Mechanotransduction in red blood cells

Lennart Kuck

BSc (Bioscience & Health), MSc (Medical Research)

Biorheology Research Laboratory

School of Health Sciences and Social Work

Griffith Health

Griffith University

Submitted in fulfilment of the requirements of the degree of

Doctor of Philosophy

August 2022

Abstract

Red blood cells (RBC), the oxygen-carriers within blood, eject their nuclei and other organelles to optimise cellular mechanics for gas exchange in capillary networks. Lack of organelles, however, strictly limits circulatory longevity of these cells, due to the inability to repair damaged cellular components. Given the turnover of RBC, the cell population within blood is inherently heterogenous, comprising RBC across the whole spectrum of *in vivo* age. Moreover, surrender of translational capacity restricts cellular signalling within RBC to modifications of existing proteins and/or flux of ions through membrane-embedded channels, rather than alterations in protein expression.

The traversal of the cardiovascular system for the purpose of gas exchange exposes RBC to varying mechanical forces. Exposure to mechanical force physically deforms the RBC membrane, which, upon cessation of force exposure, readopts its native bi-concave disc chape. Novel observations support that these mechanical forces also activate biochemical pathways that may acutely and transiently alter RBC mechanics. The molecular machinery facilitating these mechanotransduction processes in RBC, however, is largely undescribed.

The aim of the present body of work was thus to elucidate i. mechanotransductive pathways in mature, enucleated RBC; ii. the contribution of mechanically-activated signalling to the regulation of RBC mechanics; and iii.

the impact of sub-populations of RBC with abnormal mechanical properties on blood fluid behaviour.

The salient findings of the present dissertation support the presence of a relevant post-translational signalling network in circulating, enucleated RBC, some of which is sensitive to activation by mechanical forces. The cation channel Piezo1 appears to be a central mechanism of 'force sensing' in these cells. That is, opening of Piezo1 in response to mechanical force facilitates influx of calcium-ions, which regulate RBC mechanics *via* diverse mechanisms, including acute shifts in cell volume, selective removal of susceptible cells within a given RBC population, and initiation of nitric oxide production.

Collectively, the herein presented results enhance the current understanding of fundamental RBC physiology by elucidating hitherto unrecognised signalling pathways. Given the demonstrated relevance of these processes to the regulation of RBC mechanical properties, which determine blood fluid properties and effective gas exchange, components of mechanically-activated signalling in these cells may provide novel therapeutic targets. Moreover, adverse complications arising in scenarios where blood is exposed to mechanical forces far exceeding those investigated here, for example during transit of mechanical circulatory support devices or dialysis machines, may be linked to overactivation of mechanically-sensitive signalling.

Correspondence

Lennart Kuck

School of Health Sciences and Social Work

Biorheology Research Laboratory, Menzies Health Institute Queensland

Gold Coast campus, Griffith University, 4215

AUSTRALIA

Email: lennartkuck@googlemail.com

Statement of Originality

This work has not previously been submitted for a degree or diploma in any university. To the best of my knowledge and belief, the dissertation contains no material previously published or written by another person except where due reference is made in the dissertation itself.

_____

(Lennart Kuck)

Acknowledgements

The present body of work is the product of a journey that has spanned the past 7 years of my life. Its completion has required the generous support of a number of inspiring people at every stage, for which I am wholeheartedly grateful.

Assoc Prof Michael Simmonds, being in the right place at the right time for taking an opportunity or give someone an opportunity can profoundly impact their life path. Crossing paths with you, and receiving that opportunity, has transformed my personal and professional lives tremendously. I am most grateful and appreciative of your persistent support and belief in my capacity in these past 7 years, which have facilitated a growth that I myself look back on in astonishment. I believe, however, as you do, that the best still lies ahead, and I look forward to shared discoveries and amazing science in the future.

Assoc Prof Jason Peart, my interest and passion has been in cellular signalling, and it has been immensely rewarding to work with a scholar of this field with your expertise, experience, and perspective. I am grateful for your guidance and mentorship within science and beyond its borders. I am proud of the body of work we have produced together, yet I am extremely excited about the work we can do next, and I look forward to our continued collaboration.

Dr Antony McNamee, I sincerely thank you for your kinship, comradery, and for sharing your incredible scientific mind in our conversations. You were a source of motivation and support in good times and bad, and I am grateful for your selflessness in- and outside the laboratory.

To my colleagues at Griffith University and overseas, I am grateful for the collaborations I have been able to share with you and your support, engagement, and inspiring scientific discussion.

To my fellow doctoral candidates and friends, I am thankful for your continued support both from overseas and here in Gold Coast. When I needed to step away and recover from this research effort, you have been there every time, and you were always happy to lend an ear when I would go on about my red blood cells, or an arm when I needed study participation.

To my family, if this dissertation is worthy of dedication, it is to you. Your most generous love and unwavering support over the past 7 years, from first encouragements to undertake a stay at a laboratory on the other side of the globe, to final video calls in the final week of writing this dissertation, your contributions have enabled its completion. Without the knowledge of unconditional love and selfless support from you all, and a sustained belief in me, these works would not be what they became.

Contents

List of figures

List of tables

List of published works contained in this dissertation

Peer-reviewed publications

Kuck, L., Peart, J. N., & Simmonds, M. J. (2020). *Calcium dynamically alters erythrocyte mechanical response to shear*. Biochimica et Biophysica Acta (BBA)-Molecular Cell Research, 1867(11), 118802. DOI: 10.1016/j.bbamcr.2020.118802

Kuck, L., Peart, J. N., & Simmonds, M. J. (2020). *Active modulation of human erythrocyte mechanics.* American Journal of Physiology-Cell Physiology, 319(2), C250-C257. DOI: 10.1152/ajpcell.00210.2020

Richardson, K. J.*, **Kuck, L.*,** & Simmonds, M. J. (2020). *Beyond oxygen transport: Active role of erythrocytes in the regulation of blood flow.* American Journal of Physiology-Heart and Circulatory Physiology 319(4), H866-H872. DOI: 10.1152/ajpheart.00441.2020
*These authors have contributed equally to this work.

Kuck, L., McNamee, A. P., & Simmonds, M. J. (2022). *Impact of small fractions of abnormal erythrocytes on blood rheology.* Microvascular Research, 139, 104261. DOI: 10.1016/j.mvr.2021.104261

Kuck, L., Peart, J. N., & Simmonds, M. J. (2022). *Piezo1 regulates shear-dependent nitric oxide production in human erythrocytes*. American Journal of Physiology-Heart and Circulatory Physiology. DOI: 10.1152/ajpheart.00185.2022

Manuscripts in preparation

Kuck, L., Peart J. N., Simmonds M. J. *Distinct calcium-handling of density-separated human erythrocytes in response to mechanical shear.* Final draft in preparation for first submission during Q1, 2023. Target journal: Blood

Abstracts presented to scientific conferences

2018 – Joint International Conference of Three Societies in Krakow: The European Society for Clinical Hemorheology and Microcirculation, The International Society of Clinical Hemorheology, and The International Society of Biorheology (ESCHM-ISCH-ISB); **Kuck, L.**, Simmonds M. J.: *"Cell volume regulation via the Calcium-activated Potassium channel KCa3.1 contributes to red blood cell compliance under shear"*

2020 – Queensland Cardiovascular Research Network Online conference:

Kuck L., McNamee A. P., Simmonds M. J.: *"Blood fluidity is disproportionately impaired by a small fraction of abnormal red cells"*

2020 – Australian Physiological Society student and early career researcher online forum; **Kuck L.**, Peart J. N., Simmonds M. J.: *"Active regulation of red cell mechanics by nitric oxide and calcium"*

2021 – 2nd Joint International Conference of Three Societies in Fukuoka: The European Society for Clinical Hemorheology and Microcirculation, The International Society of Clinical Hemorheology, and The International Society of Biorheology (ESCHM-ISCH-ISB):

Kuck L., Peart J. N., Simmonds M. J.: "*Impaired mechanotransduction in diamide-treated erythrocytes"*

Kuck L., Peart J. N., Todd O. J., Simmonds M. J.: "*Cell age sensitivity of red cells to mechanical stresses and calcium load"*

2021 – Australian Physiological Society 60th Diamond Jubilee conference; **Kuck L.,** Peart J. N., Simmonds M. J.: *"Piezo1 regulates shear-dependent nitric oxide production in human erythrocytes"*

2021 – Society for Free Radical Research Australia Annual Meeting: **Kuck L.,** Peart J.N., Simmonds M.J.: *"Membrane thiol oxidation impairs endogenous nitric oxide generation in human erythrocytes"*

Preface

Red blood cells (RBC) are, at first glance, probably the simplest cells in the human body. Comprised of merely a lipid bilayer enclosing the cytoplasm, without sub-cellular compartments (that we know of), a cell could not be constructed in a more basic way. There is an elegance in the perceived simplicity of how red cells are designed; it is more difficult to design something in the simplest way, such that it still works perfectly, when compared with more complex cellular architectures. During differentiation from haematopoietic progenitor cells, RBC surrender their capacity to express genetic information: thus, their responsiveness to external stressors during their lifespan is limited. Given the accessibility of human blood samples even in the historic times of science, RBC (or the "red corpuscles of blood") were first depicted by the Dutch microscopist Antonie van Leeuwenhoek some 300 years ago (Fig. 1). Interestingly, he would have observed them in the presence of plasma at stasis, thus depicting them as aggregates, rather than individual cells. Red cells then played a key role in the discovery and characterisation of the lipid bilayer in studies by Gortner and Grendel in 1925 [1], as the lack of organelles in these cells facilitated extraction of the cell membrane lipids.

Fig. 1*: The first illustration of the "red corpuscles of blood" by A. van Leeuwenhoek in 1695.*

With the discovery of the molecular components that comprise genetics, RBC soon after became a less prominently researched cell type, at least from a biochemical and cell biological perspective, given they are devoid of transcriptional machinery. During this "golden era" of molecular biology, manipulation of gene expression in specific cell types or tissues – either through knock-outs/-downs or overexpression – enabled elucidation of the function of a plethora of different proteins and enzymes. Red cell studies, however, did not benefit from this leap in molecular technologies yet, as they could not easily be manipulated through changing gene expression, due to the enucleation process. Over the past two decades, however, significant advancements were made in the field of dynamic post-translational signalling, and RBC are now beginning to be "re-discovered". "Re-discovery" in this context may refer to the complex post-translational signalling presumably present in RBC, a cell type long considered biologically inert due to the absence of translational activity, which is only

recently being accessed. In most current teaching textbooks, and according to general knowledge within the scientific community, RBC remain a "boring" type of cell: a membranous sac that contains haemoglobin *en masse*. A cell that is bounced around the circulatory system at will until it eventually disintegrates because it cannot repair itself. The present dissertation is composed of a series of experimental studies supporting that RBC are overdue for a re-evaluation. The ejection of the nucleus provides such enormous advantages for maximising surface area in capillaries to facilitate diffusion of oxygen, that the metabolic demands of higher mammals required evolution of enucleated RBC. It appears that these cells, however, maintain post-translational regulation of some vital cellular properties, including cell volume homeostasis, membrane deformable properties and enzyme activity, in spite of not being capable of translation. It is my personal fascination and ambition to make meaningful contributions in this area, and to facilitate re-ignited interest in fundamental red cell research, which may well be an underestimated therapeutic target in various cardiovascular disorders where tissue perfusion is impaired.

Lennart Kuck, August 2022

Chapter 1

Introduction

1.1 The physical properties of blood facilitate efficient oxygen delivery

The delivery of oxygen to metabolically-active tissues and its efficient use to generate molecular energy is absolutely essential to sustain homeostasis in complex higher organisms [2]. Oxygen is typically transported by specialised carrier cells, where it may be bound to metalloproteins designed to facilitate efficient oxygen uptake and release, in dependence of local concentration-gradients [3]. In humans, these specialised cells are suspended in a fluid to facilitate traversal of the cardiovascular system – the blood. Blood is propelled through the vasculature, composed of large arteries and veins that are connected *via* intricate capillary networks surrounding working tissues, thus optimising oxygen delivery. As a result of comprising solid (cells) and liquid (plasma) phases, blood exhibits distinct fluid properties: blood viscosity is characteristically dynamic (i.e., blood is a non-Newtonian fluid), depending on local fluid forces. Given plasma viscosity is Newtonian, and thus shear-independent, the dynamic fluid behaviour of blood is explained by the physical properties of red blood cells (RBC), which comprise ~99% of the cellular phase in blood.

Specifically, the comparatively high viscosity of blood at stasis and under low shear (<100 s^{-1}; [4]) is due to RBC reversibly aggregating to form branched, three-dimensional structures resembling stacks of coins, fittingly termed 'rouleaux' (Fig. 2). In contrast to the endpoint of the coagulation process – irreversible formation of a thrombus – RBC aggregates are redispersed under increasing shear forces. The determinants of RBC aggregate formation are i. haematocrit, given an increased density of cells increases the probability for cell-cell contact; ii. the high surface area of RBC relative to its volume, owed to the bi-concave cellular geometry, facilitating cell-cell attachment; iii. presence of plasma proteins in the surrounding medium, especially fibrinogen, inducing and stabilising rouleaux; iv. the negative charge of the RBC membrane, mostly carried by the glycocalyx, facilitating repulsion between cells.

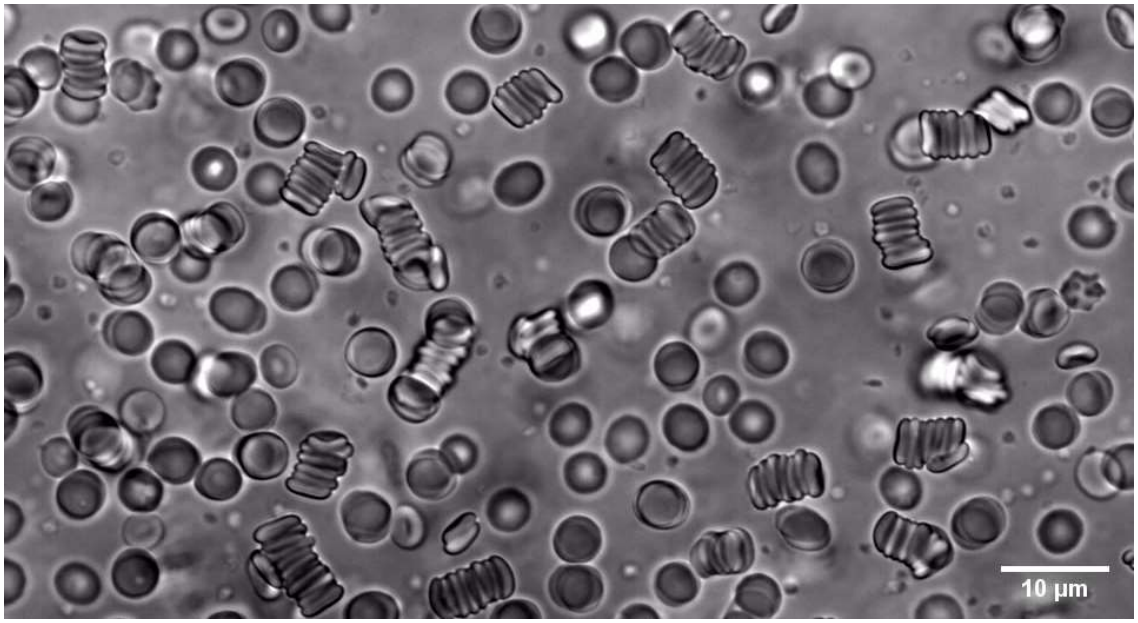

***Fig. 2**: Red blood cells (RBC) forming reversible rouleaux, suspended in autologous plasma at 0.015 $L \cdot L^{-1}$ haematocrit. The image was captured at room temperature after allowing 10 min for RBC to settle onto the coverslip and aggregate, using an objective with 600-times magnification. Note the extraordinarily low haematocrit, chosen to improve visibility of aggregates: at physiological haematocrit, aggregate formation occurs along physiologically-relevant time scales.*

The dynamic fluid behaviour of blood is also dependent on the capacity of RBC to reversibly elongate in response to mechanical forces, owed first and foremost to the ejection of the near incompressible nucleus [5]. The viscoelastic properties of the plasma membrane and the aforementioned extraordinarily high ratio of surface area to cell volume also determine the deformability of mature RBC (for an extensive review on the rheological properties of blood, see [6]). This exceptional capacity to elongate and deform impacts bulk-blood flow by facilitating axial migration of RBC; that is, due to being highly deformable, RBC

are more concentrated in the centre of the blood vessel (where velocity is highest), pushing platelets and leukocytes towards the vessel wall (Fig. 3).

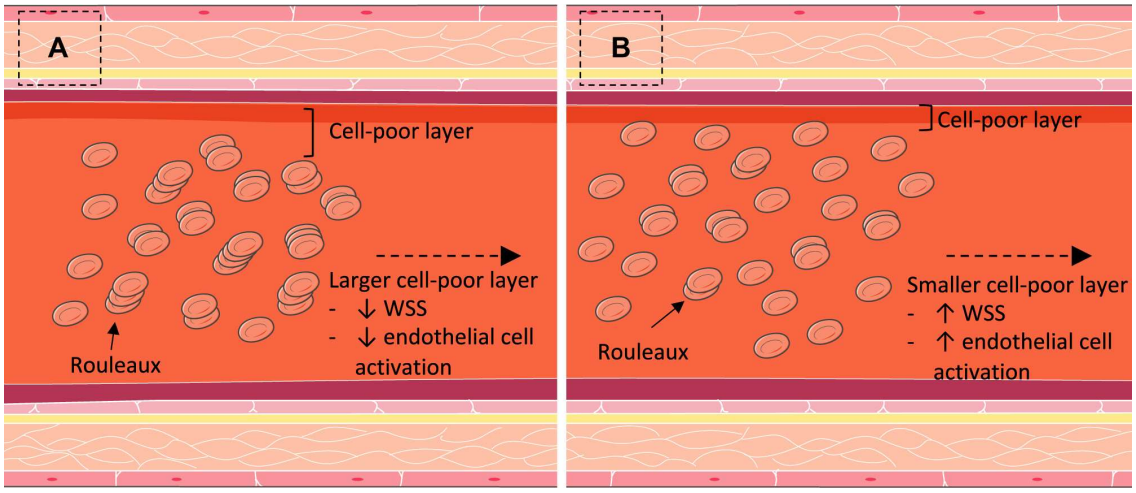

***Fig. 3**: The physiological relevance of red cell aggregate formation. A: formation of red cell aggregates ('rouleaux') is beneficial within normal limits, due to concomitant promotion of the cell-poor region. B: when aggregation levels are diminished, greater distribution of red cells within flow impacts on the cell-poor region, leading to increased wall shear stress (WSS) and, thus, also abnormally high activation of endothelial cells. Figure adapted from Richardson et al. [7].*

Placing platelets and leukocytes in spatial proximity of the vessel wall facilitates platelet aggregation during wound-healing, and lymphocyte migration to damaged tissues during immune responses [8]. The capacity of RBC to deform is also pivotal in the microcirculation, where transit of capillaries and the interendothelial slits of the spleen is required for gas exchange, despite vessel diameters much narrower (2 μm) than those of an average RBC (~8 μm). The exceptional capacity of mammalian RBC to deform, facilitated by expulsion of

the nucleus and other organelles during differentiation, ensures maximal contact area between RBC and vessel to optimise diffusion of haemoglobin-bound oxygen. While the large oxygen demands of mammalian tissues were met by evolution of RBC organelle expulsion, a process that does not occur in reptilian, amphibian or avian RBC, there appear to be adverse consequences of this process on a cellular level.

1.2 The heterogeneity of the circulating erythrocyte population

The RBC lifespan is pre-determined due to the lack of cell organelles, which precludes resynthesis of damaged cellular components. Early estimates placed the length of this lifespan around 120 days for human RBC, a number derived from landmark experiments tracking ^{59}Fe-labelled isotopes [9] – a value of RBC circulatory longevity that is now universally accepted. *In vivo* ageing of RBC interestingly follows a densification pattern, wherein density of cells increases with cell age [9, 10]. This densification may appear counterintuitive at first glance, given the well-described progressive decline in sodium-potassium exchange. This decline is likely due to decreasing copies of the responsible ion pump (Na-K-ATPase; [11]) being present with increased cell age, which would facilitate an inward leak of sodium ions (Na^+), causing osmotic swelling, not shrinkage. Accumulation of calcium-ions (Ca^{2+}) in ageing RBC [12, 13], however, dominates progressive outward shifts in cell volume through activation of a

calcium-activated potassium channel (*KCNN4*). The gradient between intracellular calcium concentration $[Ca^{2+}]_i$ and extracellular calcium concentration $[Ca^{2+}]_e$ in blood is so significant (~40,000-fold) that even brief opening of non-selective cation channels leads to significant spikes in $[Ca^{2+}]_i$, which are much larger than concurrent spikes in intracellular sodium concentration $[Na^+]_i$. The result of increased $[Ca^{2+}]_i$ is an electroneutral loss of K^+ and Cl^-, followed by osmotically-driven loss of H_2O, causing an increase in cytosolic viscosity (due to unaltered haemoglobin concentration), and thus increased cellular density (i.e., the 'Gárdos effect'; [14]). Increases in $[Ca^{2+}]_i$ are normalised by the plasma membrane calcium pump (PMCA) at the expense of molecular energy [15, 16] in the form of adenosine triphosphate (ATP). In its native state, the RBC membrane is near impermeable to Ca^{2+}, with the Ca^{2+}-leak easily corrected by a PMCA that operates well-below maximal capacity [16, 17]. Opening of non-selective cation channels, for example mechanically-activated channels during capillary transit, however, may precipitate spikes in $[Ca^{2+}]_i$ sufficient to trigger the Gárdos effect [18]. A linear decline in PMCA-activity with increasing cell age in combination with the well-documented decline in metabolic capacity of aged RBC drives increasingly frequent activation of the Gárdos effect, which is thought to contribute to *in vivo* ageing of RBC [19, 20]. Collectively, as a consequence of biosynthesis being absent in these cells, the RBC lifespan is strictly limited due to cellular damage, accumulated through constant exposure to oxidative products of haem-oxygen reactions and mechanical wear.

Due to this *in vivo* ageing pattern, RBC populations in blood are inherently heterogenous, comprising cells at different points along their 120-day lifespan. This cellular heterogeneity is often not considered in experimental studies exploring RBC properties at a population-level, given that the impact of low fractions of cells with unfavourable mechanics (e.g., senescent RBC) on overall blood fluid behaviour is poorly described. It is also possible that shifts in the composition of a given RBC population could alter bulk blood flow behaviour. Indeed, previous reports indicate that selective removal of aged RBC through exposure to non-physiological environments results in improved properties of the remaining cell population [21].

1.3 Mechanisms of erythrocyte removal from circulation

Failure to maintain low $[Ca^{2+}]_i$ appears to be a significant driver of *in vivo* ageing and may even contribute to the eventual removal of RBC from circulation. Indeed, calcium-handling may become progressively impaired in senescent RBC [15]. Cytosolic concentration of Ca^{2+} is not uniform in a given RBC population [22]: increased $[Ca^{2+}]_i$ is associated with aged RBC, while low $[Ca^{2+}]_i$ is observed in 'younger' cells [23]. It is well-known that distinct sub-populations of RBC, for example those at different stages of their *in vivo* lifespan, present with different physical, metabolic, mechanical, and biochemical properties [10, 22-26]. Heterogeneity has also been observed in the responsiveness to external

stimulation [22, 27, 28], wherein 'old' RBC generally exhibit unfavourable characteristics. While the combination of accumulative oxidative stress, ion gradient dissipation and metabolic decline drives ageing of enucleated RBC, detailed descriptions of the mechanisms that govern the eventual removal of aged RBC from circulation remain somewhat elusive [29]. It was thought that senescent RBC, which are rigid due to their high density, increased cytosolic viscosity and stiffened membrane skeleton, are retained in the filtering architecture of the spleen, and then phagocytosed [30, 31]. Patients that undergo splenectomy, however, do not lose the ability to clear aged RBC; this process appears to take place in the liver instead [32, 33]. More recent works have suggested a role of the Gárdos effect in the removal of RBC [34], and also indicate that digestion of aged RBC by macrophages is preceded by haemolysis – release of cytosolic contents – leaving behind the membrane skeleton (i.e., production of RBC ghosts; [35]). This type of haemolysis is typically caused by rapid swelling due to influx of Na^+ and Cl^- *via* transient membrane pores, hypothesised to be induced by the complement system, which is vital to innate immunity and host defence [36]. Adhesion of rigid RBC is facilitated by binding to the splenic anatomy *via* specialised molecules (e.g., laminin and CD40), wherein aged RBC exhibit increased adhesive properties [35]. An overload of intracellular Ca^{2+} appears to contribute to untimely removal of aged RBC, as observed in various anaemias [37], accelerating RBC removal through activation of proteases (e.g., calpain), and disruption of lipid asymmetry (e.g., phosphatidylserine exposure).

Collectively, the age-dependent densification of circulating RBC has been shown to be driven by repeated entry of Ca^{2+} in combination with progressive decline in ion pump function (for an extended review, refer to [38]), precipitating a distinctly heterogeneous population of circulating RBC. It also appears that haemolysis in the spleen, at least in healthy individuals, precedes removal of RBC at the end of their 120-day lifespan; however, the mechanisms of haemolysis and some aspects of RBC *in vivo* ageing remain yet unresolved.

1.4 Mechano-sensitive signalling in enucleated erythrocytes

Enucleation of mammalian RBC for the purpose of optimising oxygen-delivery during capillary transit severely limits cellular function. As one of the very few enucleated cell types in the human body, apart from platelets and keratinocytes, RBC do not have access to transcription and translation, mitochondrial energy production, or ribosomal activity. Thus, 'passive' physical characteristics were typically recognised as the primary determinants of RBC mechanics (e.g., viscoelastic membrane, surface area to volume ratio, intracellular viscosity). Over the past decade, however, a body of evidence has accumulated indicating that intracellular signalling *via* short-lived messenger molecules may acutely and transiently alter the physical properties of RBC [27, 39-42]. Given that the synthesis of new proteins is impossible, all signalling in RBC must occur at the post-translational level, which includes post-translational modifications of

existing proteins, altered activity of metabolic enzymes, and flux of ions across the cell membrane (for a detailed review of RBC membrane transport, please refer to [43]). The key mediators currently hypothesised to exert significant effects on RBC mechanics are nitric oxide (NO) – which may be produced endogenously within RBC *via* an RBC-localised nitric oxide synthase (NOS) – and acute changes in $[Ca^{2+}]_i$. The primary mechanism currently proposed to elicit activation and mobilisation of these molecules is mechanical shear [18, 28]; that is, it is thought that physical forces deforming the cell membrane may be transduced into biochemical events that stimulate signalling *via* NO and/or Ca^{2+}. The molecular machinery that facilitates mechanotransduction in RBC, however, is largely undescribed.

Ulker et al. [28] previously investigated RBC that were exposed to fluid shear stress, reporting that shear exposure led to activation of RBC-NOS3 *via* phosphorylation at serine residue^{1177} (ser^{1177}). Activation of RBC-NOS3 was accompanied by entry of Ca^{2+} into RBC, and precipitated increased intracellular concentrations of NO [28]. Grau et al. [39] proposed that endogenous NO may be reversibly incorporated into the cytoskeletal component of the cell membrane, thus affecting cellular deformability; specifically, NO may bind to exposed thiols (-SH) of cysteine-residues in α- and β-spectrin filaments, forming nitrosylated residues (S-NO), thereby altering the elasticity of the cytoskeleton. While this proposed mechanism has not been confirmed in independent studies or

structural investigations of S-nitrosylated spectrins, data supporting potential alternative mechanisms that explain how NO alters RBC mechanics are also lacking. The generation of highly sophisticated, tissue-specific RBC-NOS3 knock-out murine models in a recent landmark study provided convincing evidence that RBC-derived NO plays an important role in regulating blood pressure [44], although it is unclear whether modulation of RBC physical properties contributed to this observation.

Expression of the *bona fide* mechanosensory protein Piezo1, a cation channel thought to be activated by mechanical forces deforming the cell membrane, was recently shown in RBC membranes [45]. It appears that Piezo1 may regulate RBC volume through facilitating entry of Ca^{2+}, which triggers the Gárdos effect, thus causing RBC to shrink [45], potentially aiding transit of narrow capillaries [18]. Given that Piezo1 is instrumental to vascular function, regulating vascular tone through coupling with eNOS [46], and considering the plethora of Ca^{2+}-dependent pathways described in RBC [47], it is plausible that Piezo1 would be an important mechanotransductive mechanism in these cells. Post-translational signalling in enucleated, circulating RBC, for example through NO and regulation of RBC-NOS3, is known to be sensitive to mechanical forces, however, whether Piezo1 contributes to the activation of these pathways remains to be elucidated.

1.5 Conclusion

The properties of a given RBC population are heavily impacted by a major event in erythropoiesis: the ejection of the nucleus and other cell organelles, rendering mature, circulating RBC devoid of transcriptional machinery. As a direct result of this event, a given RBC population is inherently heterogenous, comprising cells at various stages of their lifespan, and this heterogeneity contributes to the overall physical and biochemical characteristics of blood fluid properties.

A secondary consequence of enucleation is the reliance on post-translational signalling for acute, reversible alterations of cellular properties. Convincing evidence has accumulated over the past decade establishing a significant role for NO molecules and Ca^{2+} in contributing to 'active' regulation of RBC physical properties. While several interactions and mechanisms remain to be elucidated, it can be assumed that maintaining tight control over the concentration of these messengers is pivotal for ensuring RBC homeostasis and cellular deformability, especially during ageing of RBC *in vivo*. Consequently, given that RBC deformability is a parameter known to be impaired in a vast variety of pathologies (e.g., type 2 diabetes, ischemia-reperfusion injury, coronary artery disease [48, 49]) and in physiologically-aged RBC, studying the mechanism through which NO-dependent and Ca^{2+}-regulated pathways contribute to controlling RBC mechanics, is of value. The notion that RBC are not merely passive contributors to circulatory function, but actively participate in it *via*

molecular signalling, has received significant interest only in the past decade; thus, two distinct reviews of recent advances in the scientific literature have been prepared with first author contributions by the candidate, and are published under the references below [7, 50]:

Richardson, K. J.*, **Kuck, L.***, & Simmonds, M. J. (2020). Beyond oxygen transport: Active role of erythrocytes in the regulation of blood flow. *American Journal of Physiology-Heart and Circulatory Physiology.* 319, H866–H872

*these authors contributed equally to the work.

Kuck, L., Peart, J. N., & Simmonds, M. J. (2020). Active modulation of human erythrocyte mechanics. *American Journal of Physiology-Cell Physiology*, 319(2), C250-C257.

The literature review that follows is a synthesised chapter based on the peer-reviewed papers listed above, with minor redundancies eliminated, and novel findings that were published after publication of these reviews incorporated post-hoc. Further reference to the review papers themselves was omitted in the present dissertation for the sake of clarity.

Literature review

1.6 Role of cell mechanics in oxygen delivery

Cellular respiration is vital to sustained metabolism, and therefore life, and is only possible through the integration of the cardiovascular, pulmonary, and circulatory systems. One of the challenges to oxygen loading, and subsequent transport, within the circulatory system is the extremely small apertures that blood needs to navigate: the smallest capillaries (2-3 μm) in the pulmonary and peripheral circulations are a fraction of the resting diameter (~8 μm) of RBC; consequently, the RBC is morphologically agile, with a unique ability among all mammalian cells to change shape and subsequently return to its resting state without any appreciable negative effects [51]. A pathologically reduced ability of RBC to deform has thus long been considered a precursor for heightened risk of tissue ischemia at both micro- and macro-vascular scales, given rigid cells: i. have limited capability to perfuse the rich microvascular network of organs [52]; and, ii. affect the bulk properties of blood through increasing the resistance to flow by contributing to hyperviscosity [6]. Indeed, even the capacity for oxygen dissociation from haemoglobin during tissue perfusion was reported to be limited by decreased cellular deformability [53]. Further, many disease states associated with tissue necrosis, ischemia, and/or hypoxia are characterised by poor cell mechanics of RBC [48]. A rat model was used to demonstrate, for example, that RBC with an artificially rigidified membrane were subsequently

"trapped" within the spleen, sternum, lung, femur, and liver, which collectively inferred poor global tissue perfusion [52]. Doyle et al. [54] employed a similar rigidifying process and perfused the resultant cells through isolated rat lungs; they observed a significant increase in pulmonary artery pressure, providing evidence of a multiscale (i.e., both microcirculatory and macrocirculatory) impact of poor cellular deformability. Langenfeld et al. [55] subsequently demonstrated that infusion of rigidified RBC into rats significantly increased systemic vascular resistance and decreased cardiac index, linking the cellular mechanics of blood with vascular function, and ultimately cardiac performance. These works thus provided experimental evidence for the meaningful physiological impact resulting from poor RBC deformability, and led to clinical insights into numerous pathologies that are associated with impaired cell deformability, including sickle cell disease [56], haemochromatosis [57], sepsis [58], and diabetes [59]. Translational work extends these earlier findings, given recent evidence indicating that despite attempts at compensation *via* increased conduit artery blood flow, the impaired cell mechanics in sickle cell disease significantly impair microvascular oxygenation and vascular reactivity [60]. Further, impaired capillary blood flow (RBC velocity and flux) was observed both at rest and during muscular contraction, in a murine model for heart failure [61]. Given RBC deformability is essential for capillary transit, it is plausible that these observations may be due, in part, to impaired RBC deformability, commonly reported in individuals with heart failure [62], further highlighting the multiscale

relation between the micro- and macrovasculature. Thus, despite a vital role for optimal cellular mechanics being well established, the molecular regulation of these physical properties is only recently emerging.

1.7 Physical properties that enable erythrocyte deformability

The properties of RBC that were recognised to confer their unique capacity to deform in response to mechanical stimulation included the excess surface area relative to cell volume, the intracellular viscosity, and a visco-elastic cellular membrane [51]. The excessive surface area of RBC is clearly observed when the cell is compared with a perfect sphere: while the average volume of an RBC (~90 μm^3) could be contained in a sphere with only 97 μm^2 of surface area, the surface area of an RBC is ~44% larger (~140 μm^2) and thus yields a surface area-to-volume ratio that approaches 1.5 [51]. The resultant excess surface area is provided by the bi-concave structure of the RBC membrane and facilitates significantly greater capacity to deform than a spherical shape would. The intracellular viscosity of RBC is largely determined by haemoglobin concentration suspended in the cytosol. The mean intracellular viscosity of RBC is ~7 mPa·s at normal haemoglobin content, which is comparatively higher than the viscosity of the surrounding plasma (~1.2 mPa·s; [51]). This disparity contributes to the deformation of RBC by facilitating an independent rotation of the cellular membrane around the cytoplasm, termed tank-treading [63]. While the earliest

interpretation of tank-treading indicated that the cell membrane was mostly independent of internal structures [63], advances over the last decades support that various entities complex with the intracellular surfaces of the cell membrane, which indeed may even serve to enhance the mechanical properties of the cell [64].

Further, the exceptionally deformable capacity of the RBC membrane has been long observed; this cell provides the template for lipid bilayer models of cell membranes and is noted for its exceptional capacity to deform upon exposure to shearing forces, subsequently reassuming its original bi-concave shape [6]. The RBC membrane contains a cytoskeletal mesh-network with integral proteins establishing connections with the lipid bilayer, which stabilises the characteristic bi-concave shape of RBC. Collectively, the properties that permit a remarkable capacity of RBC to deform have been studied (Fig. 4), and until recently the determinants of these properties were thought to be static. Recent advances challenge this perspective and support an 'active' regulation of mechanical properties that may acutely alter the physical properties of RBC.

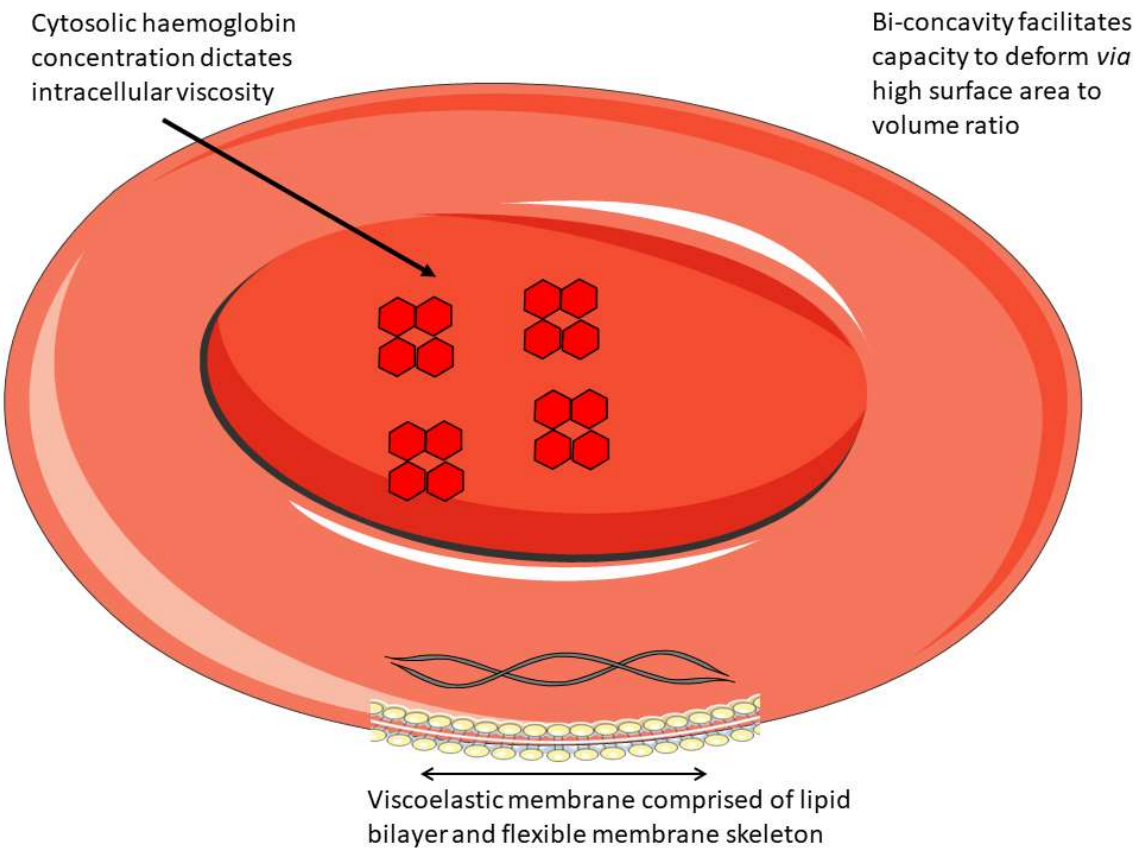

***Fig. 4**: The physical properties that facilitate the remarkable capacity of red blood cells to reversibly deform. Figure adapted from [50]*

1.8 The molecular structure of the erythrocyte membrane facilitates cellular deformability

The molecular composition of both the cytoskeletal and lipid bilayer components of RBC has been the subject of extensive study during the past century [1, 65]. The cytoskeleton consists of spectrin filaments (i.e., α- and β-subunits, which are antiparallel isomers), assembled in conjunction with filamentous actin to form hetero-tetramers in head-to-head manner (Fig. 5). These filaments are interconnected to the lipid bilayer: i. *via* complexation with integral membrane

proteins band 3 and glycophorin; or ii. *via* actin and protein 4.1 [66]. Smith et al. [67] recently demonstrated that the spectrin-actin cytoskeleton is stabilised by an isoform of non-muscular filamentous myosin (NMIIA). NMIIA is a hexameric actin-binding ATPase comprised of two heavy chains, two light chains, and two regulatory chains, and importantly is capable of contraction – which in other cell lines has been shown to be vitally important to cell function [68]. Knowledge around the role that NMIIA exerts within RBC is still developing, although it has been recently demonstrated that tension is regulated to maintain the cell's unique bi-concave shape *via* linkage to actin in the cytoskeletal component of the membrane [67]. It follows that the mechanical properties that are promoted by this unique shape are thus also integrally affected by NMIIA [67]. Indeed, when NMIIA is inhibited using a NMIIA-specific inhibitor (i.e., blebbistatin), RBC exhibit elongated morphology at rest and lose their membrane curvature [67]. How phosphorylation or other post-translational modifications may alter NMIIA-contractility and RBC mechanics, however, remains to be resolved, although it is a valid area of interest given observations regarding structure/function in other cell lines [68-70].

The lipid bilayer itself, and the distribution of cholesterol and phospholipids within it [71], appears to also have some regulatory role in RBC membrane stability and pliability [72]. Abundant lipid-anchored integral glycoproteins band 3 and glycophorin A, which structurally contribute to coupling of the

membrane skeleton and the lipid bilayer, are pivotal in determining membrane dynamics [73-75].

Collectively, although the molecular identity and structure of the RBC membrane has been largely determined, the interactive functions of numerous proteins remain unresolved, as is the dynamic re-assembly of membrane components during cellular deformation. Moreover, while the physical properties of RBC were viewed as the singular determinants of their extensive deformability, post-translational modifications of membrane proteins in particular have been suggested as novel mechanisms to acutely alter RBC mechanics [18, 39, 76].

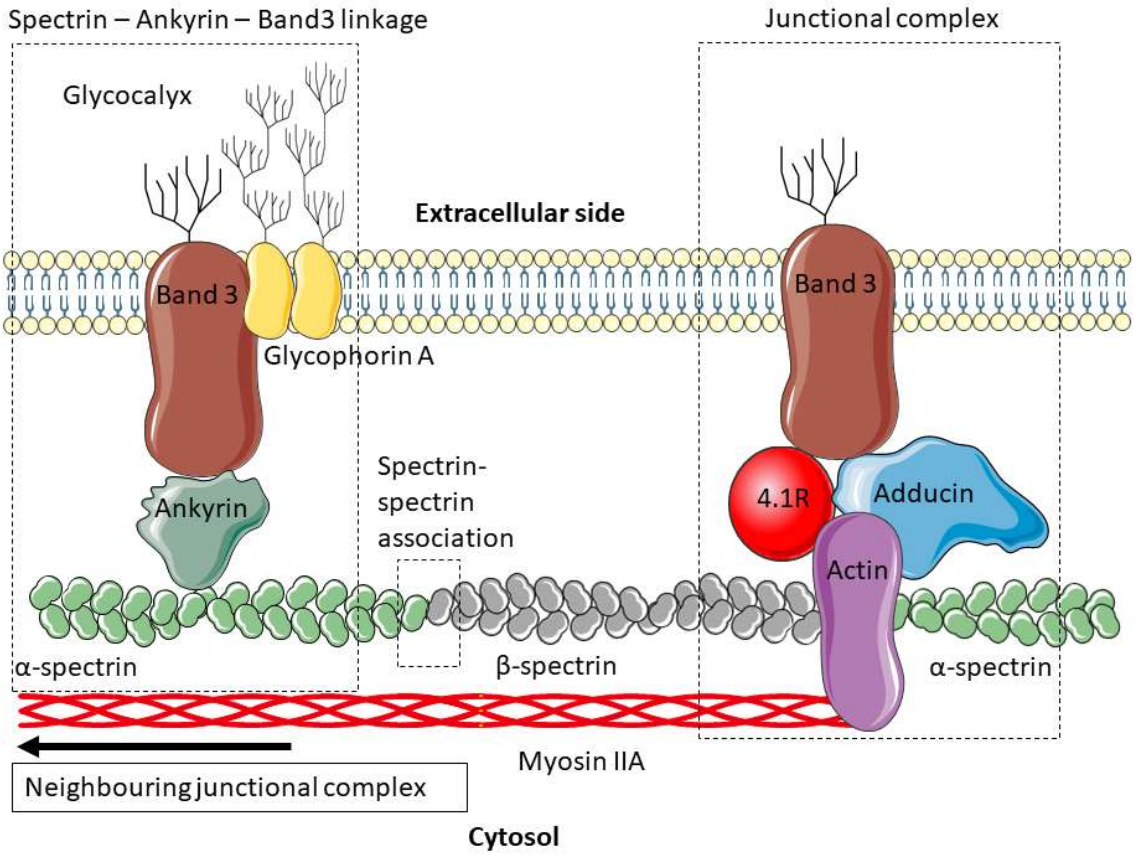

***Fig. 5**: The molecular composition of the cytoskeletal component in the RBC membrane, that resides under the lipid bilayer. α- and β-spectrins self-associate head-to-head, while each dimer is anchored to the lipid bilayer via either ankyrin or actin-4.1 complexes. Myosin IIA connects actin molecules within the junctional complexes and thus stabilises the bi-concave shape of the RBC. Figure adapted from [50]*

1.9 Red blood cells are not sedentary: the role of nitric oxide-derived species

The concept that the physical properties of RBC may be modulated "actively" – that is, dynamically altered upon exposure to mechanotransductive stimuli – has emerged only over the past decade or so. While the presence of a process responsible for generating intracellular NO in RBC was speculated for some time

[77], Kleinbongard et al. [78] only relatively recently employed independent and complimentary methods to demonstrate that RBC contain a NOS isoform that was distinct to the neuronal and inducible forms. Indeed, several key physical features were shown to reflect those of the endothelial-type NOS (eNOS).

Endothelial cells contain a NO-synthesizing enzyme (eNOS) that releases NO through catalysing the metabolic conversion of *L*-arginine to *L*-citrulline. Catalytic activity of eNOS requires organisation into homodimers, wherein each monomer possesses an oxygenase and a reductase domain – an uncommon feat for enzymes [79]. Whether native RBC-NOS3 is also present as a dimer remains to be elucidated. Co-factors for eNOS bind either to the reductase domain, which contains sites for flavin adenine dinucleotide (FAD), flavin mononucleotide (FMN), and nicotinamide adenine dinucleotide phosphate oxidase (NADPH), or the oxygenase domain, which contains bindings sites for the substrate *L*-Arginine, co-factor tetrahydrobiopterin (BH_4), and a haem centre to facilitate electron flow [80]. Molecular oxygen (O_2) is considered the final electron acceptor; in RBC, where O_2-availability is heavily contested by haemoglobin, the interaction between O_2-requirements of RBC-NOS3 and haemoglobin-O_2 binding affinity is unresolved. Activation of eNOS occurs through an association with the Ca^{2+}-carrying protein calmodulin, which initiates detachment of eNOS from lipid rafts within the cell membrane and subsequent NO-production [81]. It is thought that the increase in $[Ca^{2+}]_i$ required for calmodulin-mobilisation is caused by

activation of mechanosensitive cation channels that are sensitive to alterations in shear stress exerted by the "dragging" of blood across the vessel wall [82]. Decreased shear stress near the vessel wall, as induced by a wider cell-poor layer, was previously shown to ameliorate NO release from the endothelium, supporting rheologically mediated regulation of endothelial NO-production [83]. Moreover, once released from caveolin-1 within the lipid rafts of the cell membrane, eNOS may localise to either the Golgi complex or remain within the cytosol. The subcellular location of activated eNOS is critically important to its function, given that translocation to the Golgi complex ultimately promotes vasodilatation, while cytosolic eNOS is thought to facilitate vasoconstriction [84]. Intriguingly, RBC-NOS3 has been observed to favour membrane localisation, however, it appears that a substantial number of copies also reside within the cytosol. Given that RBC do not contain cell organelles, whether translocation of RBC-NOS3 plays a role in its function or down-stream targets is still an open question.

The activity of RBC-NOS3 was shown to be dependent on the substrate *L*-arginine, was Ca^{2+}-sensitive, and also sensitive to phosphorylation *via* the phosphoinositide 3-kinase (PI3K) pathway [78] – all properties shared with eNOS. Elucidating potential activation and down-stream targets mechanisms of RBC-NOS3 was thus of interest. Shear stress – induced either *in vitro* by exposing RBC to fluid shear in a microchannel or *in vivo* by increasing blood flow through

exercise – may act as an activator of RBC-NOS3 by inducing phosphorylation at its active residue ser^{1177} [28, 85]. Increased phosphorylation of this residue has been reported by various groups to be closely associated with increased RBC deformability [39, 76, 86], while inhibition of RBC-NOS3 was previously shown to be associated with impaired cell deformability [39]. Given RBC and endothelial cells differ significantly in structure and intracellular composition (i.e., RBC lack a nucleus and Golgi apparatus, which are pivotal in activation of endothelial NOS; [84]), further elucidation is required to examine RBC-NOS3 and discern its molecular mechanisms in higher resolution.

1.10 Activation mechanism and down-stream targets of erythrocyte-derived nitric oxide synthase

The primary mechanism currently proposed to elicit activation and mobilisation of RBC-NOS3 is mechanical stimulation [18, 28]; that is, it is thought that physical forces deforming the cell membrane may be transduced into biochemical events that stimulate NO-generation directly, or alternatively *via* an independent method involving Ca^{2+}-signalling.

Investigations aimed at discerning the effects of varying shear stress magnitudes on RBC deformability and NO-metabolism in flow led to the proposal of a dose-response relationship between shear stress and NO-production [87]. Moreover, *in vitro* application of shear stress in the physiological range during laminar flow

(i.e., comparable to forces present in the human circulatory system) was shown to elicit phosphorylation of RBC-NOS3 ser^{1177}, which occurred in concert with increased cell deformability [76]. These data support that shear stress appears to activate RBC-NOS3, and lead to predictable increases in intracellular NO-production, that may impact cellular deformability. The mechanism for shear-induced activation of RBC-NOS3 remains elusive, although Ulker et al. [28] demonstrated that while shear exposure increased the phosphorylation of RBC-NOS3 at ser^{1177}, intracellular concentrations of NO and intracellular Ca^{2+} concentration increased in tandem. Grau et al. [39] independently, demonstrated that NO produced during mechanical stimulation may reversibly incorporate into the cytoskeletal component of the cell membrane, as evidenced by increased S-nitrosylation of integral membrane proteins. Specifically, Grau et al. [39] suggested that NO appears to bind the exposed sulphur atoms in α- and β-spectrin filaments forming nitrosylated residues, and they hypothesised that this process may explain the increased cellular deformability in the presence of increased intracellular NO concentration. Further observations to confirm the S-nitrosylation of the cell membrane remain elusive, although provide a tantalising suggestion of a mechanism for shear-mediated modulation of cell deformability with implications in vascular perfusion.

It collectively appears that shear stress activates RBC-NOS3, and thus also increases intracellular availability of NO, which may impact the physical

properties of the cell membrane *via* S-nitrosylation. How the flux of Ca^{2+} during mechanical stimulation of the cell membrane – such as when RBC pass narrow capillaries to facilitate gas exchange – is related to these events remains a topic of current investigation. While these characteristics infer striking similarities between endothelial NOS and RBC-NOS3, it is stressed that these cells maintain fundamental biological differences, no less than the obvious differences in intracellular organelles. Several groups are thus currently exploring the function of RBC-NOS3 [28, 39, 76, 88], although fundamental studies into the structure of RBC-NOS3, and its potential localisation within RBC are ongoing, yet stand to deliver much greater understanding on the regulatory role of this protein. Strong genetic evidence [44, 89], supported by data derived through mass spectrometry of isolated RBC-NOS3 [88], suggests that RBC-NOS3 indeed has a genetic sequence and amino acid composition identical with that of eNOS. Although the currently available evidence points to RBC-NOS3 having the identity of eNOS, structural data of the quaternary structure of RBC-NOS3 obtained *via* X-ray crystallography or cryogenic electron microscopy would provide the absolute assurance that RBC-NOS3 does in fact assume the structure of eNOS.

1.11 Modulation of erythrocyte mechanics by intracellular calcium

Incubation of RBC with calcium has been reported to induce membrane rigidification, and thus decreased cellular deformability; at least for experiments

employing high concentrations of extracellular Ca^{2+} [23]. The mechanism of cellular rigidification, however, has never been well understood, leading to inferences of a hypothetical ionic association of Ca^{2+} with some membrane components [90]. It is clear that in RBC, $[Ca^{2+}]_i$ is maintained low (~40-60 $nmol \cdot L^{-1}$; [47]) relative to that of the surrounding plasma (~1.8 $mmol \cdot L^{-1}$; [38]), owing to the action of powerful calcium-ATPases [91]. Given RBC do not possess mitochondria, and glycolysis is the sole pathway of endogenous ATP-generation, the capacity of RBC to maintain such a tightly regulated $[Ca^{2+}]_i$ is thus dependent on the metabolic status of the cell.

O'Rear and colleagues [90] hypothesised Ca^{2+} may impair the flexibility of the cell membrane due to electrostatic interaction of this cation with the membrane lipid bilayer – at least in the context of RBC being exposed to supraphysiological shears. Increased $[Ca^{2+}]_i$ depletes cellular ATP [92], which was initially thought to be essential for maintaining RBC deformability [93], by forcing high PMCA-activity. On the other hand, Clark et al., [94] demonstrated that ATP-depletion and Ca^{2+}-accumulation have distinct effects on cellular deformability, hypothesising that the primary consequence of increased $[Ca^{2+}]_i$ is activation of the Gárdos channel (for a review, see [95]) and subsequent loss of intracellular fluid. Briefly, the Gárdos channel is a calcium-activated potassium channel embedded in the RBC membrane [14] that facilitates transport of K^+ to the extracellular space [43], and thus also water according to an osmotic shift, leading

to a decrease in cell volume (i.e., Gárdos effect; Fig. 6). Of note, while the intracellular fluid leaving the RBC contains chloride ions (Cl^-) and water, haemoglobin is unable to leave the cell *via* this mechanism. It follows that intracellular viscosity increases due to the resultant higher relative abundance of haemoglobin, which has been experimentally validated and suggested to induce impaired cellular mechanics [96]. Recent developments have led to a paradigm shift indicating that the Gárdos effect may have valuable contributions to the maintenance of cellular mechanics, at least when shear stresses and/or Ca^{2+}-flux is maintained within physiological limits.

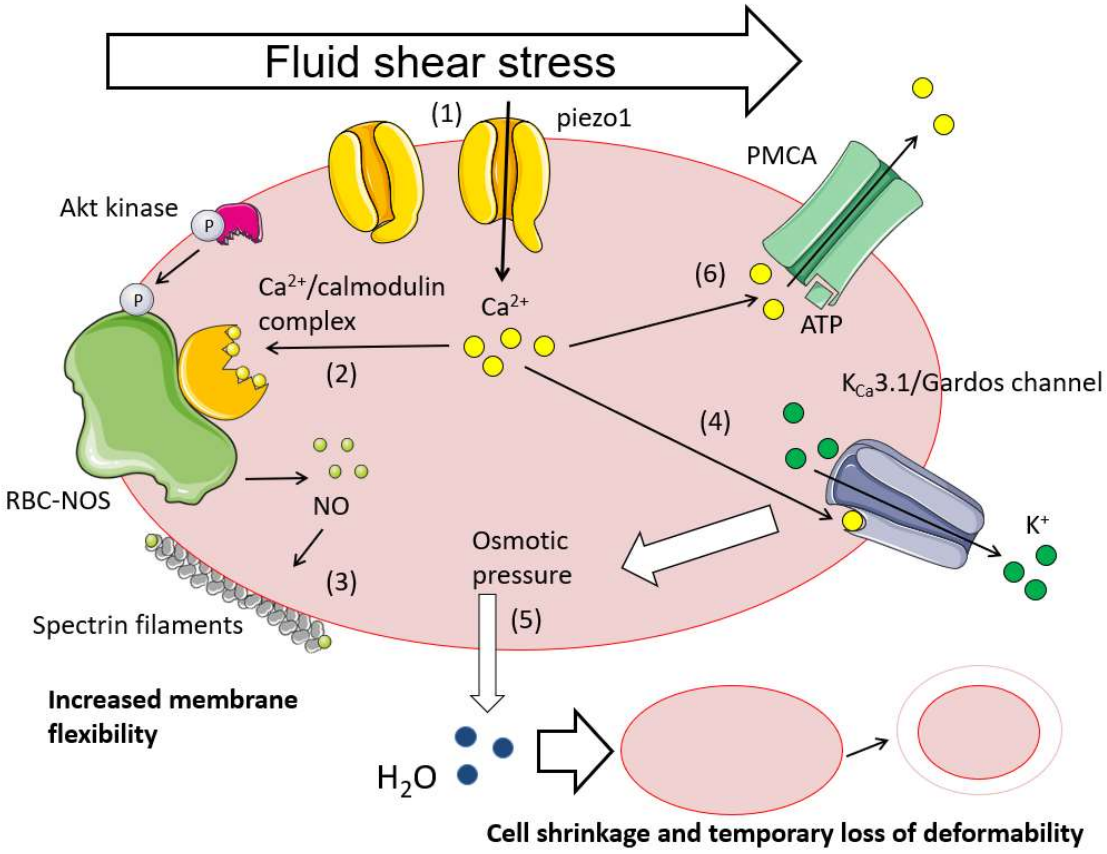

***Fig. 6**: A synthesis of the hypothesised regulatory pathways involving nitric oxide (NO) generation and calcium ion-movement (Ca^{2+}) within RBC yields a complex intracellular signalling network. Mechanical stimulation via exposure to fluid shear in blood promotes Ca^{2+}-influx via the mechanosensitive Piezo1-channel (1). Complexation of Ca^{2+} with the carrier protein calmodulin also occurs, which then collectively bind RBC-NOS3 (2). RBC-NOS3 is subsequently activated, producing NO which appears to bind to α- and β-spectrins in close proximity via S-nitrosylation of free cysteine residues, leading to increased flexibility of the cytoskeleton and improved cellular deformability (3). Activation of the Gárdos channel occurs in response to sustained Ca^{2+}-influx (4), which facilitates export of potassium ions (K^+) and leads to a loss of intracellular fluid (5). Simultaneously, Ca^{2+} is transported out of the RBC via the plasma membrane Ca^{2+}-ATPase (6).*

1.12 Mechanical stimulation, calcium, and volume regulation

Early patch-clamp experiments performed on RBC to examine stretch-activated currents found evidence of a transient Ca^{2+}-flux that occurred in immediate

response to mechanical stimulation. A negative pressure was placed onto single RBC using micropipettes to induce a reproducible deformation of the cell while isolating a membrane patch to record currents [97]. It was observed that secondary to the Ca^{2+}-trace, K^+ was transported in the opposite direction across the cell membrane [97]. The authors thus hypothesised a possible interplay between a mechanically-activated calcium channel (that was yet to be identified) and the calcium-activated potassium channel, termed the Gárdos channel. Subsequent investigations into stretch-activated ion channels in the RBC membrane became more complicated given that the gold standard method – patch clamping – itself involves applying a mechanical stimulus to the membrane which could evoke currents from mechanically-activated channels (for a review, see [98]).

Danielczok and colleagues [18] used *in vivo* and *in vitro* methods to assess transient increases in $[Ca^{2+}]_i$ within deformed RBC, visualised using a fluorescent probe. Upon cellular deformation of the RBC membrane, $[Ca^{2+}]_i$ transiently increased [18]. While anion transport across the RBC membrane occurs readily and rapidly due to the action of the abundant anion exchanger 1 protein [99], cation flux is generally more impeded, and thus Ca^{2+}-flux involves transporters/pumps residing within the membrane. A wide variety of both selective, and non-selective transports are now known, with the vast majority of these routes being voltage sensitive (for a review, see [100]). Danielczok and

colleagues [18] thus examined whether mechanosensitive cation-channels (i.e., Piezo1), shown to be expressed on the RBC membrane [45], were critically involved in the transient Ca^{2+}-response. Application of a non-specific Piezo1-blocker, the peptide GsMTx-4 [101], abolished the expected change in $[Ca^{2+}]_i$ caused by stretching of the RBC membrane. Rheological and biophysical measurements to assess the contribution of this mechanism to tissue perfusion more globally (e.g., quantification of flow velocities, shear stresses, transit times), however, were not performed in these experiments and would present a valuable addition to the observations of Danielczok and colleagues [18]. Moreover, quantifying the alterations in cell volume as RBC pass narrow capillaries is required, in conjunction with investigations aimed to discern the reversibility of this phenomenon both on a cellular (e.g., return to normal cell size) and molecular level (e.g., ion-flux during states of reduced cell volume that facilitate a restoration of cellular homeostasis). Integrative studies investigating the interplay between mechanically-activated NO generation and Ca^{2+}-signalling pathways present ambitious albeit valuable directions for full understanding of the RBC active regulation of its mechanical properties. Given the Ca^{2+}-dependency for activation of NOS observed in endothelial cells [102], in addition to existing evidence supporting a similar mechanism in the RBC [28, 78], it is plausible to suspect that cross-talk between these two signalling molecules exists.

1.13 Relevance in mechanical circulatory support and blood disorders

The mechanics of RBC are known to be impaired in a vast variety of pathologies (e.g., type 2 diabetes, coronary artery disease; [48, 59]) which manifest circulatory defects. Further, given these diseases may progress to require interventions facilitated by mechanical circulatory support (e.g., cardiopulmonary bypass; ventricular assist devices), which exert supraphysiological mechanical force on the blood [103], alterations in the sensitivity of second-messenger pathways may be particularly implicated in commonly observed post-surgical complications [104]. Impaired transduction of NO- and Ca^{2+}-regulated signalling contributing to the observed rheological impairments in clinical conditions and after high-shear exposure presents a therapeutic opportunity. Stimulating or inhibiting mechanically-activated signalling pathways by pharmacological means could ameliorate the observed deficiencies in sustaining oxygen-delivery.

Sickle cell anaemia is caused by a single point mutation in exon I of the gene coding for beta-globin [105], located on chromosome 11, which results in polymerisation of the haemoglobin beta-chain and thus 'sickling' of RBC under local hypoxia. Repeated collapses of RBC – such as through sickling when traversing the venous circulation – would provide a mechanical stimulus even stronger than shrinking induced by exposure to a hypertonic solution, which has been independently shown to induce Piezo-1 activation and Ca^{2+}-influx [18]. The Gárdos effect has been associated with sickle cell pathology (i.e., exacerbating the

'sickling'; [106]) and inhibitors of the Gárdos channel (e.g., clotrimazole and senicapoc) have been therapeutically explored, although these agents proved ineffective in reducing vascular crisis events despite decreasing the relative abundance of 'sickled' cells and haemolysis [107, 108]. Homozygous Piezo1-mutations are expressed in 20% of the sickle cell anaemia population in contrast to 5% in the general population [109]; however, preliminary clinical observations of Piezo1-mutations in sickle cell anaemia patients did not significantly associate with disease severity [110]. Independent studies established abnormal NO-metabolism in sickle cell anaemia patients; that is, sickle RBC present with increased NOS-activation and NO-production which are not associated with improved rheological characteristics [111]. It appears, however, that NO may inhibit the Gárdos channel through interaction with cysteine residues on the extracellular side of the RBC membrane, thereby ameliorating the Gárdos effect [40, 112]. Alternatively, ionic volume-regulation *via* the Gárdos effect could offset NO-dependent increases in membrane flexibility; however, further studies investigating the concrete interplay between these pathways are required.

Mutations in the genes coding for Piezo1 and the Gárdos channel have been reported in patients suffering from xerocytosis and other forms of rare anaemia [113, 114]. The rheological properties and Ca^{2+}-homeostasis of RBC were significantly altered, providing a potential mechanistic explanation for the premature haemolysis observed in these patients [37]. Collectively, it appears

that RBC-volume regulation *via* Ca^{2+}-homeostasis and endogenous NO generation play pivotal roles in blood disorders rooted in abnormal properties of RBC. Given that only symptomatic treatments currently exist for these genetic blood disorders, pharmacological interventions to correct the acute regulation of Ca^{2+} and NO within RBC is a promising approach to restore cellular mechanics and ensure tissue perfusion. For example, inhibitors of Piezo1-channels (e.g., GsMTx4) may be titrated to prevent intracellular Ca^{2+}-overload, while stimulators of RBC-NOS3 (e.g., *L*-arginine) or up-stream kinases (e.g., 740 Y-P) could increase RBC-derived NO and thus improve cell mechanics which ultimately increase tissue perfusion.

1.14 Summary

Evidence has accumulated over the past decade establishing a significant role for second-messenger molecules, such as NO and Ca^{2+}, in contributing to the *active* regulation of RBC mechanics, which ultimately affect tissue perfusion. Thus, while the last decade has provided a new perspective of the *active* regulation of RBC, integration of molecular techniques, electrophysiology, and rheological assessment of blood appears a fruitful avenue for improved therapeutic approaches for cardiometabolic and haematologic disorders, and further in the refinement of mechanical circulatory support devices that remain plagued by poor complication rates.

Aims and hypotheses

The experimental work described in the present dissertation was designed to elucidate mechanically-activated signalling in mature, enucleated RBC. Specifically, the experimental chapters were designed to investigate i. the contribution of RBC with abnormal mechanics to normal blood fluid behaviour; ii. the contribution of Ca^{2+} to regulating RBC mechanics under mechanical force; iii. the contribution of mechanically-induced entry of Ca^{2+} to RBC *in vivo* ageing and the capacity of 'young' and 'old' RBC to process intracellular spikes of $[Ca^{2+}]$; iv. the molecular machinery that enables RBC mechanotransductive processes to facilitate mechanically-stimulated NO-production *via* RBC-NOS3.

Study 1: The aim of the first study was to establish a threshold concentration of RBC with abnormal biophysical properties which was tolerable in blood (i.e., where bulk blood fluid properties were unaltered when compared with a native sample). Two distinct mechanisms of disturbing normal RBC mechanics were tested and then employed to produce mixed RBC populations: glutaraldehyde fixation and intracellular production of reactive oxygen species.

> Hypothesis: Presence of relatively low concentrations of abnormal RBC would interfere with blood fluid properties in shear flow and disrupt the normal flow behaviour of other cells.

Study 2: The aim of the second study was to determine the effect of both increased intra- and extracellular Ca^{2+} on RBC mechanics. A secondary aim was to assess the responsiveness of Ca^{2+}-treated RBC to physiological levels of mechanical shear (≤10 Pa).

> Hypothesis: Ca^{2+} entering RBC would impair cell mechanics. Impairments would be mediated by decreased cell volume and rigidification of the cell membrane. Entry of Ca^{2+} would primarily occur during mechanical shear due to the presence of mechanically-activated cation channels in the RBC membrane. Ca^{2+}-loaded RBC would be more susceptible to future impairments of their biophysical properties.

Study 3: The aim of the third study was to experimentally characterise the function and expression of the mechanically-sensitive cation channel Piezo1 across RBC populations of varying physiological age. A secondary aim was to assess whether activation of Piezo1 in aged RBC would contribute to their eventual removal from circulation.

> Hypothesis 1: Aged RBC would be less deformable and exhibit increased sensitivity to mechanical shear exposure, in particular when sheared in presence of extracellular Ca^{2+}.

Hypothesis 2: 'Old' RBC would contain increased free Ca^{2+} when compared with their physiologically 'younger' counterparts and also exhibit increased sensitivity to Piezo1-induced entry of Ca^{2+}.

Hypothesis 3: The accumulation of intracellular Ca^{2+} following prolonged stimulation of Piezo1 would overpower the Ca^{2+}-extrusion capacity of physiologically-aged RBC and lead to impaired cell mechanics.

Study 4: The aim of the fourth study was to assess whether normal levels of RBC deformability were required for mechanical activation of endogenous NO-production *via* the RBC-NOS3. A secondary aim was to investigate whether Piezo1 was involved in translating mechanical cues into biochemical activation of RBC-NOS3 *via* raising $[Ca^{2+}]_i$.

Hypothesis 1: Cellular deformation of RBC when exposed to mechanical shear, would regulate mechanical activation of RBC-NOS3, and subsequent generation of NO.

Hypothesis 2: Piezo1 would contribute to the activation of RBC-NOS3, and thus production of endogenous RBC-NO, by facilitating entry of Ca^{2+} in response to mechanical shear.

Chapter 2

General methods

Chapter 2 provides an overview of general methods that were employed in the experimental works of the current dissertation. Specific methods pertaining to individual studies, however, are described in greater detail in the respective chapters. General methods include procurement of blood samples from volunteers and preparation of isolated RBC, which was required for each study presented herein.

2.1 Recruitment of participants and experimental designs

Participants were recruited to participate in the studies outlined herein primarily from a convenience population at Griffith University, unless otherwise specified. Given that the experimental studies comprising this dissertation were designed to investigate fundamental physiological responses of RBC, the aim of participant recruitment was to obtain RBC from a homogenous sample population. Thus, only male participants were recruited to minimise variability in the blood samples due to the hormonal differences observed between sexes [115]. Volunteers were healthy males aged 18-40 years and reportedly free from any chronic pathologies including metabolic, endocrine, haematological, or neurological disorders. Moreover, participants that reported medication use,

excessive alcohol consumption, smoking habits, ingestion of supplements, recreational drug use, or having provided a high-volume blood donation (i.e., 450 mL) within the past three months (*Appendix 1*; "Questionnaire") were not considered for participation in any experimental studies. Participation was limited to one low-volume blood donation (i.e., ≤20 mL) per experiment; where one study was comprised of multiple experiments on separate testing days, participants were permitted to donate blood for each experiment if they expressed interest in doing so. The benefits and risks associated with participation were explained to the participant prior to any procedures in detail. Upon approval by the participant, witnessed consent was obtained. The experimental procedures described in the present dissertation are in accordance with the Code of Ethics of the World Medical Association (Declaration of Helsinki). All protocols were also reviewed and subsequently approved by the Griffith University Human Research Ethics Committee (Reference Numbers 2016/712, 2020/111).

2.2 Blood sample collection

Blood collection and handling of blood samples was performed under close adherence to the guidelines for haemorheological laboratory techniques [116]. A certified phlebotomist collected all blood samples. Firstly, a tourniquet was placed tightly around the upper arm of the participant. A syringe with a sterile

21-gauge needle attached was used to puncture a prominent vein in the antecubital region of the arm within 90 s of the tourniquet being tightened. Alternatively, a winged infusion set with a sterile 21-gauge needle was used when multiple blood tubes (more than 10 mL) of sample were collected. Collection tubes coated with anticoagulant (typically ethylenediaminetetraacetic acid, unless otherwise specified) were prepared and the blood sample was transferred into the collection tubes immediately. Clot formation was successfully prevented using this collection technique. The collection tubes were then inverted several times to ensure adequate mixing of the blood sample with the anticoagulant. Thereafter, blood samples were kept on a slowly rotating mixer which provided sufficient distribution within the tube and prevented sedimentation of blood cells prior to experiments. All experiments were performed within 4 h of blood collection to minimise the effects of *ex vivo* blood ageing unless blood was processed otherwise as indicated in the respective experimental chapters. Washing procedures (unless indicated otherwise) were performed using phosphate buffered saline solution (PBS), which was prepared to the standard of pH = 7.4 ± 0.5; osmolality = 290 ± 5 $mOsm \cdot kg^{-1}$. Washing procedures were carried out by diluting RBC at least ten-fold to achieve sufficient dilution of potential contaminants.

2.3 List of chemicals

Sodium chloride	Sigma Aldrich, Australia
Potassium chloride	Sigma Aldrich, Australia
Sodium phosphate dibasic	Sigma Aldrich, Australia
Potassium phosphate monobasic	Sigma Aldrich, Australia
Sodium hydroxide	Sigma Aldrich, Australia
Hydrochloric acid	Sigma Aldrich, Australia
Polyvinylpyrrolidone 360 kDa	Sigma Aldrich, Australia
D(+)-glucose monohydrate	Merck Millipore, Australia
Magnesium chloride	Sigma Aldrich, Australia
Calcium dichloride	Sigma Aldrich, Australia
N-(2-Hydroxyethyl)piperazine-N'-(2-ethanesulfonic acid); HEPES	Sigma Aldrich, Australia
Tris(hydroxymethyl)aminomethane	Merck Millipore, Australia
Paraformaldehyde	Merck Millipore, Australia
Bovine serum albumin	Sigma Aldrich, Australia
Fluo-4 acetoxymethyl ester	Thermo Fisher Scientific, Australia
Trypsin from porcine pancreas	Merck Millipore, Australia
Methanol	Sigma Aldrich, Australia
Hydrogen peroxide 30%	Merck Millipore, Australia

Polyclonal anti-phospho eNOS Rabbit antibody (Ser1177)	Cell Signaling, USA
Polyclonal anti-phospho eNOS Rabbit antibody (Ser1177)	Merck Millipore, Australia
Skim milk powder	Woolworths Supermarkets, Australia
Goat Anti-Rabbit Biotinylated Immunoglobulins	Dako, Denmark
Goat anti-rabbit cross-adsorbed Alexa Fluor 568	Thermo Fisher Scientific, Australia
Normal goat serum	Sigma Aldrich, Australia
Tween® 20 polysorbate	Merck Millipore, Australia
Horseradish peroxidase	Merck Millipore, Australia
3,3'-diaminobenzidine	Sigma Aldrich, Australia
Glucose oxidase from aspergillus niger	Sigma Aldrich, Australia
Streptavidin-horseradish peroxidase	Abcam, Australia
Ethanol undenatured 100%	Chem-supply, Australia
Xylenes	Sigma Aldrich, Australia
Entellan®	Merck Millipore, Australia
4,5-Dihydroxy-1,3-benzenedisulfonic acid disodium salt	Sigma Aldrich, Australia
Phenazine methosulfate	Sigma Aldrich, Australia

Glutaraldehyde Grade, 50% in H_2O	Sigma Aldrich, Australia
Ionophore A23187	Sigma Aldrich, Australia
Dimethyl sulfoxide	Sigma Aldrich, Australia
Sodium carbonate	Chem-supply, Australia
N,*N*,*N*′,*N*′-Tetramethylazodicarboxamide, 'Diamide'	Sigma Aldrich, Australia
Diaminofluorescein-FM diacetate	Sigma Aldrich, Australia
Insulin from bovine pancreas	Sigma Aldrich, Australia
Wortmannin	Sigma Aldrich, Australia
Yoda1	Sigma Aldrich, Australia
Peptide GsMTx4	Abcam, Australia
Nω-Nitro-L-arginine methyl ester hydrochloride	Sigma Aldrich, Australia
Percoll®	Sigma Aldrich, Australia

2.4 Application of well-controlled mechanical shear using a Couette-type shearing apparatus

Given the focus of the present body of work on the transduction of *mechanical stimuli* into cellular events, it was absolutely essential to have a precise, well-controlled, and quantifiable method of applying mechanical force onto blood. In the experimental studies described herein, the method of choice was the use of a

commercially-available Couette-type ektacytometer (LORCA MaxSis, RR Mechatronics, de Hoorn, The Netherlands). The intended use of this instrument is the quantification of RBC deformability, which requires RBC to be diluted at a low concentration (0.005 $L \cdot L^{-1}$) in a highly viscous, isotonic solution of polyvinylpyrrolidone (PVP 360 kDa; 30 ± 0.5 mPa·s, 290 ± 5 mOsm, pH 7.4 ± 0.05). This solution was prepared in-house by first preparing a solution of PVP in distilled water at a concentration of 5% $w \cdot v^{-1}$. Following dissolution of the PVP component, sodium chloride (140 $mmol \cdot L^{-1}$), potassium chloride (2.7 $mmol \cdot L^{-1}$), disodium phosphate (10 $mmol \cdot L^{-1}$), and monopotassium phosphate (1.8 $mmol \cdot L^{-1}$) were added to increase tonicity and provide buffering capacity. Viscosity of the buffered PVP solution was tested at shear rates of 750 and 1500 s^{-1} using a rotational cone-and-plate viscometer (DV-II+Pro, Brookfield Engineering Labs, Middleboro, MA) equipped with a CPA-40z spindle operated at 37°C. If required, viscosity was adjusted by either dissolving additional PVP or adding distilled water. Once the viscosity of the PVP solution was within 30 ± 0.5 mPa·s, osmolality was measured using a freezing-point depression osmometer (Model 3MO Plus, Advanced Instruments LLC, Norwood, USA). If required, osmolality was adjusted by either dissolving additional NaCl or adding distilled water. Once the osmolality of the PVP solution was within 290 ± 5 mOsm, pH was measured using a benchtop pH-meter (Model pH 209, Hanna Instruments, Woonsocket, USA). If required, pH was adjusted by either adding hydrochloric acid or sodium hydroxide. Once the pH of the PVP solution was within 7.4 ± 0.05,

both viscosity and osmolality were confirmed to be within accepted ranges once more, prior to a final confirmation measurement of pH.

The viscosity of native blood is dynamic; that is, it depends on the shear rate applied onto blood, which would complicate quantification of the shear stress RBC are exposed to. By diluting RBC at this low concentration, the RBC-PVP dilution becomes quasi-Newtonian, irrespective of the mechanical properties of RBC, thus enabling precise calculation of the applied shear stress. The geometry of the shearing system comprises a stationary inner bob, separated from a rotatable cup by a gap of 300 μm. A given sample of fluid is suspended in the gap between the bob and the cup; rotation of the cup under the precise control of a step-motor allows for the generation of laminar Couette flow in the gap (Fig. 7).

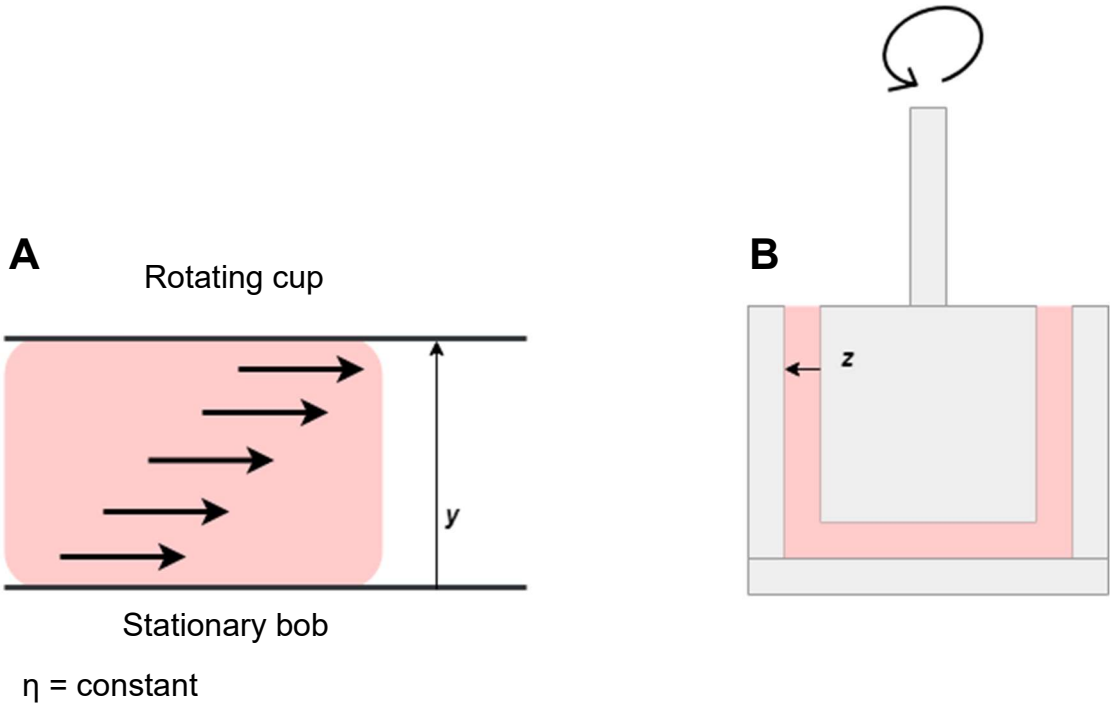

***Fig. 7**: Fluid dynamics of the Couette shearing system employed to generate a well-controlled, laminar shear field for the purposes of mechanical stimulation of blood or isolated red blood cells in shearing media [117]. The moving plane (the rotating cup) with known velocity (v) generates a shear field in the gap between itself and the stationary plane (the non-rotating bob), wherein fluid shear stresses are equal across the gap (y).*

The resultant shear forces in the flow field are constant across the gap, irrespective of the distance from either wall, thus facilitating the application of a precisely-controllable shear stress, provided shear rate and medium viscosity are known entities (Eq. 1).

$$\tau \text{ (shear stress)} = \gamma \text{ (shear rate)} \times \eta \text{ (apparent viscosity)} \quad (1)$$

Shear rate can be determined using the geometry of the shear apparatus and the rotational velocity of the moving plane (i.e., the cup) as follows [118]:

$$\gamma\ (\text{shear rate}) = 2 \times \frac{2\pi}{60} \times \frac{r_1 \times r_2}{r_2^2 - r_1^2} \times V_r \qquad (2)$$

where r_1 and r_2 reflect the radii of the inner (r_1) and outer (r_2) cylinder and V_r is the rotational velocity of the outer cylinder. Mechanical force, expressed and quantified as shear stress, was thus applied to RBC that were diluted in isotonic PVP (e.g., in *Study 2*).

Given the dynamic viscosity of blood, achieving accurate shear stresses when shearing whole blood rather than RBC-PVP suspensions requires that shear rate-specific viscosities of individual blood donors are known. For example, whole blood required to be sheared in the optimisation studies for detection of phosphorylated RBC-NOS3 (Chapter 2.5), and in *Study 4*. To this end, shear stress was calculated using Eq. 1, wherein the blood viscosity was measured on each individual day of experiments. Blood viscosity of an individual blood sample was measured across a wide range of shear rates between 75-1500 s^{-1} (example shown in Fig. 8). Using a non-linear curve-fit, blood viscosity values were interpolated across this range of shears (Fig. 8). Finally, the shear rate required to induce a specific shear stress onto the whole blood sample was determined under

consideration of the shear rate-specific viscosity of the individual sample using Eq. 2.

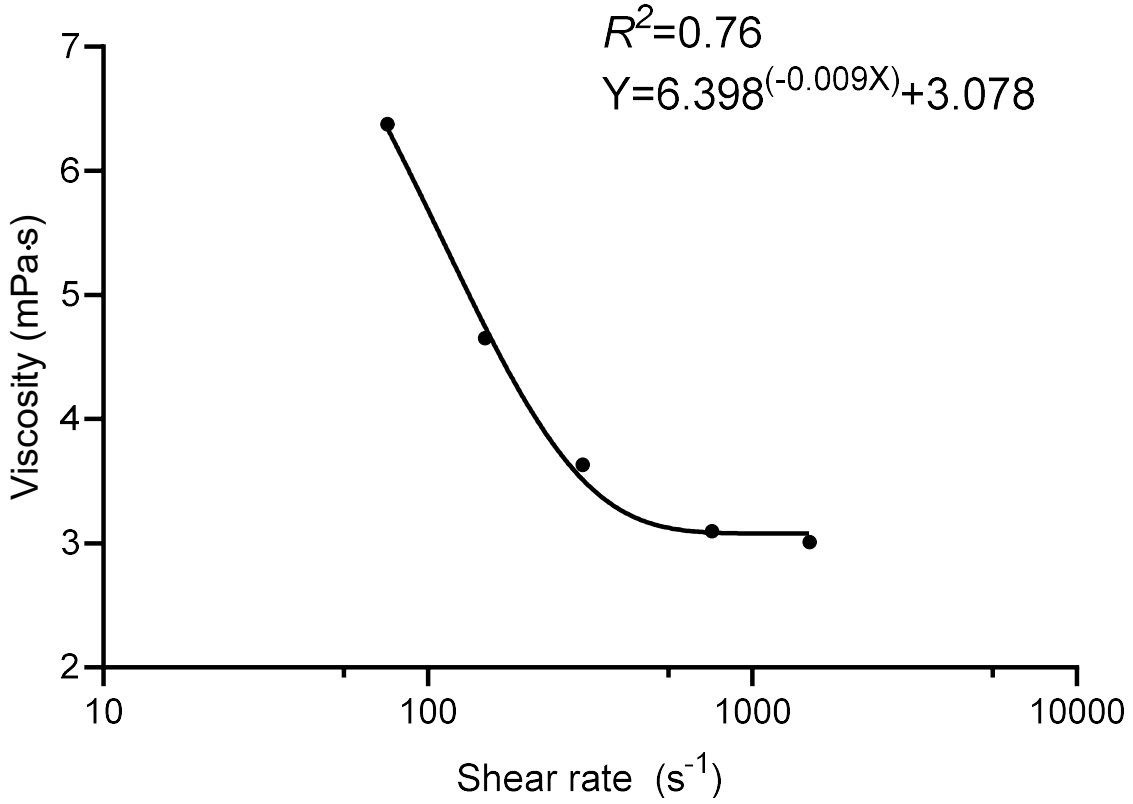

***Fig. 8**: A representation of a typical blood viscosity measurement using a sample obtained from a healthy male. Blood viscosity was assessed across an increasing range of shear rates between 75 and 1500 s^{-1}. These representative data is pooled from 15 healthy volunteers and was analysed using a non-linear curve-fit to interpolate between data points.*

2.5 Development of an immunofluorescent protocol to detect phosphorylated erythrocyte nitric oxide synthase

The existence of an active NOS isoform in RBC was debated in the literature for several years by a number of research groups [77, 119]. The landmark publication by Kleinbongard and colleagues [78] finally provided convincing evidence supporting the existence of a functionally-active NOS isoform in RBC using molecular and biophysical methods to detect the enzyme. That is, RBC-NOS3 was tagged with specific antibodies against NOS-3 or eNOS, while also employing cryo-electron force microscopy and freeze fracture coupled with immunogold labelling to detect the protein in both the cytosol and the inner leaflet of the lipid bilayer. The authors confirmed that the present isoform of NOS was resembling eNOS, given that they were able to retrieve a positive signal with application of primary antibodies against eNOS while no signal was observed using the same protocol with antibodies against neuronal NOS (NOS-1) or inducible NOS (NOS-2; [78]). Moreover, phosphorylated RBC-NOS3 could also be detected with a primary antibody raised against phosphorylated eNOS. Several subsequent investigations [39, 85, 120] employed the immunohistochemical method established by Kleinbongard et al. [78] to detect the phosphorylated serine^{1177} residue on RBC-NOS3, which is considered to reflect catalytic activity of the enzyme – as inferred from eNOS [121]. This immunohistochemical method involves fixation of fresh RBC in

paraformaldehyde (PFA); PFA was the fixative of choice given that aldehyde-based fixatives are known to preserve post-translational modifications and the most commonly used alternative, glutaraldehyde, is known to interfere with immunoreactivity and epitope retrieval [122]. Thereafter, chemically fixed RBC are transferred onto a microscope slide to yield a monolayer of cells that can be easily visualised (i.e., blood smear). Additional physical fixation is performed by applying heat to the blood smear to ensure that cells are not washed off the microscope slide. Ultimately, visualisation of immuno-tagged protein residue is facilitated by a colour change *via* a horseradish peroxidase detection system coupled with 3,3'-Diaminobenzidine. While this method was generally accepted, some technical details appear difficult to standardise (e.g., time until colour change occurs and the reaction is stopped, selection of cells given that cells appear grey under the microscope irrespective of colour change, low signal intensity). Thus, a secondary aim of the current dissertation was to establish an immunohistochemical protocol for the detection of phosphorylated ser^{1177} using a fluorescent detection system. The advantages of a fluorescence-based signal are i. reducing subjectivity in selecting cells (i.e., because cells that have not reacted with the fluorescent tag are not visible); ii. reducing error by decreasing the number of required steps; iii. increased standardisation of the background; iv. potential to amplify signal strength by modulating the laser intensity during detection. First, the HRP-DAB detection method was validated using the protocol described below. Sheared RBC were used as a positive control given that both

eNOS and RBC-NOS3 were shown to exhibit increased phosphorylation at ser^{1177} following exposure to shear [28, 121, 123], while unsheared RBC were used as the control condition. Shear conditioning of RBC was performed using whole blood, which was exposed to well-controlled shear stresses in a rotational ektacytometer (for a detailed description, refer to Chapter 2.4). Cells were fixed in PFA with a final concentration of 2% for 20 min at room temperature. Thereafter, cell suspensions were centrifuged gently at 300 × *g* to prevent cell lysis for 3 min. Following washing with double volume PBS, cell suspensions were incubated at room temperature for 5 min. Finally, cell suspensions were centrifuged again at 300 × *g* for 3 min and the supernatant was removed. The cell pellet was diluted 1:1 in PBS to yield a haematocrit which would facilitate formation of a cell monolayer, and blood smears were created on a microscope glass slide. The smears were left to dry overnight, following which they were heat fixed using a laboratory gas burner. The microscope slide with heat-fixed RBC was divided into two separate sections using a lipid pen to create a hydrophobic barrier between a large test area and a smaller control area (Fig. 9), thus providing an internal negative control to every individual slide. Incubations were carried out at room temperature unless otherwise specified.

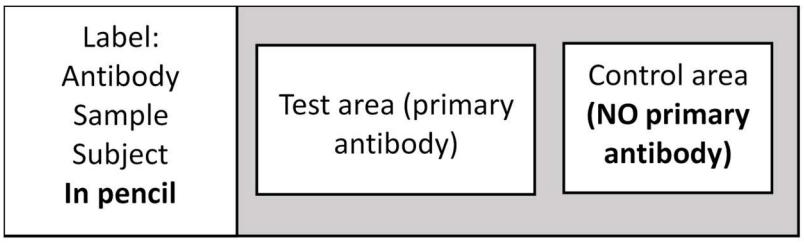

***Fig. 9**: Representation of typical microscope slide marked with clearly separated test and control area used for immunohistochemical analysis*

Both areas were washed with a tris-buffered saline solution (0.1 mol·L^{-1} TBS; pH = 7.6) and subsequently incubated with 0.1% Trypsin for 30 min at 37°C to permeabilise the cell membrane. Trypsin was inactivated with fluoride-enriched tap water, slides were washed with TBS and incubated with 2% hydrogen peroxide suspended in 80% methanol for 30 min to saturate endogenous peroxidases. Slides were washed once more with TBS and non-specific binding of the primary antibody was minimised by incubation with 3% skim milk powder diluted in TBS for 30 min. Rabbit primary antibody (anti-Phospho-eNOS^{Ser1177} diluted 1:150; Cell Signaling, Massachusetts, USA) was applied to the test area using a vehicle designed to further minimise non-specific binding and facilitate entry of antibodies (0.3% skim milk, 0.09% Tween® 20), while the control area was only treated with vehicle solution (i.e., no primary antibody). Slides were incubated for 60 min and subsequently washed carefully with TBS. Non-specific binding of the secondary antibody was minimised by incubation with 3% normal goat serum for 30 min, following which biotinylated goat anti-rabbit secondary antibody (Dako, Glostrup, Denmark) was applied to the slides

for 30 min. A streptavidin-horseradish peroxidase complex was used to tag the relevant site *via* incubation for 30 min, and 3,3'-diaminobenzidine (DAB) was used to develop the colour change (Fig. 10). Finally, the DAB was removed by extensive washing with TBS, and the slides were dehydrated in a series of alcohol solutions with increasing concentration. After removal of the hydrophobic pen residues and PFA through suspensions in Xylene, coverslips were mounted with mounting medium (Entellan®, Merck Pty Ltd., Bayswater, Australia). The slides were left to dry overnight, and light microscopy images were acquired at 400-fold magnification with an inverted high-resolution microscope (IX73, Olympus, Tokyo, Japan) coupled to a camera (optiMOS sCMOS, QImaging, Surrey, Australia).

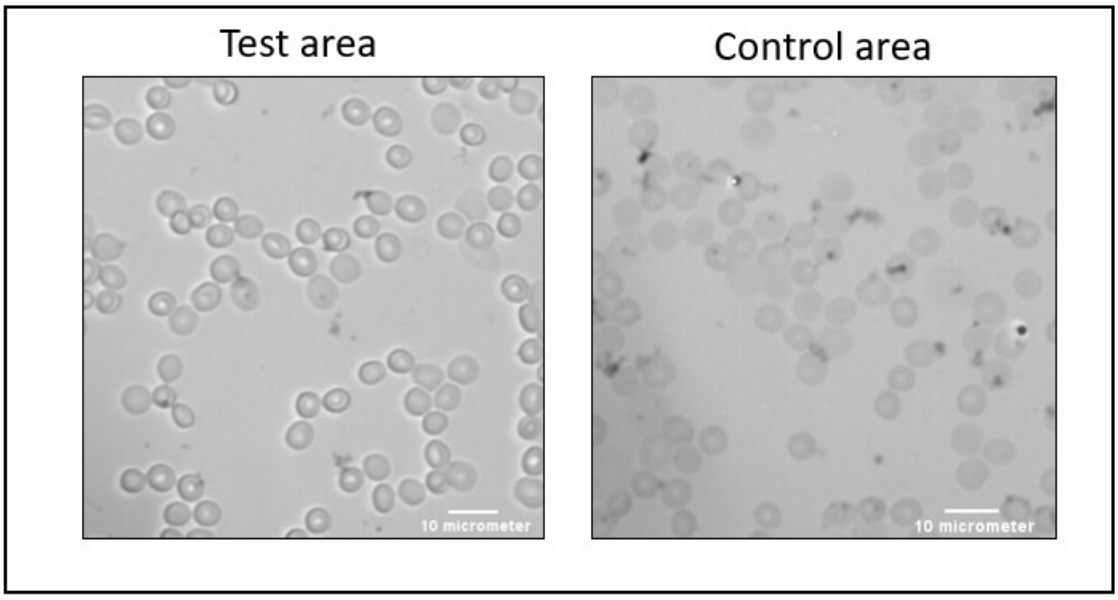

***Fig. 10**: Light microscopy micrographs of cells stained with diaminobenzidine. The test area contains primary antibody while the control area lacks primary antibody and serves to control for background staining caused by non-specific antibody binding*

Grey values of RBC randomly selected within both areas were determined using ImageJ software (FIJI package, National Institutes of Health, Bethesda, USA). The grey values of 100 individual cells were measured from three distinct fields of view on the test area, while grey values of 50 individual cells from two distinct fields of view in the control area were quantified. Moreover, the background grey intensity was assessed in three spaces within each field of view to correct the cell grey intensity for variations in background intensity. The final grey value corresponding to antibody bound to phosphorylated ser^{1177} of RBC-NOS3 (Fig. 11) was determined using the formula: Signal = (Test area background-Test area RBC) - (Control background-Control RBC).

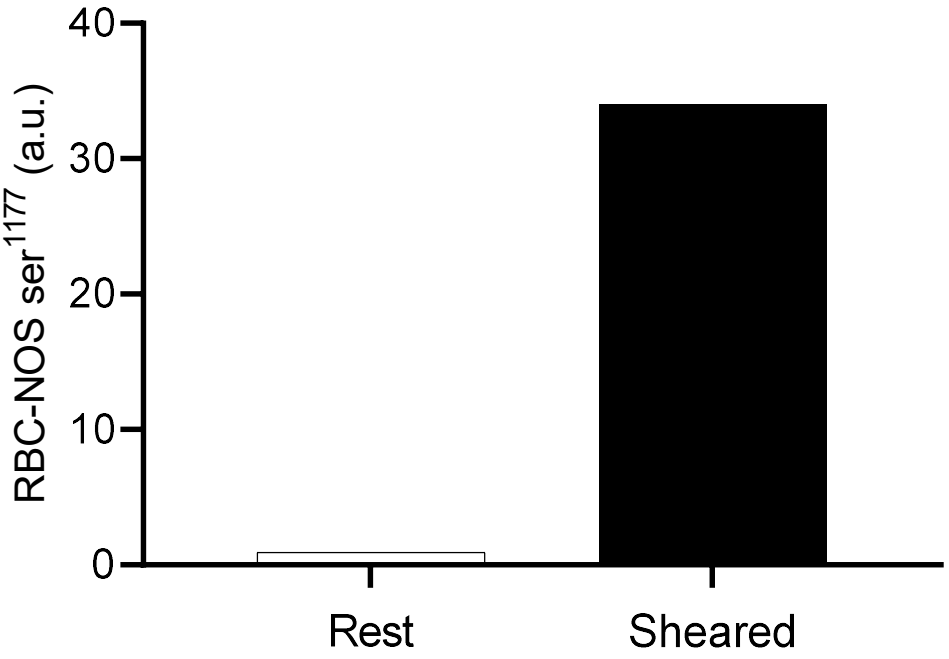

***Fig. 11**: Total signal of immunohistochemical staining of red blood cells (RBC) using diaminobenzidine. RBC were exposed to a shear conditioning protocol (10 Pa for 300s; "Sheared"); the signal is profoundly increased when compared with RBC that were not exposed to mechanical shear ("Rest"). N = 100 individual cells*

Given that an increase in HRP-derived phosphorylated ser^{1177} following exposure of RBC to shear was observed when compared with unsheared RBC, confirming previous findings [28], a protocol employing a secondary antibody conjugated to a fluorescent tag was developed. This novel protocol was based on the HRP-method, however, modified to optimise signal-to-noise ratio with the fluorescent detection method. The procedure of fixing RBC in 2% PFA prior to washing and producing blood smears was adopted. Similarly, the separation of test and control area followed by partial digestion of the membrane using 0.1% trypsin

was also identical. The colour change of DAB is initiated by reaction with hydrogen peroxide that is produced enzymatically by HRP. When using DAB-based detection, it is thus required to saturate the cells' antioxidant defence system, which acts to defuse hydrogen peroxide, *via* incubation with hydrogen peroxide in methanol. For the novel fluorescent approach, DAB was not used for detection, and this step was consequently omitted from the protocol. Non-specific binding was blocked with 3% skim milk followed by incubation with primary rabbit-raised antibody against phosphorylated RBC-NOS3 (anti-Phospho-eNOS^{Ser1177}; Cell Signalling, Massachusetts, USA) at 1:150 dilution in vehicle solution for 60 min. Excess primary antibody was washed off carefully with TBS. Non-specific binding of the secondary antibody was minimised by incubation with 3% normal goat serum. Goat-raised anti-rabbit secondary antibody conjugated to a fluorescent tag (Alexa Fluor 568, Thermo Fisher Scientific, Waltham USA) was applied for 30 min in the dark. This antibody was chosen specifically due to its peak emission (λ = 605 nm) not interfering with the spectrum of haemoglobin, which is overabundant in RBC and may cause fluorescent noise [124]. Unbound secondary antibody was removed by washing with TBS and the slides were dehydrated in a series of alcohol solutions with increasing concentrations. Finally, the slides were suspended in Xylene, and a coverslip was mounted with Entellan®. The mounted slides were left to dry over night while protected from light to prevent photobleaching of the fluorescent tag. The following day, images of RBC exposed to a laser (λ = 594 nm) were acquired

using an inverted microscope (IX73, Olympus, Tokyo, Japan) coupled to a camera (optiMOS sCMOS, QImaging, Surrey, Australia). Images were obtained from three randomly chosen areas within the test area and two randomly chosen areas within the control area (example shown in Fig. 12).

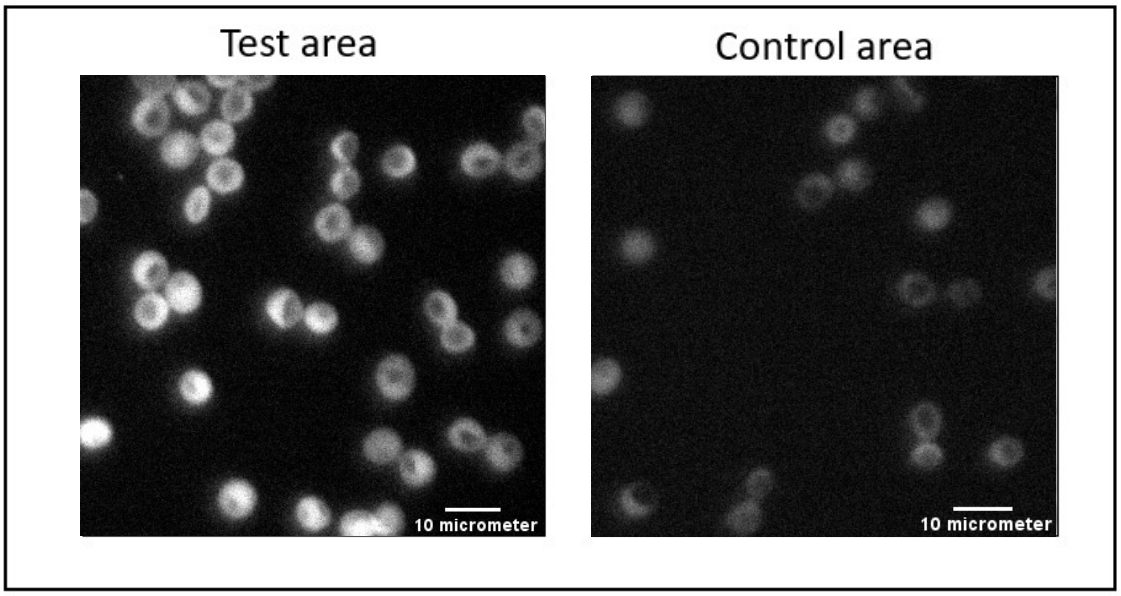

***Fig. 12**: Fluorescent microscopy micrographs of red blood cells stained with goat anti-rabbit secondary antibody coupled with a fluorescent tag. The test area contains primary antibody while control area lacks primary antibody and serves to control for background staining due to non-specific antibody binding*

ImageJ software (FIJI package, National Institutes of Health, Bethesda, USA) was then used to quantify the mean fluorescent intensity of individual RBC. The mean intensities of 100 RBC from the test area and 50 RBC from the control area were measured and the final signal was calculated from the formula: Signal = (Test RBC-Test area background) – (Control RBC-Control background).

The optical specificity of the antibody was assessed by quantifying bleeding into other wavelengths. A comparative trial was carried out to determine non-specific fluorescence emitted in the presence and absence of normal goat serum, which was used to minimise non-specific binding of the secondary antibody. It was observed that while fluorescent intensity was greatly increased in the Texas red (Txred) channel when compared to the Fluorescein isothiocyanate (FITC) channel, bleeding was observed. Application of 3% normal goat serum successfully decreased the signal in both channels (Fig. 13).

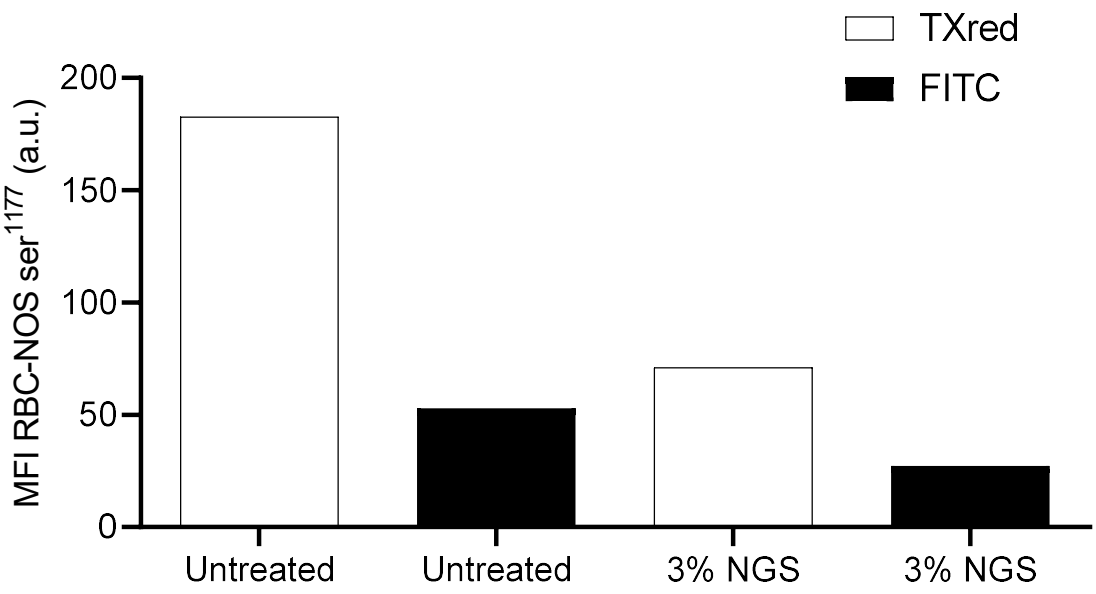

***Fig. 13**: Mean fluorescent intensity (MFI) reflecting phosphorylated serine[1177] of the erythrocyte-derived nitric oxide synthase (RBC-NOS3) exposed to light of different wavelengths (FITC: λ = 488 nm; TXred: λ = 595 nm) was decreased with the application of normal goat serum (NGS). N = 100 individual cells*

While application of 3% NGS resulted in a decrease of the final signal indicating that non-specific binding of the fluorescent-conjugated secondary antibody was

decreased, the signal on the test area was still abundant. Thus, it was concluded that non-specific binding still occurred, albeit to a lesser degree, and a trial was conducted to assess whether increasing the concentration of NGS to 6% would prompt a further decrease in non-specific binding, reflected by decreased signal in the control area.

It was observed that incubation with 6% NGS resulted in a decrease of fluorescent intensity in both test and control areas (Fig. 14). The final signal (i.e., difference between test and control area) was increased, while the absolute fluorescent intensity decreased, providing an improved signal-to-noise ratio.

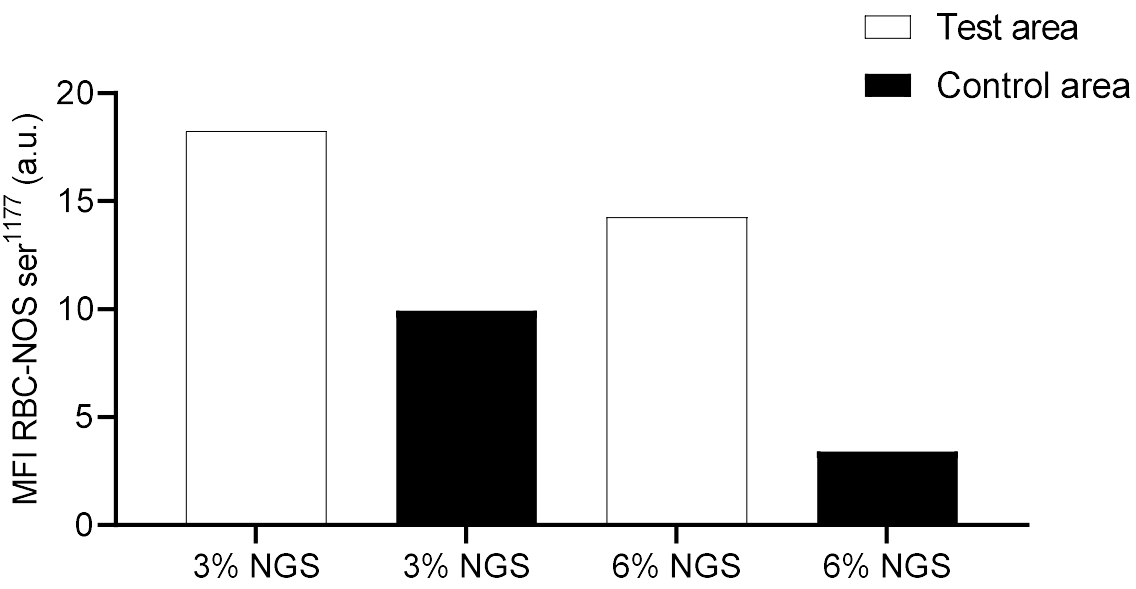

***Fig. 14**: Mean fluorescent intensity (MFI) reflecting phosphorylated serine[1177] of the erythrocyte-derived nitric oxide synthase isoform (RBC-NOS3) on test and control areas. Non-specific binding of secondary antibodies was minimised by incubation with normal goat serum (NGS); incubation with 6% NGS resulted in a decrease of fluorescent intensity compared to treatment with 3% NGS. N = 100 individual cells*

Finally, a validation trial was conducted to compare the HRP-based and fluorescent methods of detecting phosphorylated ser^{1177} of RBC-NOS3. Total RBC-NOS3 content was assessed using a primary rabbit-raised antibody against eNOS (NOS-3; Cell Signaling, Massachusetts, USA) employed within the same optimised protocols. Sheared and unsheared phosphorylated ser^{1177} were also measured using both the HRP and fluorescence method. Close associations between the final signal of both total RBC-NOS3 and phosphorylated ser^{1177} were observed between HRP and fluorescence methods (Fig. 15). Exposure to shear increased the signal when compared with unsheared RBC.

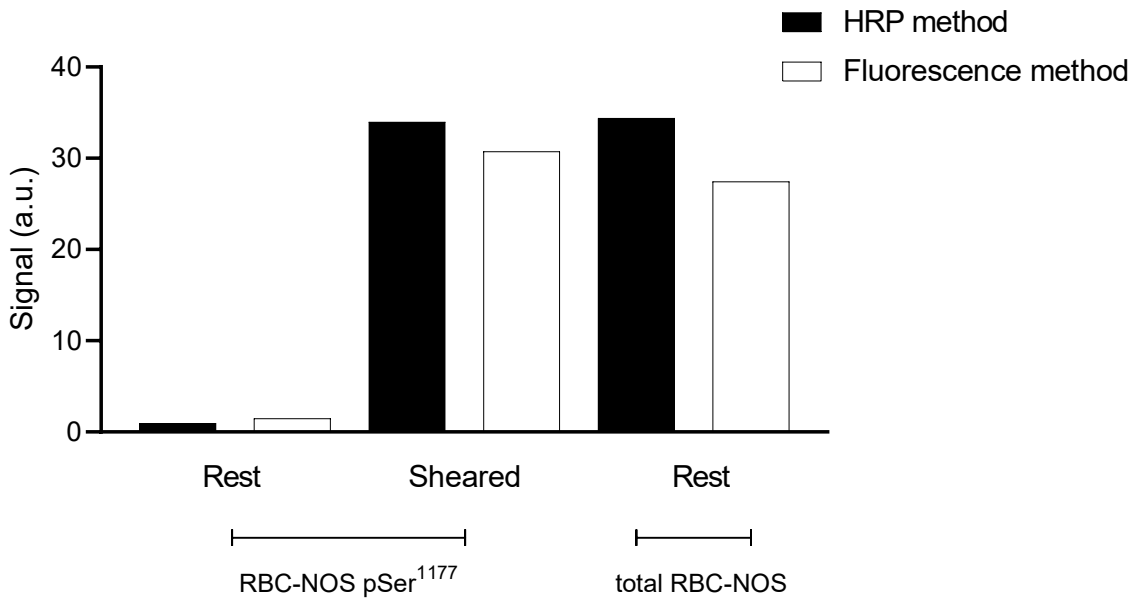

***Fig. 15**: Signal intensity reflecting total content of erythrocyte-derived nitric oxide synthase (RBC-NOS3) and RBC-NOS3 with phosphorylated serine^{1177} was assessed using both the HRP-based method (black bars) and the novel fluorescent method (white bars). Shear exposure increased the signal as measured by both methods and close association was observed between the two methods. N = 100 individual cells*

Increasing the concentration of NGS to 6% $v \cdot v^{-1}$ to minimise non-specific binding of the goat-derived anti-rabbit secondary antibody was found to be effective. Given that non-specific fluorescence was still observed on the control area, several blocking approaches targeting the primary rabbit-derived antibody were tested. Moreover, air-drying the slides following dehydration was compared to immediate wet-mounting, both using Entellan® purpose mounting medium (Merck Pty Ltd, Bayswater, Australia) to optimise the signal-to-noise ratio of the assay. Specifically, non-specific binding of the primary antibody was minimised using 3% skim milk powder as before or using 4% BSA. Traditionally, BSA is the preferred blocking agent when analysing phospho-proteins over milk powder due to the presence of phospho-proteins within skim milk (e.g., casein). In the current assay, however, skim milk was observed to produce less non-specific fluorescent signal when compared with bovine serum albumin (BSA; Fig. 16). The dry-mounting technique was also found to yield superior quality images, potentially due to decreased light refraction.

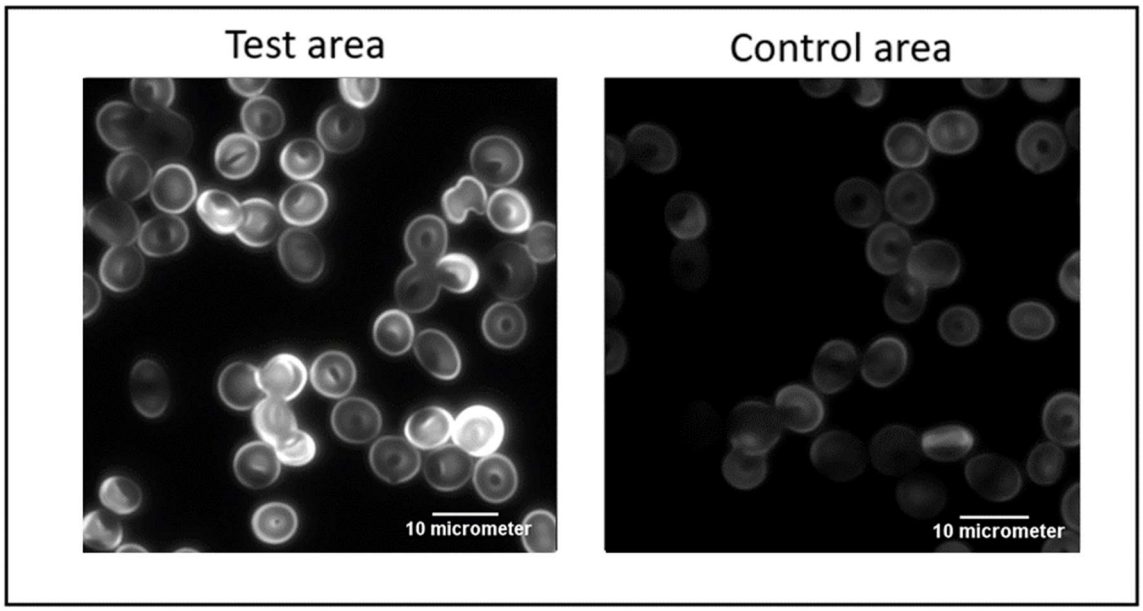

***Fig. 16**: Representative micrograph of red blood cells fluorescently labelled with rabbit-raised polyclonal antibodies against phosphorylated serine^{1177} endothelial nitric oxide synthase*

Given the close association between the novel fluorescence-based method described herein and the previously established HRP-based method for detection of RBC-NOS3, it was concluded that the novel method was suitable for the assessment of total content of RBC-NOS3 and phosphorylation at its active residue ser^{1177}. Following the optimisation of image quality using the novel fluorescent method, an automated image analysis pipeline was developed in ImageJ-software (FIJI release 1.53c, NIH, Maryland, USA). The image analysis code is provided (Appendix 2), with intermediate steps annotated below each line of code. Agreement of data obtained for a given image using both manual and automatic image analysis segmentation methods was assessed using linear regression analysis (Fig. 17; $R^2=0.95$).

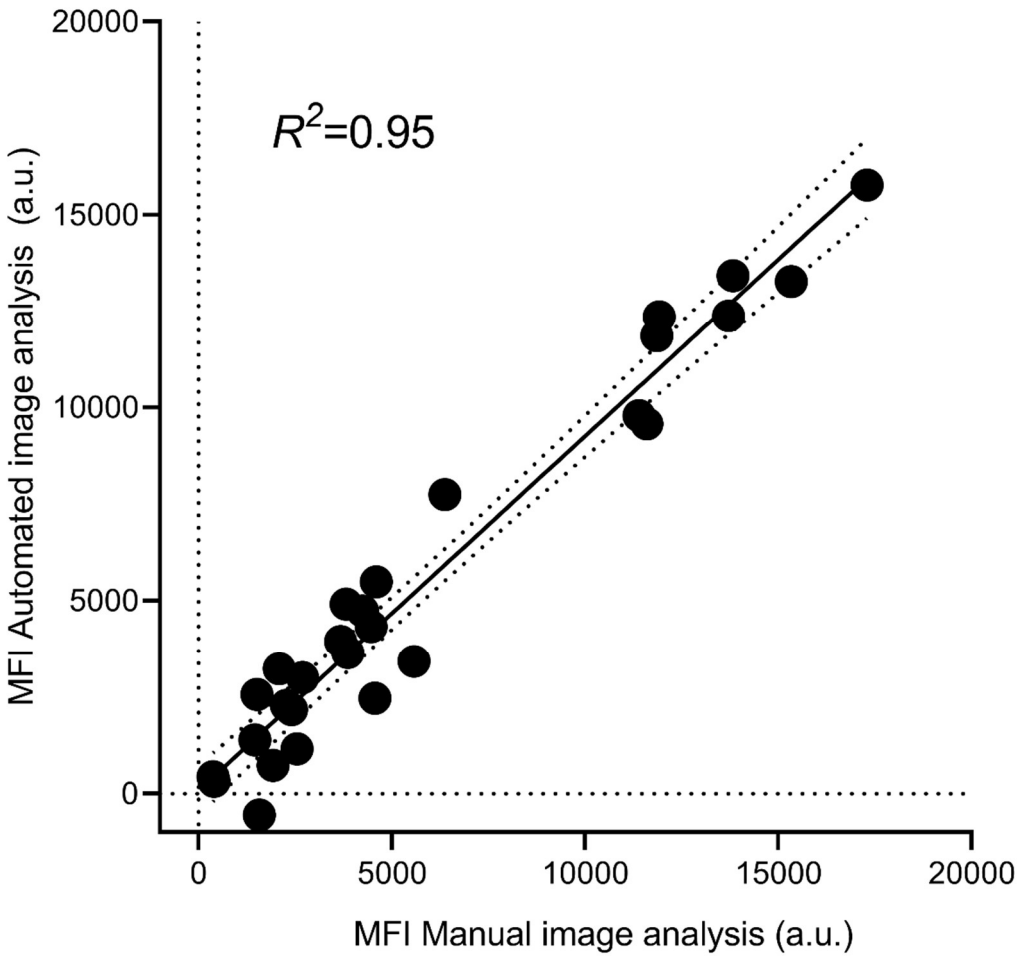

***Fig. 17**: Linear regression analysis to determine agreement between the newly developed automated image analysis (Y-axis) and the conventional manual image analysis method (X-axis). A total of 28 blood samples with mean fluorescent intensity (MFI) values ranging from 370 a.u.-17297 a.u., as determined by manual image analysis, were analysed using the newly-developed automated image analysis method for comparison.*

Moreover, to determine whether the automated image analysis method produced biased results (i.e., systematically over-, or underestimating values), the statistical analysis introduced by Bland and Altman [125] was used (Fig. 18). While acceptable spread of variability not exceeding the respective 95% CIs was observed, a bias of the automated method overestimating signal by 411 units was

also noted. Given that signals up to 17300 units are measured, the absolute magnitude of the bias was considered acceptable, and the automated method was adopted as standard operating procedure for image analysis to increase throughput and objectivity of the analysis.

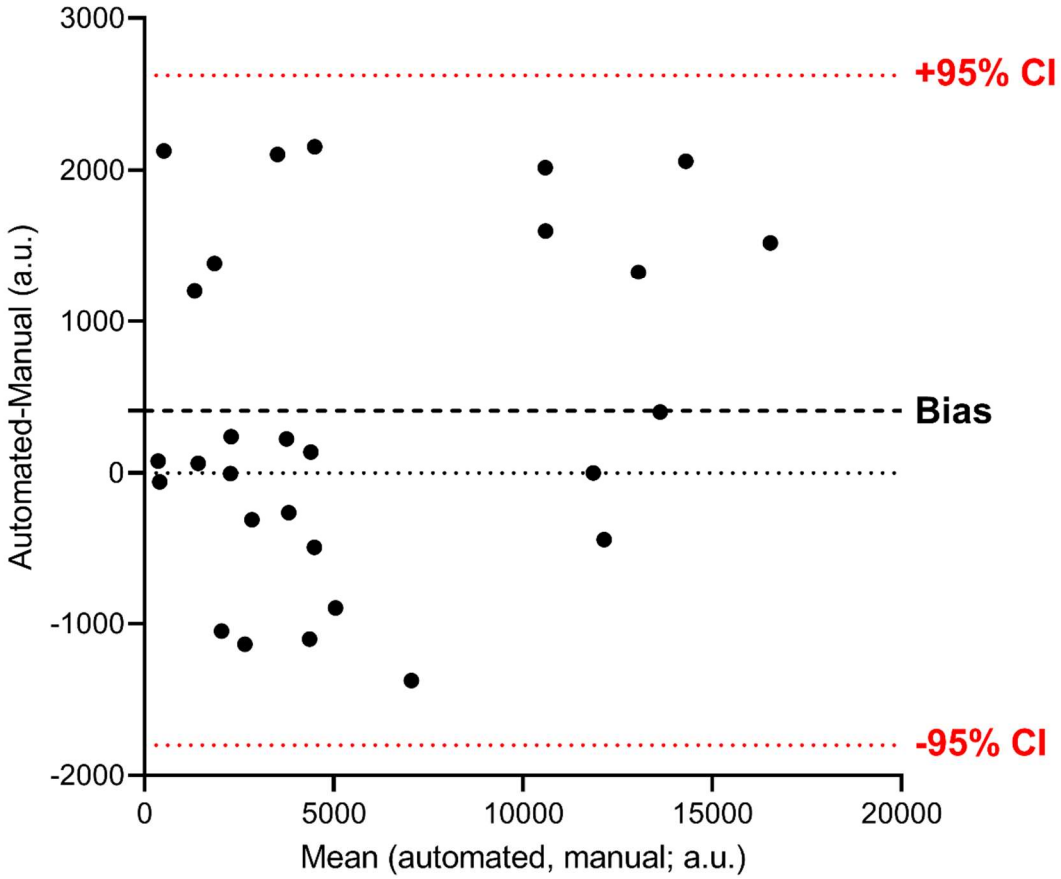

***Fig. 18**: Bland-Altman plot presenting the difference in signal obtained through manual and automated image analysis methods. In general, narrow 95% confidence intervals (CI) and a non-systematic pattern of random error reflect non-biased results.*

Chapter 3

Study 1: Impact of small fractions of abnormal erythrocytes on blood rheology

Lennart Kuck, Antony P. McNamee, Michael J. Simmonds

Chapter 3 contains works conducted as part of the present doctoral program and is presented in its peer-reviewed and published form. My contributions to this paper include concept and experimental design, data collection, data analysis and interpretation, manuscript development. All authors reviewed and approved the manuscript.

Reference: Kuck, L., McNamee, A. P., & Simmonds, M. J. (2022). Impact of small fractions of abnormal erythrocytes on blood rheology. *Microvascular Research*, *139*, 104261. PubMed ID: 34624306. DOI: 10.1016/j.mvr.2021.104261.

3.1 Preface

The physical properties of RBC are well-known to influence blood fluid properties (for a detailed explanation, please refer to Chapter 1). The RBC population present within blood, however, is inherently heterogenous, due to progressive *in vivo* ageing effects. The impact of shifts in the distribution of ageing cells, for example a larger fraction of 'old' RBC with unfavourable cell mechanics, is poorly described. Moreover, given the primary aim of the present body of work was to investigate acute regulation of RBC mechanics on a cellular level, it is of utmost importance to establish that altered cell properties have an impact on the tissue-level (i.e., on blood fluid behaviour). Thus, the following experiments were conceived to determine a threshold concentration where RBC with abnormal cellular mechanics would impact blood fluid properties.

3.2 Introduction

Blood is a two-phase suspension, consisting of cellular elements suspended in aqueous plasma. Given that the solid phase primarily (~99.9%) consists of red blood cells, the contribution of white blood cells and platelets to normal blood flow behaviour is minimal [51]; thus, the physical properties of RBC largely determine the dynamic fluid properties of blood. Blood is a shear-thinning fluid, where blood viscosity exhibits a non-linear and inverse relation with shear rate. The decreased viscosity is propagated by several physical processes: under low

flow or static conditions, viscosity is very high due to cell-cell structures that may exist in linear rouleaux or three-dimensional clusters, dramatically increasing the internal resistance to flow [6]. Upon exposure to increasing shear these "aggregates" of RBC disperse, before orientating and aligning with flow. The extent to which cells orientate and align is shear dependent, and once external forces reach a critical threshold, RBC progressively deform [126]; collectively, these physical processes each facilitate decreased local resistance to flow (and thus viscosity [51]).

Given that oxygen delivery is the primary function of RBC, and blood viscosity is a key determinant of bulk blood flow, blood viscosity is a primary parameter dictating oxygen transport to metabolically active tissues. Rigidified RBC, however, diminish the characteristic shear-thinning behaviour of blood [127] while also impairing perfusion of the microcirculation [128] – a phenotype observed in several clinical conditions [6, 48] including sickle cell anaemia [129], diabetes mellitus [59], haemochromatosis [130], and coronary artery disease [131]. Many of these conditions manifest population-wide alterations to cell integrity; for example, glycation and oxidative stress appear to broadly influence RBC properties in diabetes [132]. On the other hand, it is clear blood fluid properties may be affected by only a subset of the total RBC exhibiting abnormal properties (e.g., sickle cell disease). Whether a critical limit to normal blood flow behaviour in the presence of cells with impaired physical properties exists,

however, is poorly resolved, given the native RBC population itself is distinctly heterogenous, comprising sub-populations of varying physiological age [10], $[Ca^{2+}]_i$ [22], rheological attributes [23], and biochemical properties [86].

This heterogeneity is primarily due to circulating RBC being devoid of the ability to re-synthesise proteins [5] as a result of erythroblasts and reticulocytes ejecting cell organelles (nucleus and ribosomes) prior to maturation. This deficit is particularly relevant in RBC, given the continuous chemical stress (e.g., reactive oxygen species exposure *via* haemoglobin [133, 134]) and progressive mechanical degradation of these cells during circulation cannot be reversed by replacing damaged structures. Consequently, RBC function progressively declines *in vivo*, as cell age increases [26]. While the mechanism of RBC physiological aging is thought to involve accumulated oxidative damage [135], degradation of ion pumps [38], altered lipid distribution [136], or some combination of these factors, precise characterization remains elusive [137]. The sensitivity of blood flow behaviour towards mechanically impaired RBC, introduced for example through blood transfusion or in scenarios where a sub-population of native RBC becomes damaged, is yet to be elucidated.

Medical interventions that facilitate the introduction of mechanically impaired RBC subpopulations into whole blood are inherent to routine blood transfusion and mechanical circulatory support. Blood transfusion is one of the most common in-patient procedures performed in hospitals globally [138]. Blood

products may be stored under tightly regulated conditions for up to 42 days; however, negative metabolic and ionic alterations – termed 'storage lesions' (for a recent review, see [139]) – accumulate within days of extraction from the body [140, 141]. Blood storage precipitates impaired cell mechanics [86, 142, 143] and decreased ability to release oxygen [144], which are associated with complications following blood transfusion [138]. Introduction of a single unit of stored blood (~450 mL) into the circulation, which contains ~5,000 mL of blood, presents the human body with a significant challenge by causing inflammation [145] and requiring rapid turnover of removal-prone RBC [146, 147], precipitating adverse clinical outcomes. Moreover, it is known the high shears required for haemodynamic maintenance with mechanical circulatory support devices are damaging to RBC, causing increased membrane rigidification and altered rheological behaviour in subsequent low-shear (i.e., ≤5 Pa) flows [148-151]. It remains to be elucidated, however, whether the relatively low fraction of RBC that is damaged by the traverse of such devices is significant enough to disturb normal blood fluid properties.

Thus, the current study was designed to explore the fraction of abnormal RBC required to induce altered blood rheological behaviour by re-introducing RBC with well-defined abnormal rheological properties into the native cell population at concentrations that are reflective of clinical blood transfusions and mechanical circulatory support. Rigidification of autologous RBC was achieved through two

distinct mechanisms: i. intracellular accumulation of free radicals, which may induce oxidative stress; and ii. cross-linking of membrane and intracellular proteins. Intracellular free radicals were generated by incubation with phenazine methosulfate (PMS), which has well-described negative effects on RBC mechanics [76, 152, 153]. Cross-linking of RBC proteins was achieved by exposure to discrete concentrations of glutaraldehyde (GA; [154]). Moreover, given exposure to the supraphysiological (>20 Pa) mechanical shear forces present during the process of blood transfusion has been demonstrated to reduce RBC deformability [148], with mechanical sensitivity being improved post-transfusion [155], the susceptibility of mixed RBC populations to mechanical trauma was also investigated.

3.3 Materials and methods

3.3.1 Blood sample collection

Male participants with normal body mass index (18.5-24.9 $kg \cdot m^{-2}$) were recruited to participate in the current study. The inclusion criteria required absence of any cardiovascular, pulmonary, endocrine, or metabolic pathologies. It was also required that participants had not provided a large-volume blood donation (i.e., 450 mL) within the previous 90 days. Participants provided informed consent and blood was collected from a prominent vein in the antecubital region of the forearm. A tourniquet was applied prior to the blood draw, and the sample was

extracted within 90 s using a sterile 21-gauge needle and syringe. The obtained sample was immediately transferred into a vacuum-sealed tube coated with ethylenediaminetetraacetic acid (1.8 $mg \cdot mL^{-1}$). All procedures performed were reviewed and approved by the Human Research Ethics Committee of Griffith University and comply with the Declaration of Helsinki. The experiments were carried out within 6 h of retrieving the blood sample.

3.3.2 Sample preparation

RBC were isolated by centrifugation at 1500 × *g* for 10 min. Subsequently, isolated RBC were washed repeatedly with an isotonic, PBS solution (0.1 $mol \cdot L^{-1}$; pH = 7.42, 291 $mOsmol \cdot kg^{-1}$). Washed RBC were resuspended in PBS containing 0.1% BSA at a haematocrit of 0.4 $L \cdot L^{-1}$ and incubated with the respective agents at their final concentrations (i.e., glutaraldehyde, GA; phenazine methosulfate, PMS). All agents were sourced from Sigma (Sigma-Aldrich Pty Ltd, Castle Hill, NSW, Australia).

3.3.3 Experimental protocol

The results reported herein were obtained from successive experiments. The first experiment was designed to establish the relation between the respective treatments and resultant impairments in RBC deformability – akin to a titration step that would facilitate later experiments. Thereafter, the specific concentration

or exposure duration which induced an ~50% impairment in cellular deformability was determined *via* regression analyses. The second experiment was conducted to investigate the effects of introducing RBC with a 50% reduction in cellular deformability at increasing proportions into an untreated blood sample. These mixed populations were then exposed to supraphysiological shear stress for the determined duration (inducing a 50% reduction in cellular deformability) to determine their mechanical sensitivity.

3.3.4 Experiment One: Establishing the relations between chemical/mechanical treatment and alterations in red blood cell deformability

Washed, isolated and resuspended RBC were incubated with increasing doses of GA (0.001, 0.002, 0.005, 0.01%) for 30 min at room temperature or PMS (50, 75, 100, 150, 200 $\mu mol \cdot L^{-1}$) for 60 min at 37°C in PBS supplemented with BSA. Concurrent incubations of RBC in PBS/BSA served as control. The incubation conditions were based on previous reports on the effects of GA and PMS on RBC, which were confirmed during pilot testing. Following each treatment, RBC samples were washed and resuspended in a viscous PVP solution diluted in 0.1 $mol \cdot L^{-1}$ PBS (pH = 7.4 ± 0.5, 290 ± 5 $mOsmol \cdot kg^{-1}$, viscosity = 30 ± 0.5 mPa·s) at a haematocrit of 0.02 $L \cdot L^{-1}$ for deformability analysis. Moreover, control RBC in PVP were conditioned with a continuous shearing protocol (100 Pa for 0, 20, 30,

40, 60 s) prior to deformability analysis to determine the relation between shear stress exposure time and decreases in RBC deformability.

3.3.5 Experiment Two: Detecting the lower tolerance of abnormal RBC in a healthy cell population

A second experiment was performed to assess the effects of mixing abnormal RBC with an untreated cell population on blood fluid behaviour. The specific treatment protocol to induce ~50% impaired cell deformability (i.e., determined in "*Experiment One"*) was performed. Treated RBC were introduced into a sample of non-treated autologous RBC at progressively increasing concentrations (0, 1, 5, 25, 50, 100%). Note that RBC were kept at a normalised haematocrit of 0.4 $L \cdot L^{-1}$ following addition of treated cells, such that the sum of untreated RBC and treated RBC would make up 40% of total fluid volume in a given sample. Similarly, measures of viscosity, RBC deformability, and sensitivity to supraphysiological shear stress of these mixed populations were determined at normalised haematocrit (0.4 $L \cdot L^{-1}$).

3.3.6 Red blood cell deformability

A Couette-type ektacytometer (LORCA MaxSis, Mechatronics Instruments B.V., Zwaag, The Netherlands) was used to quantify cellular deformability at 37°C, the details of which have been discussed elsewhere [156]. Briefly, this coaxial system

consists of an outer cup rotating around a stationary inner bob. Suspensions of RBC were transferred into the gap between the cylinders (~300 μm), wherein they were exposed to a range of shear stresses (0.3-50 Pa). A laser was directed through the deforming RBC suspension, producing an increasingly elliptical diffraction pattern which was captured by a CCD video camera. An ellipse was fit to the resultant laser diffraction pattern, and the elongation index (EI) was calculated using length (a) and width (b) of the ellipse as follows: EI = (a - b)/(a + b). With increasing shear, the EI also increases as RBC populations deform.

3.3.7 Mechanical sensitivity of mixed population samples

The RBC suspensions investigated in the current study were exposed to 100 Pa shear stress for a duration determined to induce a 50% impairment in cellular deformability (i.e., determined in *Experiment 1*) to assess sensitivity to supraphysiological mechanical stress. The same Couette shearing device utilised for deformability assessment was employed to exert a precisely-controlled shear stress onto the cell suspensions.

3.3.8 Haematocrit adjustments and blood viscosity

Haematocrit of control and mixed population samples was determined using the microhematocrit method [157]; briefly, blood was drawn into a capillary glass tube, centrifuged at 12,000 × *g* for 5 min, and the volume of packed RBC relative

to plasma was determined. The haematocrit was then adjusted to 0.4 $L \cdot L^{-1}$ using autologous plasma. Viscosity of blood samples was determined over a ramped range of shear rates (75, 150, 300, 750, and 1500 s^{-1}) using a rotational cone and plate viscometer (DV-II+Pro, Brookfield Engineering Labs, Middleboro, MA) equipped with a CPA-40z spindle at 37°C. Blood was exposed to each shear rate for 30 s in a step-wise manner, and the stable torque value obtained during the last 5 s was recorded. Using the device-specific constant, shear rate-specific blood viscosities were calculated from the torque measurements.

3.3.9 Red blood cell aggregation of mixed populations

Total aggregation capacity and aggregate size of mixed GA-treated cell populations were investigated *via* high-resolution microscopy using an inverted microscope (IX73, Olympus, Tokyo, Japan) equipped with a high-speed camera (optiMOS sCMOS, QImaging, Surrey, Australia). Mixed and unmixed RBC populations were resuspended in autologous plasma at a haematocrit of 0.015 $L \cdot L^{-1}$, equilibrated to 37ºC, and subsequently transferred onto a microscope slide. An image was captured immediately at 200-times magnification to provide a 'disaggregated' image for qualitative comparisons. The RBC suspensions were then recorded at 600-times magnification for 4 min, and the visual aggregation index (VAI; Eq. 3) was determined every 10 s following the method of Chien et al. [158]:

$$VAI = \frac{Number\ of\ cells\ forming\ aggregates\ in\ the\ field\ of\ view}{Total\ number\ of\ cells\ in\ the\ field\ of\ view} \quad (3)$$

Following this period, another image of the now aggregated RBC was captured at 200-times magnification, which served to provide a larger field of view. The size of RBC aggregates was quantified by measuring the length of each rouleau present in this image. Videos and images were analysed in open-source ImageJ-software (FIJI distribution 1.53c [159], National Institutes of Health, Bethesda, MD, USA).

3.3.10 Data analysis

Raw EI-shear stress curves were parameterised using a non-linear version of the Lineweaver-Burk equation in accordance with Baskurt et al. [160] to extrapolate the maximal elongation (EI_{max}) and the shear stress required to achieve half-maximal elongation ($SS_{1/2}$); increased EI_{max} and decreased $SS_{1/2}$ are generally interpreted to reflect improved cellular deformability, and *vice versa*. The normalization of $SS_{1/2}$ to EI_{max} (i.e., $SS_{1/2}$:EI_{max} ratio) provides an accurate representation of cellular deformability and is thus used herein to reflect deformability of RBC populations. It is important to note that increased $SS_{1/2}$:EI_{max} values are interpreted as decreased RBC deformability (and *vice versa*), given that

samples exhibiting such values require increased shear stress to induce any given deformation, which is characteristic of less deformable RBC. Changes in the average deformability of a given RBC population were calculated as relative changes from the respective unmixed control RBC population (Eq. 4), with the unmixed control RBC sample serving as baseline (i.e., 0% change).

$$\Delta SS_{\frac{1}{2}}: EI_{max}\ (\%) = \frac{\left(\frac{SS_{\frac{1}{2}}n}{EI_{max}n}\right)}{\left(\frac{SS_{\frac{1}{2}}Con}{EI_{max}Con}\right)} \times 100 - 100 \quad (4)$$

Dose-response curves for GA- and PMS-treatments were analysed using linear regression. Shear-induced impairments in RBC deformability were analysed using a non-linear one-phase association equation, which is described in Chapter 3.4.

Elongation index-shear stress curves obtained post-shear exposure (100 Pa for 32 s, as determined in "*Experiment 1*") were subjected to non-linear curve-fitting under the exclusion of EI-values below 1 Pa. Previous observations have indicated abnormal RBC mechanical behaviour under low shear following supraphysiological shear exposure, resulting in a paradoxically increased EI at

shears below 1 Pa [148, 150, 161, 162]; thus, these data points were excluded from the curve-fit to obtain representative $SS_{1/2}$:EI_{max}.

3.3.11 Statistical analysis

Results are presented as mean ± standard error, unless stated otherwise. Commercial data processing software was used to conduct statistical analyses and curve-fitting procedures throughout (Prism, GraphPad Software Inc., Release 8.1.1, La Jolla, CA, USA). Standard assessments for the assumptions of parametric statistical analyses were performed to inform the appropriate tests. Parameterised indices of RBC deformability ($SS_{1/2}$:EI_{max}) were compared using one-way analysis of variance (ANOVA). Raw EI-SS data and comparisons between sheared and unsheared mixed RBC population samples was carried out using two-way ANOVAs. Viscosity profiles at specific shear rates across the experimental conditions were compared using one-way ANOVA. Post-hoc analyses of ANOVAs were carried out using Dunnett's multiple comparisons test to determine significant differences between the treatment groups and the control group. An alpha-level of 0.05 was employed to determine statistical significance. Stated *N*-values throughout refer to the number of independent experiments carried out, each using a distinct blood sample from a different donor; however, donors who provided a blood sample for *Experiment One*, which

served to inform the design for *Experiment Two* and was thus conducted independently, were not excluded from subsequent donation for *Experiment Two.*

3.4 Results

3.4.1 Glutaraldehyde exposure and cytosolic production of superoxide induce a linear concentration-dependent impairment in RBC deformability

Exposure of RBC to increasing concentrations of GA (0.001-0.01%) induced a concentration-dependent and linear impairment in cellular deformability (i.e., $SS_{1/2}$:EI_{max}; Fig. 19A). Plotting the increase in cell rigidity against the employed doses of GA yielded a linear relationship.

Similarly, inducing cytosolic generation of superoxide (O_2^-) by incubation with PMS also resulted in a linear concentration-dependent increase in $SS_{1/2}$:EI_{max} (Fig. 19B). Of note, it appears that the regression line obtained for RBC exposed to GA crosses the origin (i.e., 0% impairment in cellular deformability with 0% GA), while the regression line obtained for PMS-treated RBC crosses the x-axis at ~30 μM, indicating that impairments in cell deformability would not be observed when exposed to concentration of PMS lower than 30 μM.

3.4.2 Continuous exposure of RBC to supraphysiological shear induces a non-linear pattern of decreased cellular deformability

RBC exposed to continuous supraphysiological shear stress (i.e., 100 Pa) exhibited progressively decreased cellular deformability with increasing exposure duration. The impairment in RBC deformability, however, occurred in a non-linear manner (Fig. 19C).

The GA-dose required to impair RBC deformability by 50% [95% CI: 42-58%] was calculated to be 0.0036% by interpolating the linear relationship between GA-concentration and the associated increase in $SS_{1/2}$:EI_{max}. Using the linear relationship between PMS-concentration and increase in $SS_{1/2}$:EI_{max}, the dose required to induce a 50% [95% CI: 44-56%] reduction in cellular deformability was calculated to be 116 $\mu mol \cdot L^{-1}$. Finally, the duration of continuous shear stress exposure that would induce a 50% [95% CI: 40-60%] increase in $SS_{1/2}$:EI_{max} was calculated to be 32 s of 100 Pa.

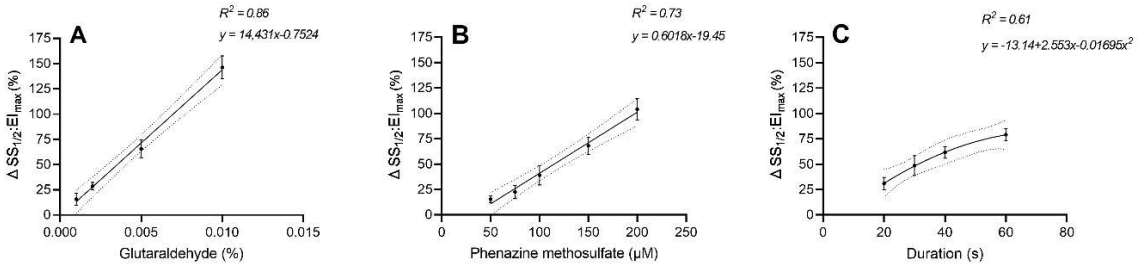

***Fig. 19**: The change in cellular deformability (expressed as a ratio of $SS_{1/2}$ to EI_{max}) was assessed in red blood cells (RBC) exposed to chemical rigidification of the cell membrane (via glutaraldehyde exposure; A), intracellular free radicals (via phenazine methosulfate exposure; B) or mechanical stress (100 Pa; C) of increasing degrees. A linear relationship was observed between impaired cell deformability (i.e., increased $SS_{1/2}$:EI_{max}) and increasing glutaraldehyde (R2 = 0.86) and phenazine methosulfate (R^2 = 0.73) concentrations, respectively. Exposure to increasing durations of mechanical shear, however, induced a non-linear increase in $SS_{1/2}$:EI_{max} (R^2 = 0.61). N = 7.*

3.4.3 The proportion of chemically rigidified RBC impacts the physical properties of mixed cell populations

Incubation of RBC with 0.036% GA or 116 µmol·L^{-1} PMS resulted in significant impairments in cell deformability. The elongation index (EI; reflective of the capacity of RBC to deform) in response to shears between 0.3-16.04 Pa was significantly decreased by both treatments when compared with untreated control RBC ($P < 0.05$; Fig. 20A). Note that the extent of impairment in GA- and PMS-treated RBC was remarkably similar, as demonstrated by their EI-shear stress curves being superimposable.

Progressively introducing increasing quantities of RBC exposed to either GA- or PMS-treatment into the untreated control cell population resulted in increasingly

impaired mean cell deformability when measured across the respective cell population, reflected by a stepwise increase in $SS_{1/2}$:EI_{max} (Fig. 20B, 20C).

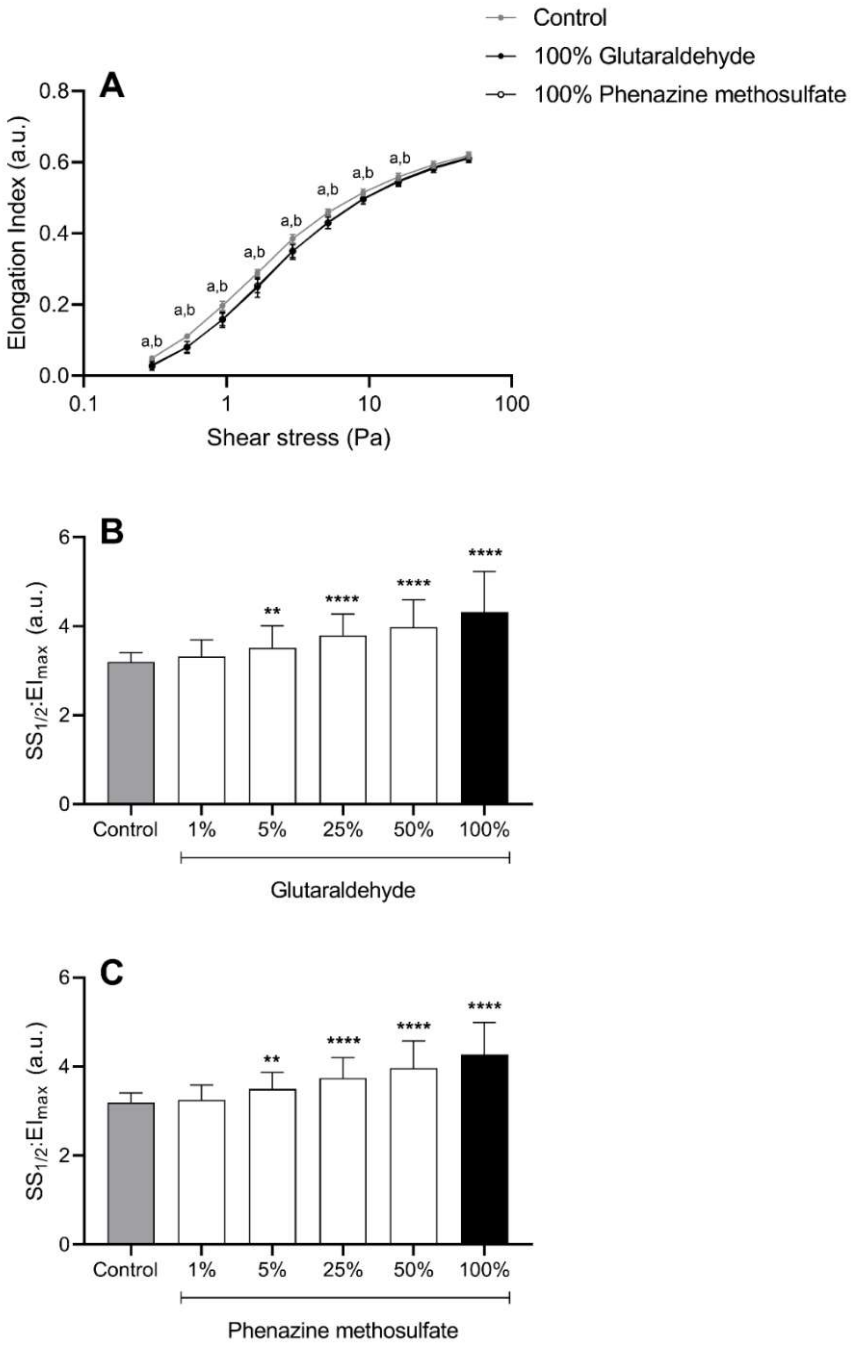

***Fig. 20**: Incubation of normal control cells with 0.036% glutaraldehyde (GA) or 116 µmol·L⁻¹ phenazine methosulfate (PMS) resulted in significantly impaired capacity of red blood cells (RBC) to deform in response to a range of shear stresses ($P < 0.05$; 0.3–16.04 Pa; A). Note that the curves of GA- and PMS-treated RBC are superimposed. Subsequently, RBC with impaired deformable capacity were progressively re-introduced into the control cell population, which precipitated decreased cellular deformability of the resultant mixed RBC population, reflected by increases in $SS_{1/2}$:EI_{max} (B; C). Data presented as mean ± standard deviation. [a]Significant differences between GA and control; [b]Significant differences between PMS and control. ****, $P < 0.0001$, **, $P < 0.01$ when compared with control. $N = 13$.*

3.4.4 Cross-linking of the cell membrane and intracellular oxidative stress precipitate near-identical impairments in deformability of the mixed red blood cell population

Mean rigidity (i.e., the average deformability of the RBC population) of mixed cell populations comprising GA- or PMS-treated RBC re-introduced into the untreated control cell population increased with increasing presence of rigid RBC (i.e., reflected by an increase in $SS_{1/2}$:EI_{max}) in a non-linear manner (Fig. 21). That is, presence of 1% rigidified RBC resulted in a 5.6 (PMS-treated RBC) and 11.5% (GA-treated) decrease in mixed population RBC deformability, respectively. Similarly, a concentration of 5% rigidified RBC resulted in an ~28% increase in rigidity, and presence of 25 or 50% rigidified sub-populations precipitated 52 and 71% increased rigidity, respectively.

While introduction of mechanically impaired RBC sub-populations resulted in non-linear increases in rigidity of the mixed cell population, no differences were observed between the rigidification treatments (i.e., exposure to GA or PMS) at 5-50% concentration.

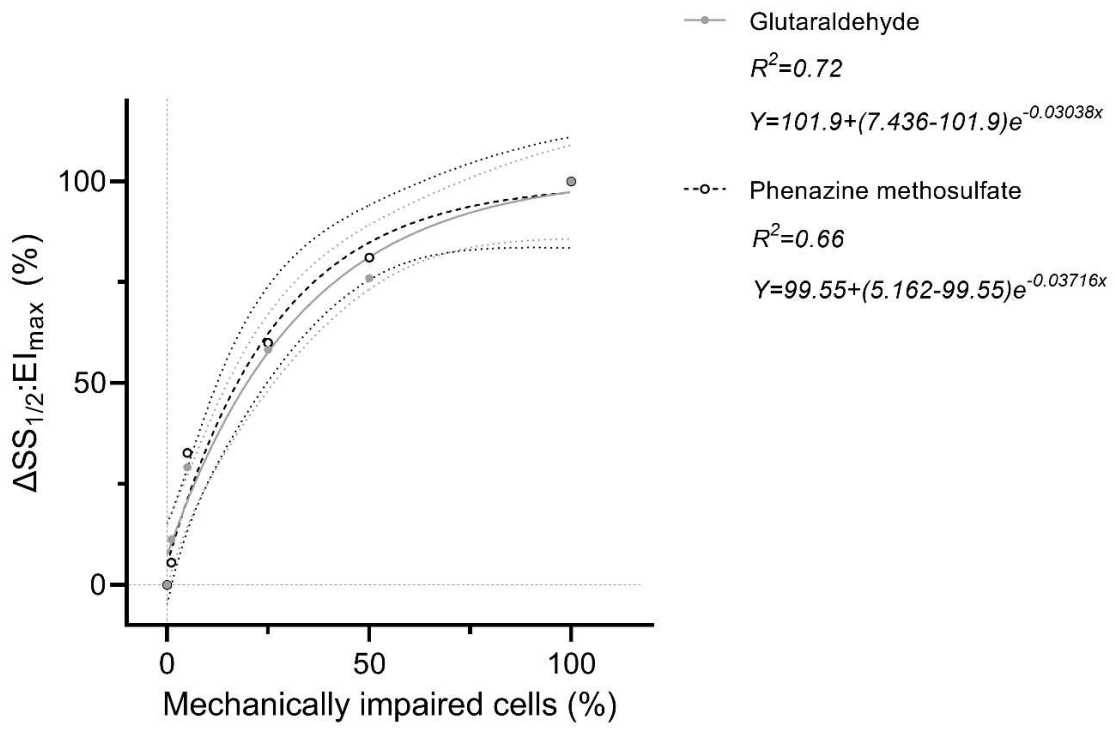

***Fig. 21**: Increased rigidity of the mixed cell population plotted against the concentration of abnormal red blood cells (RBC) re-introduced into the untreated control cell population. Non-linear curve-fitting of progressively increasing concentrations of rigidified sub-populations showed a disproportionate increase in $SS_{1/2}:EI_{max}$ ratio relative to untreated control cells (95% confidence intervals of the fit are plotted as dotted lines for glutaraldehyde in grey and phenazine methosulfate in black). N = 13.*

3.4.5 Sensitivity of RBC to supraphysiological shear stress is altered in presence of rigidified sub-populations

Red blood cell deformability following exposure to supraphysiological shear stress (100 Pa for 32 s) was impaired, reflected by a significant increase of $SS_{1/2}:EI_{max}$ (Fig. 22). In presence of rigidified sub-populations, $SS_{1/2}:EI_{max}$ ratio increased with increasing concentration of rigidified cells in a non-linear manner. Moreover, RBC samples containing a low percentage (1-5%) of sub-populations previously exposed to PMS exhibited more pronounced impairments of cellular

deformability when compared with samples containing GA-treated sub-populations. When present in higher concentrations (25-100%), however, samples containing GA-treated sub-populations resulted in more pronounced impairments of cellular deformability when compared with samples containing PMS-treated sub-populations.

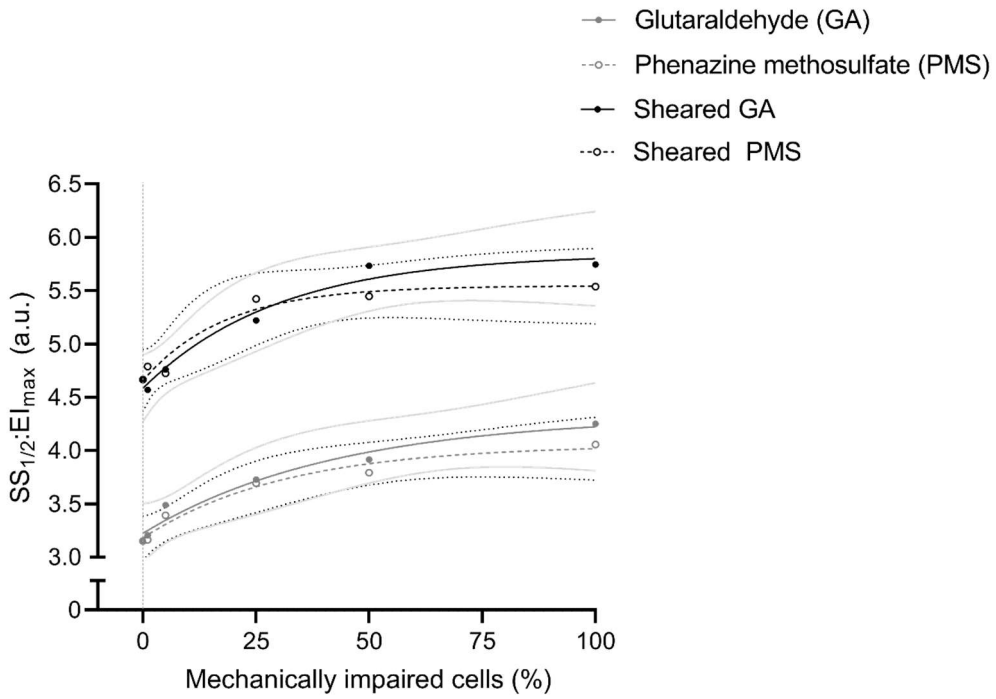

***Fig. 22**: Sensitivity of mixed red blood cell (RBC) populations to 100 Pa mechanical shear stress for 32 s. Changes in cellular deformability (i.e., $SS_{1/2}$:EI_{max} ratio) are presented with increasing proportions of cells rigidified via treatment with 0.036% glutaraldehyde (GA; closed circles) or 116 µmol·L^{-1} phenazine methosulfate (PMS; open circles) prior to (grey) and following (black) exposure to 100 Pa shear stress for 32 s. Mean data was fit with non-linear curve-fits and 95% confidence bounds of the respective fits are displayed for GA-treated (continuous lines) and PMS-treated (dotted lines) mixed RBC populations. Shear exposure statistically significantly elevated $SS_{1/2}$:EI_{max} irrespective of the fraction of mechanically impaired cells present, when compared with the matched unsheared sample. N = 8.*

3.4.6 Viscosity of mixed cell populations containing RBC treated with glutaraldehyde is altered due to impaired cellular deformability and aggregation

Whole blood viscosity of RBC suspensions containing 25% and 50% GA-treated sub-populations was significantly decreased compared with control when measured at 75 s^{-1} ($P < 0.05$ and $P < 0.01$, respectively; Fig. 23). While no changes in whole blood viscosity between control and mixed cell populations were observed at a shear rate of 150 s^{-1}, at 300 s^{-1}, viscosity of samples with 50% GA-treated RBC was significantly increased ($P < 0.05$). Moreover, viscosity of samples containing 5 ($P < 0.05$), 25 and 50% (both $P < 0.001$) GA-treated RBC was significantly increased at 750 s^{-1}. Viscosity of all samples containing GA-treated RBC was significantly elevated at 1500 s^{-1} when compared with the untreated control cell population ($P < 0.01$; Fig. 23).

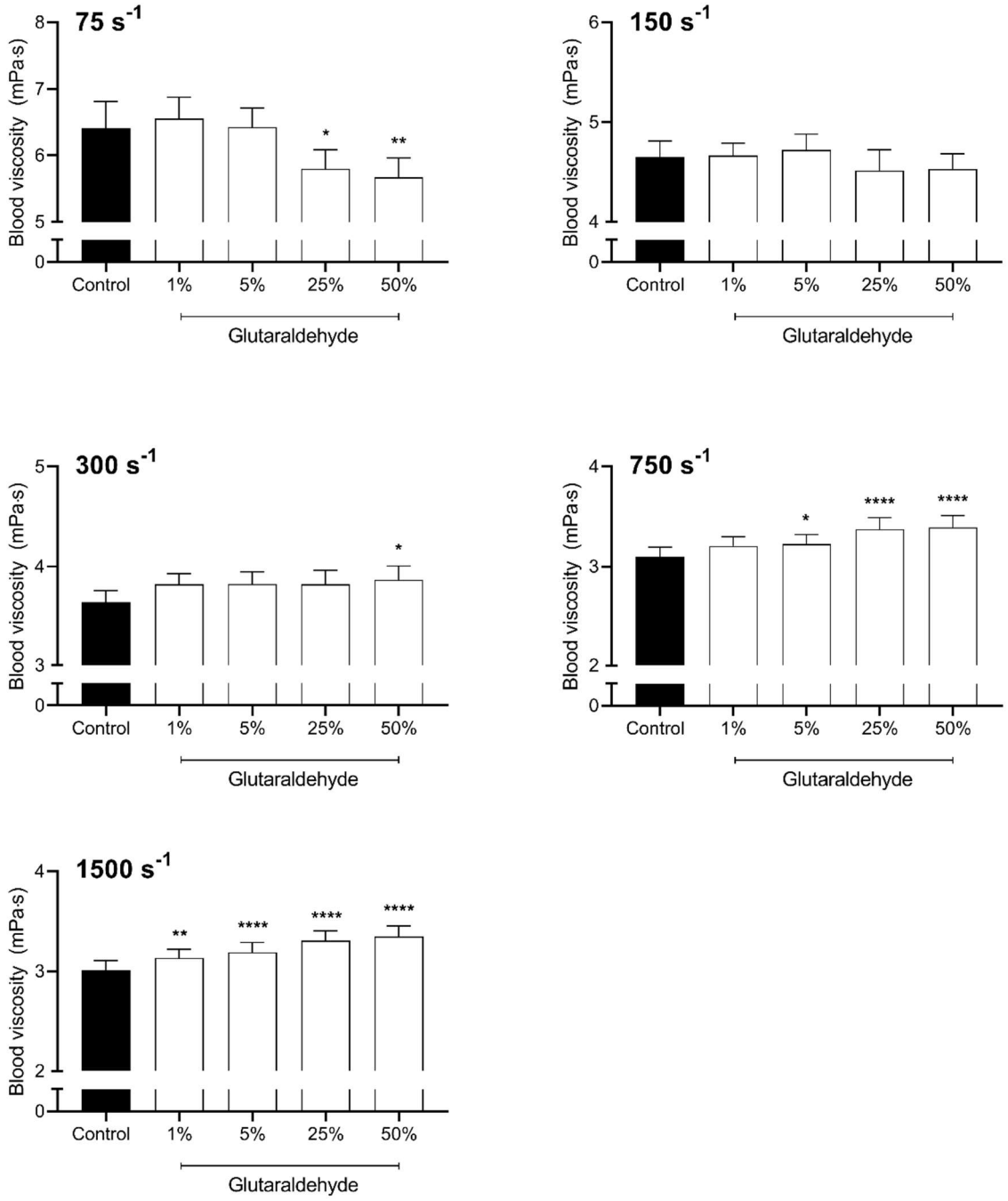

***Fig. 23**: Whole blood viscosity of samples with progressively increasing proportions of mechanically impaired red blood cells (RBC) present was quantified across a range of shear rates (75–1500 s^{-1}). Mixed cell populations were produced by re-introducing 1, 5, 25, or 50% RBC previously treated with 0.036% glutaraldehyde into a sample of untreated control cells. ***P < 0.001, **P < 0.01, *P < 0.05 compared to 'Control'; data were compared using One-Way analysis of variance. N = 14.*

Untreated control RBC populations showed a tendency to aggregate quickly within the first 30 s following transfer onto the microscope slide, while mixed populations containing 5% GA-treated cells required ~60 s to achieve a similar fraction of cells engaged in aggregate formation (Fig. 24I). The final VAI following 270 s of time allowed for aggregation was 0.92 for untreated RBC populations and 0.86 for suspensions containing 5% GA-treated cells, respectively. Mixed RBC populations with 25 and 50% GA-treated cells, however, exhibited a slower, more steady tendency to engage in aggregate formation. Moreover, the final VAIs of these mixed RBC populations were 0.68 (25% GA-treated RBC) and 0.53 (50% GA-treated RBC), indicating that only 68% and 53% of cells in the field of view were engaged in an aggregate after 270 s, compared with 92% of cells in the control sample. The mean aggregate size in the unmixed cell population was 18.2 μm (Fig. 24J), with a diverse distribution of aggregate sizes (standard deviation = 9.9). Mean aggregate size was decreased in mixed cell populations containing 5% GA-treated RBC (14.1 ± 8.0 μm), and decreased further in populations containing 25 (12.9 ± 6.2 μm) and 50% (13.6 ± 7.3 μm) GA-treated RBC, respectively. Moreover, the number of aggregates 20 μm or longer was decreased in mixed RBC populations when compared with the control cell population.

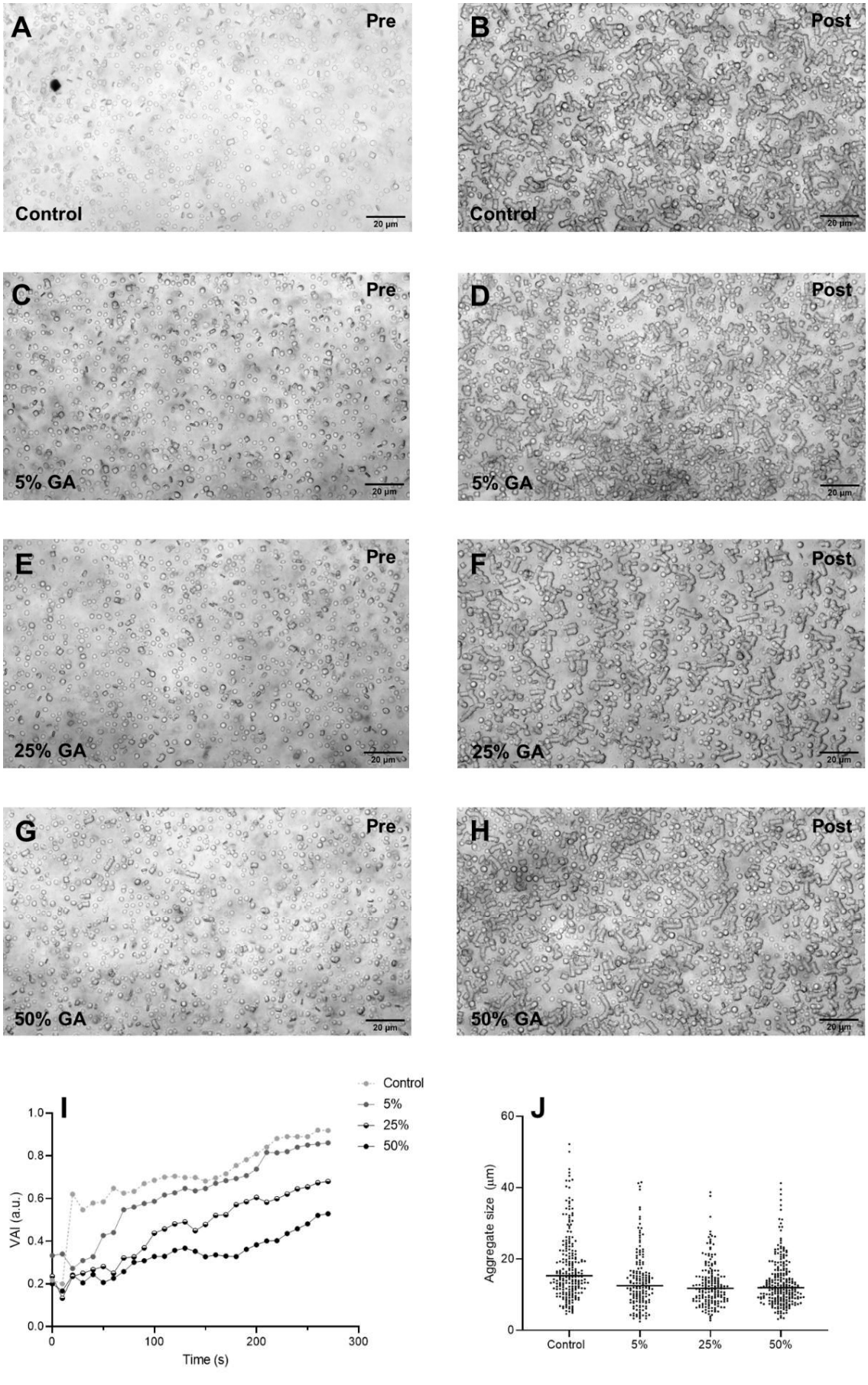
A
Pre
Control
20 µm
B
Post
Control
20 µm
C
Pre
5% GA
20 µm
D
Post
5% GA
20 µm
E
Pre
25% GA
20 µm
F
Post
25% GA
20 µm
G
Pre
50% GA
20 µm
H
Post
50% GA
20 µm
I
Control
5%
25%
50%
VAI (a.u.)
Time (s)
J
Aggregate size (µm)
Control
5%
25%
50%

***Fig. 24**: Disaggregated ('Pre'; A, C, E, G) and aggregated ('Post'; B, D, F, H) mixed red blood cell (RBC) populations containing increasing concentrations of glutaraldehyde (GA)-treated cells were imaged at 200-times magnification (0.5 NA), while the process of aggregate formation was recorded at 600-times magnification (0.85 NA) and the visual aggregation index (VAI) was quantified every 10 s (I). Following a total of 300 s of aggregate formation, the sizes of aggregates formed within the mixed RBC populations were determined from the 'Post'-images (J). N = 150–250 individual cells. Photomicrographs were captured using an Olympus IX-73 inverted microscope coupled with an optiMOS CMOS CCD camera. Cell suspensions were prepared and imaged in autologous plasma at 37 °C.*

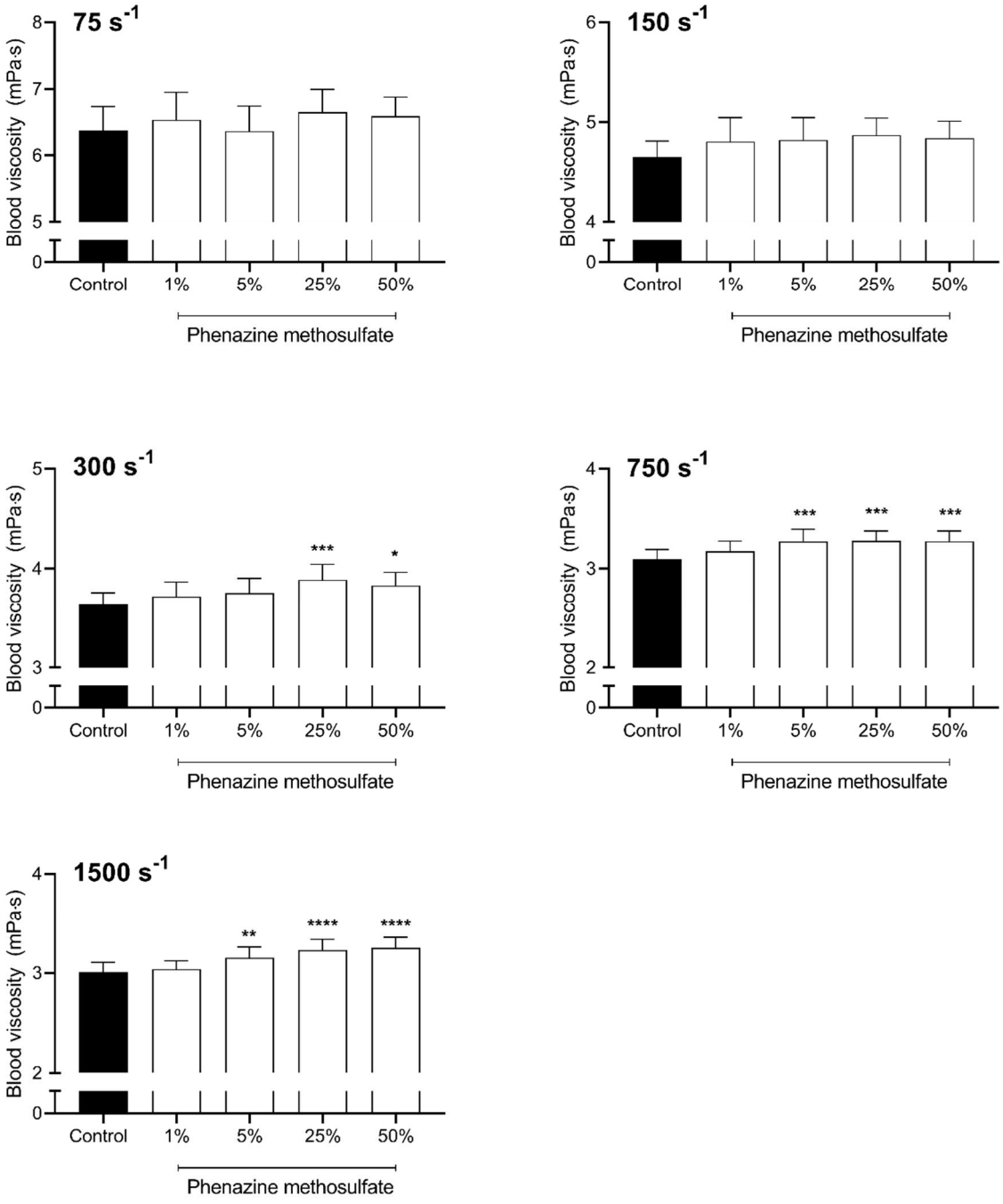

***Fig. 25**: Whole blood viscosity of samples with progressively increasing proportions of mechanically impaired red blood cells (RBC) present was quantified across a range of shear rates (75–1500 s^{-1}). Mixed cell populations were produced by re-introducing 1, 5, 25, or 50% RBC previously treated with 116 $\mu mol \cdot L^{-1}$ phenazine methosulfate into a sample of untreated control cells. ***P < 0.001, **P < 0.01, *P < 0.05 compared to 'Control'; data were compared using One-Way analysis of variance. N = 14.*

3.4.7 Mixed RBC populations containing PMS-treated cells exhibit unaltered viscosity at low shear and increased viscosity at higher shears

Addition of PMS-treated RBC sub-populations into control samples had no effect on low shear viscosity (i.e., 75 and 150 s^{-1}, Fig. 25). At 300 s^{-1}, however, blood viscosity was significantly increased in samples containing 25 and 50% PMS-treated RBC sub-populations, respectively. Moreover, at both 750 and 1500 s^{-1}, viscosity of blood samples containing 5-50% PMS-treated sub-populations was significantly elevated ($P < 0.01$).

3.5 Discussion

The salient findings of the present study indicate that the physical properties of blood suspensions are altered when a sub-population of mechanically impaired RBC is introduced. The impact of abnormal RBC on whole population cellular deformability, and blood viscosity, is non-linear; a disproportionately greater impact is observed than what would be reasonably predicted for the fraction of impaired cells present. It was also found that the mechanism of inducing impaired cell deformability (i.e., *via* cross-linking of cell membrane components or *via* cytosolic exposure to free radicals) precipitated near-identical patterns of abnormal RBC mechanics (Fig. 20); the same was *not* observed for the impact on whole blood viscosity. That is, mixed cell populations containing 25-50% GA-treated RBC exhibited significantly decreased low shear viscosity, while high

shear viscosity was increased at all concentrations. Conversely, mixed populations that contained 5-50% PMS-treated RBC exhibited *no* alteration in low shear viscosity, while high shear viscosity was significantly increased. Follow-up experiments revealed that decreased low shear viscosity, observed in samples with GA-treated sub-populations, was mediated by a decreased tendency of these mixed cell populations to form aggregates, when compared with an untreated sample (Fig. 24). Collectively, the results of the current study indicate that even small fractions (1-5%) of RBC with impaired cell mechanics significantly impact both whole blood microrheological properties and macrorheological behaviour of blood. Given medical interventions such as blood transfusion or mechanical circulatory support represent introduction of a similar fraction of abnormal RBC (1-10%; [163, 164]), the present findings suggest that both the macro- and microcirculation may be impacted by poor quality blood constituents, and may contribute, in part, to common complications observed in post-operative patients.

Incubation of RBC with rigidifying agents (*Experiment One*) induced significantly impaired cellular deformability across a range of shear stresses (Fig. 20A), despite the absence of observable morphological alteration (Fig. 26). Interestingly, while a linear increase of RBC rigidity was observed with increased concentration of the respective rigidifying agent (Fig. 19 A,B), it appears that PMS-concentrations <30 μM would not precipitate increased $SS_{1/2}$:EI_{max}. Given that PMS rigidified the

cell membrane by producing reactive oxygen species in the RBC cytosol, which is also enriched in antioxidant molecules [165], it is plausible that this observation infers that the antioxidant defence of the RBC is sufficient to quench superoxide to at least ~30 μM equivalent PMS. The rigidifying effect of GA and PMS is well-reported [52, 76, 152, 154, 166], although our unique approach enabled titration of the various agents to achieve comparable cell rigidification. This approach was effective, as evidenced by the RBC populations of rigidified cells mixed at 1-50% with untreated control cells exhibiting a highly reproducible response independent of treatment (within 1% variance; Fig. 20). For both conditions, however, a disproportionate effect was observed when relatively few treated cells were mixed with untreated blood samples: for example, only 25% of the sample required rigidification treatment to achieve 50% of the total impairment to cell mechanics (i.e., the level of rigidification observed in a sample containing 100% GA-treated RBC), while introduction of only 5% rigidified cells resulted in over 25% of the total response (Fig. 21). Presence of 1% GA-treated RBC appeared to have a more significant effect on cellular deformability (i.e., $SS_{1/2}$:EI_{max}) when compared with 1% PMS-treated RBC (Fig. 21), which may explain the increase in blood viscosity observed only in the GA-treated mixed samples (Fig. 23). It thus appears that the presence of RBC with abnormal mechanics within the native cell population precipitates significant disruptions to the overall fluid behaviour, even at concentrations ranging from 1-5%. Given that the average volume used in blood transfusions represents ~5-8% of the patient's RBC population, the

salient observation that 1-5% GA- or PMS-treated RBC is sufficient to affect mechanics of the mixed cell population is potentially clinically meaningful [163]. Estimating the physiological implications of haemorheological phenomena is not straightforward and is dependent upon the level of circulation investigated [167]. Previous reports have indicated that comparable changes in blood viscosity as were observed in the present study may significantly increase pulmonary arterial pressures and decrease regional blood flow to various organs in canine models [168]. Moreover, trapping of less deformable RBC in spleen and sternum has been observed to raise vascular resistance and decrease local blood flow [52]. While the latter experiments involved a larger fraction of hardened RBC than 1-5%, traversal of high-shear regions in long-term circulatory support in particular would stand to sustain the presence of a small fraction of abnormal RBC, which may have deleterious chronic effects.

Previous reports have indicated an increased mechanical sensitivity of PMS-treated RBC to supraphysiological shear stress exposure [166], which is corroborated in the present study. We observed a compounding effect, where mixed RBC samples containing previously rigidified sub-populations became even more rigid (Fig. 22) following exposure to 100 Pa shear stress for 32 s. Given that increasing the concentration of rigid RBC beyond 25-50% resulted in no further compounding of shear- and rigidification treatment-induced mechanical impairment (the curve reached a plateau; Fig. 22), which mirrored the effect of

shear stress on untreated RBC (Fig. 19C), it is plausible to hypothesise that untreated RBC are simply more sensitive to shear-induced impairments of cell mechanics. Previously rigidified RBC, however, may exhibit less capacity to become even more rigid. Moreover, it is possible that an upper 'threshold' of rigidity exists, prior to haemolysis, beyond which RBC do not accumulate further damage, akin to the elastic limit observed in non-biological materials. During exposure to mechanical stresses typical of mechanical circulatory support, a fraction of the total RBC population is exposed to non-physiological environments and shears (e.g., extracorporeal circulation, long-term implanted circulatory support [103]) per device transit. Thus, the number of mechanically-impaired RBC in circulation progressively increases following each pass of the mechanical pump. The salient observation that a fraction of mechanically-impaired RBC comprising only <5% of the total cell count has a measurable impact on blood viscosity, which may in turn impede blood fluidity, is therefore of clinical relevance.

Mixed RBC populations containing large proportions of RBC with cross-linked membrane proteins, and thus reduced flexibility of the cell membrane, showed decreased viscosity at low shears (Fig. 23). This observation was unexpected, given it is well reported that rigid spheres/rigidified cells produce an elevated blood viscosity response, independent of shear rate [169]. To explore the reason for our observation, we investigated whether the capacity of RBC to aggregate

was altered by GA-treatment, given that the capacity of RBC to form reversible three-dimensional aggregate structures largely determines the fluid properties of blood at stasis/low shear. The magnitude of aggregation (i.e., the number of cells engaged in aggregates relative to the local haematocrit, reflected by the VAI; Fig. 24I) was decreased in RBC samples containing GA-treated cells, which occurred concurrent with a decrease in both mean aggregate size and the number of aggregates larger than 25 μm (Fig. 24J). Given membrane flexibility is a vital determinant of cell-cell contact [170, 171], it is plausible that RBC with rigid plasma membranes may be unable to form stable aggregates, or at least prevent the formation of large aggregates (Fig. 27) by effectively 'capping' rouleaux on both ends, depending on the number of rigid cells present. That is, presence of a larger fraction of abnormally rigid RBC would increase the likelihood of these cells being engaged into an aggregate, while simultaneously decreasing the probability of this particular aggregate being extended. This observation prompts questions that warrant further investigation, for example, whether RBC preferentially aggregate with cells of either similar or strongly dissimilar membrane properties *in vivo* (e.g., RBC on either end of the cell-density spectrum). It is important to note that the tentative data presented here requires confirmation through direct approaches, for example optical tweezers, which have recently been used to provide quantitative data on RBC interactions [126, 172]. Mixed cell populations with PMS-treated RBC did not exhibit altered low-shear viscosity when compared with control RBC (Fig. 25); it thus appears that

intracellular oxidative stress, despite propagating an equivalent increase in cellular rigidity, may not affect RBC aggregation to the same extent, which has previously been reported by Baskurt et al. [152]. Cell charge is a vital determinant of RBC aggregation, given that increased negative charge, conferred onto the RBC primarily by its glycocalyx [173], promotes cell-cell repulsion [174]. It is plausible that treatment with GA altered the cell charge [175], thus increasing the repulsive forces that prevent cellular aggregation, while PMS – which requires intracellular metabolites to activate [176] – does not interfere with the RBC glycocalyx.

The impairment in RBC mechanics provoked in the current investigation is comparable in magnitude to that observed in RBC stored under controlled conditions for less than one week [143]. Previous investigations have been conducted in a similar manner, albeit employing rigidification far above those that could reasonably be expected even in a pathophysiological scenario [177]. Given that the average length of storage for a transfused unit of RBC in the United States is ~21 days [178], it is suggested that the state of fresh RBC exposed to GA or PMS in the current study provides a useful estimate of stored RBC used in transfusion practices. We observed significant increases in high shear blood viscosity even for samples with impaired physical properties at concentrations as low as 1% (GA-treated; Fig. 23) and 5% (PMS-treated; Fig. 25). The average transfusion procedure replaces ~9% of native RBC with stored RBC [163], which

are exposed to considerable mechanical stresses and artificial environments in the process, thus plausibly exacerbating pre-existing impairments in cell mechanics (e.g., due to *ex vivo* aging). Increased blood viscosity is commonly reported in recipients post-transfusion [179], which cannot be explained by changes in haematocrit alone, and may indeed counteract the desired aim of increasing RBC count to enhance oxygen delivery [180].

Collectively, the present results indicate that a small fraction (1-5%) of RBC with abnormal mechanics may alter bulk blood fluid properties; the observed alterations in viscosity appear to be mediated by impaired microrheological properties of RBC. The specific physical properties that determine cellular deformability seem to be of importance, given that inducing a matched level of rigidity *via* distinct treatments induced discrete effects on blood viscosity. Reducing the flexibility of the RBC membrane specifically impairs cell deformability and limits cell-cell aggregation, which altered blood viscosity across a range of shears in the present study. Intracellular generation of free radicals, however, primarily impaired cell deformability, translating to unaltered low-shear blood behaviour, although substantially affected viscosity under high shears. The salient observations may, in part, explain adverse clinical events associated with blood transfusion and mechanical circulatory support, wherein a sub-population of RBC with abnormal properties is present amongst native blood.

3.6 Supplemental material: Impact of small fractions of abnormal erythrocytes on blood rheology

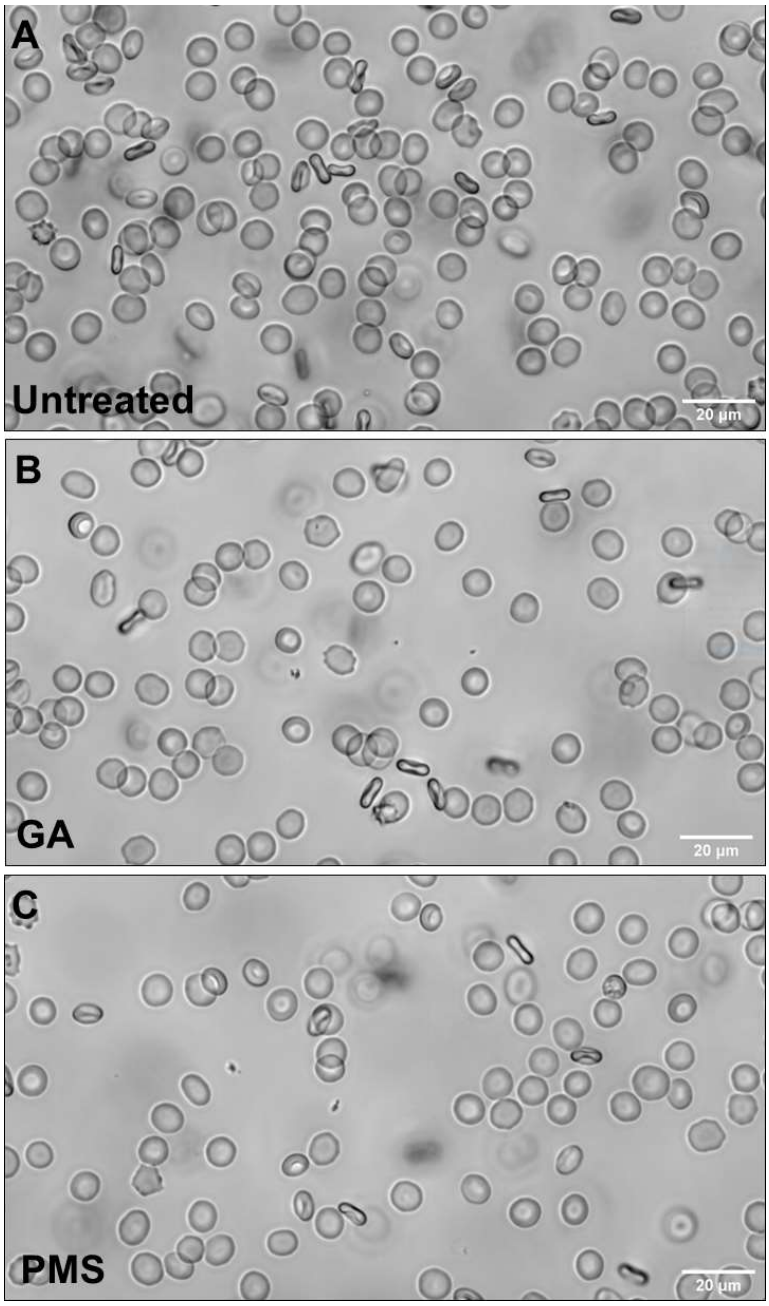

***Fig. 26**: Representative images of red blood cell (RBC) populations incubated with phosphate buffered saline (A) as control, 0.036% glutaraldehyde (B), or 116 µmol·L^{-1} phenazine methosulfate (C), imaged at 600-times magnification (0.85 NA). Exposure to the rigidifying agents did not precipitate observable morphological alterations of RBC. Photomicrographs were captured using an Olympus IX-73 inverted microscope coupled with an optiMOS CMOS CCD camera. Cell suspensions were prepared and imaged in isotonic phosphate-buffered saline at room temperature.*

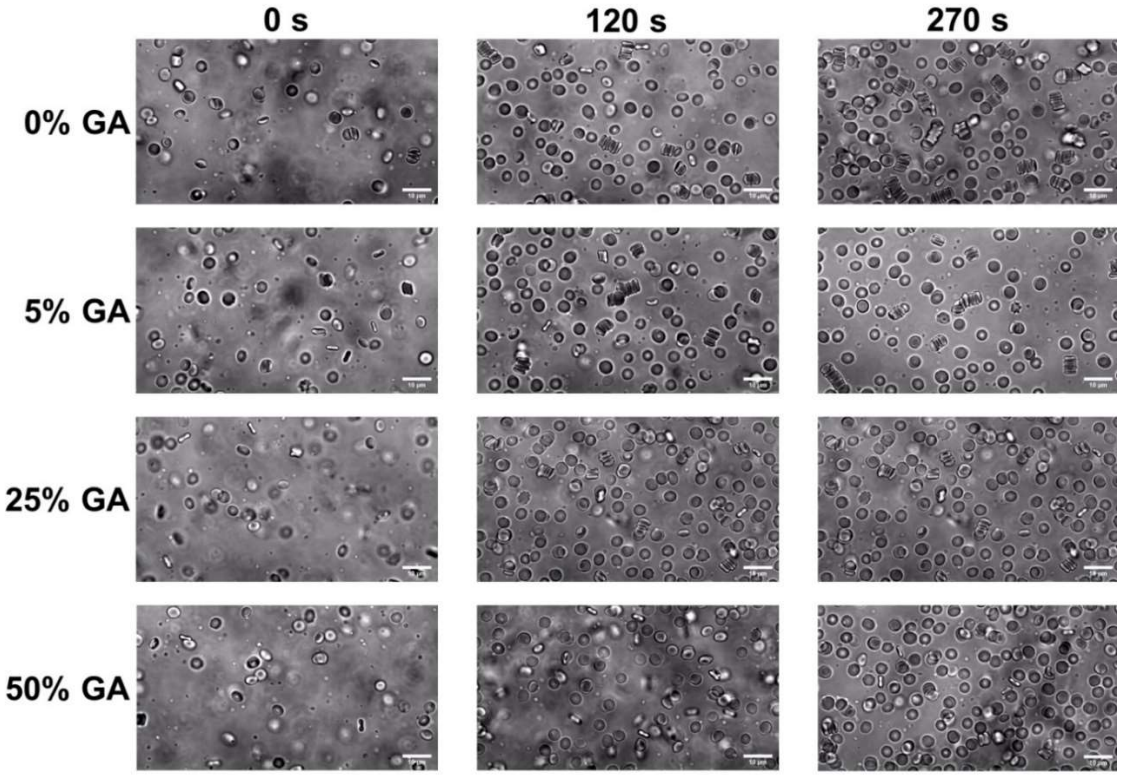

***Fig. 27**: Micrographs of mixed red blood cell (RBC) populations containing increasing fractions of glutaraldehyde-treated RBC aggregating in autologous plasma. Over time, formation of aggregates in the control RBC population (i.e., 0% GA) occurred, precipitating large aggregates that contain a high number of cells and multiple branches (top right image). In contrast, mixed RBC populations tended to preferentially form doublets and triplets, even after longer periods of stasis (270 s; bottom right image) and failed to form branched aggregates containing large numbers of cells.*

3.7 Results of Study 1 in the context of the present dissertation

The primary conclusions from the results of *Study 1* support that a fraction of only 1-5% RBC with altered mechanical properties may have significant effects on bulk blood biophysics. This observation is clearly relevant to transfusion-related complications, but also demonstrates the significance of sub-populations comprising a given RBC population. That is, it appears that disturbances by a sub-population of chemically-altered RBC present at low fractions are relevant to overall blood flow behaviour.

The heterogeneity of the RBC population is a direct result of these cells surrendering transcriptional capacity during maturation. Without the ability to re-synthesise proteins or membrane components, the chemical and mechanical stresses exerted upon RBC during their 120-day transit of the cardiovascular system predetermine the limited lifespan of these cells. It is nonetheless remarkable that the bulk of RBC are able to maintain their mechanical properties for most of their lifespan, merely deteriorating immediately prior to removal from circulation. The mechanisms of this removal process, which is thought to occur primarily in the spleen, but may be shifted somewhat to the liver in patients that underwent splenectomy, are still unclear.

Chapter 4

Study 2: Calcium dynamically alters erythrocyte mechanical response to shear

Lennart Kuck, Jason N. Peart, Michael J. Simmonds

Chapter 4 contains works conducted as part of the present doctoral program and is presented in its peer-reviewed and published form. My contributions to this paper include concept and experimental design, data collection, data analysis and interpretation, manuscript development. All authors reviewed and approved the manuscript.

Reference: Kuck, L., Peart, J. N., & Simmonds, M. J. (2020). Calcium dynamically alters erythrocyte mechanical response to shear. *Biochimica et Biophysica Acta (BBA)-Molecular Cell Research*, 1867(11), 118802. PubMed ID: 32717279. DOI: 10.1016/j.bbamcr.2020.118802

4.1 Preface

Increased $[Ca^{2+}]_i$ is commonly considered to progress the *in vivo* ageing process of RBC, and may ultimately contribute to their demise (for recent detailed reviews on Ca^{2+} in RBC ageing and anaemias, the interested reader is directed to [47] and [37]). Ca^{2+} entering RBC is thought to facilitate a deterioration of RBC mechanics through rigidification of the cell membrane and/or inducement of cell volume loss. Only very recently, it has been proposed that an influx of Ca^{2+} into RBC that marginally raises $[Ca^{2+}]_i$ may have benefits for RBC capillary transit [18]. Surprisingly, the bulk of studies conducted to interrogate the role Ca^{2+} plays in regulating RBC mechanics were performed at stasis – despite blood seldomly pooling in healthy humans. Traditional dogmas dictate that RBC are biologically inert, due to the lack of gene expression capacity, and the biological relevance of mechanical cues to the post-translational regulation of RBC homeostasis is a novel concept. It is thus plausible that these factors were not considered in previous designs of studies investigating interactions between Ca^{2+} and RBC mechanics. With the recent discovery of Piezo1, however, a cation channel expressed in RBC opening in response to mechanical forces, a revisit of past findings is timely. Thus, the following study was designed to provide a comprehensive assessment of the regulatory role Ca^{2+} plays in altering the physical properties of RBC using both static and dynamic models.

4.2 Introduction

The mechanical properties of RBC are primary determinants of both bulk blood flow and microcirculatory transit (for review, see [51]). It has long been understood that the unique properties of RBC enabled high levels of cellular deformability [6]. The biconcave disc-shape of RBC, for example, provides an unusually high surface area-to-volume ratio compared with other cells of equivalent volume. Moreover, the RBC membrane is composed of a lipid bilayer attached to an underlying cytoskeleton by lateral protein junctions, which maintains structural integrity while facilitating extensive deformation, that is reversible when shear exposure is within physiological limits [181, 182]. The resultant exceptional level of cellular deformability was believed to be largely a passive response to the external environment [6]. Similarly, decreased levels of cell deformability, as present in various pathological conditions (e.g., membrane disorders, metabolic disorders or oxidative stress conditions; [48]), were thought to be caused by fundamental dysregulation of these passive determinants of cell deformability.

Increased $[Ca^{2+}]_i$, for example, has long been known to induce impairments in RBC deformability and increased osmotic fragility [23, 90, 183-185]. Ca^{2+}, upon entering the RBC, activate the Ca^{2+}-dependent potassium K^+-channel $K_{Ca}3.1$, commonly referred to as the 'Gárdos channel' [14]. Gárdos channels facilitate K^+-efflux, which results in loss of intracellular fluid ('Gárdos effect'); however, RBC

possess powerful Ca^{2+}-ATPase pumps, which in combination with a membrane that is near impermeable to Ca^{2+}, maintain a ~40,000-fold concentration gradient between the cytosol (~30-60 $nmol \cdot L^{-1}$) and the extracellular fluid (i.e., plasma: ~1.8 $mmol \cdot L^{-1}$; [47]). Over the 120 day-lifespan of the RBC, the activity of the Ca^{2+}-ATPase decreases, propagating a heterogenous cell population composed of cell fractions with different cell ages [16, 38], which likely explains the heterogenous $[Ca^{2+}]_i$ observed in RBC [186]. Intact cellular deformability, which requires low $[Ca^{2+}]_i$, is maintained by Ca^{2+}-ATPase activity under utilisation of ATP. It is important to note that these ATPases are fuelled exclusively by anaerobic glycolysis given RBC do not possess cell organelles to conduct aerobic metabolism. Collectively, disturbances in Ca^{2+}-metabolism were thought be resultant of fundamental dysregulation or physiological aging and thus primarily investigated in static conditions.

Over the past decade, however, a substantial body of evidence has accumulated indicating that the physical properties of RBC may be acutely modulated by what appears to be biochemical mediators – including production of nitric oxide-derived species and acute shifts in $[Ca^{2+}]_i$ – when exposed to external stimuli. Piezo1, a mechanically-activated cation-channel in the RBC membrane, has been shown to facilitate influx of Ca^{2+} when RBC are exposed to mechanical stimulation, such as physical deformation of the membrane [18, 45]. It is currently proposed that an interplay between Piezo1 and the Gárdos channel leads to

release of small amounts of intracellular fluid when traversing capillaries; cell volume and cell size thus each decrease, enhancing RBC transit within the microcirculation [18]. Further, subtle Ca^{2+}-influx has previously been reported to transduce a conformational change in junctional proteins in the cytoskeleton, which is hypothesised to facilitate flexibility of the cell membrane [187]. Exposure of RBC to shear stress in the physiological range (i.e., ≤10 Pa) facilitates a temporary increase in cell deformability [76, 162, 188, 189], and Ca^{2+}-shifts have been suggested as a potential mechanism explaining this response. Thus, given that traditional experimentation was primarily conducted in a static environment, however, more dynamic approaches demonstrate substantial mechano-sensitive processes affecting RBC properties, it remains unknown whether the previously reported determinants of RBC deformability (e.g., hydration status, membrane flexibility) are altered within the novel, dynamic model.

Therefore, we sought to investigate Ca^{2+}-flux in a dynamic environment that would reflect *in vivo* conditions and assess the active regulation of RBC mechanics. $[Ca^{2+}]_i$ was altered in a dose-dependent manner using an ionophore (A23187) known to facilitate Ca^{2+}-transport across the RBC membrane [16], which has been shown to decrease cell volume and deformability. To elucidate whether cell volume was a determinant of the Ca^{2+}-mediated responses, potassium chloride (KCl) was titrated into the extracellular medium to eliminate the native

K^+-gradient between RBC (~100 mmol·L^{-1}) and the surrounding plasma (5 mmol·L^{-1}; [38]), which inhibits the 'Gárdos effect'. The effects of intracellular and extracellular Ca^{2+} on RBC mechanics both at stasis and under shear were subsequently assessed in separate experiments.

4.3 Materials and methods

4.3.1 Blood sample collection

Participants were healthy, male volunteers (N = 8; age: 25 ± 2 years; height: 182 ± 6 cm; body mass: 82 ± 4 kg) free of any known cardiovascular, pulmonary, endocrine, or metabolic diseases. Moreover, participants had not provided a large-volume blood donation (i.e., 450 mL) within the previous year, and were not taking any medication. Written consent was obtained after educating the participants about the risks and benefits involved in participating in the current study. Blood samples were collected from a prominent vein in the antecubital region of the arm. The blood draw procedure was performed within 90 s of applying a tourniquet to the upper arm, using a sterile needle and syringe, which was drawn slowly at 0.5 mL·s^{-1} to minimise shear. Blood was immediately transferred into a vacuum-sealed tube coated with ethylenediaminetetraacetic acid (1.8 mg·mL^{-1}) and gently mixed for ~10 s. The experimental procedures were reviewed and approved by the Human Research Ethics Committee of Griffith University (Gold Coast, QLD, Australia), and are consistent with the Declaration

of Helsinki. All experimental procedures were carried out within 4 h of blood collection. Chemicals were sourced from Sigma Aldrich Pty Ltd (Castle Hill, NSW, Australia), unless stated otherwise.

4.3.2 Sample preparation

RBC were separated from white blood cells, platelets (i.e., buffy coat) and plasma by centrifugation at 1500 × *g* for 10 minutes. Isolated RBC were then washed twice using an isotonic, PBS (0.1 $mol \cdot L^{-1}$; pH = 7.41, osmolarity = 289 $mOsmol \cdot kg^{-1}$) supplemented with 5 $mmol \cdot L^{-1}$ glucose (in the following, this specific solution is referred to as "glucose solution"). Isolated RBC were incubated with glucose solution (Control) and the respective agents at 37°C for 20 min. One aliquot was incubated with 2.5 $\mu mol \cdot L^{-1}$ A23187 alone, while further aliquots were prepared containing A23187 in combination with 0.5 or 5 $\mu mol \cdot L^{-1}$ extracellular calcium chloride ($CaCl_2$). A final RBC sample was incubated with A23187 and 5 $\mu mol \cdot L^{-1}$ extracellular $CaCl_2$ in glucose solution supplemented with 150 $mmol \cdot L^{-1}$ KCl. Packed RBC were subsequently centrifuged at 1500 × *g* for 5 min and washed twice with glucose solution. Washed RBC were diluted in glucose solution at a haematocrit of ~0.4 $L \cdot L^{-1}$ and suspended in a viscous PVP solution (PVP in 0.1 $mol \cdot L^{-1}$ phosphate-buffered saline; 360 kDa, pH = 7.4 ± 0.5, 290 ± 5 $mOsmol \cdot kg^{-1}$, viscosity = 30 ± 0.5 mPa·s) at a final haematocrit of 0.005 $L \cdot L^{-1}$. Further RBC samples were resuspended in PVP solutions containing 2 $mmol \cdot L^{-1}$ $CaCl_2$. Fresh

RBC-PVP suspensions were prepared prior to each measurement to avoid extended exposure of RBC to $CaCl_2$ prior to deformability assessments.

4.3.3 Experimental protocol

The results reported herein were obtained from two distinct experiments, performed using a given blood sample. Specifically, the first experiment was designed to interrogate the effects of loading RBC *intracellularly* with Ca^{2+} through ionophore A23187 on RBC deformability, mean cell volume (MCV) and cell sensitivity to physiological shear exposure. In contrast, the second experiment was conducted to assess the effects of *extracellular* Ca^{2+} on the mechanical properties of RBC at stasis and under shear.

4.3.4 Experiment One

Washed, isolated and resuspended RBC were incubated with 2.5 μM of the calcium ionophore A23187 and with/out varying concentration of $CaCl_2$ (0.5, 5 μM) in glucose solution at 37°C for 20 min. Concurrent incubations of RBC in glucose solution served as control. Thereafter, incubated RBC samples were washed and resuspended in PVP solution. Samples were suspended in PVP immediately prior to deformability assessments to prevent prolonged exposure to the medium and to minimise any change in $[Ca^{2+}]_i$; cells were thus suspended in PVP, mixed thoroughly, and cell mechanics were analysed within 45-60 s. An

un-sheared, control measurement of RBC suspensions in PVP was performed using a ramped protocol (0.3-50 Pa), following which the same sample was exposed to a constant shear conditioning protocol (10 Pa for 300 s). Immediately post-shear conditioning, another measurement of deformability was conducted using the same ramped shear regime. Free haemoglobin, an index of cell destruction (i.e., haemolysis), was also quantified after the shear conditioning protocol. Haematological parameters including MCV were determined using an automated hematology analyser (DxH 600, Beckman Coulter, Brea, USA). In development stages of the current study, we systematically validated cell volume derived *via* the automated analyser with direct micropipette observations (using 1.5-5.0 μm inner diameter borosilicate glass capillaries) and micromanometer regulated suction forces; it was found that at "extreme" cell volumes of 90 fL and 82 fL, measurements derived using automated analysis and manual criterion methods agreed within 1%. Subsequent measurements were thus conducted using the automated analyser to increase experimental throughput.

4.3.5 Experiment Two

A second experiment was performed to assess the effects of $[Ca^{2+}]_e$ on RBC deformability. Isolated washed RBC were incubated with glucose solution and 2 $mmol \cdot L^{-1}$ $CaCl_2$ or autologous plasma – which also contains ~2 $mmol \cdot L^{-1}$ Ca – at 37°C for 20 min. Thereafter, RBC were centrifuged at 1500 × *g* for 5 min, washed

and resuspended in glucose solution for measurements. Resuspended RBC were diluted in PVP solution containing 2 mmol·L^{-1} $CaCl_2$ or control PVP at 0.005 L·L^{-1} haematocrit immediately prior to being sheared continuously at 10 Pa for 300 s. During the shear conditioning protocol, the resultant RBC deformation was recorded and analysed to provide cellular elongation over time. Thus, progressive changes in deformable capacity of RBC populations were assessed with/out $CaCl_2$ present. Immediately post-shear conditioning, an additional measurement of RBC deformability over a ramped range of shears (0.3-50 Pa) was performed on the discrete "post-sheared" sample to assess the effects of the shear conditioning protocol in combination with Ca^{2+}-supplementation on global cell deformability. To determine whether overt cell destruction occurred during shear conditioning, free haemoglobin concentration was measured for each sample.

4.3.6 RBC deformability measurements

A rotational ektacytometer (LORCA MaxSis, Mechatronics Instruments B.V., Zwaag, The Netherlands) was used to quantify cellular deformability, which has been described in detail [190]. The coaxial system consists of an outer cup rotating around a stationary inner bob. RBC suspensions were inserted into the gap between the two cylinders (300 μm), where the cell suspensions were exposed to a range of well-controlled shear stresses (0.3-50 Pa). A low-powered laser is

emitted from the stationary bob and through the RBC suspension under shear; the laser diffracts around the RBC, producing a diffraction pattern that reflects the cell orientation and deformation at a given shear stress. The diffraction patterns were captured by a CCD video camera and analysed in real-time by fitting an ellipse to the region of interest, where an elongation index (EI) was calculated using the length (a) and width (b) of the ellipse as follows: EI = (a - b)/(a + b).

4.3.7 Shear conditioning of blood samples

RBC suspensions in PVP were exposed to a discrete magnitude-duration combination of shear conditioning (i.e., 10 Pa for 300 s) known to improve cellular deformability, as described before [162]. During shear conditioning, the resultant laser diffraction patterns were recorded with a frequency of 1 Hz, which allowed for monitoring of EI throughout the shear conditioning. The shear conditioning procedures were carried out using the rotational ektacytometer described above, operated at 37 ± 0.2 °C.

4.3.8 Quantification of free haemoglobin

Immediately following shear conditioning, RBC suspensions in PVP were collected from the cup of the shearing device. Collected samples were centrifuged at 1500 × *g* for 5 min and the supernatant was diluted in 0.01% sodium

bicarbonate (Na_2CO_3) solution at a 1:5 ratio. Free haemoglobin was quantified using the Harboe method [191]: absorbance was quantified at multiple wavelengths (380, 415, and 450 nm) using an automated plate-reader (FLUOstar Omega, BMG Labtech, Mornington, VIC, Australia). A three-point correction was employed to filter noise caused by other heme-based products (e.g., bilirubin) and accurately represent the concentration of oxy-haemoglobin (Eq. 5).

$$\text{free Hb } (\text{mg}\cdot\text{dL}^{-1}) = \left(\frac{167.2\ (415\ \text{nm}) - 83.6\ (380\ \text{nm}) - 83.6\ (450\ \text{nm})}{10}\right) \times \frac{1}{\text{Na}_2\text{CO}_3\ \text{dilution factor}} \quad (5)$$

4.3.9 Fluo-4 imaging of intracellular calcium-levels

Isolated RBC were washed three times with a modified Tyrode's buffer containing (in $\text{mmol}\cdot\text{L}^{-1}$): 135 NaCl, 5.4 KCl, 10 glucose, 1 $MgCl_2$, 1.8 $CaCl_2$ and 10 HEPES with the pH adjusted to 7.35. RBC were then loaded with Fluo-4 AM (Thermo Fisher Scientific, Waltham, USA), a fluorescent probe suitable to assess intracellular Ca^{2+}-levels in living RBC [186], for 60 min at room temperature and protected from light. Fluo-4-loaded RBC were then washed three times with modified Tyrode's buffer and suspended in Tyrode's at a haematocrit of ~0.001 $\text{L}\cdot\text{L}^{-1}$. RBC suspensions were placed on glass coverslip and 20 minutes were allowed for the cells to sediment and for intracellular esterases to activate the dye. Fluo-4-loaded RBC were excited at λ = 488 nm and the fluorescent signal

was captured at $\lambda = 505$ nm using an inverted microscope (IX73, Olympus, Tokyo, Japan) with an integrated camera (optiMOS sCMOS, QImaging, Surrey, Australia) at 600-fold magnification. Fluorescent images were recorded for 10 s and averaged to provide a baseline signal (F_0), following which 2.5 $\mu mol \cdot L^{-1}$ A23187 was added onto the coverslip. Thereafter, the fluorescence of cells in the same field of view was recorded for another 10 s. Fluorescent intensity was determined in open-source software (Image J, National Institutes of Health, Bethesda, USA). At least 15 individual RBC from two independent donors were used to determine fluorescent intensity; the background intensity was quantified at 5 randomly chosen regions in the field of view and subtracted from the RBC intensity to give the final signal. It is important to note that Fluo-4-related fluorescence monitored in these cells does not quantitatively reflect $[Ca^{2+}]$, but rather provides a qualitative reflection of changes in intracellular Ca^{2+} over time.

4.3.10 Data analysis

Raw elongation index-shear stress (EI-SS) curves were parameterised using a non-linear version of the Lineweaver-Burk equation [160] to give EI_{max} and $SS_{1/2}$. The significant volume-shifts observed in some samples in the current study (Fig. 30C) resulted in RBC populations with uncharacteristically low EI_{max}-values (Fig. 29A). Thus, we modified the conventional analysis of the raw EI-SS curves to adequately correct for the alterations in EI_{max} and report global cell deformability

as $SS_{0.3}$:EI_{max} herein. A detailed description of the modifications is provided in the supplementary methods.

The curve describing the $SS_{0.3}$:EI_{max}-MCV relationship was obtained by non-linear regression curve-fitting (Eq. 6):

$$Y(x) = \left(Y_0 - Y_{inf}\right)e^{-Kx} + Y_{inf} \quad (6)$$

Y_0 is the theoretical $SS_{0.3}$:EI_{max} ratio at 0 MCV (i.e., Y-intercept), Y_{inf} represents the theoretical $SS_{0.3}$:EI_{max} at infinite MCV (i.e., plateau), K is the rate constant of the curve. Y(x) represents the $SS_{0.3}$:EI_{max} calculated for a given MCV (i.e., x).

Further, we correlated EI_{max} data (Fig. 33) and raw EI data (obtained at 3 Pa; Fig. 34) with the MCV of the respective sample and analysed the relationship using non-linear regression curve-fitting (Eq. 7):

$$Y(x) = Y_0 + \left(Y_{inf} - Y_0\right)(1 - e^{-K}\ ) \quad (7)$$

Y_0 is the theoretical EI at 0 MCV (i.e., Y-intercept), Y_{inf} represents the theoretical EI at infinite MCV (i.e., plateau), K is the rate constant of the curve. Y(x) represents the EI calculated for a given MCV (i.e., x).

Deformation of RBC populations over 300 s of constant shear exposure was recorded at a frequency of 1 Hz and slopes were calculated using linear regression analysis.

4.3.11 Statistical analysis

Results are presented as mean ± standard error of the mean (SEM), unless stated otherwise. Commercial data processing software was used to conduct statistical analyses and curve-fitting procedures throughout (Prism, GraphPad Software Inc., Release 8.1.1, La Jolla, CA, USA). Normality of the data was assessed with the D'Agostino and Pearson test of normality, which informed appropriate statistical analyses. Raw EI-SS data were compared using a two-way ANOVA with repeated measures. MCV and free haemoglobin data were compared using a one-way ANOVA. $SS_{0.3}$:EI_{max} ratio data between conditions were compared using the non-parametric Friedman-test. Post-hoc comparisons were performed with Bonferroni-correction. Pre- and post-SS comparisons of $SS_{0.3}$:EI_{max} ratios within the same condition were conducted using a two-tailed t-test. Analyses of the pre-and post-shear $SS_{0.3}$:EI_{max} ratios in Ca^{2+}-exposed samples sub-sets were conducted using a one-tailed t-test given that they were grouped based on whether they showed an increase or decrease, thus providing the direction of the effect. An alpha level of 0.05 was used throughout to determine statistical significance.

4.4 Results

4.4.1 Ionophore A23187 increases cytosolic calcium-related fluorescence

The fluorescent intensity obtained from imaging individual live RBC loaded with the Ca^{2+}-sensitive dye Fluo-4 over time are presented in Figure 28. When ionophore A23187 (2.5 μM) was added to RBC suspended in Tyrode's buffer, Fluo-4-emitted fluorescent intensity increased ~5.5-fold (Fig. 28A) when compared with baseline (i.e., -10-0 s).

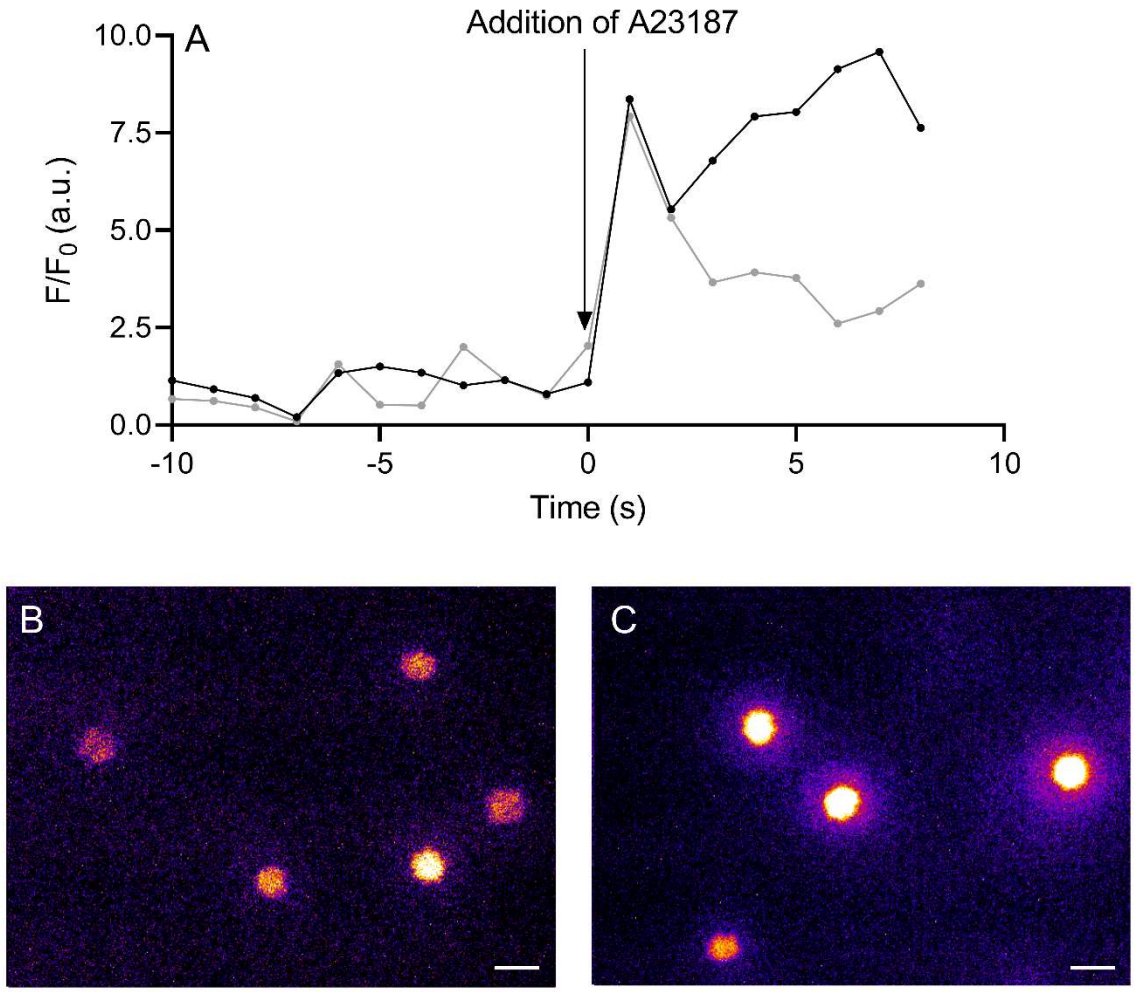

***Fig. 28**: Cytosolic calcium-concentration, measured using the fluorescent probe Fluo-4, was significantly increased upon the addition of the ionophore A23187 to the red blood cell (RBC) sample. Baseline fluorescence of RBC suspended in saline containing 5 µM calcium chloride ($CaCl_2$) was recorded over 10 s (representative image is shown in B). 2.5 µM A23187 was added to the RBC sample (representative image is shown in C). The change in fluorescence relative to baseline (F_0) is shown in (A), where F_0 was the mean fluorescence recorded over the 10 s before addition of A23187. Following addition of A23187, F/F_0 showed a sustained significant increase. N = 2 independent experiments with samples from different donors; at least 15 individual RBC were measured, respectively. The representative images were changed into the 'fire' look-up table for accentuation. Scale bar = 10 µm.*

4.4.2 Increased intracellular calcium impairs global cell deformability and reduces mean cell volume (MCV)

RBC incubated with ionophore A23187 exhibited slightly decreased capacity to deform under shears >3 Pa (Fig. 29A), reflected by a decreased EI. When $CaCl_2$ was added to the incubation medium, impairments in cell deformability were exacerbated in a dose-dependent manner: RBC suspensions exposed to 5 μM $CaCl_2$ (open circles) presented with significantly impaired capacity to deform under shears >0.94 Pa compared to control RBC (open circles) and incubations in high-KCl medium (diamonds; Fig. 29A). $SS_{0.3}$:EI_{max}, a parameter representing global cell deformability, was also increased with increased loading of Ca^{2+} in a dose-dependent manner, reflecting a progressive impairment in RBC deformability (Fig. 29B). When RBC were incubated with A23187 and $CaCl_2$ in KCl, no impairment in cellular deformability was observed at any applied shear stress. Moreover, RBC exposed to A23187 presented with decreased MCV, and the combination of A23187 and $CaCl_2$ further decreased MCV in a dose-dependent manner (Fig. 29C). When KCl was added to the incubation medium with A23187 and $CaCl_2$, however, no decrease in MCV was observed when compared with control (Fig. 29C).

4.4.3 RBC loaded with calcium exhibit no alterations in elongation under constant exposure to physiological shear stress

Deformability of RBC suspensions exposed to A23187 in combination with $CaCl_2$ exhibited decreased cellular deformability at stasis (Fig. 29A). When exposed to shear, RBC loaded with Ca^{2+} maintained this decreased capacity to deform during the shearing protocol (i.e., 10 Pa for 300 s), as the EI remained near-constant throughout (Fig. 29D). Linear regression revealed the slope of untreated RBC was -2.889×10^{-5}, while Iono samples exhibited a slope of -3.941×10^{-5}. LoCa, HiCa and $HiCa^{+K}$ samples had slopes of -5.477×10^{-5}, -2.341×10^{-5}, and -1.927×10^{-5}, respectively.

Moreover, no difference in the concentration of free Hb, a primary marker of overt cell destruction, was observed between the conditions (Fig. 29E) post-shear conditioning.

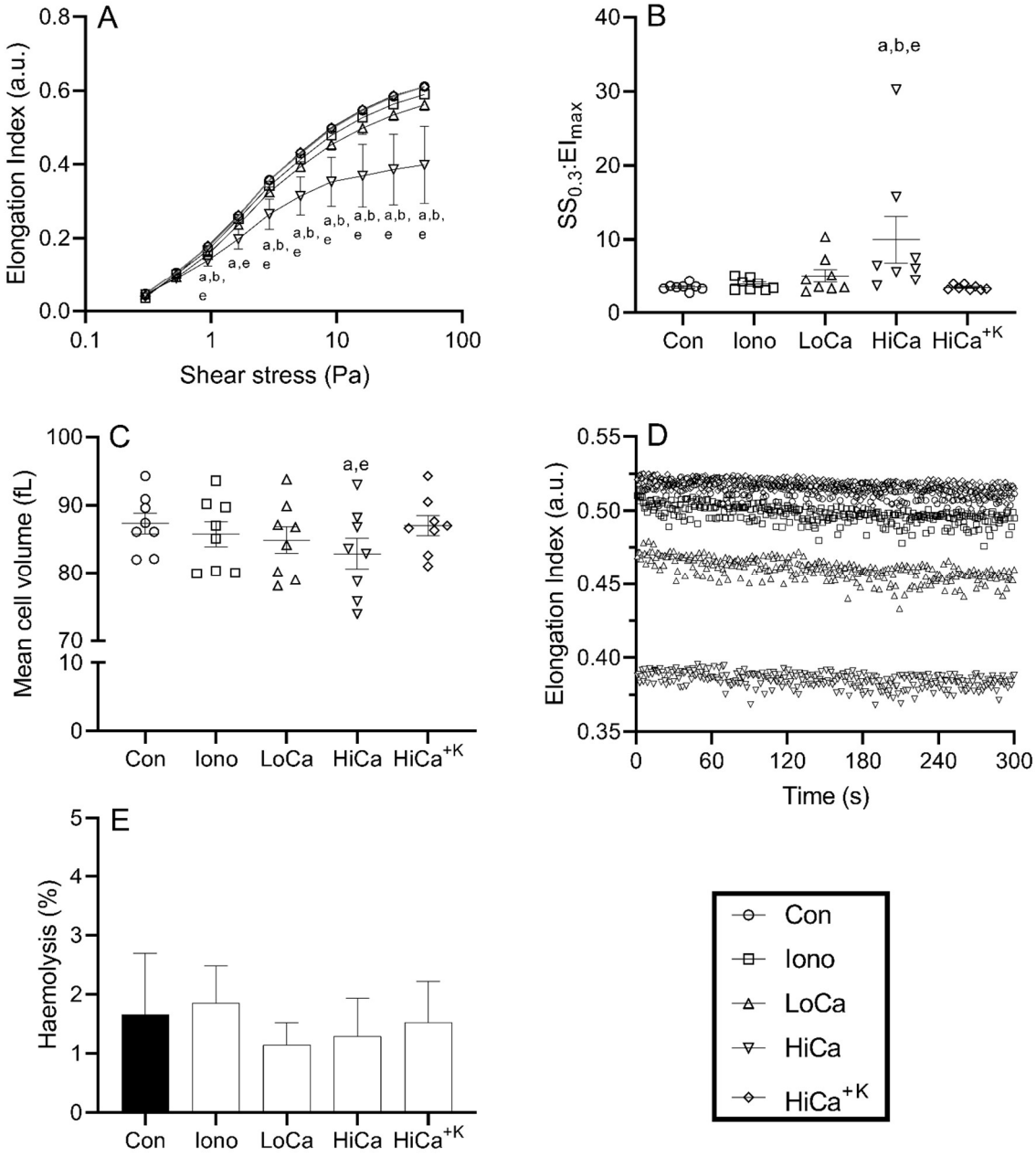

***Fig. 29**: Red blood cell deformability (RBC) and mean cell volume (MCV) in response to increased cytosolic calcium-concentration are presented pre- and post-shear. RBC deformation (i.e., elongation index) was measured over a ramped range of shear stress (0.3-50 Pa) (A). Deformability of ionophore-treated RBC (Iono; squares) with added calcium chloride ($CaCl_2$) in the suspending medium at 0.5 µM (LoCa; triangles) or 5 µM (HiCa; inverted triangles) is compared with the deformability of RBC treated with ionophore and 5 µM $CaCl_2$ in presence of 150 mM extracellular potassium chloride ($HiCa^{+K}$; diamonds). Increased intracellular calcium induced an increase in $SS_{0.3}$:EI_{max} (index of global deformability; B) accompanied by a decrease in mean cell volume (MCV) in a dose-dependent manner (C). Deformation of RBC during the shearing protocol remained constant over time (D). Free haemoglobin concentration, the primary marker of*

red cell destruction (i.e., haemolysis), was not altered after the shearing protocol (E). N = 8 (mean ± SEM); significant differences (P < 0.05) compared to (a) Control, (b) 2.5 μM A23187, (c) 0.5 μM $CaCl_2$, (d) 5 μM $CaCl_2$, (e) 5 μM $CaCl_2$ in KCl determined by two-way ANOVA (panel A), one-way ANOVA (B) and non-parametric Friedman test (C).

4.4.4 RBC deformability post-shear conditioning is dependent upon mean cell volume rather than calcium-exposure

Exposure to 10 Pa continuous shear for 300 s induced an ~26% decrease in $SS_{0.3}$:EI_{max} ratio (Fig. 30A). Moreover, in presence of A23187, global cell deformability improved by ~20%. Upon further addition of 5 μM $CaCl_2$ and 150 mM KCl in the incubation medium, global RBC deformability improved by ~24%.

When RBC treated with the ionophore A23187 and $CaCl_2$ in glucose solution were exposed to the shear conditioning protocol, deformability changed in a non-uniform manner. Shear exposure either improved or impaired global cell deformability, irrespective of the $CaCl_2$-concentration employed (Fig. 30B). Individual samples were accordingly clustered into sub-groups based on whether $SS_{0.3}$:EI_{max} increased or decreased following shear exposure. RBC suspensions exposed to 0.5 μM $CaCl_2$ with a mean MCV of 88.4 ± 3.7 fL presented with a 13% decrease in $SS_{0.3}$:EI_{max} (i.e., improvement in global cell deformability), while RBC exposed to the same protocol with a mean MCV of 79.2 ± 1.5 fL exhibited a 28% increase in $SS_{0.3}$:EI_{max} (i.e., impairment in global cell deformability). Similarly, RBC suspensions exposed to 5 μM $CaCl_2$ with a mean

MCV of 87.6 ± 5.1 fL showed a 22% improvement in global cell deformability post-shear conditioning, while samples with a mean MCV of 81.1 ± 6.2 fL exhibited a 170% increase in $SS_{0.3}$:EI_{max} when compared with the unsheared condition. Collectively, exposure to 10 Pa of shear stress for 300 s further compromised cellular deformability of RBC with lower MCV, while enhancing deformability of RBC with higher MCV (Fig. 30B).

Thus, to assess the relationship between MCV and RBC deformability in untreated cells and cells loaded with 0.5 μM or 0.5 μM $CaCl_2$, $SS_{0.3}$:EI_{max} of all individual samples was plotted against the respective MCV of that sample, irrespective of treatment. When $SS_{0.3}$:EI_{max} ratio (Fig. 30C), EI_{max} (Fig. 33), or EI at 3 Pa (Fig. 34) were plotted against the respective MCV of a given blood sample, we found a strong, statistically significant relationship between MCV – altered by increases in $[Ca^{2+}]_i$ – and RBC deformability (all $R^2 > 0.95$).

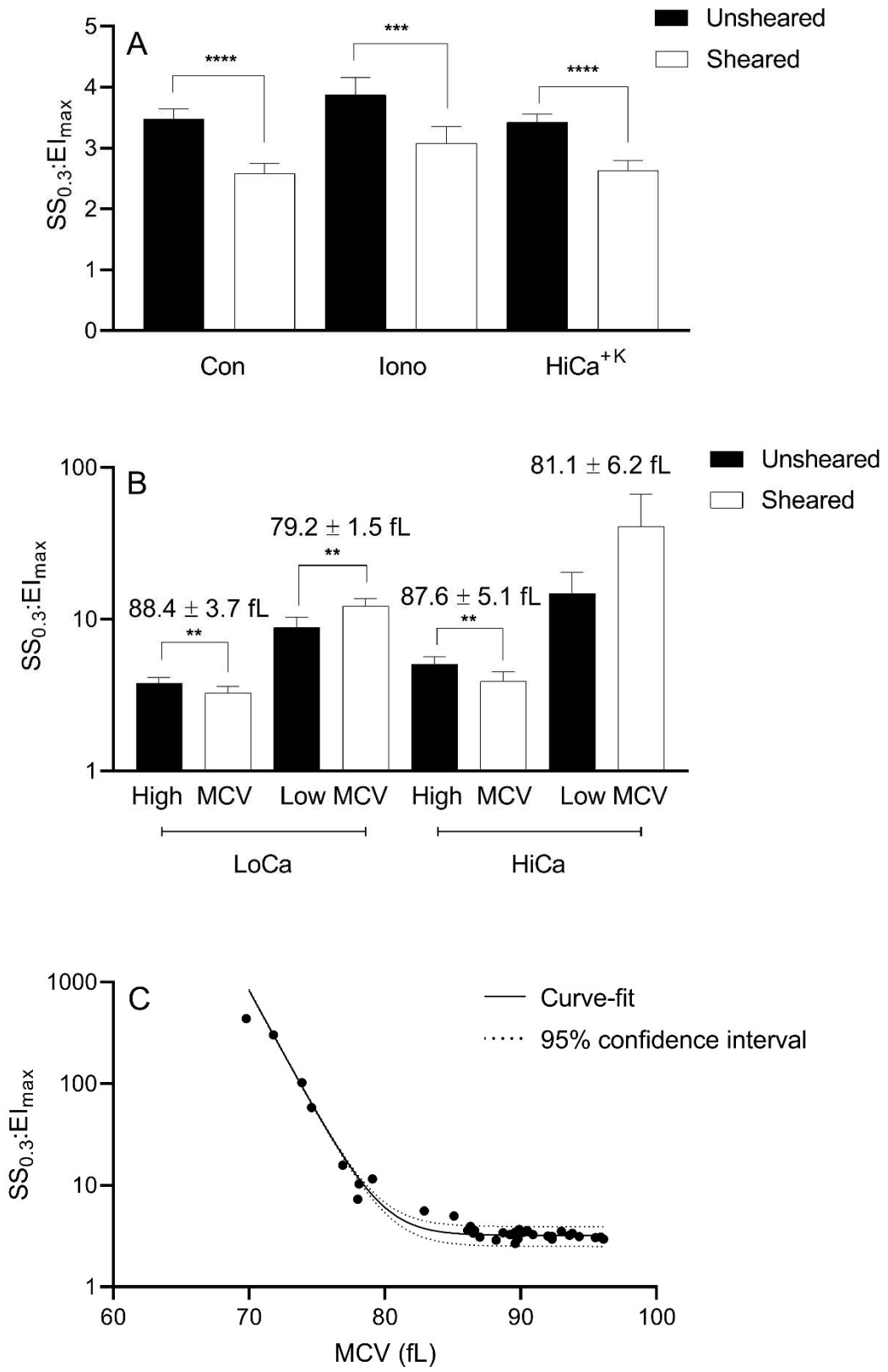

***Fig. 30**: Mechanical sensitivity is dependent upon cell volume rather than calcium-exposure. Global cell deformability expressed as a single parameter ($SS_{0.3}$:EI_{max}) improved post-shear conditioning at 10 Pa for 300 s (A) for red blood cell (RBC) suspensions*

incubated with 2.5 μM ionophore A23187 alone (Iono) and A23187 with 5 μM calcium chloride ($CaCl_2$) in potassium chloride (150 mM; $HiCa^{+K}$). Pre- and post-shear conditioning $SS_{0.3}$:EI_{max} of grouped subsets of RBC suspensions incubated with A23187 and 0.5 (LoCa) or 5 μM $CaCl_2$ (HiCa) was altered (B) in dependence of their respective mean ± s.d. of the mean cell volumes (MCV); note that the $SS_{0.3}$:EI_{max}-data (Y-axis) is presented on a log_{10}-scale (B, C). LoCa and HiCa RBC showed improved global cell deformability when MCV was higher and vice versa. N = 8 (mean ± SEM); significant differences between linked variables: $^{****}P < 0.0001$, $^{***}P < 0.001$, $^{**}P < 0.01$, $^{*}P < 0.05$. Global cell deformability expressed as a single parameter ($SS_{0.3}$:EI_{max}) is closely associated with the mean cell volume of the respective individual sample (C) irrespective of the prior treatment (i.e., Control, 2.5 μM A23187, 2.5 μM A23187 + 0.5 μM calcium chloride, 2.5 μM A23187 + 5 μM calcium chloride, 2.5 μM A23187 + 5 μM calcium chloride in KCl). N = 40; individual data was obtained by pooling the results of 8 distinct experiments wherein the samples were exposed to 5 different conditions. $R^2 = 0.998$, determined by non-linear regression curve-fit

4.4.5 Increased extracellular calcium has no effect on RBC deformability and MCV at stasis

When incubated with 2 mM extracellular $CaCl_2$ at stasis, RBC exhibited no alterations in the capacity to deform under a given shear (Fig. 31A) compared to control. Concurrent incubations with autologous plasma yielded a tendency for lower EI values at low shear (1.65 Pa) which, however, was not statistically significant. $SS_{0.3}$:EI_{max} ratio tended to increase in plasma- and $CaCl_2$-incubated RBC (Fig 31B), albeit no statistically significant differences were observed. Accordingly, a tendency for decreased MCV was observed in RBC incubated with plasma when compared with control RBC (Fig. 31C) and RBC incubated with $CaCl_2$.

4.4.6 RBC sheared in calcium-rich suspensions exhibit progressively improved cell deformability accompanied by haemolysis

When RBC were exposed to a constant shear (10 Pa) over prolonged durations (300 s), the presence of Ca^{2+} in the shearing medium induced a significantly reduced EI upon the commencement of the shearing protocol (Fig. 31D). Over time, however, the cell population appeared to exhibit progressively improved capacity to deform under shear, represented by the increasing EI. While RBC suspensions previously incubated with $CaCl_2$ (2 mM) or autologous plasma exhibited a similar increase in EI over the duration of shearing protocol, RBC sheared in Ca^{2+}-free medium presented with a constant EI.

RBC suspensions previously incubated in either glucose solution (Control) or $CaCl_2$ (Calcium) exhibited no haemolysis in response to physiological-level shear exposure (10 Pa for 300 s; Fig. 31E). When $CaCl_2$ (2 mM) was added to the shearing medium (PVP), however, ~30% of RBC ruptured in response to the same shear conditioning protocol, releasing free haemoglobin into the supernatant. Cell suspensions previously incubated with plasma exhibited significant haemolysis post-shear conditioning (~25% of RBC lysed), albeit less when compared with the other conditions.

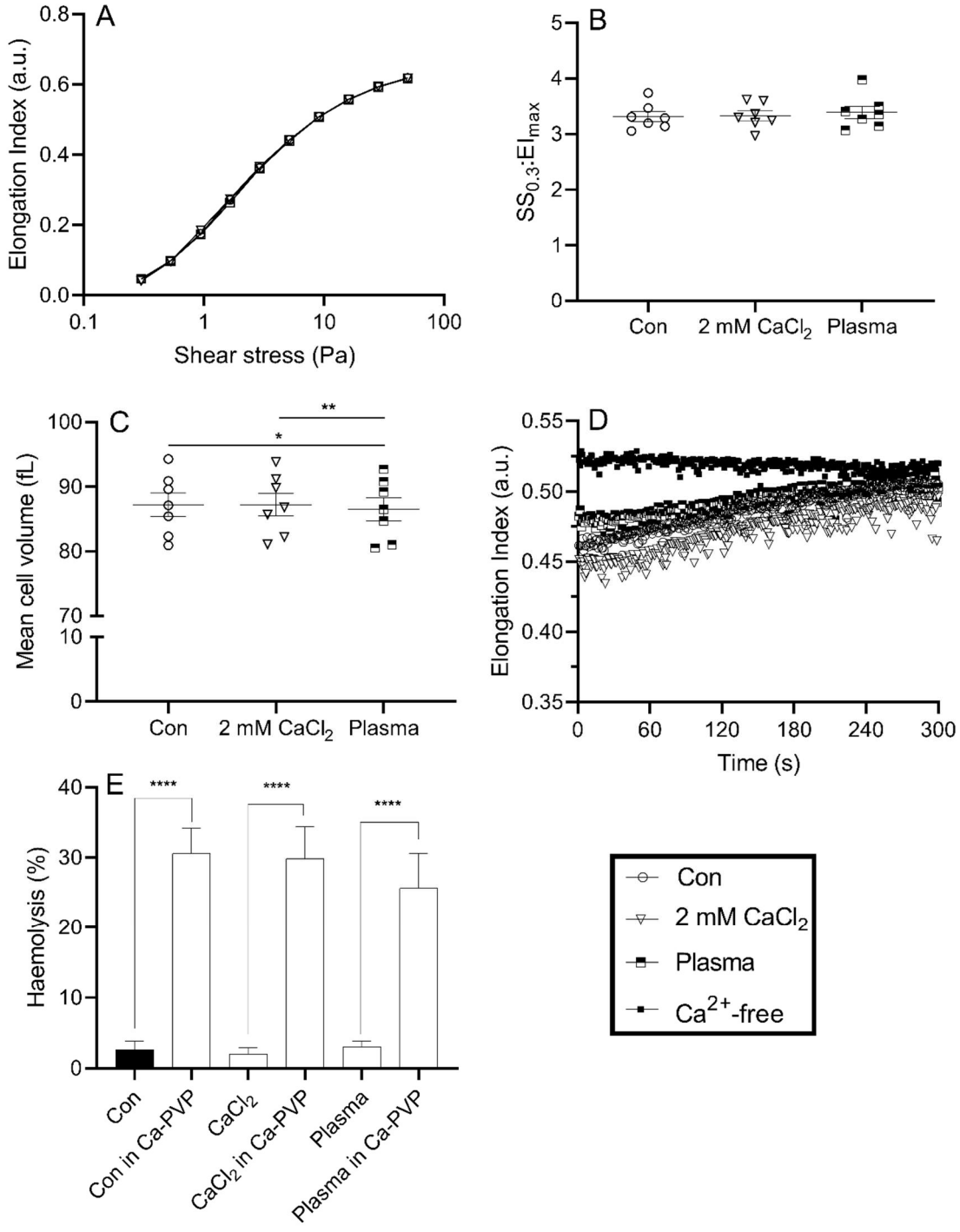

***Fig. 31**: Red blood cell deformability (RBC) and mean cell volume (MCV) in response to increased extracellular calcium-concentration are altered under shear. Elongation index (EI) for a given shear stress was assessed in RBC suspensions that were incubated with isotonic saline (Control; circles), plasma-equivalent levels of calcium chloride ($CaCl_2$; inverted triangle) or autologous plasma (half-shaded squares) at 37°C (A). Global deformability ($SS_{0.3}$:EI_{max}) was unaltered between the conditions (B). MCV showed some changes when RBC were pre-incubated with plasma (C). Deformation of RBC sheared in calcium-free medium (closed squares) remained constant, while deformation of RBC*

sheared in a calcium-rich medium (circles) increased over time (D). Moreover, elongation of RBC previously incubated in 2 mM calcium chloride ($CaCl_2$; inverted triangles) or autologous plasma (half-shaded squares) also increased over time (D). Free haemoglobin concentration, the primary marker of red cell destruction (i.e., haemolysis; E), in suspensions exposed to 10 Pa shear stress in calcium-rich media (Control in Ca-PVP, Calcium in Ca-PVP, Plasma in Ca-PVP) was significantly increased compared to calcium-free (Control in PVP, Calcium in PVP, Plasma in PVP). N = 8 (mean ± SEM); significant differences between linked variables: $^{***}P < 0.001$, $^{**}P < 0.01$, $^{*}P < 0.05$ determined by one-way ANOVA (B, C) or two-tailed t-test (E).

Global cell deformability, expressed as $SS_{0.3}$:EI_{max} ratio, improved following shear exposure by 31% (Control), 27% (2 mM Calcium) and 30% (Plasma), respectively (Fig. 32).

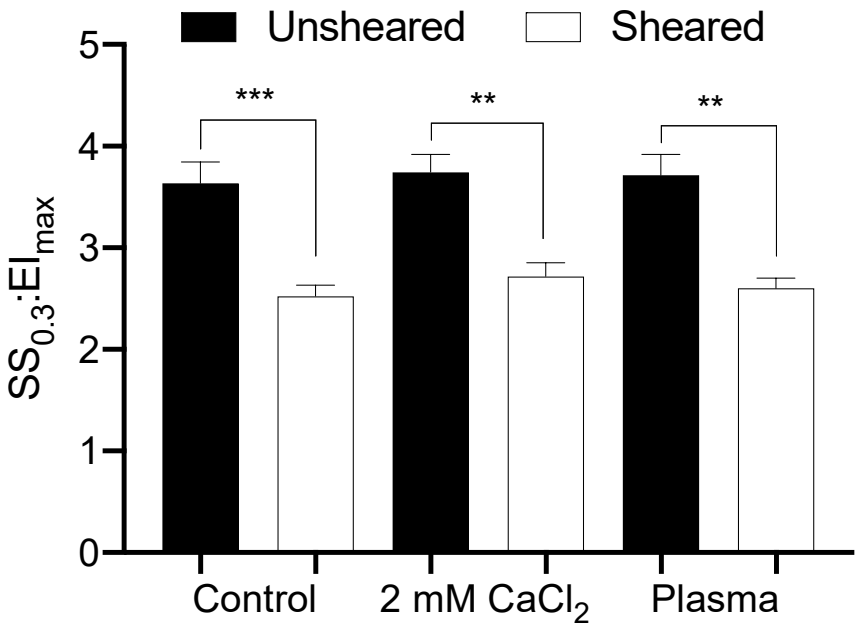

***Fig. 32**: Red blood cell (RBC) deformability is improved after shear conditioning in high calcium media. Cellular deformability (expressed as $SS_{0.3}$:EI_{max}) of RBC suspensions previously incubated with 2 mM calcium chloride ($CaCl_2$) or autologous plasma improved after shear conditioning at 10 Pa for 300 s in a shear medium that also contained 2 mM $CaCl_2$. N = 8 (mean ± SEM); significant differences between linked variables: $^{***}P < 0.001$, $^{**}P < 0.01$, $^{*}P < 0.05$*

4.5 Discussion

The salient findings of the present study indicate that $[Ca^{2+}]_i$ in RBC contributes to regulation of cellular deformability through shifts in cell volume facilitated by a potassium-gradient, most likely involving the 'Gárdos channel'. Indeed, increases in $[Ca^{2+}]_i$ propagated significant impairments in cellular deformability only when accompanied by a decrease in MCV (Fig. 30C). This response was entirely abrogated when the potassium-gradient across the cell membrane was removed (Fig. 29), which confirms prior independent findings [40, 183]. Further, we observed that exposure of RBC with profoundly decreased cell volume – independent of Ca^{2+}-loading – to physiological-levels of shear stress exacerbated impaired cell deformability, while RBC with less profoundly decreased volume exhibited improved cellular deformability (Fig. 30B). Thus, the results of the current study provide evidence to support that Ca^{2+}-related impairment of RBC deformability is primarily caused by decreased cell volume facilitated by loss of intracellular fluid due to the 'Gárdos effect' [94, 192], rather than alterations in membrane flexibility, as previously proposed [25, 90, 93] – at least under the acute conditions presented in the current study. Moreover, we found that the presence of $[Ca^{2+}]_e$ augments cellular deformability only under shear, indicating that a mechanically-activated process facilitates flux of Ca^{2+} across the RBC membrane. Collectively, the present data indicate that Ca^{2+} contributes to acute regulation of cellular deformability by altering cell volume, which profoundly

affects the physical properties of RBC by increasing cytosolic viscosity and decreasing cell size. The behaviour of RBC was found to be fundamentally altered when investigated in flow rather than at stasis, which highlights the significance of conducting experiments that reflect *in vivo* conditions of flow, and the complex molecular machinery present in these cells.

Increasing $[Ca^{2+}]_i$ using A23187 induces a decrease in RBC deformability when measured using ektacytometry [40, 183]. This impairment is obvious when studying the capacity of RBC populations to deform under a given shear (Fig. 29A). The observation that RBC exhibit a reduced capacity to elongate under higher shears (>5 Pa), while retaining the ability to deform under lower shears (<5 Pa) may indicate that RBC with reduced MCV are limited by their size rather than a rigidification of the membrane [193]. With intact capacity to deform under shears <5 Pa (Fig. 29A), which RBC are primarily exposed to in larger vessels – e.g., brachial artery: ~1 Pa [194], conjunctival pre-capillary arterioles: ~2 Pa [182] – bulk blood flow containing low-MCV RBC should not be altered. That is, given cellular deformability under these physiological shears is essential for optimal flow as flexible cells are more likely to orientate with flow and migrate from the vessel wall, alterations in cell orientation and axial migration are not expected to occur even when a substantial portion of RBC has been exposed to excess $[Ca^{2+}]_i$ [51].

Increased $[Ca^{2+}]_i$ was associated with decreased MCV in a dose-dependent manner; however, upon addition of 150 mmol·L^{-1} extracellular KCl, increased $[Ca^{2+}]_i$ had no effect on MCV (Fig. 29C). These observations are in agreement with the hypothesis that upon entry of Ca^{2+} into RBC, the Ca^{2+}-sensitive potassium channel (i.e., Gárdos channel) is activated, which facilitates K^+-loss, followed by water [14, 40, 195]. When the potassium gradient that is present in whole blood between RBC (~100 mmol·L^{-1}) and plasma ~5 mmol·L^{-1} [38] is abrogated (i.e., raising the extracellular concentration of K^+ to >100 mmol·L^{-1}), opening of the Gárdos channel no longer results in efflux of K^+ or water. Thus, although Ca^{2+} enters the RBC, MCV and cellular deformability are unaffected (Figs. 29, 30), at least in the acute conditions presented herein. Potential adverse chronic effects may arise with a temporal delay for example due to the presumably compacted cytoskeleton during loss of intracellular fluid or alterations in membrane fluidity mediated by lipid asymmetry (e.g., exposure of phosphatidylserine on the outer membrane leaflet [196]). These potential chronic effects notwithstanding, it appears that acute Ca^{2+}-loading does not affect global deformability as quantified using ektacytometry in the absence of altered hydration status. Given that the herein presented experiments served to characterise the mean response of a heterogenous cell population (i.e., ektacytometry and cell counts using the coulter principle assess >1,000,000 cells), investigations into these effects on a single-cell level are warranted.

Cell suspensions with increased $[Ca^{2+}]_i$ were subjected to a continuous shear conditioning protocol (10 Pa for 300 s) previously reported to trigger a temporary improvement of cellular deformability [162, 189]. Elongation of RBC throughout the continuous shear conditioning protocol (10 Pa for 300 s), which represents the upper level of the physiological shear range – shear stresses in larger arteries are estimated to range from 1-7 Pa [197], while shears in the microvascular capillaries (e.g., vessels in the retina) may peak around 15 Pa [182] – remained constant (Fig. 29D). Following shear conditioning, RBC incubated with A23187 and control RBC presented with significantly improved cellular deformability, as reported before for healthy RBC samples [162]. Given that RBC were incubated with A23187 and $CaCl_2$ prior to the shearing procedure and subsequently washed, it is unlikely that A23187 is still retained in the cell membrane at this point. Previous reports have proposed both Ca^{2+} and NO as potential mediators of the temporary improvement observed after mechanical stimulation of RBC with physiological-level shear stress (≤ 15 Pa; [76, 162, 189, 198]). NO in RBC may be produced enzymatically by RBC-NOS3, which is known to be activated by mechanical stimulation and increasing $[Ca^{2+}]_i$ [27, 28, 76]. Thus, the observed beneficial effects of physiological-level shear conditioning may be mediated by increased RBC-NOS3 activation and subsequent NO-production. While mechanical stimulation increased cell deformability in control conditions, RBC loaded with intracellular Ca^{2+} using A23187 presented with a non-linear response relative to resting values (Fig. 30B). A23187 mediates entry of Ca^{2+} into the cell

through the electroneutral exchange with two protons (H^+; [16]). The loss of H^+ is equilibrated by the also electroneutral Jacobs-Stewart mechanism in combination with the CO_2 shunt, co-transporting H^+ and Cl^- in exchange for HCO_3^- *via* anion exchanger 1 (for a detailed description, see [199]). It is thought that A23187 facilitates ion-transport until equilibrium is achieved (i.e., intracellular [Ca] = extracellular [Ca]); therefore, $[Ca^{2+}]_i$ should be approximately 0.5 μM and 5 μM when incubated with these concentrations of extracellular $CaCl_2$ in the present study, given that $CaCl_2$ dissociates rapidly in water to form 2 Cl^- and Ca^{2+}. We acknowledge, however, that $[Ca^{2+}]_i$ was not measured directly in this study, thus leaving the possibility that a very small level of residual extracellular free Ca^{2+} (or complexed with EDTA) remained, which would be consistent for all conditions. Nevertheless, the extensive washing procedures employed would certainly have diminished the level of residual native Ca^{2+}, prior to addition of $CaCl_2$ and A23187. This 10-fold difference in intracellular Ca^{2+}-availability notwithstanding, it appears that the resultant decrease in cell volume dictates deformability of the RBC population (Fig. 30C) and also the sensitivity to mechanical stimulation (Fig. 30B). That is, RBC with a lower MCV, irrespective of intracellular [Ca], exhibit impaired deformability post-shear; however, cellular deformability of RBC populations with a higher MCV may be improved by mechanical stimulation. It is yet to be elucidated whether this increased sensitivity to shear with decreased cell volume also occurs when cell volume is altered by Ca^{2+}-independent mechanisms.

When RBC were exposed to physiological shear conditioning in a medium that contained plasma-equivalent [Ca^{2+}] (2 mmol·L^{-1} $CaCl_2$), deformation of the cell populations increased over time in a linear manner (Fig. 31D). Mechanical stimulation, specifically exposure to shear stress in the physiological range (≤15 Pa), is known to promote permeability of RBC to cations [200, 201]. The presence of Piezo1, a mechanosensitive cation-channel, is linked to RBC volume regulation and microvascular transit [18, 45]. It is thus plausible to hypothesise that Piezo1 opens in RBC sheared in the presence of $CaCl_2$ in the shear medium to facilitate Ca^{2+}-influx, altering cellular deformability. Conversely, while increasing $[Ca^{2+}]_i$ impairs RBC deformability (Fig. 29A, B), elongation increased over the shear conditioning protocol (Fig. 31D). We observed, however, that significant haemolysis occurred after the shear conditioning protocol, despite the employed magnitude-duration of shear being well-below the reported haemolytic and even sub-haemolytic thresholds [148, 202]. It appears that shear-induced uptake of Ca^{2+} triggered progressive haemolysis, which produced an altered cell population with improved physical properties (Fig. 32). Supraphysiological shear stress exposure is known to induce "preferential" haemolysis; that is, more susceptible RBC sub-populations rupture first, which probably had impaired physical properties in the first instance (e.g., RBC approaching senescence [21]). Similarly, haemolysis may occur due to increased shear sensitivity and overactivation of the Gárdos channel, followed by irrecoverable water loss. Dehydrated RBC, as present in sickle cell anaemia patients, have been shown to

be destroyed by low shear exposure in these patients, induced either *in vivo* through exercise or *in vitro* using a cone-and-plate viscometer [203]. The significant improvement in RBC deformability following shear exposure in high-Ca^{2+} media is thus likely induced by selective destruction of a more susceptible fraction of the original RBC population, potentially characterised by reduced cell volume and deformability [204], leaving behind a cell population with 'improved' properties [148, 149, 161].

4.6 Conclusion

Collectively, the results of the present study indicate that global cell deformability may be acutely modulated by Ca^{2+}. While in the present study, direct quantification of $[Ca^{2+}]_i$ was not performed, and indeed microscopic calcium-precipitation may have occurred in the presence of phosphates, the dose-response observed in impaired biophysical measurements per change in Ca^{2+} loading supports the primary aims of the study. It indeed appears that the primary mechanism of Ca^{2+}-regulated RBC deformability are shifts in cell volume facilitated by the Gárdos channel. Loss of intracellular fluid increases cytosolic viscosity and decreases cell size, which specifically impairs the capacity of RBC to deform under shears >5 Pa, confirming previous reports [193, 205]. Shear stress of this magnitude is common in the microcirculation and altered deformability may impact tissue perfusion and plasma skimming effects, ultimately affecting

oxygen delivery [52]. Physiological levels of shear exposure may also lead to premature clearance of RBC by facilitating entry of Ca^{2+}, which has profound effects on the bulk flow behaviour of the remaining sub-population. Further investigations into whether the association of cell volume and deformability holds true on a single cell-level are required. Moreover, molecular targeting of the interplay between Ca^{2+}-entry under shear (e.g., Piezo1) and down-stream targets (e.g., Gárdos channel) is of interest to develop drugs that may correct dysfunctional volume regulation in patients with sickle cell anaemia, hereditary xerocytosis or spherocytosis.

4.7 Supplementary material: Calcium dynamically alters erythrocyte mechanical response to shear

4.7.1 Supplementary methods

RBC populations presented with a significantly impaired capacity to deform under moderate to high shears (i.e., >1 Pa), which resulted in a significant reduction in EI_{max}. EI_{max} is calculated using a modified version of the Lineweaver-Burk equation [25]. Global RBC deformability is commonly expressed as the ratio of the shear stress required to induce $SS_{1/2}$ over EI_{max}. The robustness of this model was originally explored and validated when either the whole RBC population was rigidified, or part of the cell population was exposed to high concentrations of a rigidifying agent [160]. The EI-SS curves in the present study, however, were congruent at low shear (i.e., <1 Pa), while EI was significantly decreased at higher

shears (>1 Pa; Fig. 29A). Non-linear regression indicated that the global parameter of $SS_{1/2}$ was decreased, signifying improved deformability (Fig. 35) in RBC populations with obviously impaired capacity to deform (at least under shears >1 Pa). EI_{max} was found to adequately represent the respective EI-SS curves (Fig. 35B), showing a significant decrease in conditions of high cytosolic Ca^{2+}-loading and impaired capacity to deform under shears >1 Pa. Given that the $SS_{1/2}$ parameter is derived from the EI_{max} extrapolated for each individual curve during non-linear regression analysis, an EI_{max} of 0.4 (5 μM $CaCl_2$; Fig. 29A), for example, would yield the shear stress required to induce half of EI_{max} of 0.2 (i.e., the $SS_{1/2}$ parameter). The resultant $SS_{1/2}$ is thus paradoxically low, specifically in RBC populations with impaired capacity to deform under shears <1 Pa, as determined from the EI-SS curves, compared to the SS1/2 values obtained for normal healthy cells, owing largely to the superior EI_{max} (Fig. 29A). It follows that $SS_{1/2}$ is deceptively low (i.e., in general indicating improved cell deformability) in RBC populations with dramatically decreased EI_{max} because $SS_{1/2}$ is determined based on the individual EI_{max} of the respective EI-SS curve, rather than an independent reference value. Thus, it was required to find an appropriate comparison between the cell populations with extreme differences in cell volume that is not dependent upon the individual EI_{max}. We used the mean EI measured at 50 Pa (i.e., $EI_{50\ Pa}$ = 0.602; refer section *2.4 RBC deformability measurements*) of all 'control' samples assessed in the current study as a reference point reflecting 'baseline' RBC property and calculated the shear stress required to achieve half of $EI_{50\ Pa}$ (termed

'$SS_{0.3}$'; the shear stress to induce EI = 0.3) based on the curve-fit obtained from the Lineweaver-Burk equation. Global deformability of RBC samples with dramatic volume shifts is thus presented as the ratio of $SS_{0.3}$ of the individual samples to their respective EI_{max}. Using this modification, we obtained parameters of global RBC deformability, which more adequately represent the alterations in the raw EI-SS curves, when compared with the conventional method [25]. We propose the analysis presented herein to be used in specific cases, where EI-SS curves differ significantly in high-shear deformation, to correct for resultant deceptively decreased $SS_{1/2}$-values (Fig. 36).

4.7.2 Supplementary figures

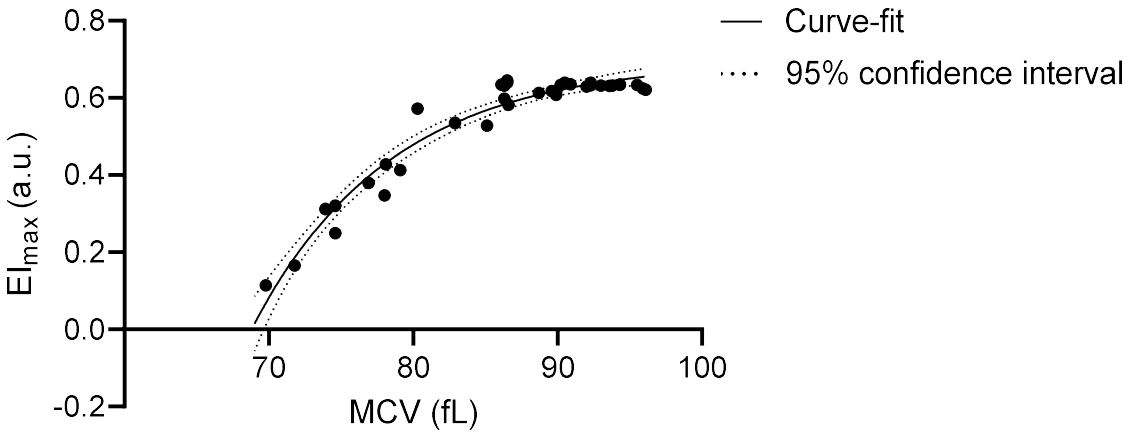

***Fig. 33**: Maximal theoretical elongation (EI_{max}) of individual red blood cell (RBC) samples plotted against the corresponding mean cell volume (MCV), irrespective of the prior treatment (i.e., Control, 2.5 μM A23187, 2.5 μM A23187 + 0.5 μM calcium chloride, 2.5 μM A23187 + 5 μM calcium chloride, 2.5 μM A23187 + 5 μM calcium chloride in KCl). N = 40 individual data was obtained by pooling the results of 8 distinct experiments wherein the samples were exposed to 5 different conditions. R^2 = 0.955.*

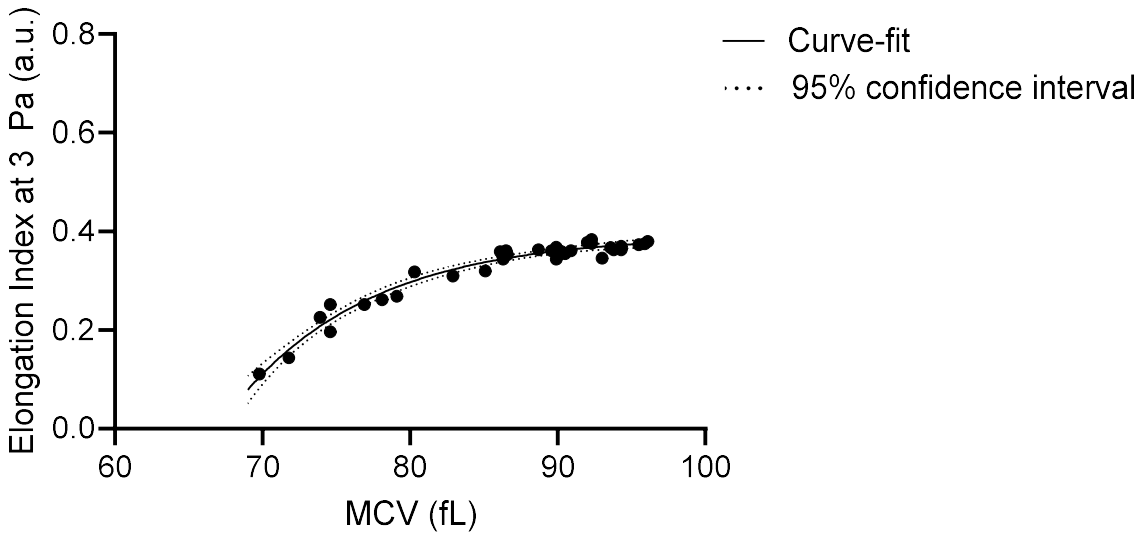

***Fig. 34**: Elongation index (EI) of red blood cell (RBC) suspensions measured at 3 Pa plotted against the corresponding mean cell volume (MCV), irrespective of the prior treatment (i.e., Control, 2.5 µM A23187, 2.5 µM A23187 + 0.5 µM calcium chloride, 2.5 µM A23187 + 5 µM calcium chloride, 2.5 µM A23187 + 5 µM calcium chloride in KCl). N = 40; individual data was obtained by pooling the results of 8 distinct experiments wherein the samples were exposed to 5 different conditions. $R^2 = 0.962$.*

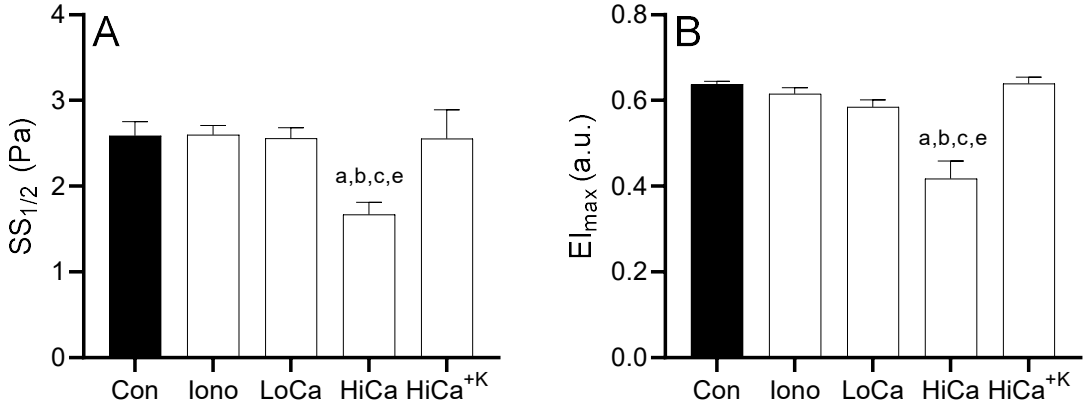

***Fig. 35**: Global parameters representing cellular deformability (i.e., $SS_{1/2}$, A; and EI_{max}, B) were sensitive to high calcium loading, which was abrogated in the presence of potassium. N = 8 (mean ± SEM). Significantly different (P < 0.05) compared to [a]Control (Con), [b]2.5 µM A23187 (Iono), [c]0.5 µM $CaCl_2$ (LoCa), or [e]5 µM $CaCl_2$ in KCl ($HiCa^{+K}$) determined by one-way ANOVA. Note: for clarity sake, no designation for [d], as HiCa was different to all others.*

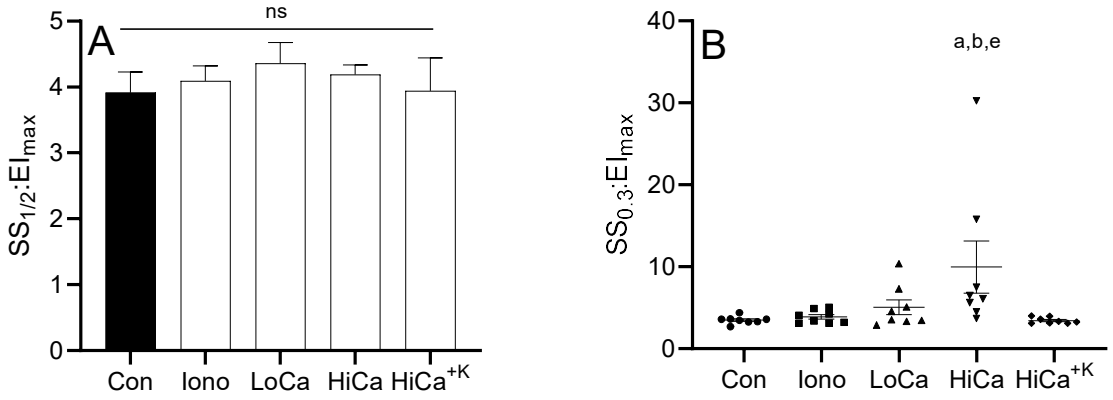

***Fig. 36**: The parameters obtained from curve-fitting the raw elongation index-shear stress (EI-SS) curves in the present study using the conventional (A) and currently proposed (B) methods. N = 8 (mean ± SEM). Significantly different (P < 0.05) compared to [a]Control (Con), [b]2.5 µM A23187 (Iono), or [e]5 µM $CaCl_2$ in KCl ($HiCa^{+K}$) determined by one-way ANOVA (A) or non-parametric Friedman-test (B). Note: no designation for [c] or [d], although the designations were kept consistent for all supplementary material.*

4.8 Results of Study 2 in the context of the present dissertation

The results obtained in *Study 2* indicate that the acute effect of Ca^{2+}-entry on the physical properties of RBC is mediated by altering cell volume *via* the Gárdos effect, which may be initiated by exposure to shear stress. While we were unable to find evidence for any acute membrane-associated effect of Ca^{2+}, it is plausible to hypothesise that – given the plethora of pathways activated by Ca^{2+} [47] – failure to maintain or return to low basal $[Ca^{2+}]_i$ may adversely impact the RBC membrane, as occurs during *in vivo* ageing.

The observation that physiological-level shear stress in presence of extracellular $CaCl_2$ resulted in selective destruction of RBC supports the impact of the distinct sub-populations that comprise a given RBC population on blood physical properties on a population-level. It is plausible to hypothesise that RBC with unfavourable characteristics (i.e., physiologically 'old' RBC) were preferentially removed, thus improving cell mechanics of the 'surviving' cell population, given the impact a small population of rigid RBC may have on overall blood fluid properties (*Study 1*). It is possible that the acute Ca^{2+}-overload, induced by shear-mediated Ca^{2+}-uptake may play a role in the removal of aged RBC *in vivo*, wherein the role of Piezo1 should be of considerable interest.

Chapter 5

Study 3: Distinct calcium-handling of density-separated human erythrocytes in response to mechanical shear

Lennart Kuck, Jason N. Peart, Michael J. Simmonds

Chapter 5 contains works conducted as part of the present doctoral program and is presented in journal article form, intended for future publication. My contributions to this paper include concept and experimental design, data collection, data analysis and interpretation, manuscript development.

5.1 Preface

Studies aimed at assessing distinct sub-populations of RBC date back several decades [26, 204, 206], following the development of separation techniques based on RBC density. It has long been established that RBC ageing is accompanied by densification, a phenomenon thought to be driven by entry of Ca^{2+} and cell volume loss *via* the Gárdos effect (please refer to Chapter 1.3). The discovery of Piezo1 in RBC membranes by the Patapoutian lab [45] has prompted several lines of investigation to decipher its physiological significance. It is currently hypothesised that Piezo1 is responsible for acute volume shifts of RBC in response to mechanical force and/or membrane deformation ([18]; *Study 2*), which may aid capillary transit and traversal of the narrow interendothelial slits of the spleen. It is also suggested that Piezo1-induced entry of Ca^{2+} modulates cell deformability by altering membrane dynamics [207], although this was not observed in the present dissertation (*Study 2*). Computational studies suggest that repeated Piezo1-mediated Ca^{2+}-entry during traversal of narrow capillaries dictates RBC circulatory longevity [20, 38] and it is hypothesised that Piezo1 plays a role in the terminal removal of aged RBC [35, 208]. In light of the earlier findings reported here, which characterised the significance of RBC sub-populations with abnormal properties to blood flow (*Study 1*) and elucidated the dynamic effects of increased $[Ca^{2+}]_i$ on RBC mechanics (*Study 2*), the following series of experiments was designed to assess Piezo1-function in density-

separated RBC sub-populations that reflect cells at different stages of their circulatory life cycle.

5.2 Introduction

The elasticity of RBC, enabled by a concave disc-geometry, viscoelastic cell membrane, and a cytosolic viscosity higher than that of the suspending plasma, facilitates their traversal of the cardiovascular system, which may continue for 120 days [6, 51]. While these properties contribute to minimising the internal resistance of blood to flow in wider arteries, the unique capacity of RBC to reversibly deform is required for capillary passage, where vessels may be narrower (~2 μm) than the RBC itself (~8 μm). During the ~120 days of vascular transit, RBC undergo a progressive decline of metabolic function, culminating in splenic removal by macrophages [31, 204, 209]. Novel observations suggest that attachment of RBC to the red pulp of the spleen is a preliminary step in the process of removal; indeed, it appears that the formation of ghosts (i.e., release of cytosolic contents due to membrane rupture) precedes phagocytotic digestion of the remaining membrane components [35, 208]. During attachment, RBC are exposed to prolonged fluid shear, which is unusual compared with the transient and dynamic mechanical stresses experienced during normal circulation. The interaction between RBC and mechanical stimuli, including fluid shear stress, was thought to be purely physical: the elasticity of the RBC membrane and excess

surface area relative to cell volume allow for reversible deformation under shear. Recent advances, however, support the emergence of additional, biochemical effects: it appears that RBC also respond to mechanical cues with activation of cellular signalling pathways [7, 50]. The anatomical architecture of the spleen provides a unique stimulus of prolonged, low-level mechanical force to attached RBC, which is unlike the intermittent exposure to mechanical deformation during capillary transit.

Mechanical forces have recently re-emerged as vital cues involved in the regulation of diverse biological mechanisms ranging from early development and cell fate determination to cellular homeostasis, differentiation, and apoptosis (for a recent review, see [210]). Mechanotransduction, the translation of physical forces into biochemical signalling, is commonly initiated by mechano-sensors, such as ion channels. Enucleated RBC express the *bona fide* mechanosensory protein Piezo1, which appears to transduce mechanical cues through influx of Ca^{2+}, and is implicated in RBC volume regulation and nitric oxide metabolism [18, 45, 211]. This discovery has contributed to a step-change in understanding of RBC physiology, providing support to the hypothesis that relevant and active post-translational signalling networks are present in enucleated, mature RBC.

Given erythroid pre-cursor cells eject the nucleus and other organelles, leaving mature erythrocytes devoid of mitochondria, and thus unable to generate energy through oxidative phosphorylation, the reliance of RBC-ATP production solely

on glycolysis severely limits metabolic capacity [212]. Moreover, RBC are not equipped with the translational machinery required to resynthesise essential proteins, rendering the process of cellular aging irreversible. As a result, physiologically-aged RBC exhibit decreased cytosolic ATP-levels, metabolic flux, and PMCA-capacity [11, 15, 213, 214] when compared with their 'younger' counterparts. Given the large difference in $[Ca^{2+}]$ between the RBC cytosol (30-90 $nmol \cdot L^{-1}$) and the suspending plasma (1-2 $mmol \cdot L^{-1}$), opening of cation channels results in significant spikes of Ca^{2+}-influx. Entry of Ca^{2+} thus places metabolic strain onto these cells [16, 17, 92], since transport of Ca^{2+} against this concentration gradient *via* PMCA1 is metabolically expensive. Consequently, owing to the fact that aged RBC present with limited metabolic function, it may be that impaired calcium-handling results in diminished capacity to resist significant challenges of increased $[Ca^{2+}]_i$; however, experimental evidence to support this hypothesis is scarce.

Ageing of RBC results in a progressive increase in density, which allows for separation of RBC sub-populations [26]. This densification is primarily attributed to the Gárdos effect, driven by an accumulation of $[Ca^{2+}]_i$ due to repeated spikes of increased $[Ca^{2+}]_i$ during each capillary transit [14, 20, 215]. Increases in $[Ca^{2+}]_i$ activate the calcium-activated potassium channel $K_{Ca}3.1$ (i.e., the 'Gárdos channel'), which is highly sensitive to subtle increases in $[Ca^{2+}]_i$ (~1 μM activation threshold; [47]). Activation of the Gárdos channel results in K^+-efflux that causes

loss of volume due to local osmotic gradients; a well-reported phenomenon referred to as the 'Gárdos effect'. While recent computational studies provide compelling evidence to support that Piezo1 is involved in regulating circulatory longevity of RBC [20], and indeed drive their ageing patterns [19], experimental evidence has not yet been provided. Thus, the aim of the current study was to i. separate the distinct RBC sub-populations of distinct physiological ages; ii. investigate the sensitivity of light, middle, and dense RBC to mechanical forces in presence of absence of Ca^{2+}; and iii. assess Piezo1-function in light, middle, and dense RBC.

5.3 Materials and methods

5.3.1 Blood sample collection

Participants were healthy, male volunteers, reportedly free of any known cardiovascular, pulmonary, endocrine or metabolic diseases. Moreover, participants had not provided a large-volume blood donation (i.e., 450 mL) within the last 3 months, and were not taking any medication. Written consent was obtained after educating the participants about the risks and benefits involved in contributing a blood sample to the current study. Blood samples were extracted from a prominent vein in the antecubital region of the arm. The blood draw was performed within 90 s of applying a tourniquet to the upper arm, using a sterile needle and syringe. Blood was immediately transferred into a vacuum-

sealed tube coated with ethylenediaminetetraacetic acid (1.8 mg·mL^{-1}). The experimental procedures were reviewed and approved by the Human Research Ethics Committee of Griffith University (Gold Coast, Australia), and are in line with the Declaration of Helsinki. All experimental procedures were carried out within 6 h of blood collection.

5.3.2 Sample processing and density separation of erythrocyte sub-populations

White blood cells, platelets (i.e., buffy coat) and plasma were separated from RBC by centrifugation at 1500 × *g* for 10 minutes. Isolated RBC were then washed with an isotonic PBS solution supplemented with BSA (0.8 g·mL^{-1}) and 5 mmol·L^{-1} glucose (GASP; pH = 7.4 ± 0.05, 290 ± 5 mOsmol·kg^{-1}) and centrifuged at 1500 × g for 5 minutes. This washing procedure was repeated twice, before the isolated RBC were resuspended 1:1 in a serum albumin-HEPES buffer (SAH; pH = 7.1 ± 0.05, 26 g·L^{-1} albumin) and layered upon a gradient of Percoll®-SAH mixtures of distinct densities (1.07, 1.075, 1.08, and 1.085 g·ml^{-1}). Separation was achieved by centrifugation at 3260 × *g* for 40 minutes at room temperature as previously described [24]. Three distinct RBC sub-populations were isolated based on their densities (Fig. 37A; 'dense', 'middle' and 'light' fractions; in the following referred to as 'young', 'middle' and 'old' RBC), washed with GASP-buffer and centrifuged at 1500 × *g* for 5 min. The supernatant was discarded, and isolated RBC sub-populations were used for further analyses.

5.3.3 Haematological analysis

Haematological parameters of isolated RBC sub-populations obtained from each fraction were analysed to confirm cell age, using an automated cell counter operating under the Coulter principle (DxH 500, Beckman Coulter, Brea, USA). The same device was also used to assess changes in mean cell volume (MCV) following exposure to prolonged mechanical shear.

5.3.4 RBC deformability

A rotational ektacytometer (LORCA, MaxSis, Mechatronics Instruments B.V., Zwaag, The Netherlands) was used to quantify cellular deformability, the details of which have been discussed elsewhere [156]. Briefly, this coaxial system consists of an outer cup rotating around a stationary inner bob, which enables precise control over applied shear rate and shear stress. RBC suspensions were submitted into the gap between the cylinders (300 μm), wherein cell suspensions were exposed to a range of shear stresses (0.3-50 Pa). A laser diffracts around the elongating RBC populations, producing an increasingly elliptical diffraction pattern, which is captured by a CCD video camera and analysed in real-time. An ellipse was fit to the resultant laser diffraction pattern, and the EI was calculated using length (a) and width (b) of the ellipse as follows: $EI = (a - b)/(a + b)$; with increasing deformation, resultant of increased shear exposure, EI also increases.

5.3.5 Shear conditioning of blood samples

Isolated RBC were resuspended in a viscous solution (PVP 360 kDa dissolved in PBS; pH = 7.4 ± 0.5, 290 ± 5 mOsmol·kg^{-1}, viscosity = 30 ± 0.5 mPa·s) at a haematocrit of 0.005 L·L^{-1}. For some experiments, the PVP solution also contained 2 mmol·L^{-1} $CaCl_2$, as specified. RBC suspensions in PVP were exposed to a discrete magnitude-duration combination of shear conditioning (i.e., total exposure of 10 Pa for 300 s) using the couette shearing device used to measure RBC deformability as described before [76, 162, 215]. The shear conditioning procedures were carried out at 37 ± 0.2 °C.

5.3.6 Quantification of free haemoglobin

Immediately following shear conditioning, RBC-PVP suspensions were collected from the cup of the shearing device. The supernatant was obtained through centrifugation at 3000 × *g* for 10 min and diluted in 0.01% Na_2CO_3 solution at a 1:1 ratio. Free haemoglobin was measured using the Harboe method [191]: absorbance was quantified at multiple wavelengths (380, 415, and 450 nm) using an automated plate-reader (FLUOstar Omega, BMG Labtech, Mornington, Australia). A 3-point correction was employed to filter noise caused by other haem-based products (e.g., bilirubin) and accurately reflect the concentration of oxy-Hb (Eq. 5). A negative control was prepared by lysing 0.005 L·L^{-1} RBC in

distilled H_2O, and haemolysis is expressed relative to the negative control to facilitate interpretation.

5.3.7 Live cell calcium-imaging

Changes in $[Ca^{2+}]_i$ upon stimulation with various agents that modulate the properties of the Piezo1 cation channel were monitored using Fluo-4 AM, the most appropriate intracellular fluorescent probe for Ca^{2+}-imaging in RBC [186]. Isolated RBC were washed three times with modified Tyrode's buffer (pH 7.35) supplemented with HEPES and glucose. Following the washing procedure, isolated RBC were loaded with 5 μM Fluo-4 at a haematocrit of 0.001 $L \cdot L^{-1}$ in the dark for 60 min at room temperature. Loaded RBC were then washed twice more with Tyrode's buffer, and subsequently suspended in the same buffer at a low haematocrit for imaging. After plating RBC onto coverslips, 15 min in the dark were allowed for the cells to settle, and for de-esterification of the dye. Individual RBC were then exposed to an argon laser (excitation λ = 488 nm / emission λ = 508 nm); at least four distinct areas on each coverslip were selected at random for image recording. Following capture of baseline fluorescent images, RBC were exposed to 15 μM of the Piezo1-specific activator Yoda1 for a total of 10 min on the coverslip. Immediately following exposure to Yoda1, images of one region of interest (ROI) were captured with a frequency of 0.067 Hz for 2 min. Images of

four randomly selected areas on the coverslip were then captured following 10 min of Yoda1-exposure, respectively.

5.3.8 Immunofluorescent detection of Piezo1

Following density fractionation and isolation of young, middle and old RBC sub-populations, autologous plasma was added to each RBC sub-fraction to produce a 0.4 $L \cdot L^{-1}$ cell suspension. Cell suspensions were then fixed in 4% PFA for 20 min as previously described [85], following which the PFA was removed by centrifugation at 300 × *g* for 3 min, and RBC were washed in PBS. Blood smears were prepared on glass microscope slides following further centrifugation at 300 × *g* for 3 min and resuspension in PBS. The glass slides were left to dry overnight and then exposed to heat using a laboratory burner to fix the cells onto the glass. A test area and a smaller control area were drawn onto each slide using a PAP pen (Sigma-Aldrich, Castle Hill, Australia). The slides were washed thrice using 0.1 M TBS (pH 7.6), prior to incubation with 0.1% Trypsin at 37°C for 30 minutes. Both areas were then blocked with 5% BSA, following which only the test area was incubated with diluted primary antibody (1:500; rabbit anti-Piezo1, Protein Group Inc., Rosemont, USA), while the control area was treated with only vehicle (5% BSA, 0.02% Tween®20). Slides were washed twice with TBS, blocked using 6% normal goat serum, and primary antibodies were detected with goat anti-rabbit secondary antibody (1:400 dilution; Alexa Fluor 568, Thermo Fisher,

Scoresby, Australia). Dehydration and removal of PAP pen was facilitated by short exposure of slides (3-5 s) to increasing concentrations of ethanol and xylenes. Purpose-mounting medium (Entellan®, Merck Pty Ltd, Bayswater, Australia) was used to facilitate coverslip attachment prior to imaging. Imaging of fluorescently-labelled Piezo1 was performed using an inverted microscope (IX73, Olympus Corp., Tokyo, Japan) with an integrated camera (optiMOS sCMOS, QImaging, Surrey, Australia) at 600-fold magnification.

5.3.9 Data analysis

Raw EI-SS curves were parameterised using a non-linear version of the Lineweaver-Burk equation as outlined in Baskurt et al. [160], adapted to most accurately represent mechanical properties of RBC with diverse cell volume [215]. Briefly, calculating the shear stress required for half-maximal deformation relative to the theoretical maximal deformation, which is limited by cell size, and thus cell volume, overestimates cellular deformability in these RBC populations. Instead, the shear stress required for half-maximal elongation of cells with abnormal mechanics is calculated relative to the maximal theoretical deformation of normal RBC. Fluorescent intensity of immunolabelled or Fluo-4-loaded RBC was determined using open-source software (FIJI version 1.53c [159], National Institutes of Health, Bethesda, MD). A minimum of 150 individual RBC were analysed for Fluo-4 mean fluorescent intensity, a minimum 100 individual cells

for the test areas of immuno-tagged Piezo1, and a minimum of 50 individual cells for the respective control areas not containing Piezo1-specific antibodies.

5.3.10 Statistical analysis

Results are presented as mean ± standard deviation (SD), unless stated otherwise. Differences in EI-shear stress curves were analysed using a two-way ANOVA. Distribution of data was tested for normality using the Shapiro-Wilk test. Depending on normality of distribution, differences between grouped means were determined using either a conventional one-way ANOVA with Dunnett's post-hoc test for multiple comparisons or a Friedman test. Commercial data processing software was used to conduct statistical analyses and curve-fitting procedures throughout (Prism, GraphPad Software Inc., Release 9.2.0, La Jolla, CA, USA).

5.4 Results

5.4.1 Density-separated sub-populations exhibit distinct cellular properties and distributions

Baseline haematological data of the three separated RBC sub-populations obtained from healthy donors and the respective unfractionated control RBC populations are presented in Fig. 37. While the middle RBC fraction presented with MCV that was comparable to that of the unfractionated control population,

the least dense fraction ('young' cells) of RBC exhibited slightly higher MCV, while the most dense fraction had significantly lower MCV ('old' cells; Fig. 37B, $P < 0.001$). No alterations in red cell distribution width (RDW) or red cell distribution width standard deviation (RDW-SD) were observed following separation of the distinct RBC sub-populations when compared with the unfractionated control cell population (Fig. 37C,D).

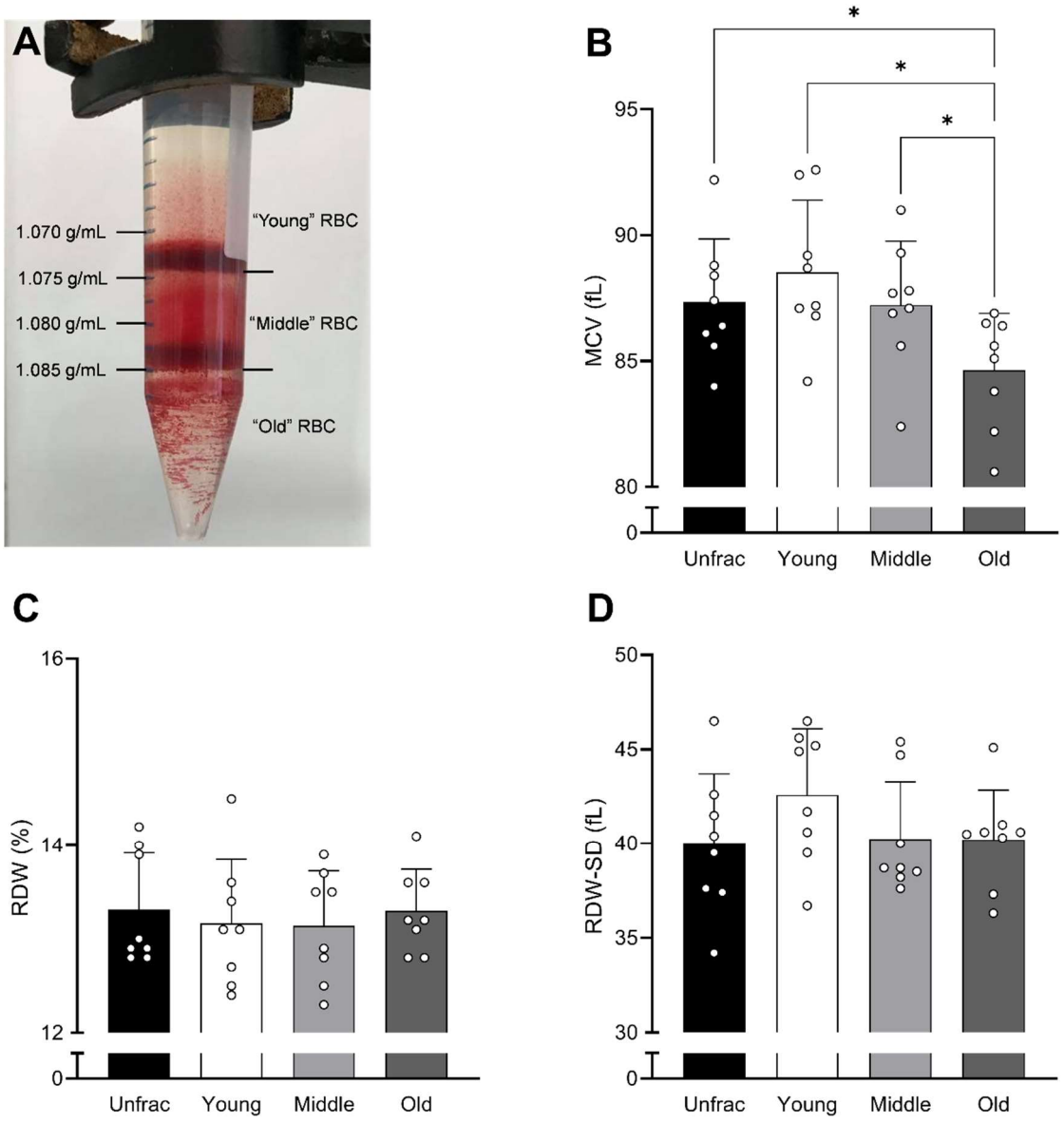

***Fig. 37**: Generation and characterisation of three distinct red blood cell (RBC) sub-populations based on distinct densities. A representative result of the density fractionation process is presented in A. Typically, two distinct bands were visible when separating RBC obtained from healthy donors; thus, RBC with densities of 1.075 g·mL^{-1} and lower were extracted and labelled as the 'young' cell fraction, RBC with densities between 1.080 and 1.085 g·mL^{-1} as the 'middle' fraction, and RBC with densities greater than 1.085 g·mL^{-1} were considered 'old' cells. Haematological characteristics of RBC sub-populations were assessed using an automated analyser (B-D). Data presented as means ± SD; N = 8*

5.4.2 Red blood cell sub-populations exhibit distinct mechanical properties during shear

Cellular deformability of the isolated RBC sub-populations was determined using a ramped shear stress protocol (0.3-50 Pa; Fig. 38). When assessed without $CaCl_2$ present in the shearing medium, the most dense ('old') RBC sub-fraction exhibited significantly decreased deformability under most shears when compared with the other cell populations ($P < 0.05$ for shears between 0.94-9.09 Pa; Fig. 38A). Following the shearing protocol (10 Pa for 300 s), deformability (reflected by the elongation index) was improved in all RBC populations when compared with unsheared cells, although old RBC remained significantly more rigid ($P < 0.05$ for shears between 0.94-9.09 Pa; Fig. 38B). Upon addition of $CaCl_2$, cellular deformability of all RBC populations was significantly blunted (Fig. 38C), which could be partly reversed following application of 10 Pa for 300 s, although old RBC remained less deformable than the other RBC sub-populations ($P < 0.05$ for shears between 0.94-5.15 Pa, and between 16.04-50 Pa; Fig. 38D).

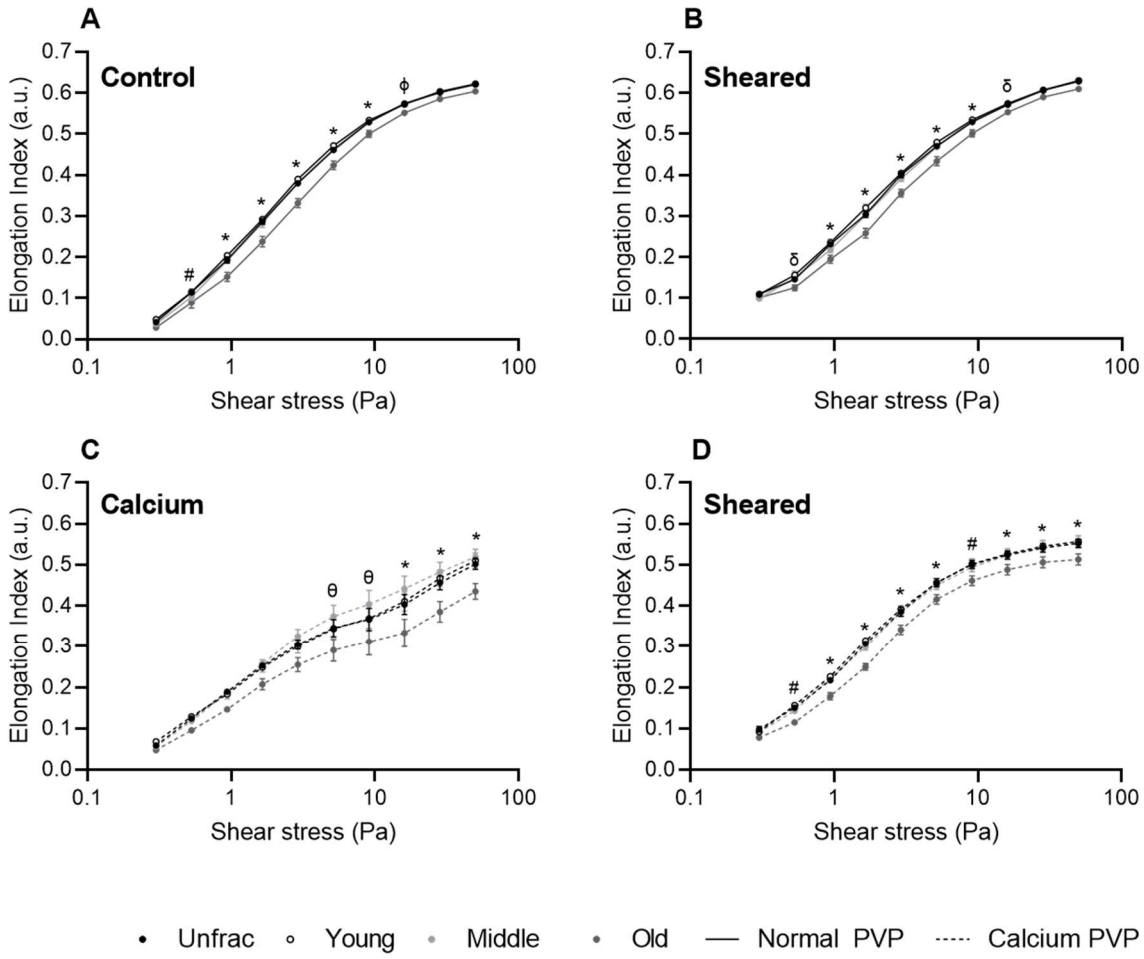

***Fig. 38**: The deformable capacity of red blood cell (RBC) sub-populations obtained from healthy donors , reflected by the elongation index (EI), was measured across ten distinct shear stresses. Deformability was assessed prior to (A, C) and immediately following (B, D) exposure to the shear conditioning protocol, which was conducted in isosmotic shearing media (A, B) or with the addition of 2 mmol·L^{-1} calcium chloride (C, D). Symbols indicate significant differences: $^{\#}$unfrac and young significantly different from old; $^{\Phi}$unfractionated and middle significantly different from old; $^{\delta}$young and middle significantly different from old; $^{\theta}$middle significantly different from old; *unfractionated, young, middle significantly different from old. Data presented as means ± SD; N = 8*

5.4.3 Non-random removal of dense erythrocytes during physiological-level shear stress exposure is dependent on calcium

Cellular deformability of RBC sub-populations significantly increased ($P < 0.05$; Fig. 39A-D) following stimulation with mechanical shear ('Post'), relative to unsheared baseline values ('Pre'). While baseline capacity of old RBC to deform under shear was lowest when compared with their young and middle counterparts (i.e., reflected by high values of $SS_{0.3}$:EI_{max}; A,B; and lowest values of EI; C,D), the improvement in overall cell deformability of the old RBC sub-population was most pronounced, in particular in presence of 2 mmol·L^{-1} $CaCl_2$. This latter improvement occurred in concert with significantly greater haemolysis when compared with that observed in the untreated, young, or middle RBC populations (Fig. 39F) and significantly increased MCV (Fig. 39G) following shear. Shear conditioning at 10 Pa for 300 s in absence of extracellular $CaCl_2$ precipitated only negligible amounts of haemolysis (<2%; Fig. 39E) across all RBC sub-populations. Accordingly, a weak, albeit statistically significant correlation ($R^2 = 0.16$, $P < 0.05$; Fig. 39H) was observed between haemolysis levels following shear conditioning without presence of Ca^{2+} and corresponding improvements in RBC deformability. In presence of 2 mmol·L^{-1} $CaCl_2$, however, spikes in haemolysis during shear were more strongly and significantly correlated with corresponding changes in $SS_{0.3}$:EI_{max} ($R^2 = 0.41$, $P < 0.0001$; Fig. 39I).

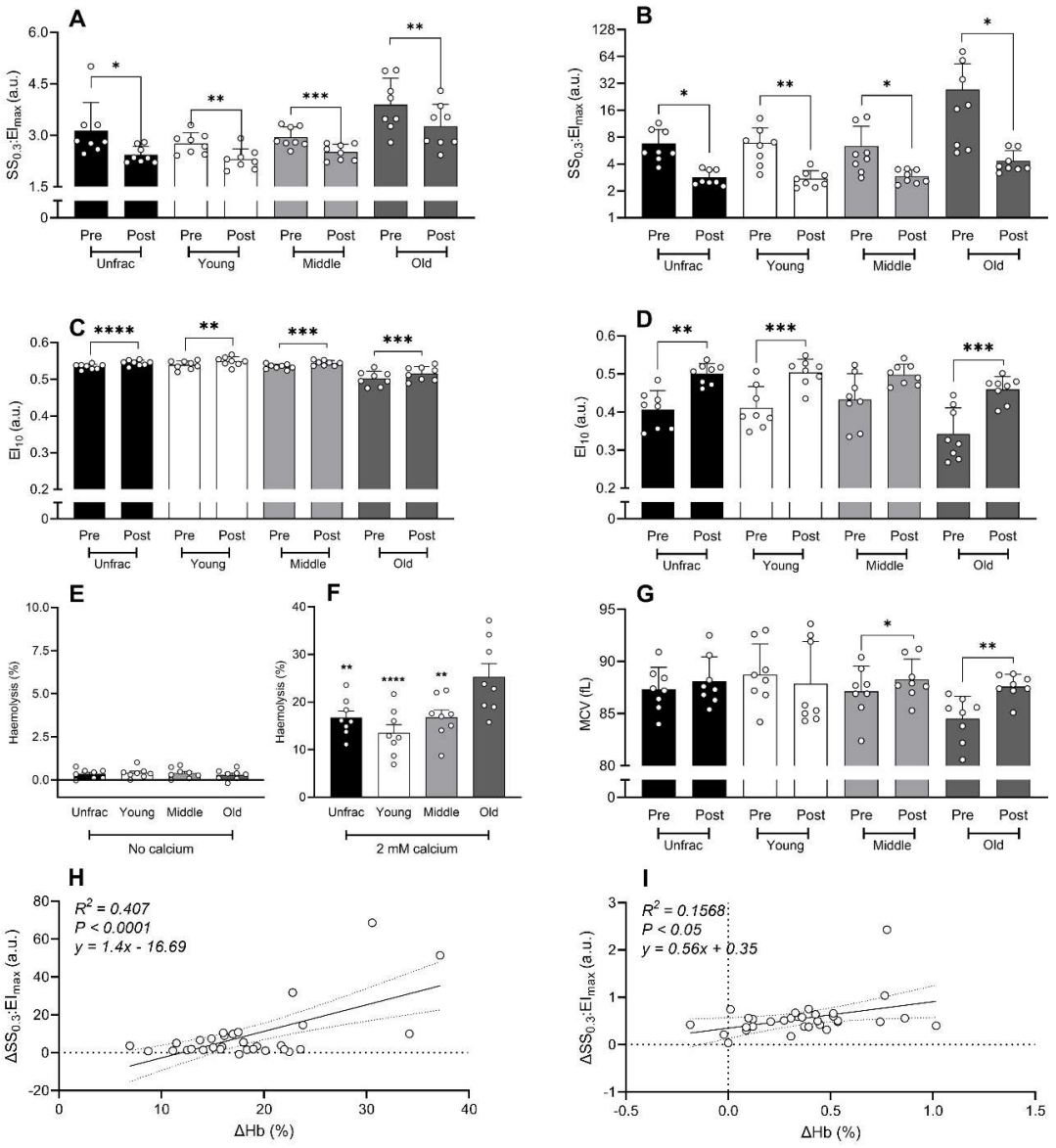

***Fig. 39**: The effect of the mechanical force application (10 Pa for 300 s) on red blood cell (RBC) sub-populations of distinct physiological ages, in dependence of extracellular calcium. Parameters were measured prior to ("Pre") and immediately following ("Post") exposure to mechanical shear. Shear conditioning was carried out in an identical manner using isotonic shear media (left column) or shear media supplemented with 2 mmol·L^{-1} calcium chloride (right column, unless otherwise specified). Changes in RBC deformability are presented as an integrated index ($SS_{0.3}$:EI_{max}; A,B) and as elongation measured under 10 Pa of shear (C,D). Destruction of RBC as a result of the shearing protocol is presented as haemolysis (E,F), while changes in cell volume are shown only for RBC sub-populations sheared in presence of calcium chloride (G). Linear regression analyses relating the extent of haemolysis and change in $SS_{0.3}$:EI_{max} for 'Pre' and 'Post' samples are shown in (H,I). $^{****}P < 0.0001$, $^{***}P < 0.001$, $^{**}P < 0.01$, $^{*}P < 0.05$ between designated pairs or when compared with the 'old' RBC (F). Data presented as means ± SD; N = 8*

5.3.5 Dose-dependent calcium-influx into RBC of varied physiological ages in response to the Piezo1-activator Yoda1

We aimed to probe the mechanisms that underlie the distinct calcium-handling capacities of physiologically-aged RBC under mechanical shear (Fig. 39); thus, we employed the specific small molecule activator of the mechanically-activated cation channel Piezo1: Yoda1 [216]. Dose-response curves of increased $[Ca^{2+}]_i$ with exposure to increasing concentrations of Yoda1 (0.15-60 μM), reflected by increased fluorescent intensity of the distinct Fluo-4-loaded RBC sub-populations, showed non-linear Ca^{2+}-influx with exposure to increasing concentrations of Yoda1 (Fig. 40). The maximal response to Yoda1 for old and middle RBC appeared to be achieved at only 15 μM, with further increases in Yoda1-concentration not precipitating further increases in Fluo-4-related fluorescence, while young RBC seemed to possess some capacity for further stimulation at 30 and 60 μM Yoda1. Thus, to ensure comparability between the distinct cell populations, while also providing a significant calcium-challenge to assess calcium-handling capacity, the dose of 15 μM Yoda1 was used in the following experiments.

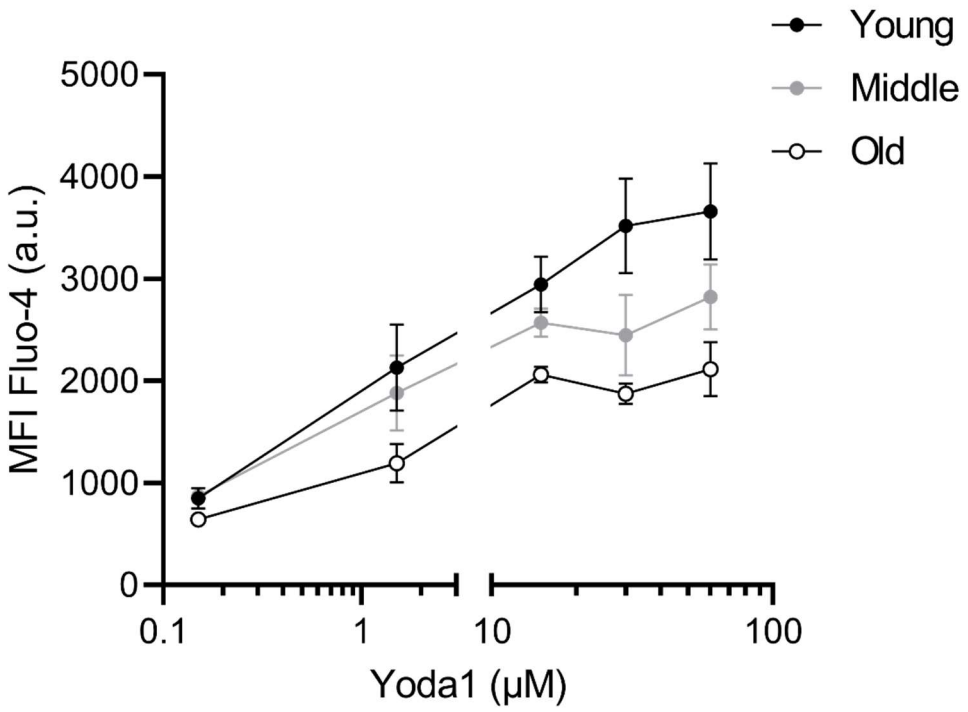

***Fig. 40**: Dose-response curves of calcium-influx into red blood cells (RBC) of distinct physiological ages following exposure to the Piezo1-specific activator Yoda1 at increasing concentrations (0.15, 1.5, 15, 30, and 60 μM). Data presented as means ± SD; N = 3*

5.3.6 Calcium-handling capacity is impaired in physiologically-aged RBC despite decreased Piezo1-abundance

Resting Fluo-4-related fluorescent intensity was highest in RBC obtained from the middle fraction of the Percoll-separation column, while old RBC exhibited the lowest intensity ($P < 0.01$; Fig. 41A). Following stimulation of RBC with Yoda1, RBC presented with dramatically increased fluorescent intensity, irrespective of cell age, when compared with resting values. Sustained exposure to Yoda1 resulted in more pronounced increases of fluorescent intensity in young RBC when compared to that of their old counterparts ($P < 0.01$; Fig. 41B).

Calcium-handling capacity of the distinct RBC sub-fractions was significantly impaired in old RBC when compared with their young and middle counterparts: young and middle RBC exhibited a decrease in fluorescent intensity following the initial spike in Fluo-4-related fluorescence caused by acute Yoda1-exposure, while Fluo-4-related fluorescence in old RBC failed to decrease during this period (Fig. 41C).

Abundance of Piezo1 was examined in old and middle RBC relative to that of the youngest RBC, wherein relative abundance of Piezo1 significantly decreased in physiologically-aged RBC ($P < 0.05$; Fig. 41D).

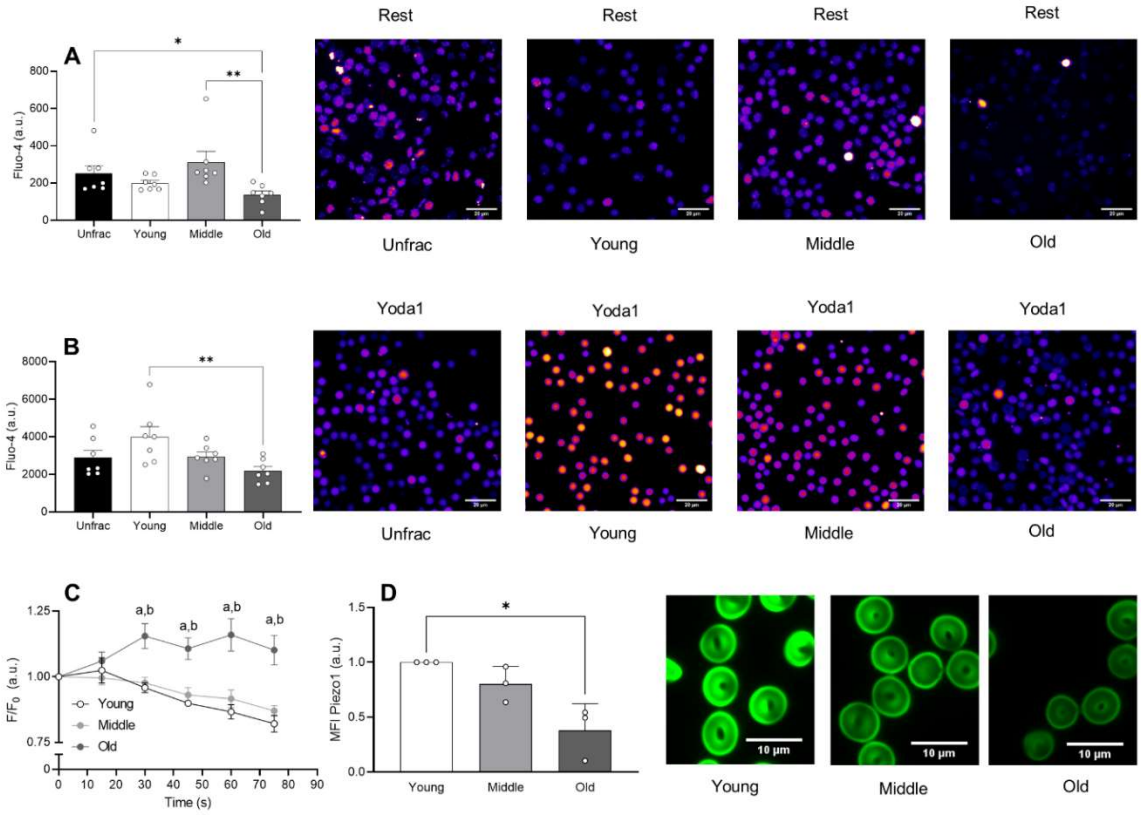

***Fig. 41**: Red blood cell (RBC) sub-populations of different in vivo ages exhibit altered calcium-handling capacities. Fluo-4-related fluorescent intensity was measured in resting RBC following gradient-density separation (A), and after 10 min of incubation with the Piezo1-specific activator Yoda1 (B). Dynamic changes in fluorescent intensity of RBC sub-populations were tracked immediately following stimulation with Yoda1 (15 µM; C). Relative changes in abundance of Piezo1 itself were also assessed in RBC of varying physiological ages (D). [a]young significantly different from old. [b]middle significantly different from old. $^{**}P < 0.01$, $^{*}P < 0.05$.*

5.3.7 Sustained Piezo1-activation precipitates morphological alterations and causes lysis of old RBC

Visual inspection of Fluo-4-loaded RBC sub-populations following sustained exposure to Yoda1 showed comparable morphology; however, distinct, qualitative differences in the responses to the Piezo1-activator Yoda1 were observed. The initial response, occurring irrespective of cell age, was acute

densification within s of Yoda1-application, wherein RBC shrunk, but then maintained their decreased volume for the following 10 min of treatment (Fig. 42). Cells from the young fraction tended to increase in density and adopt a spherical shape rapidly (~2 min), while middle and old RBC tended to exhibit an intermediate stage of echinocytosis (Fig. 42). While morphology of young and middle RBC would most often stabilise into low-volume spherocytes, ghost-formation through haemolysis was commonly observed amongst old RBC between 5-10 min of sustained exposure to Yoda1.

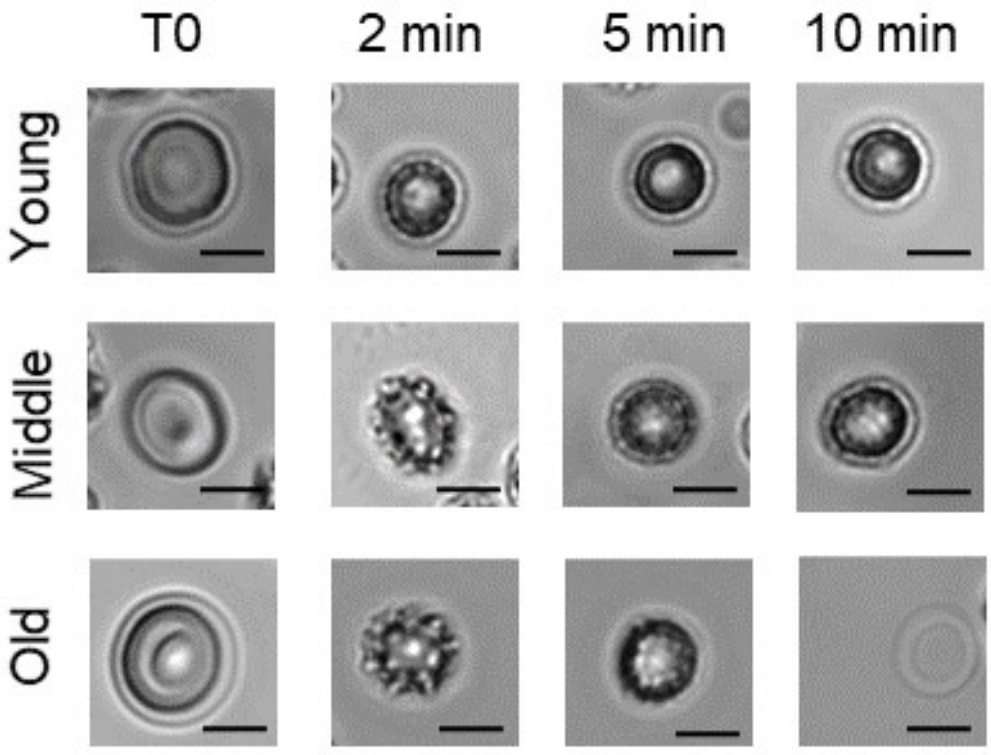

***Fig. 42**: Time-course of representative morphological responses of red blood cell (RBC) sub-populations to sustained Piezo1-stimulation through Yoda1-exposure. Young, middle, and old RBC were exposed to 15 μM Yoda1 while images were recorded over a period of 10 min. Scale bars = 5 μm*

5.4 Discussion

The salient results of the present experiments indicate that RBC exhibit impaired capacity to maintain their mechanical properties in response to increased $[Ca^{2+}]_i$ towards the end of their physiological lifespan. Moreover, it appears that Piezo1-expression progressively decreases during *in vivo* RBC ageing, which may serve to balance the impaired calcium-handling capacity of these cells. It is possible, however, that once RBC are poised for removal from circulation, an overload of $[Ca^{2+}]_i$ caused by sustained Piezo1-activation through mechanical force (i.e., when old RBC are adhered to the extracellular matrix of the spleen) contributes to the formation of ghosts and release of cytosolic contents, and ultimately the selective removal of these cells from circulation.

Separation of RBC sub-populations using density-dependent separation on layered gradients (e.g., Percoll®) has been performed for decades [26]. Successful separation of ageing RBC was confirmed herein through assessing MCV, which was decreased with increasing cell density (Fig. 37). Moreover, isotonic deformability of aged RBC was markedly decreased when compared with their middle and young counterparts (Fig. 38A), another hallmark of advanced cell age [24, 217]. Following mechanical stimulation, deformability of all RBC sub-populations improved; however, the oldest RBC remained more rigid when compared with deformability of young and middle RBC post-shear (Fig. 38B), confirming previous observations [218]. Similarly, when Ca^{2+} was present in the

shearing medium, old RBC had markedly reduced deformability when compared with their middle and younger counterparts (Fig. 38C); following mechanical stimulation, however, cellular deformability of the old RBC sub-population improved most dramatically (Fig. 38D). Previous reports indicate that prolonged exposure of RBC to 10 Pa shear stress produced haemolysis only when Ca^{2+} was added to the shearing media [215], and that 'surviving' cell populations had significantly improved properties [21]. It was hypothesised that Ca^{2+}-dependent removal was selective for RBC with unfavourable cell mechanics, for example old RBC.

We confirm here that aged RBC are selectively removed under mechanical shear in a Ca^{2+}-dependent manner, thus precipitating a surviving cell population that exhibits significantly improved cellular deformability ($P < 0.05$; Fig. 39B,D) and increased MCV ($P < 0.05$; Fig. 39G). Ca^{2+}-dependent haemolysis in response to mechanical shear was significantly more pronounced in the old RBC fraction when compared with the young ($P < 0.0001$) and middle fractions ($P < 0.01$), respectively (Fig. 39F), and the extent of haemolysis was significantly positively correlated with the observed improvements in cell deformability ($R^2 = 0.41$, $P < 0.0001$; Fig. 39J). It thus appears that aged, and more rigid RBC are selectively removed, leaving behind a population of RBC with improved cell mechanics. Haemolysis was near-absent when $CaCl_2$ was not added to the shearing media (Fig. 39E). It thus appears that prolonged mechanical shear in presence of

extracellular $CaCl_2$ results in selective removal of physiologically-aged RBC. Whether Ca^{2+}-dependent haemolysis is facilitated by dehydration following loss of KCl^- due to the Gárdos effect, as previously hypothesised [219], remains to be elucidated.

Despite the obvious clinical relevance of haemolysis – cell rupture of RBC and subsequent release of cytosolic contents – the precise mechanisms underlying this process are surprisingly poorly resolved (for a recent review, see [220]). Direct Ca^{2+}-dependent lysis of RBC has not been reported, rather, increased $[Ca^{2+}]_i$ is considered a driving force behind accelerated *in vivo* ageing of these cells, thus facilitating splenic clearance of still-intact, but more fragile RBC. Increased $[Ca^{2+}]_i$ has been reported to increase osmotic fragility of healthy RBC not through altered cell volume, but through causing membrane area loss due to exovesicle production [185, 221]. Sustained Piezo1-activation through Yoda1-exposure was observed to cause membrane blebbing and production of exovesicles under the conditions studied here (Fig. 43). In a recently proposed model of erythrophagocytosis [208], it is suggested that RBC become attached to the splenic architecture *via* adhesion molecules [34] – a process potentially facilitated by the Gárdos effect – where exposure to prolonged mechanical shear induces vesicle generation, and eventually ghost formation [35]. We provide evidence here to support this hypothesis: we observed that i. old RBC are preferentially lysed under mechanical shear in the presence of Ca^{2+}; ii. old RBC present with

impaired capacity to handle spikes in $[Ca^{2+}]_i$ induced by Piezo1-activation (i.e., mechanical force), which triggers the Gárdos effect; and iii. significant production and release of extracellular vesicles occurs in response to sustained Piezo1-activation.

It is thought that $[Ca^{2+}]_i$ increases linearly with RBC age [12, 13]. In our experiments, however, we observed that the middle fraction exhibited the highest Fluo-4-intensity at rest; this discrepancy may be explained by distinct separation techniques. While previous studies have used Percoll®-gradients, only two distinct RBC sub-populations were typically separated (i.e., 'light' and 'dense'). It is likely that the 'dense' fraction included RBC that were contained in the middle fraction in our experiments, given that we aimed to isolate only the densest of RBC as the old fraction (Fig. 37A). It is also possible that leukocytes, platelets or reticulocytes introduced noise into these measurements, given that blood constituents other than mature RBC possess substantial potential to generate artefact, even when present in low concentrations [222]. A clear advantage of the direct visualisation techniques employed herein is that the identity of each individual cell can be confirmed prior to analysis, thus increasing the signal quality provided by isolated and confirmed RBC.

Old RBC exhibit decreased Ca^{2+}-extrusion rates [15, 223], likely related to decreased metabolic capacity, and lower basal ATP-content [213, 214, 224]. It is plausible that these metabolic deficits underpin our observation that old RBC

were unable to efficiently clear increased $[Ca^{2+}]_i$ following stimulation with Yoda1 (Fig. 41C). It is important to note that, although Yoda1-concentration was standardised, the distinct RBC sub-populations exhibited distinct responses to the standardised treatment. It was unexpectedly observed that old RBC generally responded with a less pronounced influx of Ca^{2+} when stimulated with a range of Yoda1-concentrations (Fig. 40, Fig. 41B), which may plausibly be due to age-dependent loss of membrane-bound Piezo1 (Fig. 41D). Given the absence of translational processes, rather than down-regulation of gene expression, it appears that RBC may actively release Piezo1-molecules (e.g., through exocytosis); however, additional evidence is required to ascertain this hypothesis. It is also possible that existing Piezo1-molecules decline in function with increased cell age, or undergo conformational changes, resulting in diminished Ca^{2+}-influx. We have previously shown that membrane cross-linking may directly interfere with Piezo1-dependent Ca^{2+}-movement [211] and it is well-known that oxidative modifications are increasingly prevalent in aged RBC [133].

Collectively, it appears that calcium-handling capacity of older RBC is significantly impaired, despite a loss of Piezo1-abundance, and thus decreased Ca^{2+}-uptake in response to mechanical forces. It is plausible that this adaption of old RBC serves to balance the loss of metabolic capacity in these cells, which likely limits the ability to clear a large, acute influx of Ca^{2+} (Fig. 41C). When exposed to sustained mechanical forces, which uniquely occurs during

attachment of RBC to the splenic architecture – the primary RBC removal site in healthy individuals – old RBC appear to be selectively removed through ghost formation by increasing $[Ca^{2+}]_i$ beyond concentrations that this RBC sub-population is able to buffer.

5.5 Supplemental figure: Distinct calcium-handling of density-separated human erythrocytes in response to mechanical shear

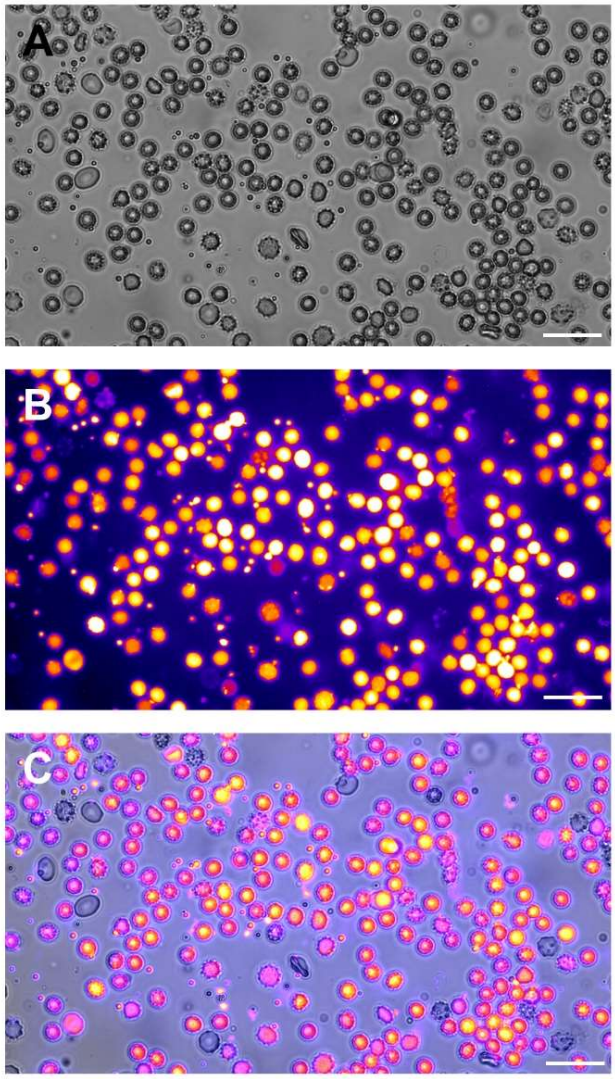

***Fig. 43**: Unfractionated red blood cells (RBC) exposed to 15 µM Yoda1 for 5-10 min produce extracellular vesicles. Note the large cell-to-cell variability in fluorescent intensity, which extends to the produced vesicles. A: Brightfield image captured at 600-times magnification. B: Fluorescent image of the same region of interest. C: Composite image of A and B. Scale bar: 20 µm*

5.6 Results of Study 3 in the context of the present dissertation

The observations of *Study 3* suggest that entry of Ca^{2+} in response to prolonged mechanical shear may be detrimental to RBC homeostasis. Moreover, it appears that the mechanically-activated cation channel Piezo1 plays a significant role in transducing mechanical cues by facilitating spikes in $[Ca^{2+}]_i$. While RBC are exposed to prolonged shears in the splenic architecture, transit of the spleen does not occur frequently. During frequent capillary transit, RBC are exposed to more transient shear stresses, where spikes in $[Ca^{2+}]_i$ are less sustained and less pronounced. It is thus plausible to hypothesise that Piezo1 may mediate shear-dependent activation of other pathways independent of the Gárdos effect, given the plethora of Ca^{2+}-dependent pathways present in RBC [47].

Intracellular NO-signalling, which is thought to not only affect the physical properties of RBC, but also mediate interactions with other cell-types, appears to be dependent on increased $[Ca^{2+}]_i$ (for a review, see [225]). The primary source of NO – NOS – is present within RBC and thought to be largely identical to the isoform of NOS present in endothelial cells (i.e., eNOS; [88]), and thus dependent on binding of Ca^{2+}-calmodulin for activation. Moreover, in keeping with the congruence of RBC-NOS3 and eNOS, RBC-derived NO-production occurs in response to mechanical shear [28, 76, 87, 226]. The mechanisms that enable RBC to sense mechanical forces, and subsequently stimulate activation of RBC-NOS3, and NO-production, remain to be elucidated.

Chapter 6

Study 4: Piezo1 regulates shear-dependent nitric oxide production in human erythrocytes

Lennart Kuck, Jason N. Peart, Michael J. Simmonds

Chapter 6 contains works conducted as part of the present doctoral program and is presented in its peer-reviewed and published form. My contributions to this paper include concept and experimental design, data collection, data analysis and interpretation, manuscript development. All authors reviewed and approved the manuscript.

Reference: Kuck, L., Peart, J. N., & Simmonds, M. J. (2022). Piezo1 regulates shear-dependent nitric oxide production in human erythrocytes. *American Journal of Physiology-Heart and Circulatory Physiology*. H24-H37. PubMed ID: 35559724. DOI: 10.1152/ajpheart.00185.2022.

6.1 Preface

The concept that the RBC may "actively", acutely alter their properties in immediate response to some stimulus – that is, dynamic alterations in for example cell deformability arise acutely upon specific stimulation – has emerged only over the past decade. Various studies had provided observations that RBC may carry a functional NOS-type enzyme, which facilitates endogenous production of nitric oxide [27, 28, 39, 76, 80, 85, 227]. In 2006, Kleinbongard et al. [78] provided evidence that RBC express a NOS-3 protein (i.e., endothelial-type NOS), while lacking NOS-1 or NOS-2, using immunofluorescent, histological, and scan-electron microscopy-based methods. Moreover, this RBC-NOS3 was shown to be – analogous to eNOS – dependent on its substrate *L*-arginine, Ca^{2+}-sensitive and phosphorylatable *via* the PI3K pathway [78]. Subsequent studies focussed on elucidating potential activation mechanisms (e.g., shear stress) of RBC-NOS3 and potential down-stream targets; it was found that shear stress acts as an activator of RBC-NOS3 by inducing phosphorylation at ser^{1177} [28, 85], and increased phosphorylation of this residue appears closely associated with increased RBC deformability [76].

A landmark study performed by Leo et al. [44] has recently provided convincing evidence of the involvement of RBC-NOS3 in physiological regulation of circulatory capacity on a systemic level. The authors used state-of-the-art molecular techniques to generate tissue-specific knock-out models of RBC-NOS3

and eNOS to investigate the contribution of RBC-NOS3 to circulatory function. Moreover, they also generated a global knock-out model of NOS in both RBC and endothelial cells to serve as a negative control. It was observed that RBC-derived NO or NO-species play an independent role in blood pressure regulation, given that mice with either endothelial-specific or RBC-specific NOS-knock outs exhibited increased mean arterial pressure and systemic vascular resistance to a similar degree. The global knock-out mice had compounded increases in blood pressure and resistance exceeding either tissue-specific single knock-out, indicating that RBC-generated NO has some compensatory capacity in scenarios where endothelial NO generation is compromised. The molecular mechanisms that allow RBC-generated NO to escape the extraordinary capacity of haemoglobin to neutralise it, and thus exert paracrine effects that contribute to blood pressure regulation, are still unclear and remain strongly debated in the scientific literature. Moreover, activation mechanisms and regulatory players that affect activation of RBC-NOS3, and thus RBC-derived NO, remain to be elucidated.

6.2 Introduction

The primary function of red blood cells (RBC) is the delivery of oxygen to working tissues, coupled with the removal of metabolic waste products. Traversal of capillary beds surrounding working tissues requires an adaptive

morphology, given apertures of microcirculatory blood vessels decrease to only a quarter of the average diameter of RBC [6, 51, 228]. While the physical properties that govern the remarkable capacity of RBC to deform are traditionally considered 'passive', recent investigations have elucidated several acute mechanosensitive signalling pathways in RBC, which appear to influence RBC mechanics (for a recent review, see [50]). The primary signalling pathways thought to be sensitive to mechanical shear or cellular deformation in human RBC are mediated by increased intracellular Ca^{2+} concentration and involve endogenous NO-production. In RBC, NO may be generated enzymatically through RBC-NOS3, or through reduction of nitrite (NO_2^-) *via* deoxyhaemoglobin [78, 229]. It appears that RBC-NOS3 is functionally and structurally congruent with eNOS, sharing sensitivity to: Ca^{2+}-availability, phosphorylation by upstream kinases such as Akt/Protein Kinase B, and local concentration of *L*-Arginine [28, 76, 80, 85, 88]. Despite the RBC cytosol being rich in haemoglobin tetramers (~5 mM) – which effectively scavenge NO – it appears that RBC-derived NO still escapes the cell through yet unresolved mechanisms, exerting extracellular effects on the vasculature [230-232]. For example, RBC-NOS3 was recently shown to independently contribute to the regulation of blood pressure in tissue-specific murine knock-out models [44]. A candidate mechanism for export of NO-species from RBC could *via* be the channel aquaporin-1, which has previously been shown to function as an NO-transporter in endothelial cells [233].

Given RBC are exposed to varying mechanical forces during their transit of the circulatory system, it is logical that mechanosensitive signalling would have developed in these abundant cells. While changes in the physical properties (e.g., morphological; mechanical) of RBC in response to mechanical stimuli are well described, emerging evidence supports that mechanical forces may be translated into biochemical signals during deformation of the cell membrane, which subsequently triggers auto-regulatory effects [50]. Influx of Ca^{2+} into RBC is known to occur in response to application of mechanical force, which may be regulated by mechanically-gated ion channels such as Piezo1 [18, 27, 28, 45, 97, 200]. The downstream effects of this Ca^{2+}-flux are generally poorly understood, although the associated activation of the Gárdos channel and resultant efflux of K^+ and H_2O is known to impair cell mechanics [215]. Independent works have demonstrated that RBC-NOS3 is stimulated when RBC are exposed to mechanical force; a process that appears sensitive to local Ca^{2+} concentration [76, 78, 226]. Despite these developments, the signalling cascade that integrates cellular deformation with RBC-NOS3 activation remains unresolved.

Mechanically-activated Ca^{2+}-influx *via* Piezo1 has been shown to upregulate ATP release from RBC during hypoxia, thus contributing to regulation of vascular tone [234]. Importantly, the extent of ATP release under this condition appears to be associated with the capacity of RBC to deform under a given shear stress [235, 236]. Accordingly, dampened ATP release has been demonstrated in both

RBC that were experimentally rigidified with the thiol-oxidizing agent diamide, and also less deformable RBC isolated from older adults; each model resulted in impaired vascular reactivity [237, 238]. An interdependence of RBC deformability and endogenous NO-production *via* RBC-NOS3 has not yet been explored, although may present as a fundamental advancement in cell physiology; the aim of the present investigation was to thus interrogate i. whether rigid RBC exhibit decreased capacity to enzymatically produce NO; ii. if normalizing cellular deformation in previously rigidified cells would restore native levels of NOS-phosphorylation and NO-production; and iii. the dependence of active RBC-NOS3 on Piezo1-mediated Ca^{2+}-movement.

6.3 Materials and methods

6.3.1 Participants and blood sampling procedure

Blood samples obtained from a pool of nine apparently healthy male volunteers (age: 26 ± 5 yr) were used in present study. Volunteers were non-smokers and confirmed freedom of known neurological, cardiovascular, endocrine, or metabolic disorders. Following provision of written and informed consent, 10 mL of blood were obtained from a prominent vessel in the antecubital region. The blood draw was carefully performed within 90 s of tourniquet application to the upper arm using a sterile 21-g needle and syringe to minimise shear exposure of the sample, which was immediately transferred to a tube containing 1.8 $mg \cdot mL^{-}$

[1] ethylenediaminetetraacetic acid for anticoagulation prior to further processing. The present experimental protocols were reviewed and approved by the Human Research Ethics Committee of Griffith University (Gold Coast, Australia) and align with the Declaration of Helsinki. All agents used in the herein described experiments were sourced from Sigma (Sigma-Aldrich Pty Ltd, Castle Hill, Australia), unless stated otherwise.

6.3.2 Red blood cell preparation

Red cells were isolated from whole blood samples by centrifugation at 1500 × *g* for 10 min and the buffy coat was discarded, while plasma was stored at 4ºC until further use. Isolated RBC were washed twice with isotonic PBS (0.1 M; 293 mOsmol·kg^{-1}, pH 7.39). The RBC were then incubated in PBS supplemented with 0.1% BSA and the respective concentration of N,N,N′,N′-tetramethylazodicarboxamide ('diamide'; 600, 750, or 1000 μM); RBC were also incubated in PBS/BSA free of diamide as a negative control (i.e., 'untreated'). All incubations were maintained at 37°C for 60 min. Validation testing confirmed that the diamide-treatment did not induce toxic effects (e.g., increased fragility, altered morphology; Figs. 45, 46) independent of the intended rigidification of the RBC membrane. Immediately following incubation, suspensions were centrifuged at 1500 × *g* for 10 min and washed twice with PBS. The final

supernatant was discarded, and isolated RBC were resuspended in autologous plasma at a haematocrit of 0.4 $L \cdot L^{-1}$.

6.3.3 Experimental design

The present study involved progression through three successive experimental phases. The aim of *Experiment One* was to explore whether mechanically-induced activation of RBC-NOS3, and consequential intracellular NO-production, was sensitive to the capacity of RBC to deform under a given shear stress. *Experiment Two* aimed to assess whether increasing the shear stress in RBC suspensions where deformability was experimentally impaired, to match the cellular deformation of untreated RBC (i.e., normalised strain), would restore native NOS-activation and NO generation. *Experiment Three* included deeper investigation in potential up-stream shear-sensitive NOS-activation pathways, including Piezo1-mediated movement of Ca^{2+}.

6.3.4 Experiment One

Diamide-treated RBC were exposed to a shear conditioning protocol known to stimulate both phosphorylation of RBC-NOS3 at ser^{1177} and intracellular NO-production [198, 226]. Shear stress reflective of microcirculatory transit (5 Pa; [239]) was applied for 120 s in a Couette shearing device (LORCA MaxSis, RR Mechatronics, Hoorn, The Netherlands) using RBC resuspended in autologous

plasma (for phosphorylation of RBC-NOS3) or isolated RBC diluted in PBS supplemented with 1.8 mM $CaCl_2$ (for NO-related fluorescence), following which both phosphorylation of RBC-NOS3 and cytosolic NO-production were assessed.

6.3.5 Experiment Two

Diamide-treated RBC were exposed to individualised shear protocols designed to standardise the amount of stretch on the RBC membrane, independent of basal rigidity. This was achieved by measuring RBC deformability and RBC-plasma suspension viscosity at a standardised haematocrit of 0.4 $L \cdot L^{-1}$, and then calculating the shear stress required to equalise cell membrane stretch – wherein diamide-treated and thus more rigid RBC required higher shear stress to achieve the same cellular deformation (Table 2). Following the specific shear conditioning protocols, phosphorylation of RBC-NOS3 and cytosolic NO-production were assessed.

6.3.6 Experiment Three

Based on the findings obtained in *Experiments One* and *Two*, a third experimental phase was designed to determine whether the diamide-treatment itself fundamentally interfered with the capacity of RBC to sense shear. To this end, diamide-treated (750 μM) and untreated control RBC were incubated with specific compounds known to stabilise either the open-state or closed-state of the

mechanically-activated cation channel Piezo1. The compounds ("Yoda1", a specific Piezo1 activator [216, 240], and "GsMTx4", a Piezo1 inhibitor [101]; Abcam, Melbourne, Australia) were dissolved and stored as stock solutions according to manufacturer's instructions. On the day of experimental testing, a fresh aliquot of each compound (Yoda1: final concentration 15 μM; GsMTx4: final concentration 3.3 μM) was produced in isotonic PBS. Piezo1-induced Ca^{2+}-flux into untreated and diamide-treated RBC was assessed using the fluorescent probe Fluo-4.

Moreover, the effects of Piezo1-activation in the absence of shear, and the inhibition of Piezo1 during shear, on phosphorylation of RBC-NOS3 ser^{1177} were assessed. To this end, untreated and diamide-treated RBC-plasma suspensions were incubated with Yoda1, prior to immunodetection of phosphorylated RBC-NOS3 ser^{1177}. Untreated RBC were also incubated with GsMTx4 prior to being exposed to 5 Pa of shear for 120 s for the measurement of phosphorylated RBC-NOS3 ser^{1177}. Incubations were carried out at room temperature for 10 min on a roller mixer, operated at minimal rotational velocity to avoid sedimentation of RBC. Finally, RBC-NOS3-dependent intracellular NO-production in response to mechanical shear (5 Pa for 120 s) or the Piezo1-activator Yoda1 was assessed in untreated RBC and RBC pre-incubated with 5 mM of the NOS-inhibitor N(G)-Nitro-*L*-arginine methyl ester (*L*-NAME) for 60 min at room temperature.

6.3.7 Blood viscosity

Application of precise shear stress necessitates that viscosity of the sheared medium is accurately quantified. The shear stress acting upon a fluid in a Couette shearing system is given as: τ (shear stress) = γ (shear rate) × η (apparent viscosity)

Given blood is a non-Newtonian fluid (i.e., dependent upon shear rate), the shear rate-specific blood viscosity of each sample (i.e., RBC suspension) was measured in a cone-and-plate viscometer operated with a CPA-40z spindle (DV-II+Pro, Brookfield Engineering Labs, Middleboro, USA) at 300, 750, and 1500 s^{-1}. This device is equipped with torque-sensors which enable the calculation of viscosity at any given shear rate using a device-specific constant determined *via* pre-experimental calibration. Using the donor- and shear rate-specific blood viscosity values, the shear rates required to yield 5 Pa of shear stress (Table 1) or the shear stress required to induce normalised cell stretch (Table 2) were calculated for RBC-plasma suspensions.

6.3.8 Red blood cell deformability measurements and shear stress application

The capacity of RBC (untreated and treated with diamide) to elongate when exposed to a given shear stress was quantified using a commercial ektacytometer (LORCA MaxSis, RR Mechatronics, Hoorn, The Netherlands), the details of which have been discussed in some detail elsewhere [156]. In brief, the device

employs a Couette shearing system, composed of an inner stationary bob and an outer rotatable cup; a 300 μm gap between the cup and bob provides a no-slip shearing region. Isolated RBC, suspended in a highly viscous solution of PVP dissolved in PBS (30.2 mPa·s, 288 mOsmol·kg^{-1}, pH 7.42), were dispensed into the gap under very-low rotational velocities (0.1 rev·s^{-1}) to minimise pre-conditioning of the samples. A low-powered laser is housed within the static bob and projects through the RBC-PVP suspension, generating laser diffraction patterns – reflective of the bulk mechanical behaviour of RBC in the gap – which are captured by a CCD camera. With increased shear, the diffraction patterns become more elliptical, and EI may be calculated based on the major (a) and minor (b) axes of the ellipse, using the formula: EI = (a-b)/(a+b). Given the LORCA ektacytometer allows for application of precisely controlled shear stresses, in the current study this device was also used to expose RBC to mechanical stimulation by adjusting the shear rate for individually measured shear rate-specific blood viscosity.

6.3.9 Intracellular nitric oxide generation

Changes in intracellular NO were monitored using the NO-sensitive probe diaminofluorescein-FM diacetate (DAF-FM DA; [241]). Briefly, DAF-FM DA is a non-fluorescent cell permeable agent which is hydrolysed by cytosolic enzymes (e.g., esterases) to yield DAF-FM. DAF-FM then irreversibly reacts with NO to

form a fluorescent benzotriazole. Loading of RBC with DAF-FM DA was achieved by incubating isolated and washed RBC with the compound at room temperature on a rolling mixer while protected from light for 30 min. Loaded RBC were then washed twice with PBS, following which an additional 15 min were allowed for de-esterification of the dye. Washed RBC loaded with DAF-FM DA were then exposed to the respective shear conditioning protocol using the Couette shearing system described earlier (LORCA MaxSis, RR Mechatronics, Hoorn, The Netherlands) and subsequently analysed. A sample of washed RBC from the same aliquot was treated identically except rather than being exposed to shear, this sample was placed in the shearing system while the cup was maintained at stasis, thus providing a direct reference value for *unsheared* DAF-FM-related fluorescence (i.e., unsheared control), which was required given the semi-quantitative nature of this method. Thus, changes in DAF-FM-related fluorescence between the sheared sample and respective unsheared control (i.e., Δmean fluorescence intensity), which were always collected in immediate temporal proximity, are reported. Following retrieval of RBC from the Couette shearing system, sheared and unsheared RBC were placed on a coverslip and allowed to settle onto the glass for 10 min. The coverslip with settled RBC was subsequently exposed to an argon laser (excitation: λ = 488 nm, emission: λ = 505 nm) and fluorescent RBC were imaged on at least 5 randomly selected regions of the coverslip. Light exposure of each individual sample was minimised to prevent artefactual increases in fluorescent signal; all coverslips were analysed

within seconds of light exposure in a highly-standardised and uniform manner. Laser exposure and fluorescent imaging were performed using an inverted microscope (IX73, Olympus Corp., Tokyo, Japan) with an integrated camera (optiMOS sCMOS, QImaging, Surrey, Australia) at 600-fold magnification.

6.3.10 Immunodetection of phosphorylated RBC-NOS3

Following mechanical stimulation of RBC-plasma suspensions that contained diamide-treated or untreated control RBC, samples were immediately fixed in 4% paraformaldehyde for 20 min. Fixed RBC were then washed with PBS and smears were produced on glass slides using published protocols [85, 111]. A test area and a negative control area were marked on each slide and separated with a lipid pen (PAP pen). The slides were washed thrice with 0.1 M TRIS-buffered saline (TBS; pH 7.6) and RBC were permeabilised using trypsin. Non-specific binding was minimised using skim milk powder prior to application of primary antibodies (1:150 dilution; rabbit anti-phospho eNOS ser^{1177}, Merck Pty Ltd, Bayswater, Australia) to the test area. The control area was simultaneously treated with only the vehicle solution used to deliver the primary antibodies (0.3% w·v^{-1} skim milk, 0.09% Tween 20 v·v^{-1}; Merck Pty Ltd, Bayswater, Australia). Following a further three washes with TBS, both areas were blocked with 6% v·v^{-1} normal goat serum, and then incubated with secondary antibodies (1:400 dilution; goat anti-rabbit Alexa Fluor 568, Thermo Fisher, Scoresby,

Australia) for signal detection. The slides were again washed with TBS thrice and then dehydrated *via* exposure to an increasingly concentrated series of ethanol solutions (70, 90, and 100% $w \cdot v^{-1}$) and the marks drawn with the lipid pen were dissolved using Xylene. Coverslips were mounted onto slides with dehydrated samples using mounting medium (Entellan®, Merck Pty Ltd., Bayswater, Australia). Micrographs were subsequently recorded using an inverted microscope (IX73, Olympus Corp., Tokyo, Japan) with integrated camera (optiMOS sCMOS, QImaging, Surrey, Australia) at 600-fold magnification, while mounted RBC were exposed to an argon laser (λ = 594 nm), with emission recorded at λ = 610 nm using the same microscope and imaging system. Validation experiments were performed to confirm that this method was sensitive to changes in phosphorylated RBC-NOS3 ser^{1177}; ser^{1177}-phosphorylation was induced pharmacologically using insulin, a stimulator of the up-stream PI3K-pathway, or inhibited using Wortmannin, an inhibitor of PI3K (Fig. 47).

6.3.11 Intracellular calcium-content

The fluorescent probe Fluo-4 AM (Thermo Fisher, Scoresby, Australia) was employed to indicate changes in Ca^{2+}-content. Given the spectrum of haemoglobin overlaps with some fluorescent Ca^{2+}-probes, Fluo-4 was employed as it has been identified as the most appropriate for use in human RBC [186]. Isolated untreated or diamide-treated RBC were washed thrice with a modified

Tyrode's buffer (containing in mM: 135 NaCl, 5.4 KCl, 10 glucose, 1 $MgCl_2$, 1.8 $CaCl_2$ and 10 HEPES; pH 7.35) following which loading with 5 μM Fluo-4 AM was performed for 60 min at room temperature on roller mixer. Loaded RBC were then washed thrice more with Tyrode's solution prior to plating on a coverslip. De-esterification of the accumulated dye was allowed for 15 min and individual RBC were then excited at λ = 488 nm. Images were captured at λ = 505 nm using an inverted microscope (IX73, Olympus, Tokyo, Japan) with integrated camera (optiMOS sCMOS, QImaging, Surrey, Australia) at 600-fold magnification. RBC were then incubated with 15μM Yoda1 for 10 min on the coverslip, following which individual RBC were imaged as described above once more.

6.3.12 Data analysis

Raw EI-shear stress data were fit with a non-linear modification of the Lineweaver-Burk equation as reported previously [160]. Curve fitting was deemed acceptable using an R^2 cut-off of ≥0.98, thus enabling precise interpolation of the EI-shear stress relation; elongation indices were subsequently calculated for the desired shear stresses (*Experiment One)* and *vice versa* (*Experiment Two).*

MFI of individual RBC was measured using open-source software (FIJI version 1.53c [159], National Institutes of Health, Bethesda, MD). A minimum of 200

individual cells from at least four random areas of each coverslip were analysed for DAF-related fluorescence, a minimum of 200 cells from at least three random areas per test area were analysed for immunodetected phosphorylated RBC-NOS3, and a minimum of 100 cells from at least two random areas were analysed per control area (i.e., non-specific fluorescence). At least 300 individual cells were analysed for Fluo-4-related fluorescent intensity to determine changes in $[Ca^{2+}]_i$, using images captured from least four random areas of the coverslip.

6.3.13 Statistical analysis

Differences in EI at various shear stresses were determined using a two-way ANOVA with Tukey's post-hoc test. Differences in individual EI values determined *via* curve-fit, blood viscosity at specific shear rates, shear rate, and shear stress values were detected using a one-way ANOVA. Normality of NO-production, phosphorylation of RBC-NOS3, and Fluo-4 data was determined using the D'Agostino & Pearson omnibus normality test, following which significant differences between untreated and diamide-treated RBC were calculated using either a one-way ANOVA with Dunnett's correction or Friedman's test with Dunn's correction. Values of n denoted throughout refer to the number of independent experiments conducted each using a blood sample obtained from a different donor. A subset of the same nine donors returned to the laboratory to donate additional blood samples to the respective experimental

phases (i.e., *Experiments One, Two, Three*). An alpha level of 0.05 was used to determine statistical significance; all data analyses and statistical tests were performed using commercially available software (Prism, GraphPad Software Inc., Release 9.20, San Diego, USA).

6.4 Results

6.4.1 Erythrocyte exposure to diamide precipitates a dose-dependent impairment in cellular deformability

Exposure of isolated RBC to the thiol-oxidizing agent diamide resulted in a dose-dependent decrease of the cells' capacity to deform in shear (Fig. 44A). Briefly, the capacity of RBC to deform was assessed under a range of shear stresses between 0.3-50 Pa, wherein EI is reflective of the mean deformable capacity of a given RBC population for each shear stress. Diamide treatment significantly decreased cellular deformability (i.e., EI); specifically, for 600 μM, differences in EI were observed at all shears 0.94-5.15 Pa; for 750 μM, differences were observed at all shears <50 Pa; and for 1000 μM, differences were observed at all shears tested (0.3-50 Pa; Fig. 44A). In an effort to explore cellular deformability at a standardised shear stress, interpolation of the EI-shear stress relationship facilitated extraction of a discrete EI at a physiologically-relevant shear stress (5 Pa); again, a dose-dependent decrease of the EI induced by 5 Pa was observed for the diamide-treated RBC, when compared with untreated RBC (Fig 44B). Further,

each dose of diamide treatment progressively increased the rigidification (i.e., decreased the EI at 5 Pa) in a dose-dependent manner (Fig. 44B).

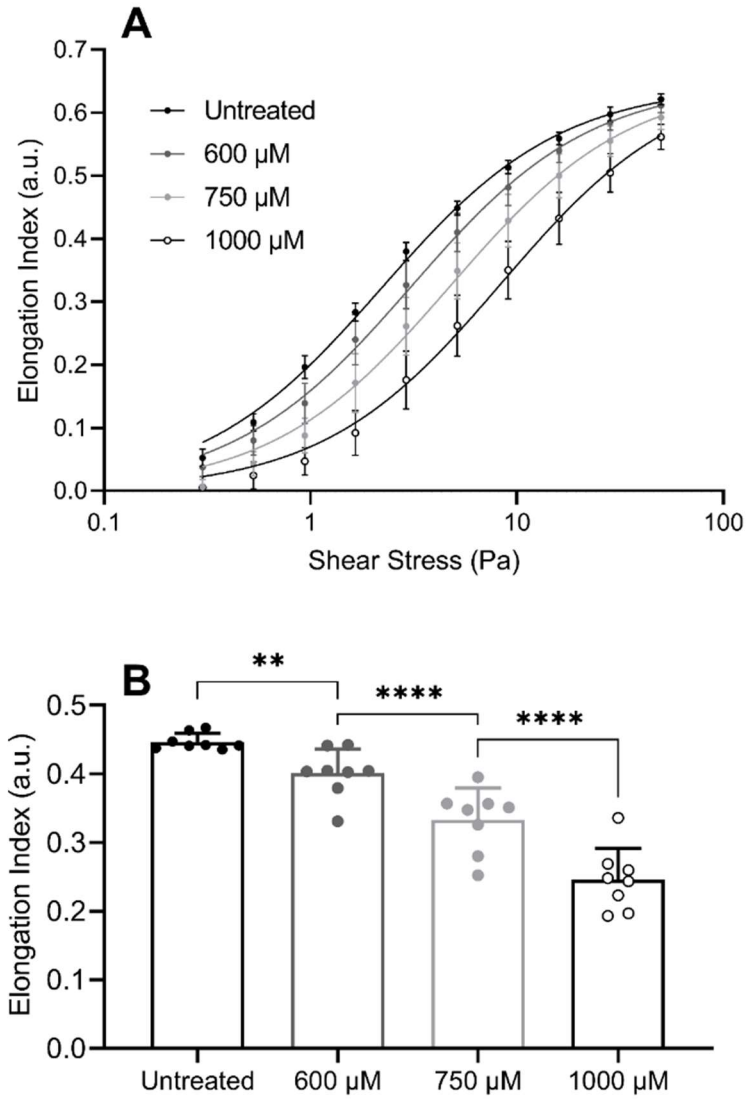

***Fig. 44**: Deformability of isolated red blood cells (RBC) treated with increasing concentrations of diamide. Diamide-treatment significantly decreased cellular deformability ($F(3,28) = 47.29$, $P < 0.0001$; two-way analysis of variance (ANOVA)) of isolated RBC in a dose-dependent manner. Diamide-treated RBC (600–1,000 µM), and untreated control cells, were exposed to a ramped shear stress protocol (A) to quantify cellular deformability (i.e., elongation index). Interpolation of the data presented in A facilitated extraction of the specific elongation index measured at a standardised shear stress of 5 Pa (B), which was decreased with increasing concentrations of diamide ($F(3,29) = 129.3$, $P < 0.0001$; two-way ANOVA with Bonferroni's post hoc test, $^{****}P < 0.0001$, $^{**}P < 0.01$). Data are presented as means ± SD; N = 8 independent experiments performed using blood obtained from distinct donors.*

Viscosity of RBC-plasma suspensions with a normalised haematocrit of 0.4 $L \cdot L^{-1}$ tended to increase due to diamide-treatment, thus discrete shear rates were required to be calculated and applied on an individual basis to produce the desired standardised shear stress of 5 Pa (Table 1).

Table 1. *Shear rate-specific viscosities and shear rates required to apply standardised shear stress*

Diamide concentration	Viscosity (mPa·s)	Shear rate (s^{-1})	Shear stress (Pa)
0 μM; Untreated	2.77 ± 0.24	1825 ± 158	5.03 ± 0.02
600 μM	2.79 ± 0.26	1815 ± 169	5.03 ± 0.02
750 μM	2.87 ± 0.26*	1758 ± 149**	5.01 ± 0.03
1000 μM	2.92 ± 0.26***	1731 ± 158***	5.02 ± 0.03

Data presented as mean ± standard deviation. Significantly different to untreated sample: $^{***}P < 0.001$, $^{**}P < 0.01$, $^{*}P < 0.05$ (one-way analysis of variance with Bonferroni's post-hoc analysis).

6.4.2 Shear-induced cytosolic nitric oxide-production is impaired in diamide-treated erythrocytes

Untreated RBC exhibited an increase in DAF-FM-related fluorescence (Fig. 45A) following 120 s exposure to 5 Pa (paired t-test: $P < 0.01$; rest data not shown to facilitate comparisons of shear-dependent effects between untreated and diamide-treated RBC). This shear-induced increase in DAF-FM-related fluorescence, reflecting intracellular NO-production, was impaired in diamide-treated RBC (Fig 45E): treatment with 600 μM diamide decreased shear-induced

NO generation by 77%, although this was not statistically significant (P = 0.07; Fig. 45B), while treatment with 750 or 1000 μM diamide significantly decreased shear-induced NO generation by 92% (P < 0.01; Fig. 45C) and 88% (P < 0.01; Fig. 45D), respectively.

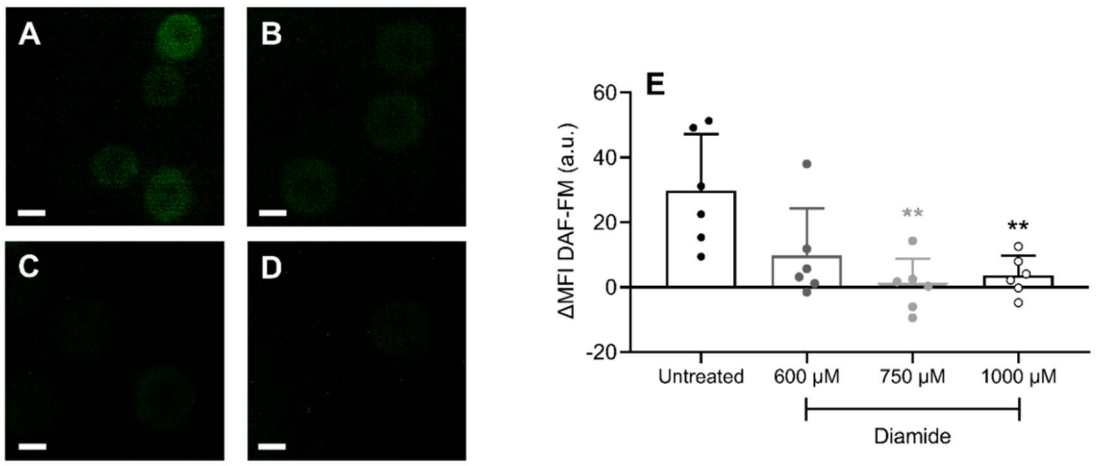

Fig. 45*: Shear-induced intracellular production of nitric oxide (NO) was significantly impeded in diamide-treated red blood cells (RBC) in a stepwise manner. The delta (absolute difference) between resting and sheared RBC is presented to reflect the distinct effect of the shearing procedure on intracellular NO-related fluorescence. A–D: representative images of post-shear samples containing untreated RBC (A) and RBC treated with 600 μM (B), 750 μM (C), or 1,000 μM (D) diamide; scale bars = 5 μm. Individual data for the quantitative analyses are presented in E. Significantly different to untreated sample: $^{**}P < 0.01$ ($\chi^2(3) = 10.35$, $P < 0.05$; Friedman test with Dunn's post hoc analysis). Data are presented as means ± SD; N = 6 independent experiments performed using blood obtained from distinct donors.*

6.4.3 Shear-induced phosphorylation of nitric oxide synthase is impaired in diamide-treated erythrocytes

Untreated RBC exhibited increased phosphorylation of RBC-NOS3 at ser^{1177} (Fig. 46A) following 120 s exposure to 5 Pa (Wilcoxon matched-pairs signed rank test:

$P < 0.01$; rest data not shown). This shear-induced increase in phosphorylated RBC-NOS3, reflecting activated NOS, was impaired in diamide-treated RBC (Fig. 46E): treatment with 600 µM diamide did not significantly alter phosphorylation of RBC-NOS3 (Fig. 46B), although 750 and 1000 µM significantly decreased shear-induced phosphorylation of RBC-NOS3 by 86% (Fig. 46C) and 96% (Fig. 46D), respectively.

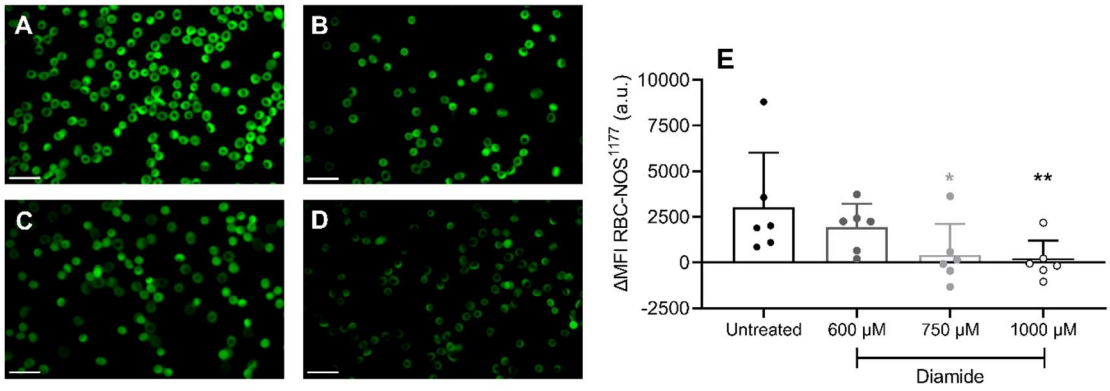

***Fig. 46**: Shear-induced phosphorylation of red blood cell-derived nitric oxide synthase (RBC-NOS3) at serine^{1177} was significantly impeded in diamide-treated RBC. The delta (absolute difference) between resting and sheared RBC suspensions is presented to reflect the distinct effect of the shearing protocol on phosphorylated RBC-NOS3. Representative images of post-shear samples containing untreated RBC (A) and RBC treated with 600 µM (B), 750 µM (C), or 1,000 µM (D) diamide; scale bars = 20 µm. Individual data points used for the quantitative analyses are presented in E. Significantly different to untreated sample: $^{**}P < 0.01$, $^{*}P < 0.05$ ($\chi^2(3) = 10.03$, $P < 0.05$; Friedman test with Dunn's post hoc analysis). Data are presented as means ± SD; n = 6 independent experiments performed using blood obtained from distinct donors.*

6.4.4 Increasing cellular deformation does not recover shear-induced enzymatic NO-production in diamide-treated RBC

The deformation of RBC populations during shear stress exposure was modulated by applying an individualised shear stress magnitude on the various diamide-treated RBC, and untreated control RBC (Table 2); this approach enabled determination of whether standardised cell deformation, rather than equal shear stress loading, might normalise the impaired NO-generation in diamide-treated RBC. A step-wise increase of the shear stress required to induce standardised deformation of diamide-treated RBC was observed (Table 2), reflecting the equivalent decrease in cellular deformability of these RBC populations (Fig. 44).

***Table 2**. Shear rate-specific blood viscosities, shear rates, and shear stresses required to standardised cell stretch (i.e., membrane strain)*

Diamide concentration	Viscosity (mPa·s)	Shear rate (s^{-1})	Shear stress (Pa)
0 μM; Untreated	2.79 ± 0.22	479 ± 46	1.42 ± 0.16
600 μM	2.82 ± 0.27	793 ± 204	2.38 ± 0.84
750 μM	2.93 ± 0.24**	1291 ± 736**	4.01 ± 2.53*
1000 μM	3.01 ± 0.17***	2102 ± 854****	6.56 ± 3.19***

Data presented as mean ± standard deviation. Significantly different to untreated sample: $^{****}P < 0.0001$, $^{***}P < 0.001$, $^{**}P < 0.01$, $^{*}P < 0.05$ (one-way analysis of variance with Bonferroni's post-hoc analysis).

Despite applying increased shear stress to diamide-treated RBC to induce an equivalent strain on the cell membrane, shear-induced NO-production remained significantly impaired in diamide-treated RBC, when compared with untreated control RBC (Fig. 47E). Specifically, treatment with 600 µM diamide significantly decreased shear-induced NO-generation by 68% (Fig. 47B) when compared with untreated cells (Fig. 47A), while treatment with 750 or 1000 µM diamide abolished shear-induced NO-production entirely (Fig. 47C-E).

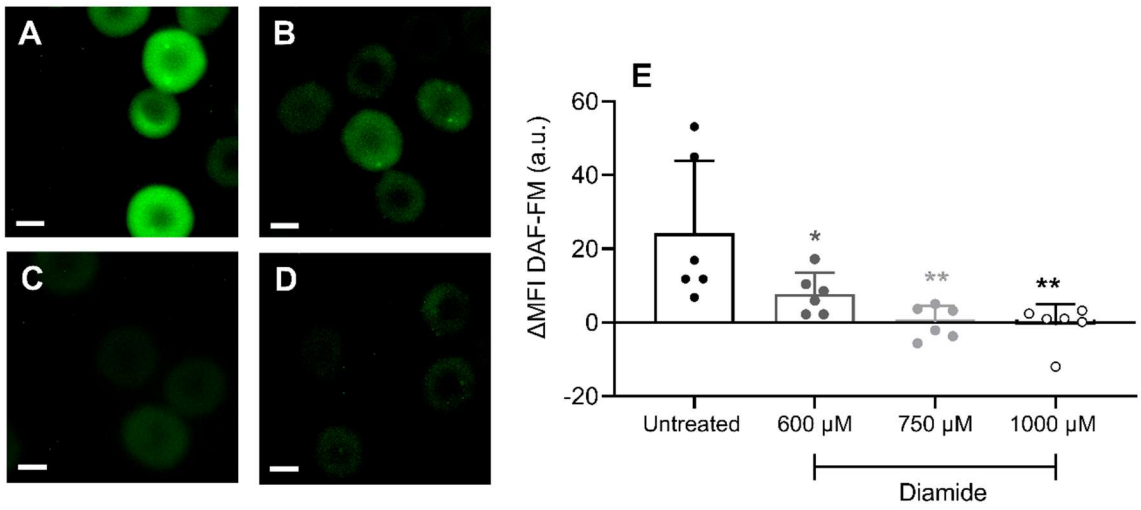

Fig. 47*: Shear-induced intracellular production of nitric oxide (NO) was significantly impeded in diamide-treated red blood cells (RBC) in a stepwise manner. The delta (absolute difference) between resting and sheared RBC is presented to reflect the distinct effect of the shearing protocol on intracellular NO-related fluorescence. Representative images of post-shear samples containing untreated RBC (A) and RBC treated with 600 µM (B), 750 µM (C), or 1,000 µM (D) diamide; scale bars = 5 µm. Individual data points used for the quantitative analyses are presented in E. Significantly different to untreated sample Significantly different to untreated sample: $^{**}P < 0.01$, $^{*}P < 0.05$ ($F(3,15) = 7.44$, $P < 0.05$; one-way analysis of variance with Dunnett's post hoc analysis). Data are presented as means ± SD; N = 6 independent experiments performed using blood obtained from distinct donors.*

Phosphorylation of RBC-NOS3 at ser^{1177} in response to shear was not normalised by increased strain for diamide-treated RBC (Fig. 48E). Specifically, while shear-induced NOS-activation was not significantly impaired following treatment with 600 μM diamide (Fig. 48B), treatment with 750 and 1000 μM significantly decreased phosphorylation of RBC-NOS3 in response to shear by 76% (Fig. 48C) and 81% (Fig. 48D), respectively.

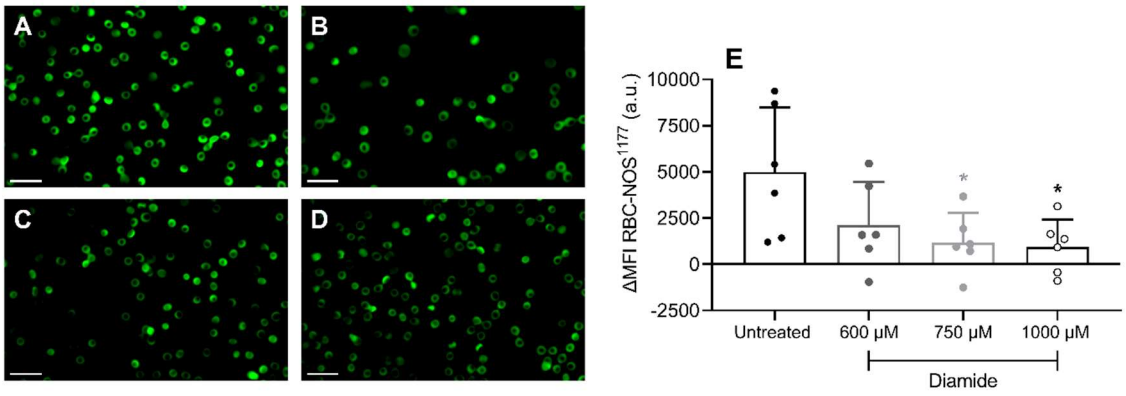

***Fig. 48**: Shear-induced phosphorylation of red blood cell-derived nitric oxide synthase (RBC-NOS3) at serine^{1177} was significantly impeded in diamide-treated RBC, even when cellular deformation was normalised using individualised shearing protocols. The delta (absolute difference) between resting and sheared RBC suspensions is presented to reflect the distinct effect of the shearing procedure on phosphorylated RBC-NOS3. Representative images of post-shear samples containing untreated RBC (A) and RBC treated with 600 μM (B), 750 μM (C), or 1,000 μM (D) diamide; scale bars = 20 μm. Individual data points used for the quantitative analyses are presented in E. Significantly different to untreated sample: $^{*}P < 0.05$ ($F(3,15) = 4.59$, $P < 0.05$; one-way analysis of variance with Dunnett's post hoc analysis). Data are presented as means ± SD; N = 6 independent experiments performed using blood obtained from distinct donors.*

6.4.5 Cross-linked Piezo1 exhibits impaired calcium-permeability and abrogates mechanically-induced nitric oxide synthase activation

The sensitivity of Piezo1 to its specific activator Yoda1 was assessed to determine whether diamide-treatment (750 μM) directly impaired its capacity to facilitate Ca^{2+}-influx into RBC. In untreated RBC, Yoda1-exposure induced a significant increase in $[Ca^{2+}]_i$ (Fig. 49A), reflected by a 6.8-fold increase in Fluo-4-related fluorescence. While no difference in baseline fluorescence was observed in diamide-treated RBC when compared with untreated RBC (Fig. 49A), upon stimulation with Yoda1, a 3.9-fold increase in Fluo-4-related fluorescence was observed over baseline values (Fig. 49A). Thus, following Yoda1-exposure, diamide-treated RBC presented with a significantly ameliorated increase in Fluo-4-related fluorescence (Fig. 49A), reflecting a less pronounced increase in $[Ca^{2+}]_i$.

The distribution of Fluo-4-related fluorescent intensity in diamide-treated RBC at baseline appeared to show a decrease in most cells that was accompanied by an increased frequency of highly fluorescent RBC (Fig. 49B, C; note use of "heat map" colouring emphasises such differences). Upon exposure to Yoda1, however, the population of untreated RBC exhibited a larger portion of highly fluorescent RBC (i.e., >2 standard deviations from the mean) when compared with diamide-treated RBC (Fig. 49B).

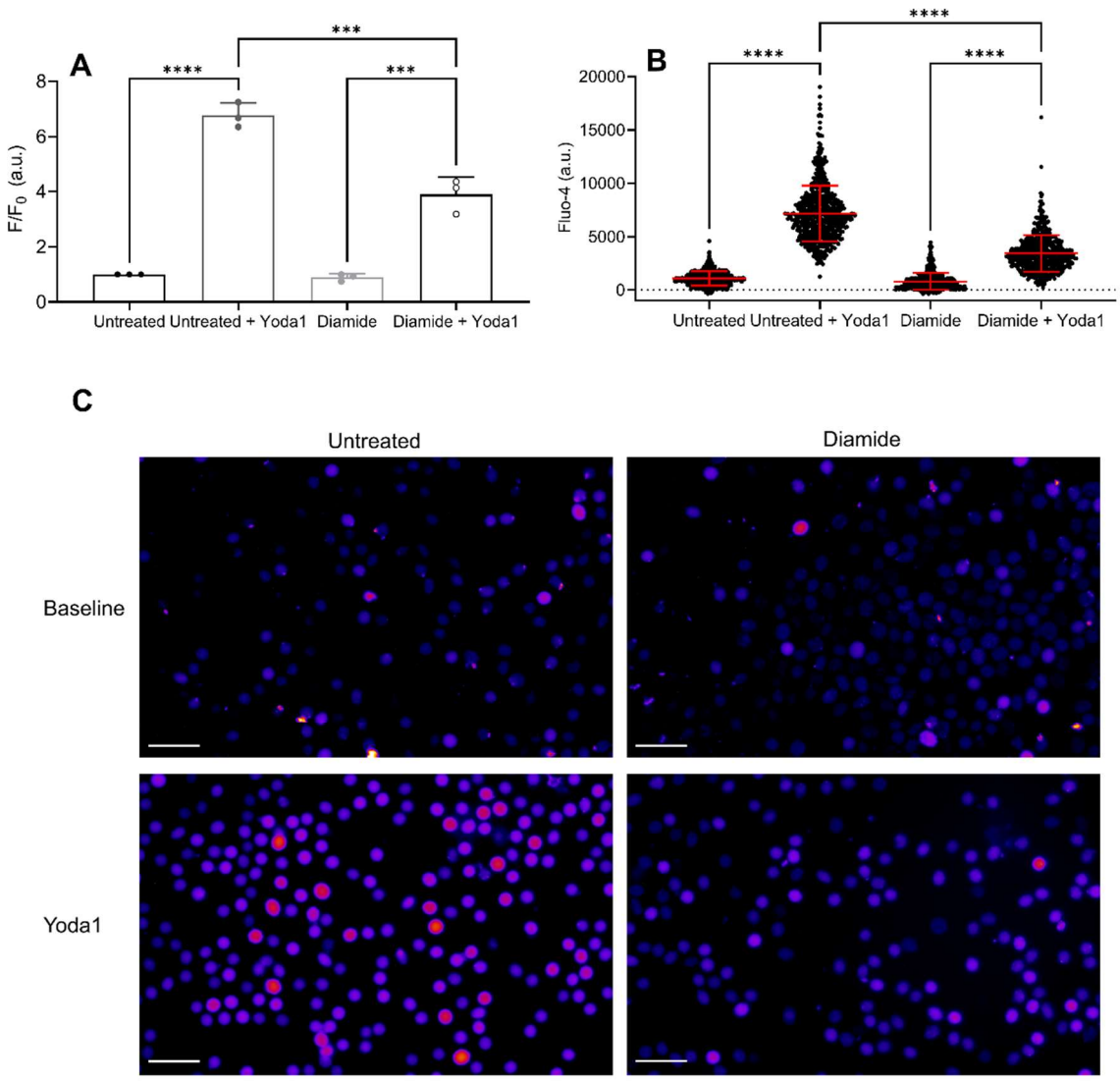

***Fig. 49**: Untreated and diamide-treated (750 μM) red blood cells (RBC) were loaded with the calcium-sensitive fluorescent dye Fluo-4 before Piezo1 stimulation. Changes in fluorescent intensity are presented as a grouped response (A) following addition of the Piezo1-specific activator Yoda1 and expressed relative to the untreated baseline (F_0); N = 3 independent experiments performed using blood obtained from distinct donors. Absolute fluorescent intensity of individual RBC obtained from a representative experiment is also presented (B) to demonstrate changes within the cell population. Representative images of Fluo-4-loaded RBC before and following exposure to Yoda1 are also shown (C), with distribution of fluorescent intensities emphasised through colouring using a "heat map" ("Fire" look-up table; scale bars = 20 μm); lighter colours represent increased intensity/signal. Data are presented as means ± SD. Significantly different between designated pairs: $^{****}P < 0.0001$, $^{***}P < 0.001$ (one-way analysis of variance with Bonferroni's post hoc analysis).*

Untreated and diamide-treated RBC were exposed to mechanical stimulation (5 Pa for 120 s) as described in *Experiment One.* Unsheared RBC-NOS3 ser^{1177}-levels (i.e., "rest") were not different between untreated and diamide-treated RBC (Fig. 50A). Exposure to the shearing protocol resulted in significantly increased phosphorylation of RBC-NOS3 at ser^{1177} (Fig. 50A) in untreated RBC; however, in diamide-treated RBC, a significantly blunted shear-induced increase in phosphorylation of RBC-NOS3 was observed (Fig. 50A*)*.

When control RBC were pre-treated with the specific Piezo1-inhibitor GsMTx4, exposure to the same shearing protocol failed to stimulate phosphorylation of RBC-NOS3 (Fig. 50A). Treatment with the specific Piezo1-activator Yoda1, in the absence of shear, led to an increase in phosphorylation of RBC-NOS3 (Fig. 50A) that was comparable to the level observed following shear exposure. Concurrently, increased DAF-related fluorescence, indicative of intracellular NO-generation, was observed to a similar extent when RBC were exposed to mechanical shear (5 Pa for 120 s) or the Piezo1-activator Yoda1 (Fig. 50B). Both shear- and Yoda1-dependent increases in DAF-related fluorescence were sensitive to treatment of RBC with the NOS-inhibitor *L*-NAME, which prevented significant increases of DAF-related fluorescence (both $P < 0.05$; Fig. 50B). Exposure of diamide-treated RBC to the Piezo1-activator Yoda1 failed to produce an increase in phosphorylation of RBC-NOS3 (Fig. 50A).

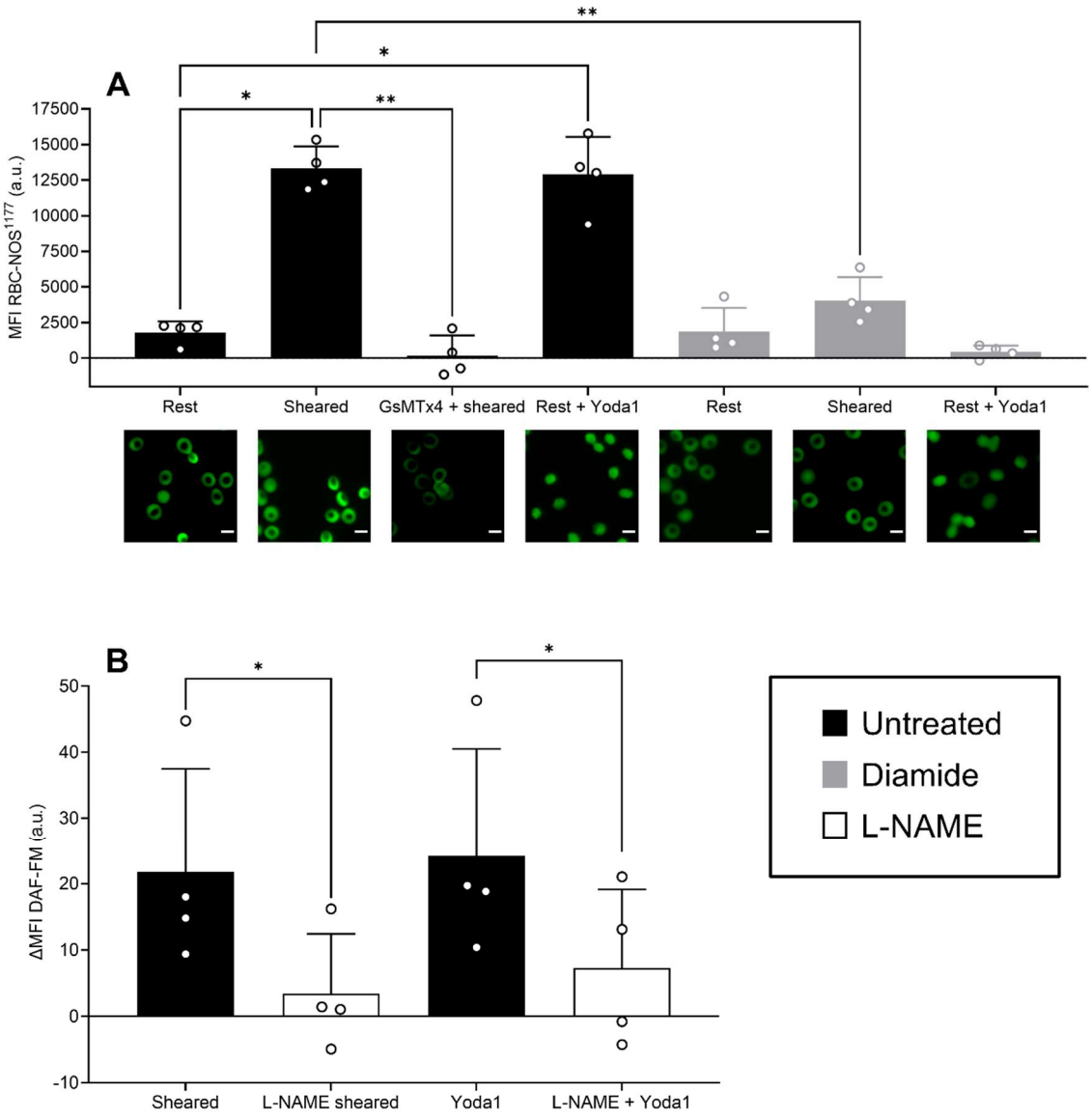

***Fig. 50**: Phosphorylation of red blood cell-derived nitric oxide synthase (RBC-NOS3) at residue serine^{1177} is sensitive to both mechanical stimulation and pharmacological interventions directly targeting the mechanosensitive cation channel Piezo1. Untreated and diamide-treated RBC were exposed to mechanical stimulation (i.e., sheared) and pharmacological interventions (i.e., GsMTx4 = inhibitor; Yoda1 = activator) targeting Piezo1. Representative images following the treatments and immunofluorescent detection of RBC-NOS3 serine^{1177} are provided below the respective data (A); scale bars = 5 μm. Untreated RBC and RBC preincubated with the NOS-inhibitor Nω -nitro-l-arginine methyl ester (L-NAME) were sheared or exposed to the Piezo1-activator Yoda1 (B). Significantly different between designated pairs: $^{**}P < 0.01$, $^{*}P < 0.05$ (one-way analysis of variance with Bonferroni's post hoc analysis, A; t-test, B). Data are presented as means ± SD; N = 4 independent experiments performed using blood obtained from distinct donors.*

6.5 Discussion

The salient findings presented herein provide evidence of a molecular signalling network in mature, circulating RBC, which is responsive to mechanical shear. It appears that physical stimuli may be transduced through a combination of ion-flux and kinase-activity, ultimately resulting in activation of the NO-producing enzyme RBC-NOS3. This signalling cascade was sensitive to thiol oxidation, which had a direct impact upon some membrane components that transduce mechanical stimulation, and also down-regulated enzyme activation downstream. The mechanically-activated cation channel Piezo1 was observed to be essential in integrating shear-flow with NOS-activation through influx of Ca^{2+}; ameliorated Ca^{2+}-influx in diamide-treated RBC *via* Piezo1 may explain the impaired capacity of these cells to generate NO in response to shear. Our observations emphasise the important role of post-translational cellular signalling in mature RBC, given these cells are enucleated and contain no complex organelles or sub-cellular compartments. Indeed, the perceived simplicity of the RBC has unravelled in the past decade with increasing availability of, for example, specialised fluorescent probes, revealing a more sophisticated cell type than previously assumed. Thus, the discovery of a multitude of signalling pathways in enucleated RBC may lead to a step-change in the fundamental understanding of these cells, and provide novel molecular

targets that could serve as biomarkers or for the development of pharmacological interventions.

The presence of a catalytically active and physiologically relevant NOS-isoform in RBC has been ascertained in various studies [44, 76, 78, 85, 88]. Moreover, activation of RBC-NOS3 through phosphorylation at ser^{1177} and subsequent intracellular NO-production has been linked to mechanical shear exposure [27, 76, 85, 198, 226], which appears to be a Ca^{2+}-dependent process [28]. We previously reported that shear stress may successfully recover RBC-NOS3 ser^{1177} phosphorylation, and thus NO-production, in RBC exposed to intracellular oxidative stress [76]. Whether deformability of the membrane itself, however, determined shear-induced activation of RBC-NOS3, remained unknown. In the current study, it was observed that shear-induced NO-production in RBC was significantly impaired following treatment with diamide (Fig. 45), which occurred in concert with decreased phosphorylation of RBC-NOS3 at ser^{1177} (Fig. 46). The reduced membrane strain in the rigidified cells (i.e., decrease EI for a given shear; Fig. 44) could have resulted in diminished signal propagation to downstream mechanosensitive pathways. The negative effects of the thiol-oxidizing agent diamide on RBC deformability have been well-described and are primarily attributed to the formation of spectrin-spectrin cross-links [242-244]. Previous studies have thus employed diamide to alter RBC membrane flexibility to assess whether membrane deformability regulates ATP release from these cells

[237]. We chose to use this compound for the same reason; however, given thiol oxidation of the RBC membrane appears to interfere with the function of dynamic signalling processes (e.g., Piezo1; Fig. 49), the use of similar compounds in biochemical studies aimed at assessing RBC mechanics should be carefully considered.

A second experiment was performed to determine whether decreased NO-production and activation of RBC-NOS3 could be 'restored' through increased shear exposure of diamide-treated RBC, which would force these cells to 'stretch' to the same extent as untreated RBC. Our observations were that despite a standardised cellular deformation (i.e., membrane strain), neither RBC NO-production (Fig. 47) or activation of RBC-NOS3 (Fig. 48) were restored to the levels of the untreated cells. Given we have previously demonstrated that shear stress could restore basal RBC-NOS3 activation when the intracellular signalling cascade was suppressed in the absence of shear (i.e., impaired Akt kinase activity; [76]), it was hypothesised that the diamide-treatment might affect the mechanism that translates mechanical shear into biochemical signals. The mechanosensitive cation channel Piezo1 has been implicated in force sensing across a variety of tissues [245-248] and was thus targeted as a potential player involved in mechanical shear responses in RBC. Piezo1 is expressed in the RBC membrane and appears to regulate cell volume through down-stream effects, which may contribute to RBC senescence – eryptosis – and also facilitate traversal of narrow

capillaries [18, 45]. Tissue-specific mutations of RBC-Piezo1 result in developmental defects and are associated with several hereditary blood disorders [110, 114, 249, 250]. In diamide-treated RBC, we observed that the capacity of the specific Piezo1-activator Yoda1 to stimulate Ca^{2+}-flux was significantly ameliorated, while basal Ca^{2+}-levels were unaltered (Fig. 49), indicating that shear-induced Piezo1-opening is likely sensitive to thiol oxidation. Given Piezo1 was recently implicated in the direct initiation of ATP release from RBC [234], it is possible that the diamide-induced ameliorations in Piezo1-function reported herein (Fig. 49) may have also contributed to impaired signal transduction in those previous reports, and ultimately led to the observed decrease in ATP release. Piezo1 contains a total of 57 cysteine-residues that may be vulnerable to cross-linking *via* thiol oxidation [251]. The structure of Piezo1 has been resolved in detail, revealing a homotrimer composed of three blade-like sub-units that form a structure resembling a propeller [252, 253]. Inter-subunit cross-links that restrict conformational flexibility of the blade and cap regions have been shown to ameliorate the capacity of Piezo1 to sense mechanical force [251, 254], which may explain the decreased capacity of Piezo1 to facilitate Ca^{2+}-flux observed herein. Given increased $[Ca^{2+}]_i$ is thought to be a vital step in the activation of RBC-NOS3, it is possible that diamide-treated RBC did not respond with an adequate influx of Ca^{2+} during the shear condition protocol to induce activation of RBC-NOS3 (Fig. 49), which would explain the lack of NO-production and NOS-activation in diamide-treated RBC in response to shear.

Clinically, loss-of-function mutations in the *PIEZO1* gene may present with diminished capacity to regulate blood pressure, specifically during scenarios where shear-induced NO is relevant (e.g., exercise).

RBC-NOS3 is thought to be a functional twin of its endothelial counterpart [80]; for example, it may be detected with eNOS-specific antibodies [88, 255], supporting the hypothesis that RBC-NOS3 is in fact identical to eNOS [88]. Moreover, genetic global knock-out models of eNOS produce RBC devoid of NOS-activity [44, 89], and mass spectrometric studies reveal congruent sequences of RBC-NOS3 and eNOS [88]. Given the profound cellular discrepancies between enucleated RBC and endothelial cells, however, and the importance of, for example, sub-cellular localization to the function of eNOS [84], extending the functions of eNOS onto the RBC-derived NOS must be carefully considered. Nevertheless, phosphorylation of eNOS at ser^{1177} and subsequent NO-production are thought to require Piezo1-dependent Ca^{2+}-influx [46, 256]. Piezo1-knock out murine models present with high embryonal mortality [257], while Piezo1-knock down animals develop hypertension and impaired vascular reactivity, among other circulatory defects [46, 256]. Given that RBC-NOS3 has previously been implicated in the regulation of blood pressure [44, 258], it is possible that the absence of RBC-derived NO may have contributed to the development of hypertension in these animals. We show here, using freshly obtained human RBC, that inhibition of Piezo1 by the peptide GsMTx4 abolished

shear-induced phosphorylation of RBC-NOS3 ser^{1177} (Fig. 50A). The inhibitor peptide was not used in the highly rigidified RBC experiments induced by diamide, given that both mechanical stimulation, and Yoda1, were inadequate to generate an increase in NOS signal (Figs. 46, 48, 50A); our exclusion does not suggest this peptide is ineffective at altering Ca^{2+}-flux for rigid cells, although it does appear that the absolute impact would be diminished in this scenario.

Application of the specific Piezo1-activator Yoda1 stimulated NO-generation through phosphorylation of RBC-NOS3 in the absence of shear, which was inhibited by the NOS-inhibitor *L*-NAME (Fig. 50B); these observations collectively indicate that shear-induced influx of Ca^{2+} *via* Piezo1 is required for acute activation of RBC-NOS3. It can be speculated that the Ca^{2+}-carrier calmodulin, which in RBC exhibits a half-activation Ca^{2+} concentration of 100-920 nM [259], is recruited to bind RBC-NOS3, as is known to occur in endothelial cells [102]; however, this has yet to be confirmed in RBC. Studies in neuronal cells have shown that local increases in cytosolic Ca^{2+}-concentration [260], that may be evoked by opening of Piezo1-channels, couple PI3K activation with Akt phosphorylation; whether the RBC-isoform of PI3K may also require local influx of Ca^{2+} through Piezo1 to facilitate downstream phosphorylation of Akt and subsequently RBC-NOS3 remains an open question. Resolving these mechanisms may not be trivial, given the fundamental cellular differences between these cell types (e.g., excitability, presence of sub-cellular compartments). Yoda1-

stimulation resulted in a 6.8-fold increase of Fluo-4-related fluorescence in untreated RBC, indicating that the basal free Ca^{2+} content (~40-60 nM; [47]) was sufficiently increased to precipitate detectable NO-formation secondary to calmodulin-NOS complexation. In diamide-treated RBC, however, impeded Ca^{2+}-flux may have been insufficient to initiate activation of RBC-NOS3 (Fig. 49). Further, given that *L*-NAME effectively prevented increased cytosolic NO-content following both mechanical shear and chemical activation of Piezo1 (Fig. 50B), it can be assumed that NO generated through reduction of nitrite *via* deoxyhaemoglobin was negligible.

Collectively, we provide evidence that Piezo1 is a vital molecular player in the capacity of RBC to sense shear and subsequently respond with NO generation *via* activation of RBC-NOS3; our working hypothesis for the interplay in this pathway is summarised in Figure 51. This capacity of RBC to actively alter enzyme activation *via* endogenous signalling appears to be sensitive to thiol oxidation of membrane components, including Piezo1. Given the involvement of RBC-NOS3 in regulating vascular tone and blood pressure, thiol oxidation of RBC membrane proteins and functional assessments of Piezo1 may prove useful as potential biomarkers for the progression of various circulatory disorders.

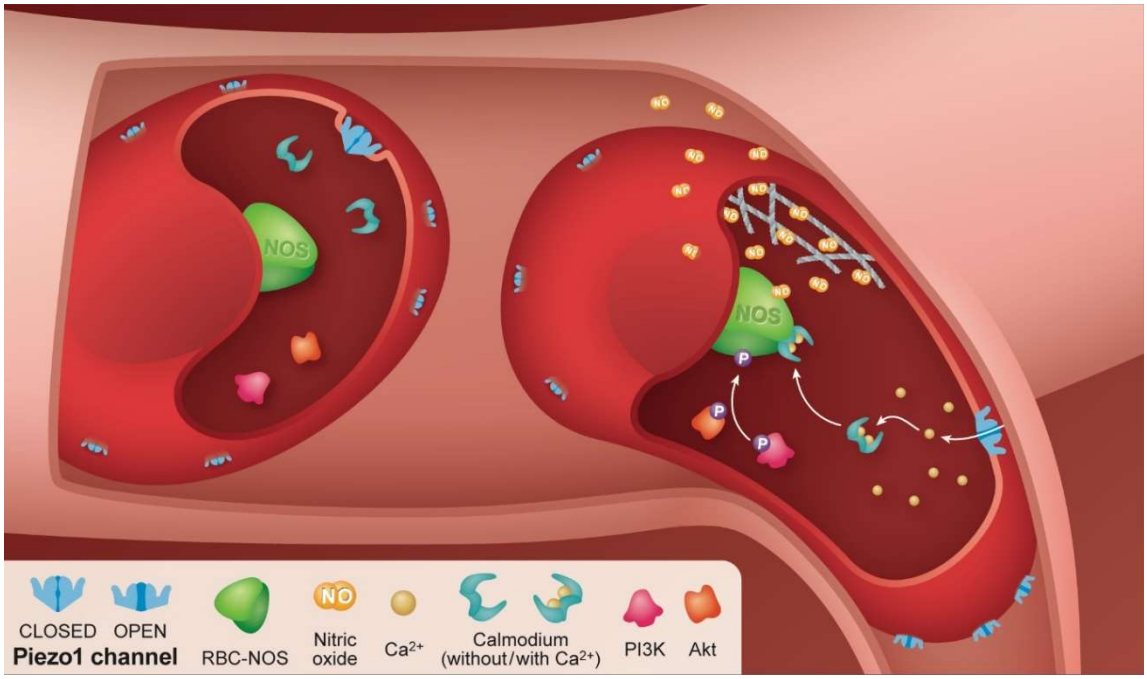

***Fig. 51**: A graphical representation of the proposed signalling pathway is presented: mechanical stimulation of red blood cells (RBC), as occurs when traversing a narrow capillary that requires cellular deformation, causes Piezo1-channels embedded in the RBC membrane to open. Calcium ions pass the cell membrane and, provided enough calcium is accumulated in the cytosol, bind to the calcium-carrying protein calmodulin, which subsequently forms a complex with RBC-derived nitric oxide (NO) synthase (RBC-NOS) to initiate production of NO. Activation of RBC-NOS is regulated through phosphorylation of Ser^{1177} via upstream kinases phosphoinositide 3-kinase (PI3K) and Akt/protein kinase B, and NO produced by RBC-NOS may participate in autocrine or paracrine signalling. It is important to note that the exertion of potential extracellular effects of RBC-borne NO is a highly controversial topic due to the scavenging properties of haemoglobin, with substantial evidence provided to support and combat this hypothesis, while no consensus has been reached yet.*

6.6 Supplementary figures: Piezo1 regulates shear-dependent nitric oxide production in human erythrocytes

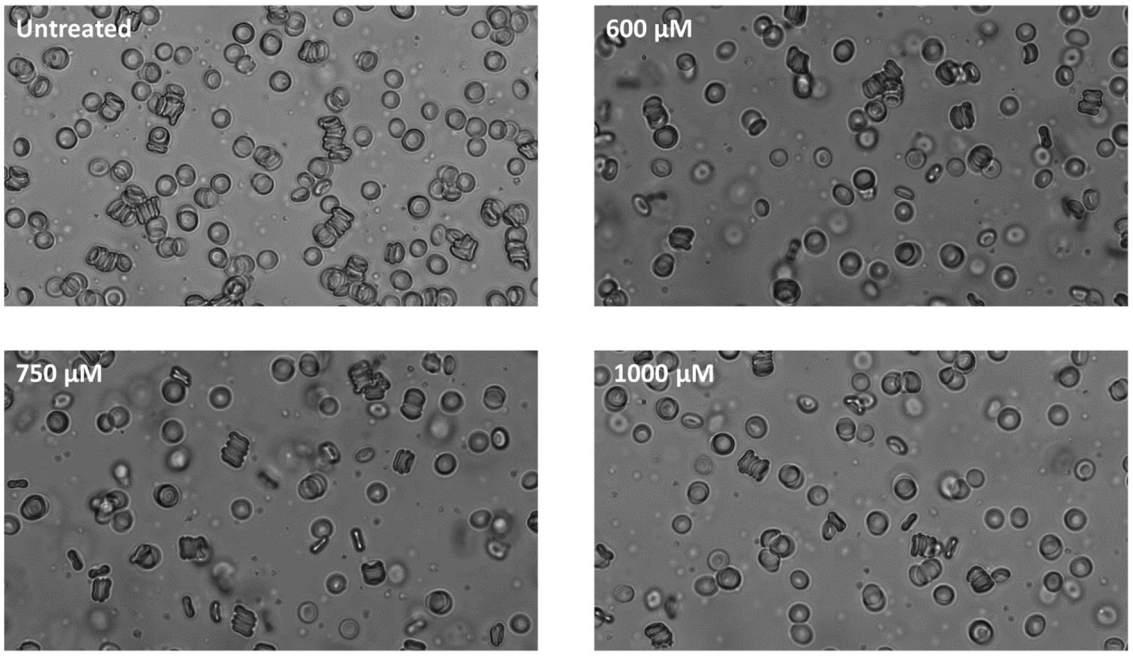

Fig. 52*: Morphological features of red blood cells (RBC) following incubation with increasing concentrations of diamide (600-1000 µM) or PBS as control (i.e., untreated). RBC were suspended in autologous plasma at a 0.1% haematocrit to facilitate imaging of individual cells. Imaging was performed at room temperature using an inverted microscope (IX73, Olympus Corp., Tokyo, Japan) with an integrated camera (optiMOS sCMOS, QImaging, Surrey, Australia) at 600-fold magnification.*

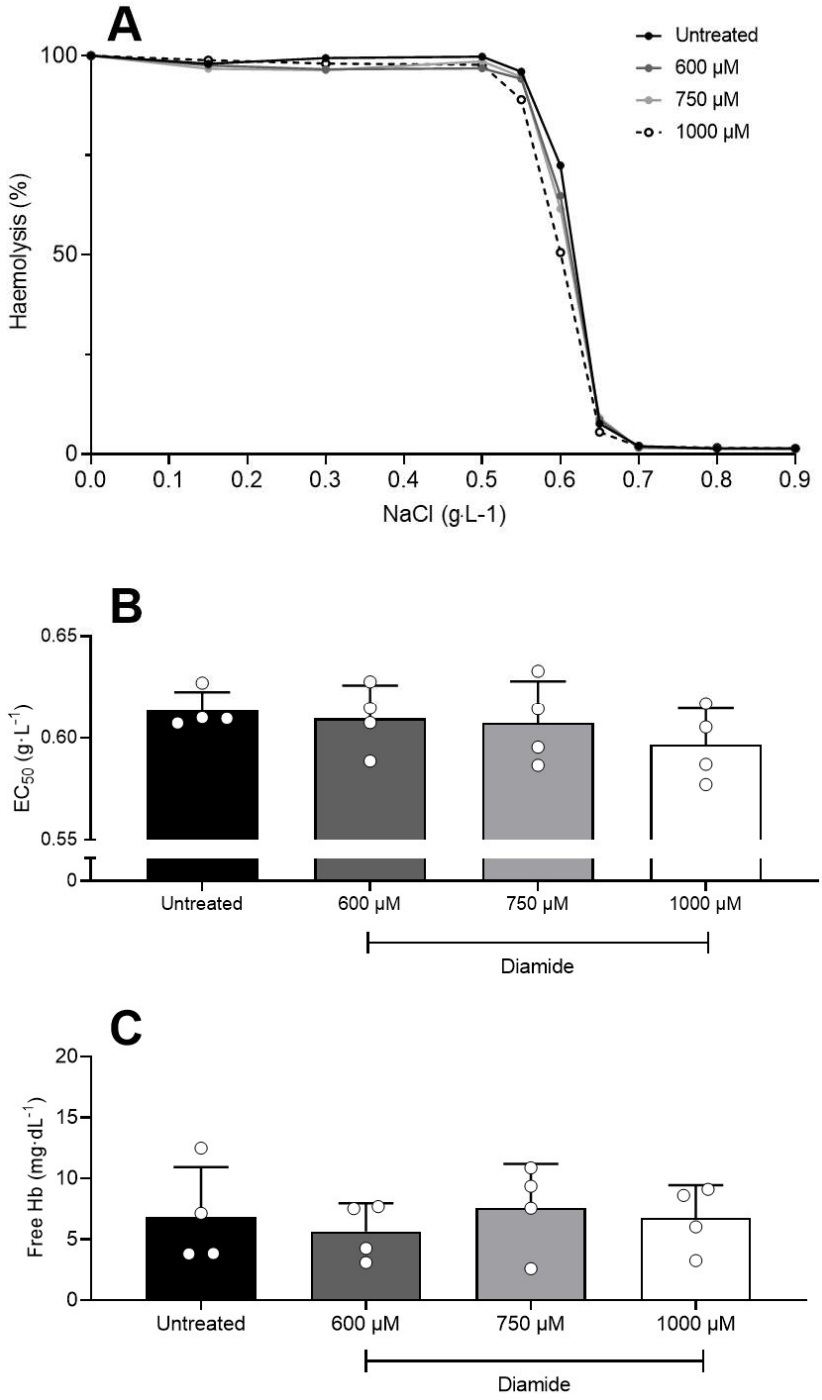

***Fig. 53**: Fragility (i.e., efflux of haemoglobin) of red blood cell (RBC) samples, previously incubated with increasing concentrations of diamide or PBS as control, plotted against increasing [NaCl] in the suspending medium (A). RBC treated with 1000 µM diamide presented with a decrease in osmotic fragility, as evidenced by a decreased efflux of haemoglobin at a given salinity. Extraction of [NaCl] where 50% of RBC haemolyse ("EC_{50}") provides an index of RBC fragility (B). Free haemoglobin in the supernatant recovered following the incubation procedures indicates toxicity of the treatment is absent (C). Data presented as Mean ± standard deviation (B, C), error bars were omitted in (A) to increase clarity. N = 4*

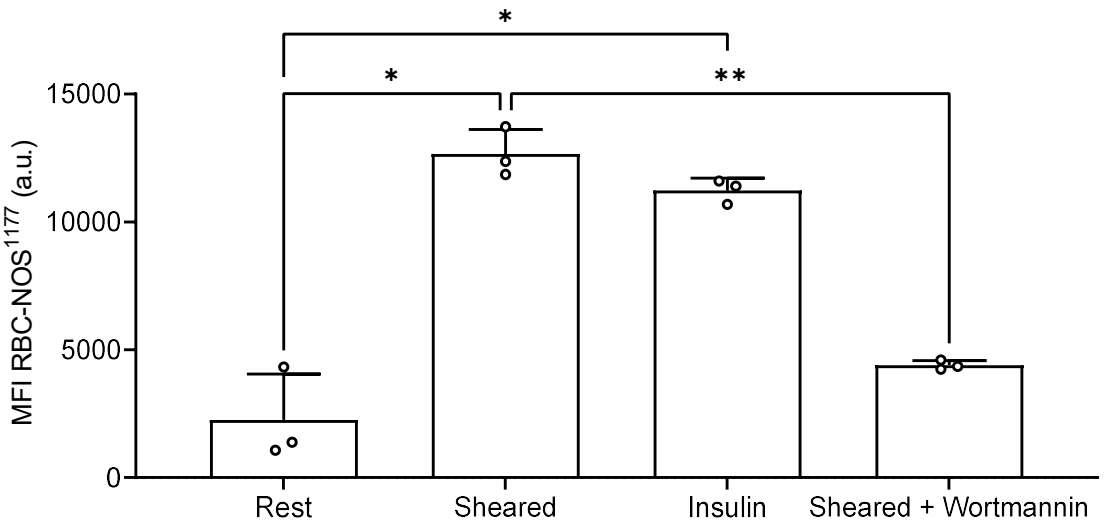

***Fig. 54**: Semi-quantitative immunofluorescent detection of phosphorylated serine^{1177}-residue of red blood cell-derived nitric oxide synthase (RBC-NOS3 ser^{1177}) was validated through pharmacological stimulation or suppression of this post-translational modification. We stimulated phosphorylation of RBC-NOS3 ser^{1177} using insulin (350 pM), which activates the PI3K/Akt kinase pathway, and inhibited it with Wortmannin (5 μM), an irreversible inhibitor of PI3K. Phosphorylated RBC-NOS3 ser^{1177} increased following mechanical stimulation (i.e., shearing) over resting values; phosphorylation could similarly be increased by stimulation with insulin in the absence of shear, while mechanical stimulation in cells treated with Wortmannin failed to elicit increased phosphorylation. $^{**}P < 0.01$, $^{*}P < 0.05$ determined using One-Way analysis of variance with Holm-Šídák post-hoc comparisons applied to preselected pairs. N = 3*

6.7 Conclusion

The observations of *Study 4* provide a glimpse into a complex, mechanically-activated, post-translational cellular signalling in enucleated, circulating RBC. A description of this signalling network is yet to be developed, given that the traditional view of RBC does not consider these newly-discovered processes. It appears that the mechanosensitive cation channel Piezo1 is a major nexus of

mechanotransductive signalling, in accordance with observations from *Studies 2* and *3*. Restriction of Piezo1-induced influx of Ca^{2+}, whether through shifting the activation threshold well-above the forces applied in *Study 4 via* the peptide GsMTx4 [101], or through treatment with the thiol oxidising agent diamide, abrogates activation of Ca^{2+}-sensitive proteins like RBC-NOS3. It could not be resolved whether the shear stress that RBC are exposed to, or indeed the resultant deformation of the cell membrane, are the driving force behind increased opening of Piezo1-channels due to the direct action of the diamide-treatment on Piezo1-dependent Ca^{2+}-flux; however, the observation of Piezo1-dependent Ca^{2+}-flux being sensitive to thiol oxidation is valuable and warrants deeper investigations. Of note, the RBC populations assessed in *Study 4* were not separated according to density; that is, these cell populations contain RBC of highly variable *in vivo* ages. It is possible that increased oxidation, a hallmark of RBC ageing, limits Piezo1-efficiency in 'old' RBC, as was observed in *Study 3*.

Collectively, it appears that entry of Ca^{2+} has not only detrimental (e.g., *Study 2; Study 3*), but also beneficial effects (e.g., *Study 4)* that may be essential for RBC physiology. Piezo1 appears to be the primary mechanism that enables RBC sensing of mechanical forces, with RBC-NOS3 as an important down-stream target, given the role of RBC-derived NO in blood pressure regulation [44, 258].

Chapter 7

Conclusion

7.1 Summary of findings

The salient findings of the experimental procedures outlined in the present thesis support that i. the composition of the heterogeneous RBC population, a direct consequence of surrendering transcriptional capacity, impacts blood fluid behaviour and RBC physical properties in humans; ii. the physical properties of RBC, which determine blood fluidity, underlie acute, biochemical regulation; iii. these biochemical pathways are activated and/or regulated, at least in part, through mechanical cues; iv. opening of the mechanically-activated cation channel Piezo1 is a primary mechanism of mechanotransduction in RBC. These tantalising observations contribute to a step-change in the contemporary understanding of RBC physiology and suggest that RBC are, in contrast to traditional views, a responsive cell type, which may indeed serve as a pharmacologically viable therapeutic target. Mounting evidence, accumulated over the past decade, supports the active role of RBC in the regulation of haemodynamics, and thus vascular distribution of RBC and delivery of oxygen to working tissues. Within these signalling processes, particular emphasis is placed on Ca^{2+} and NO, given that their involvement in the regulation of RBC mechanics has long been suspected [50]. In the present work, Ca^{2+} was observed

to be a critical second messenger, regulating cell volume (*Study 2*), contributing to acute removal of aged RBC (*Study 3*), and initiating production of endogenous NO (*Study 4*). Piezo1 was identified as the major transducer of changes in $[Ca^{2+}]_i$ in response to mechanical forces and appears to be central to a multitude of cellular signalling processes in enucleated RBC. In summation, it was observed that the role of RBC as passive carriers of haemoglobin should be expanded to include their more 'active' functions, which are supported by a unique, exclusively post-translational signalling network. Yet to be identified targets of Ca^{2+}-dependent signalling beyond RBC-NOS3 and the Gárdos channel may present promising avenues of future study, and other mechanically-activated mechanisms alluded to, but not investigated in detail here, warrant further study (e.g., microvesicle trafficking, extracellular targets of RBC-derived signals, relevance of intracellular signalling pathways in RBC to systemic homeostasis).

The physical properties of RBC are highly relevant to normal blood fluid behaviour. Remarkably, these properties are largely maintained over the RBC lifespan, despite the absence of intracellular machinery to facilitate removal and replacement of damaged components; it is, nonetheless, thought that modified haemoglobin molecules that may become harmful to cellular homeostasis, and probably other cell components, are periodically released from mature RBC through exocytosis [221]. Consequently, RBC increase in density over the course of their lifespan, and exhibit decreased abundance of some proteins (e.g., Piezo1,

as evidenced in *Study 3*). Given that only small fractions of abnormal cells may alter cell-cell interactions within the RBC population, and indeed macrorheological fluid behaviour (*Study 1*), limiting the fraction of the physiologically 'oldest' cells appears crucial to circulatory health.

7.2 Heterogeneity of RBC populations

A consistent observation throughout the present body of work, which was alluded to in recent reports [22, 186], is the need to consider that RBC within a given blood sample comprise a heterogenous cell population, due to progressive *in vivo* ageing. It appears that a small fraction of abnormal RBC is relevant to blood fluid behaviour and cell-cell interactions (*Study 1*), and that removal of some RBC through mechanically-activated Ca^{2+}-pathways seems to alter bulk RBC mechanics (*Studies 2, 3*). Distinct capacity to handle influx of Ca^{2+} within a given RBC population appears related to physiological cell age (*Study 3*) and sensitive to oxidative modulation (*Study 4*). Despite minimal differences observed in baseline properties (e.g., morphology, deformability; *Study 3*), the sensitivity of these distinct RBC sub-populations to mechanical or chemical stimulation may differ substantially (*Studies 2, 3*). It is thus suggested that distribution of RBC sub-populations in a given sample may yield relevant clinical information, for example pertaining to the relative abundance of 'light' and 'dense' cell fractions. Altered distribution of subfractions reflecting 'young' and

'old' RBC, respectively, may indicate pathologically accelerated clearance / cell ageing or diminished erythropoiesis.

Further investigations aimed at elucidating some of the mechanisms that determine distinct properties of 'young' and 'old' RBC to extend the salient findings described in *Study 3* would be of great value. An intriguing extension of *Study 3* would be to perform metabolomic analysis of the discrete RBC sub-populations both at rest and in response to Yoda1, given the Ca^{2+}-influx provoked by Yoda1, which simulates Ca^{2+}-movements evoked by mechanical force *via* opening of Piezo1-channels, was observed to precipitate differential responses in these cell populations. It is plausible that metabolic insufficiency limits the calcium-handling capacity of physiologically aged RBC, however, measurements of specific changes in glycolytic metabolites would provide mechanistic underpinnings to the herein presented hypothesis. Previous reports have shown that Piezo1-activation through mechanical force accelerates RBC metabolism [261], likely depleting ATP-reserves of old RBC more rapidly, which then also require longer periods of time to replenish.

7.3 Clinical implications and future directions

The herein presented four experimental studies aimed at providing novel insights into fundamental physiological responses of human RBC. Given the novel concepts and signalling pathways elucidated here, the present body of

work contributes to a step-change in our understanding of RBC physiology. Future extensions of this work, however, should consider how these pathways are altered in, and potentially contribute to, the development of pathophysiological scenarios. Three distinct pathophysiological phenomena should be of particular relevance: i. clinical scenarios where blood is exposed to mechanical forces beyond those occurring in the human cardiovascular system (e.g., mechanical circulatory support); ii. hereditary RBC disorders linked to mutations in Piezo1 and/or dysfunctional cell volume regulation; and iii. pathologies potentially related to abnormal RBC-NOS3 signalling.

7.3.1 Supraphysiological mechanical forces

The experiments conducted in the present thesis provide some insight into mechanotransduction processes of RBC, stimulated by mechanical cues that were designed to mimic those present in the human body, with magnitudes ≤10 Pa [76, 162, 228]. Patients with end-stage heart failure that are in critical need of a heart transplant, however, are commonly equipped with mechanical circulatory support devices as bridge-to-transplant therapy, given the severe shortage of viable donor hearts [262]. Moreover, insertion of bypass grafts or replacement heart valves in patients requires rerouting of blood through an extracorporeal cardio-pulmonary circuit to facilitate open-heart surgery. While acutely life-saving, these devices subject blood to mechanical forces exceeding those present

in the human body by several orders of magnitude (up to 1000 Pa; [103]). Given the importance of mechanically-activated signalling pathways to RBC homeostasis demonstrated within the present works, exposure to mechanical forces of significantly larger magnitude could be absolutely detrimental to cell function. Previous work from our laboratory has indicated that, for example, shear-mediated activation of RBC-NOS3 [226], and subsequent production of NO [198], are sensitive to the magnitude of shear applied. It is thus plausible that excessive mechanical force exposure may lead to over-activation of Piezo1-dependent pathways, depleting RBC of intracellular ATP [261]. Diversion of significant quantities of ATP to maintaining ionic homeostasis by increasing ATPases that correct substantial influx of Ca^{2+} may have severe impacts on the antioxidant defence system. Glutathione reductase, a vital reducing agent [263], requires redirection of glucose to maintain sufficient levels of NADPH for recycling. Given that RBC lack mitochondria and are thus dependent on glycolysis for ATP-production, which in turn is required for ion homeostasis, redirection of glucose to increase NADPH-generation and prevent accumulation of free radicals may severely unbalance cellular homeostasis. Moreover, overproduction of RBC-NOS3-dependent NO in response to mechanical shear may contribute to a disturbance of homeostasis through nitrosative stress, as NO and abundant O_2^- react rapidly to form cytotoxic $ONOO^-$ [76, 264].

Excessive mechanical forces have been shown to provoke generation of RBC-derived microvesicles *in vitro* [265]. Moreover, patients with implanted cardiac assist devices are known to exhibit accumulation of Ca^{2+} in the RBC cytosol [266], and present with increased levels of RBC-derived microparticles [267]. It is tantalising to hypothesise that increased release of microvesicles from RBC is a Piezo1- and Ca^{2+}-dependent process, similar to that observed in *Study 3*. Further studies are required, however, to ascertain this mechanistic link.

Collectively, the field of mechanotransduction is emerging, and elucidation of mechanically-activated signalling in enucleated RBC in healthy scenarios is in its infancy. An obvious clinical application is the study of impairments in RBC induced by mechanical forces far exceeding those found in normal physiology, which could explain some of the severe complications associated with the use of mechanical circulatory assist devices [262].

7.3.2 Blood disorders precipitated by mutations in PIEZO1

Haematological disorders caused by mutations in the *PIEZO1*-gene are increasingly reported, and affected individuals typically exhibit abnormal RBC morphology and/or cell volume regulation [249]. Gain-of-function mutations cause increased sensitivity or prolonged de-activation kinetics of Piezo1, manifesting larger spikes or longer periods of increased $[Ca^{2+}]_i$, respectively [110, 114, 250, 268]. Increased $[Ca^{2+}]_i$ is thought to result in RBC dehydration through

overactivation of the Gárdos channel (*Study 2*), which precipitates accelerated clearance of RBC (*Study 3*), thus causing anaemia. Given that the Gárdos effect provokes leakage of K^+ from RBC into the surrounding plasma, common symptoms include pseudo-hyperkalaemia, which may cause cardiac arrhythmias [269]. Interestingly, loss-of-function mutations cause a distinct phenotype, where affected individuals exhibit lymphatic dysplasia with non-immune foetal hydrops [270], although how these symptoms are associated with abnormal RBC Ca^{2+}-permeability remains unclear; it is speculated instead that Piezo1 is essential for vascular development of the lymphatic system. It appears that the balanced interplay between Piezo1 and the Gárdos channel is highly clinically relevant [271], thus, targeting modulation of either channel is of value. Post-translational modifications that alter sensitivity of either channel [40], or coordination with other proteins / lipids that are likely to affect local membrane properties [272, 273], for example, are poorly described in RBC, and would present fruitful avenues of investigation.

7.3.3 Dysfunctional intracellular signalling cascades

Intracellular signalling in mature, circulating RBC has received attention only recently. Given the emerging physiological significance of RBC-signalling, demonstrated by the independent contribution of RBC-NOS3 to blood pressure regulation [44], it is possible that other components of the RBC-NOS3 pathway

and/or other cellular signalling contribute to a role of RBC beyond being mere transport vessels of haemoglobin [7]. It is suggested that eNOS underlies regulation by Ca^{2+}-dependent and -independent activation mechanisms, although both may be initiated by shear stress [274]. At present, it is thought that RBC-NOS3 is activated by shear stress in a Ca^{2+}-dependent manner, given that the shear-mediated activation mechanism appears entirely dependent upon Piezo1 (*Study 4*). Activation may also occur, however, following stimulation *via* insulin in the absence of mechanical shear (*Study 4*), which is likely transduced through the PI3k/Akt kinase pathway. Whether this pathway may be activated through shear in a Ca^{2+}-dependent or -independent manner, is not yet resolved. It is possible that initial activation of RBC-NOS3 requires complexation with Ca^{2+}/calmodulin, while sustained activation does not require further Ca^{2+}-stimulation and/or mechanical force, as suggested for eNOS [275]. It is clear that direct experimental evidence, rather than inferences from eNOS, is required to ascertain the subtle regulatory processes that balance activation of RBC-NOS3 and NO-production within RBC.

During transit of the arterial and venous networks, oxygen tensions within blood vary due to offloading of O_2 from RBC. Oxygen content of RBC (i.e., bound to haemoglobin) significantly alters intracellular NO-pathways and especially interactions of NO with haemoglobin. While activation of RBC-NOS3 is down-regulated in conditions of low cellular O_2 because O_2 is required as a co-factor,

there is evidence to suggest that NOS may exhibit nitrite reductase-like function. That is, while not producing NO itself, RBC-NOS3 catalyses the conversion of NO_2^- to bioactive NO [255]. Moreover, deoxy-haemoglobin also acts as a source of NO by reducing NO_2^- [276]. The effect of mechanical stimulation on RBC-NOS3 under conditions of varying O_2-availability, however, remains to be elucidated.

To date, no direct clinical relevance of dysfunctional regulation of RBC-NOS3 has been reported. Indirect evidence suggests that abnormal RBC-NOS3, however, is present in blood-related pathologies including sickle cell disease [111, 277], diabetes mellitus [24], and hypertension [88]. Moreover, it is possible that some pathological effects currently attributed to mutations in *PIEZO1* (e.g., hypertension in murine models carrying *PIEZO1*-mutations [256]) are precipitated by dysfunctional regulation of downstream RBC-NOS3, and Piezo1-dependent NO-production (*Study 4*). Probing these signalling pathways with the *ex vivo* techniques developed and applied in the present body of work is useful, albeit limitations including antibody-specificity, off-target effects of inhibitory compounds and effects of blood removal from the organism demand careful interpretation of results. Tissue-directed genetic knock-outs in suitable model organisms present a unique and state-of-the-art avenue for confirming the physiological relevance of the herein observed RBC signalling pathways, circumventing the aforementioned limitations.

7.4 Conclusion

The importance of mechanotransduction, the conversion of mechanical cues into biochemical or electrophysiological signals, is increasingly recognised. In 2021, resolving the molecular identity of what appears to be a family of mechanosensory proteins central to many mechanically-regulated processes, Piezo-ion channels, was awarded the highest scientific honour – the Nobel prize. The concept of mechanotransduction seems intuitively significant to how we perceive the world with our sense of touch, however, the mechanistic underpinnings of this process had remained elusive. Touching an object causes changes in pressure on peripheral neurons, 'sensed' by Piezo-channels. Changes in pressure cause these channels to open, thus inducing altered membrane potential in the neuron, which is passed on *via* action potentials. Astonishingly, mechanotransduction occurs in enucleated, circulating RBC, although for a different purpose. Signals are likely not passed on to other cells, but instead, are crucial to autocrine regulation of RBC physical and biochemical properties.

The discovery of 'active' RBC signalling in response to acute mechanical cues from their environment supports that these cells may be significantly more involved in circulatory function than previously assumed. Given the constant exposure of these cells to mechanical forces that are highly variable across the cardiovascular system, it is logical that mechanotransductive signalling exists in RBC to facilitate traversal of this dynamic environment. The findings of the

present body of work elucidate some mechanotransductive signalling pathways that are relevant to RBC function, but it is likely that there are more to be unravelled.

The framing of RBC as passive bodies demands revisiting, given the herein observed responsiveness to external (mechanical) cues.

List of symbols and units:

× *g* – acceleration due to gravity

cm – centimetre

cP – centipoise

°C – degrees Celsius

Δ – delta, absolute difference

g – gram

Hz – hertz

h – hour

kDa – kilo Dalton

kg – kilogram

L – litre

m – metre

μL – microlitre

μm – micrometre

μM – micromole per litre

mg – milligram

mL – millilitre

mm – millimetre

mM – millimole per litre

mOsm – milliosmole

mPa – millipascal

ms – milliseconds

mV – millivolt

min – minute

M – mole per litre

nm – nanometre

nM – nanomole per litre

Pa – pascal

π – pi

pH – potentia hydrogenii

r – radius

s – second

γ – shear rate

τ – shear stress

σ – standard deviation

t – time

V – velocity

η – viscosity

$L \cdot L^{-1}$ – volume per volume

λ – wavelength

Glossary of abbreviated terms:

ATP – adenosine triphosphate

ANOVA – analysis of variance

a.u. – arbitrary units

BSA – bovine serum albumin

$CaCl_2$ – calcium chloride

A23187 – calcium ionophore

Ca^{2+} – calcium ion

$K_{Ca}3.1$ – calcium-activated potassium channel

CO_2 – carbon dioxide

CCD – charge-coupled device

χ^2 – chi-squared

Cl – chloride

Cl^- – chloride ion

CD40 – Cluster of Differentiation 40

R^2 – coefficient of determination

DAB - 3,3'-Diaminobenzidine

DAF-FM DA – 4-amino-5-methylamino-2',7'-difluorofluorescein diacetate

EI – elongation index

eNOS, NOS-3 – endothelial-type nitric oxide synthase

EDTA – ethylenediaminetetraacetic acid

FAD – flavin adenine dinucleotide

FMN – flavin mononucleotide

FITC – fluorescein isothiocyanate

KCNN4 – gene encoding $K_{Ca}3.1$

GASP – glucose- and albumin-supplemented buffer

GA – glutaraldehyde

Hb – haemoglobin

NOS-2 – inducible nitric oxide synthase

LORCA – laser-assisted optical rotational cell analyser

$MgCl_2$ – magnesium chloride

EI_{max} – maximal theoretical elongation

MCV – mean cell volume

MFI – mean fluorescent intensity

O_2 – molecular oxygen

L-NAME – N(G)-nitro-*L*-arginine methyl ester

NOS-1 – neuronal nitric oxide synthase

NO – nitric oxide

NO_2^- – nitrite

NMIIA – non-muscle myosin IIA

NGS – normal goat serum

NA – numerical aperture

PFA – paraformaldehyde

PMS – phenazine methosulfate

PBS – phosphate-buffered saline

PI3K – phosphatidylinositol-3-kinase

PMCA – plasma membrane calcium pump

PVP – polyvinylpyrrolidone

KCl – potassium chloride

K^+ – potassium ion

H^+ – proton

RBC – red blood cell

RDW – red cell distribution width

RDW-SD – standard deviation of the red cell distribution width

NADPH – reduced nicotinamide adenine dinucleotide phosphate

ROI – region of interest

ser^{1177} – serine residue 1177

SAH – serum albumin-supplemented HEPES buffer

$SS_{1/2}$ – shear stress required for half-maximal elongation

S-NO – *S*-nitrosothiol

Na_2CO_3 – sodium carbonate

Na^+ – sodium ion

Na-K-ATPase – sodium-potassium exchanger pump

SD – standard deviation

SEM – standard error of the mean

O_2^- – superoxide

BH_4 – tetrahydrobiopterin

TXred – Texas red filter

-SH – thiol group

TBS – Tris-buffered saline

VAI – visual aggregation index

Water – H_2O

Appendices

Appendix 1: Medical screening questionnaire

This appendix provides the screening form that was used to collect participant data on their medical history and ensure they fit inclusion criteria of the experimental studies conducted within the frame of the present dissertation.

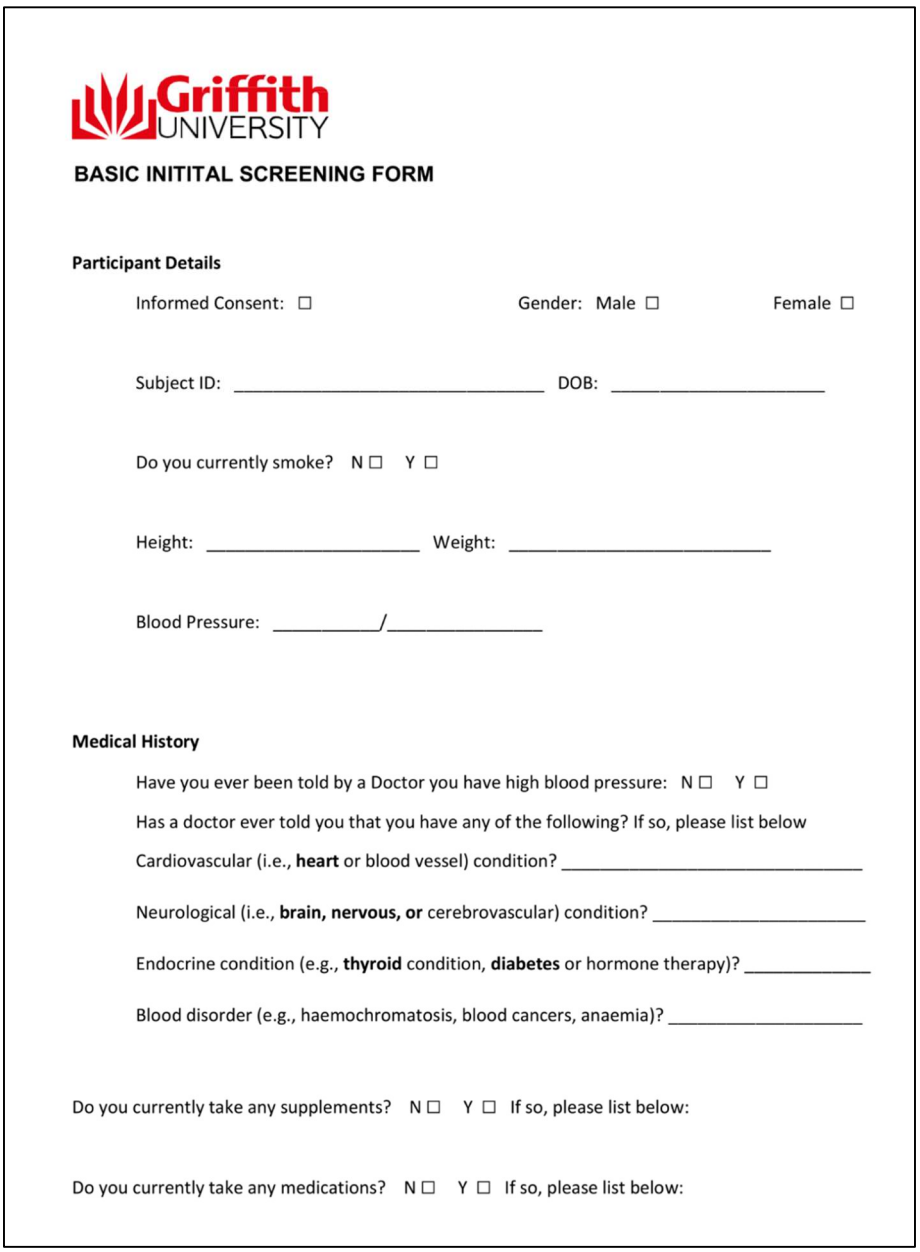

Griffith UNIVERSITY

BASIC INITITAL SCREENING FORM

Participant Details

Informed Consent: ☐ Gender: Male ☐ Female ☐

Subject ID: _____ DOB: _____

Do you currently smoke? N ☐ Y ☐

Height: _____ Weight: _____

Blood Pressure: _____/_____

Medical History

Have you ever been told by a Doctor you have high blood pressure: N ☐ Y ☐

Has a doctor ever told you that you have any of the following? If so, please list below

Cardiovascular (i.e., **heart** or blood vessel) condition? _____

Neurological (i.e., **brain, nervous, or** cerebrovascular) condition? _____

Endocrine condition (e.g., **thyroid** condition, **diabetes** or hormone therapy)? _____

Blood disorder (e.g., haemochromatosis, blood cancers, anaemia)? _____

Do you currently take any supplements? N ☐ Y ☐ If so, please list below:

Do you currently take any medications? N ☐ Y ☐ If so, please list below:

Appendix 2: Automated image analysis for fluorescent RBC

Cell detection, thresholding and binarisation

This appendix provides a step-by-step description of the image analysis routine developed for the purpose of analysing fluorescent RBC, as described, and validated in Chapter 2.5. This routine uses automated thresholding to detect the cells present in a given image using a copy of the original image, produces an overlay that is imposed onto the original image to extract grey values of fluorescent RBC.

1. Cell detection is performed on a copy of the original image to preserve the captured grey values. Automated thresholding is used to generate a binary image (i.e., rather than grey values of varying intensities, the image only contains white or black pixels), which enables edge detection of cells, wherein every single pixel is either part (white) or not part (black) of the signal.

```
idOrig = getImageID();
//This defines the title of the selected image and makes all following commands generally applicable
run("Duplicate...", "title=[My duplicated image]");
//Duplicates the relevant image so that raw image data is not altered
idDuplicate = getImageID();
//Defines image ID of duplicated image
run("Auto Threshold", "method=Otsu white");
//Thresholding that should work for identifying cells of high fluorescent intensity with good edge
detection
```

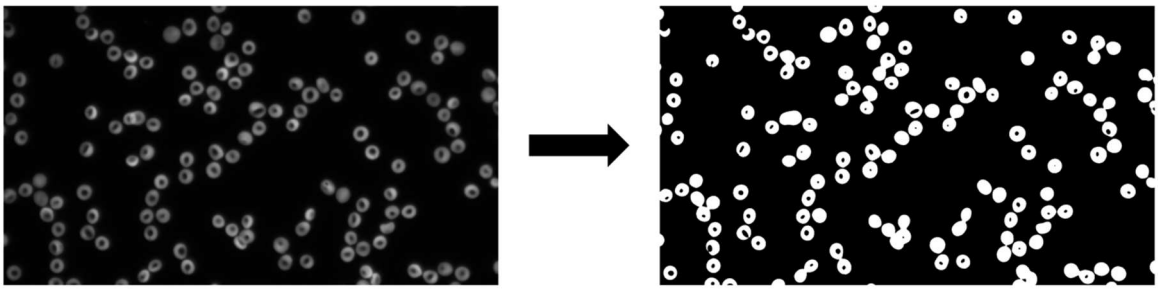

2. White and black pixel values are then inverted create an image that contains white background (i.e., pixel value has maximum grey intensity)

```
run("Invert");
//Invert binary 'colours'
```

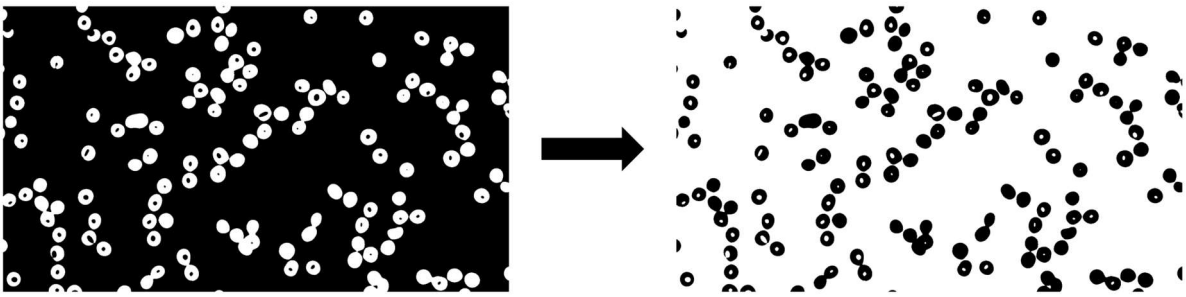

3. An overlay is detected selecting cells, wherein only cells are included that match inclusion criteria of pixel sizes between 400-3000 and exhibit reasonable circulatory. While all cells should fall within these criteria and no other objects should be present on an image, these criteria exclude clustered doublets of cells which may have erroneous grey values due to overlap or cell fragments.

```
run("Analyze Particles...", "size=400-3000 circularity=0.60-1.00 exclude add");
//Create an overlay for detected cells and stores it in the ROI manager
selectImage(idOrig);
//Switches active image to raw data
close(idDuplicate);
//Close cuplicate used to create overlay; not necessary but to avoid running analysis on thresholding
image
```

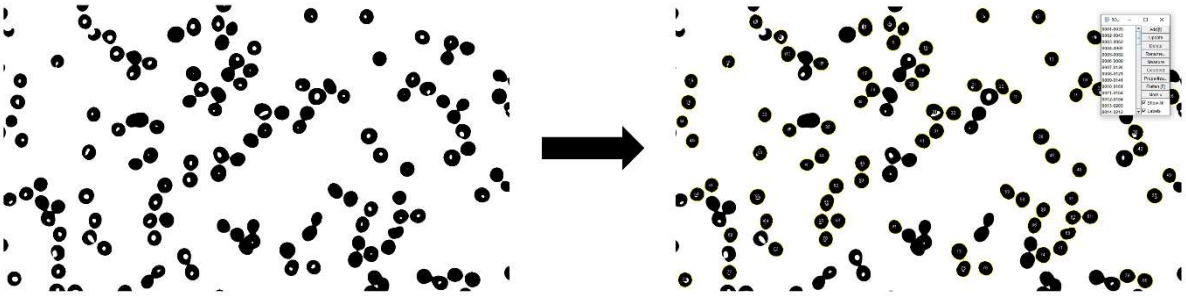

4. The overlay is stored in FIJI's ROI manager and projected onto the original image. Background is subtracted using a rolling ball algorithm and background-corrected fluorescence in each ROI is measured and displayed.

```
run("Subtract Background...", "rolling=50");
//On raw data image; detects background and subtracts it from the whole image
roiManager("Show None");
//Deselect all ROIs in ROI manager if applicable
roiManager("Show All");
//Select all ROIs in overlay from ROI manager
roiManager("Measure");
//Returns background-corrected fluroescence values to Results window
```

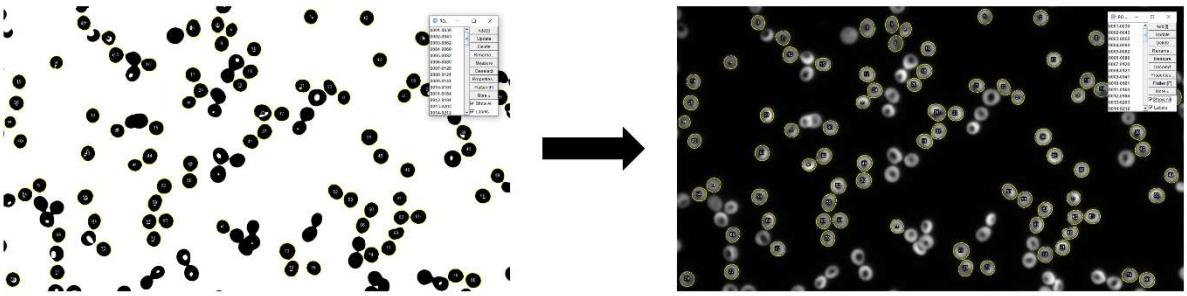

Bibliography

1. Gorter, E. and F. Grendel, *On Bimolecular Layers of Lipoids on the Chromocytes of the Blood.* J Exp Med, 1925. **41**(4): p. 439-43.
2. Wilson, D.F., *Oxidative phosphorylation: regulation and role in cellular and tissue metabolism.* J Physiol, 2017. **595**(23): p. 7023-7038.
3. Mairbaurl, H. and R.E. Weber, *Oxygen transport by hemoglobin.* Compr Physiol, 2012. **2**(2): p. 1463-89.
4. Simmonds, M.J., H.J. Meiselman, and O.K. Baskurt, *Blood rheology and aging.* J Geriatr Cardiol, 2013. **10**(3): p. 291-301.
5. Moras, M., S.D. Lefevre, and M.A. Ostuni, *From Erythroblasts to Mature Red Blood Cells: Organelle Clearance in Mammals.* Front Physiol, 2017. **8**: p. 1076.
6. Baskurt, O.K. and H.J. Meiselman, *Blood rheology and hemodynamics.* Semin Thromb Hemost, 2003. **29**(5): p. 435-50.
7. Richardson, K.J., L. Kuck, and M.J. Simmonds, *Beyond oxygen transport: Active role of erythrocytes in the regulation of blood flow.* Am J Physiol Heart Circ Physiol, 2020.
8. Litvinov, R.I. and J.W. Weisel, *Role of red blood cells in haemostasis and thrombosis.* ISBT Sci Ser, 2017. **12**(1): p. 176-183.
9. Borun, E.R., W.G. Figueroa, and S.M. Perry, *The distribution of Fe59 tagged human erythrocytes in centrifuged specimens as a function of cell age.* J Clin Invest, 1957. **36**(5): p. 676-9.
10. Franco, R.S., et al., *Changes in the properties of normal human red blood cells during in vivo aging.* Am J Hematol, 2013. **88**(1): p. 44-51.
11. Joiner, C.H. and P.K. Lauf, *Ouabain binding and potassium transport in young and old populations of human red cells.* Membr Biochem, 1978. **1**(3-4): p. 187-202.
12. Romero, P.J., E.A. Romero, and M.D. Winkler, *Ionic calcium content of light dense human red cells separated by Percoll density gradients.* Biochim Biophys Acta, 1997. **1323**(1): p. 23-8.
13. Romero, P.J. and E.A. Romero, *Effect of cell ageing on Ca2+ influx into human red cells.* Cell Calcium, 1999. **26**(3-4): p. 131-7.
14. Gardos, G., *The function of calcium in the potassium permeability of human erythrocytes.* Biochim Biophys Acta, 1958. **30**(3): p. 653-4.
15. Lew, V.L., et al., *Effects of age-dependent membrane transport changes on the homeostasis of senescent human red blood cells.* Blood, 2007. **110**(4): p. 1334-42.
16. Lew, V.L., et al., *Distribution of plasma membrane Ca2+ pump activity in normal human red blood cells.* Blood, 2003. **102**(12): p. 4206-13.
17. Dagher, G. and V.L. Lew, *Maximal calcium extrusion capacity and stoichiometry of the human red cell calcium pump.* J Physiol, 1988. **407**: p. 569-86.
18. Danielczok, J.G., et al., *Red Blood Cell Passage of Small Capillaries Is Associated with Transient Ca(2+)-mediated Adaptations.* Front Physiol, 2017. **8**: p. 979.
19. Rogers, S. and V.L. Lew, *Up-down biphasic volume response of human red blood cells to PIEZO1 activation during capillary transits.* PLoS Comput Biol, 2021. **17**(3): p. e1008706.
20. Rogers, S. and V.L. Lew, *PIEZO1 and the mechanism of the long circulatory longevity of human red blood cells.* PLoS Comput Biol, 2021. **17**(3): p. e1008496.

21. Sakota, D., et al., *Mechanical damage of red blood cells by rotary blood pumps: selective destruction of aged red blood cells and subhemolytic trauma.* Artif Organs, 2008. **32**(10): p. 785-91.
22. Wang, J., et al., *Morphologically homogeneous red blood cells present a heterogeneous response to hormonal stimulation.* PLoS One, 2013. **8**(6): p. e67697.
23. Shiga, T., et al., *Cell age-dependent changes in deformability and calcium accumulation of human erythrocytes.* Biochim Biophys Acta, 1985. **814**(2): p. 289-99.
24. Bizjak, D.A., et al., *Increase in Red Blood Cell-Nitric Oxide Synthase Dependent Nitric Oxide Production during Red Blood Cell Aging in Health and Disease: A Study on Age Dependent Changes of Rheologic and Enzymatic Properties in Red Blood Cells.* PLoS One, 2015. **10**(4): p. e0125206.
25. Zanner, M.A. and W.R. Galey, *Aged human erythrocytes exhibit increased anion exchange.* Biochim Biophys Acta, 1985. **818**(3): p. 310-5.
26. Bosch, F.H., et al., *Characteristics of red blood cell populations fractionated with a combination of counterflow centrifugation and Percoll separation.* Blood, 1992. **79**(1): p. 254-60.
27. Ulker, P., et al., *Mechanical stimulation of nitric oxide synthesizing mechanisms in erythrocytes.* Biorheology, 2009. **46**(2): p. 121-32.
28. Ulker, P., et al., *Shear stress activation of nitric oxide synthase and increased nitric oxide levels in human red blood cells.* Nitric Oxide, 2011. **24**(4): p. 184-91.
29. Thiagarajan, P., C.J. Parker, and J.T. Prchal, *How Do Red Blood Cells Die?* Front Physiol, 2021. **12**: p. 655393.
30. de Back, D.Z., et al., *Of macrophages and red blood cells; a complex love story.* Front Physiol, 2014. **5**: p. 9.
31. Safeukui, I., et al., *Sensing of red blood cells with decreased membrane deformability by the human spleen.* Blood Adv, 2018. **2**(20): p. 2581-2587.
32. Anosa, V.O., *Postsplenectomy blood values, marrow cytology, erythrocyte life-span, and sequestration in mice.* Am J Physiol, 1976. **231**(4): p. 1254-7.
33. Buchanan, G.R. and C.A. Holtkamp, *Pocked erythrocyte counts in patients with hereditary spherocytosis before and after splenectomy.* Am J Hematol, 1987. **25**(3): p. 253-7.
34. Klei, T.R.L., et al., *The Gardos effect drives erythrocyte senescence and leads to Lu/BCAM and CD44 adhesion molecule activation.* Blood Adv, 2020. **4**(24): p. 6218-6229.
35. Klei, T.R.L., et al., *Hemolysis in the spleen drives erythrocyte turnover.* Blood, 2020. **136**(14): p. 1579-1589.
36. Acosta, J.A., et al., *The transient pore formed by homologous terminal complement complexes functions as a bidirectional route for the transport of autocrine and paracrine signals across human cell membranes.* Mol Med, 1996. **2**(6): p. 755-65.
37. Hertz, L., et al., *Is Increased Intracellular Calcium in Red Blood Cells a Common Component in the Molecular Mechanism Causing Anemia?* Front Physiol, 2017. **8**: p. 673.
38. Lew, V.L. and T. Tiffert, *On the Mechanism of Human Red Blood Cell Longevity: Roles of Calcium, the Sodium Pump, PIEZO1, and Gardos Channels.* Front Physiol, 2017. **8**: p. 977.
39. Grau, M., et al., *RBC-NOS-dependent S-nitrosylation of cytoskeletal proteins improves RBC deformability.* PLoS One, 2013. **8**(2): p. e56759.

40. Barodka, V., et al., *Nitroprusside inhibits calcium-induced impairment of red blood cell deformability.* Transfusion, 2014. **54**(2): p. 434-44.
41. Andrews, D.A., L. Yang, and P.S. Low, *Phorbol ester stimulates a protein kinase C-mediated agatoxin-TK-sensitive calcium permeability pathway in human red blood cells.* Blood, 2002. **100**(9): p. 3392-9.
42. Tanaka, T., et al., *Ca2(+)-dependent regulation of the spectrin/actin interaction by calmodulin and protein 4.1.* J Biol Chem, 1991. **266**(2): p. 1134-40.
43. Lauf, P.K. and N.C. Adragna, *Properties and membrane transport mechanisms of erythrocytes*, in *Erythrocytes: Physiology and pathophysiology*. 2012, World Scientific. p. 57-228.
44. Leo, F., et al., *Red Blood Cell and Endothelial eNOS Independently Regulate Circulating Nitric Oxide Metabolites and Blood Pressure.* Circulation, 2021. **144**(11): p. 870-889.
45. Cahalan, S.M., et al., *Piezo1 links mechanical forces to red blood cell volume.* Elife, 2015. **4**.
46. Li, J., et al., *Piezo1 integration of vascular architecture with physiological force.* Nature, 2014. **515**(7526): p. 279-282.
47. Bogdanova, A., et al., *Calcium in red blood cells-a perilous balance.* Int J Mol Sci, 2013. **14**(5): p. 9848-72.
48. Tomaiuolo, G., *Biomechanical properties of red blood cells in health and disease towards microfluidics.* Biomicrofluidics, 2014. **8**(5): p. 051501.
49. Kayar, E., et al., *Red blood cell rheological alterations in a rat model of ischemia-reperfusion injury.* Biorheology, 2001. **38**(5-6): p. 405-14.
50. Kuck, L., J.N. Peart, and M.J. Simmonds, *Active modulation of human erythrocyte mechanics.* Am J Physiol Cell Physiol, 2020. **319**(2): p. C250-C257.
51. Chien, S., *Red cell deformability and its relevance to blood flow.* Annu Rev Physiol, 1987. **49**: p. 177-92.
52. Simchon, S., K.M. Jan, and S. Chien, *Influence of reduced red cell deformability on regional blood flow.* Am J Physiol, 1987. **253**(4 Pt 2): p. H898-903.
53. Wang, C.H. and A.S. Popel, *Effect of red blood cell shape on oxygen transport in capillaries.* Math Biosci, 1993. **116**(1): p. 89-110.
54. Doyle, M.P., W.R. Galey, and B.R. Walker, *Reduced erythrocyte deformability alters pulmonary hemodynamics.* J Appl Physiol (1985), 1989. **67**(6): p. 2593-9.
55. Langenfeld, J.E., et al., *Correlation between red blood cell deformability and changes in hemodynamic function.* Surgery, 1994. **116**(5): p. 859-67.
56. Vaya, A., et al., *Erythrocyte deformability and aggregation in homozygous sickle cell disease.* Clin Hemorheol Microcirc, 2014. **58**(4): p. 497-505.
57. Richardson, K.J., A.P. McNamee, and M.J. Simmonds, *Mechanical sensitivity of red blood cells improves in individuals with hemochromatosis following venesection therapy.* Transfusion, 2020.
58. Baskurt, O.K., D. Gelmont, and H.J. Meiselman, *Red blood cell deformability in sepsis.* Am J Respir Crit Care Med, 1998. **157**(2): p. 421-7.
59. Simmonds, M.J., et al., *Heart rate variability is related to impaired haemorheology in older women with type 2 diabetes.* Clin Hemorheol Microcirc, 2010. **46**(1): p. 57-68.
60. Detterich, J.A., et al., *Sickle cell microvascular paradox-oxygen supply-demand mismatch.* Am J Hematol, 2019. **94**(6): p. 678-688.
61. Richardson, T.E., et al., *Effects of chronic heart failure on skeletal muscle capillary hemodynamics at rest and during contractions.* J Appl Physiol (1985), 2003. **95**(3): p. 1055-62.

62. Tikhomirova, I., et al., *Microcirculation and blood rheology abnormalities in chronic heart failure.* Clin Hemorheol Microcirc, 2017. **65**(4): p. 383-391.
63. Fischer, T.M., M. Stohr-Lissen, and H. Schmid-Schonbein, *The red cell as a fluid droplet: tank tread-like motion of the human erythrocyte membrane in shear flow.* Science, 1978. **202**(4370): p. 894-6.
64. Lux, S.E.t., *Anatomy of the red cell membrane skeleton: unanswered questions.* Blood, 2016. **127**(2): p. 187-99.
65. Gulliver, G., *Medical Times and Gazette.* London: John Churchill & Sons, 1862.
66. Takakuwa, Y., T. Ishibashi, and N. Mohandas, *Regulation of red cell membrane deformability and stability by skeletal protein network.* Biorheology, 1990. **27**(3-4): p. 357-65.
67. Smith, A.S., et al., *Myosin IIA interacts with the spectrin-actin membrane skeleton to control red blood cell membrane curvature and deformability.* Proc Natl Acad Sci U S A, 2018. **115**(19): p. E4377-E4385.
68. Shutova, M.S. and T.M. Svitkina, *Common and Specific Functions of Nonmuscle Myosin II Paralogs in Cells.* Biochemistry (Mosc), 2018. **83**(12): p. 1459-1468.
69. Cai, Y., et al., *Cytoskeletal coherence requires myosin-IIA contractility.* J Cell Sci, 2010. **123**(Pt 3): p. 413-23.
70. Yoon, C., et al., *Myosin IIA-mediated forces regulate multicellular integrity during vascular sprouting.* Mol Biol Cell, 2019. **30**(16): p. 1974-1984.
71. Forsyth, A.M., et al., *The effects of membrane cholesterol and simvastatin on red blood cell deformability and ATP release.* Microvasc Res, 2012. **83**(3): p. 347-51.
72. Manno, S., Y. Takakuwa, and N. Mohandas, *Identification of a functional role for lipid asymmetry in biological membranes: Phosphatidylserine-skeletal protein interactions modulate membrane stability.* Proc Natl Acad Sci U S A, 2002. **99**(4): p. 1943-8.
73. Kuo, M.S., et al., *Different Involvement of Band 3 in Red Cell Deformability and Osmotic Fragility-A Comparative GP.Mur Erythrocyte Study.* Cells, 2021. **10**(12).
74. Chasis, J.A., N. Mohandas, and S.B. Shohet, *Erythrocyte membrane rigidity induced by glycophorin A-ligand interaction. Evidence for a ligand-induced association between glycophorin A and skeletal proteins.* J Clin Invest, 1985. **75**(6): p. 1919-26.
75. Anong, W.A., T.L. Weis, and P.S. Low, *Rate of rupture and reattachment of the band 3-ankyrin bridge on the human erythrocyte membrane.* J Biol Chem, 2006. **281**(31): p. 22360-22366.
76. Kuck, L., et al., *Shear Stress Ameliorates Superoxide Impairment to Erythrocyte Deformability With Concurrent Nitric Oxide Synthase Activation.* Front Physiol, 2019. **10**: p. 36.
77. Mehta, J.L., P. Mehta, and D. Li, *Nitric oxide synthase in adult red blood cells: vestige of an earlier age or a biologically active enzyme?* J Lab Clin Med, 2000. **135**(6): p. 430-1.
78. Kleinbongard, P., et al., *Red blood cells express a functional endothelial nitric oxide synthase.* Blood, 2006. **107**(7): p. 2943-51.
79. Govers, R. and T.J. Rabelink, *Cellular regulation of endothelial nitric oxide synthase.* Am J Physiol Renal Physiol, 2001. **280**(2): p. F193-206.
80. Ozuyaman, B., et al., *RBC NOS: regulatory mechanisms and therapeutic aspects.* Trends Mol Med, 2008. **14**(7): p. 314-22.

81. Tran, J., et al., *Activation of Endothelial Nitric Oxide (eNOS) Occurs through Different Membrane Domains in Endothelial Cells.* PLoS One, 2016. **11**(3): p. e0151556.
82. Lhomme, A., et al., *Stretch-activated Piezo1 Channel in Endothelial Cells Relaxes Mouse Intrapulmonary Arteries.* Am J Respir Cell Mol Biol, 2019. **60**(6): p. 650-658.
83. Baskurt, O.K., et al., *Modulation of endothelial nitric oxide synthase expression by red blood cell aggregation.* Am J Physiol Heart Circ Physiol, 2004. **286**(1): p. H222-9.
84. Sanchez, F.A., et al., *Functional significance of differential eNOS translocation.* Am J Physiol Heart Circ Physiol, 2006. **291**(3): p. H1058-64.
85. Suhr, F., et al., *Moderate exercise promotes human RBC-NOS activity, NO production and deformability through Akt kinase pathway.* PLoS One, 2012. **7**(9): p. e45982.
86. Grau, M., et al., *Decrease in red blood cell deformability is associated with a reduction in RBC-NOS activation during storage.* Clin Hemorheol Microcirc, 2015. **60**(2): p. 215-29.
87. Horobin, J.T., et al., *Shear-stress mediated nitric oxide production within red blood cells: A dose-response.* Clin Hemorheol Microcirc, 2018.
88. Cortese-Krott, M.M., et al., *Human red blood cells at work: identification and visualization of erythrocytic eNOS activity in health and disease.* Blood, 2012. **120**(20): p. 4229-37.
89. Yang, J., et al., *Arginase regulates red blood cell nitric oxide synthase and export of cardioprotective nitric oxide bioactivity.* Proc Natl Acad Sci U S A, 2013. **110**(37): p. 15049-54.
90. O'Rear, E.A., et al., *Reduced erythrocyte deformability associated with calcium accumulation.* Biochim Biophys Acta, 1982. **691**(2): p. 274-80.
91. Pasini, E.M., et al., *In-depth analysis of the membrane and cytosolic proteome of red blood cells.* Blood, 2006. **108**(3): p. 791-801.
92. Lew, V.L., et al., *Physiological [Ca2+]i level and pump-leak turnover in intact red cells measured using an incorporated Ca chelator.* Nature, 1982. **298**(5873): p. 478-81.
93. Weed, R.I., P.L. LaCelle, and E.W. Merrill, *Metabolic dependence of red cell deformability.* J Clin Invest, 1969. **48**(5): p. 795-809.
94. Clark, M.R., et al., *Separate mechanisms of deformability loss in ATP-depleted and Ca-loaded erythrocytes.* J Clin Invest, 1981. **67**(2): p. 531-9.
95. Maher, A.D. and P.W. Kuchel, *The Gardos channel: a review of the Ca2+-activated K+ channel in human erythrocytes.* Int J Biochem Cell Biol, 2003. **35**(8): p. 1182-97.
96. von Tempelhoff, G.F., et al., *Correlation between blood rheological properties and red blood cell indices(MCH, MCV, MCHC) in healthy women.* Clin Hemorheol Microcirc, 2016. **62**(1): p. 45-54.
97. Dyrda, A., et al., *Local membrane deformations activate Ca2+-dependent K+ and anionic currents in intact human red blood cells.* PLoS One, 2010. **5**(2): p. e9447.
98. Kaestner, L., *Channelizing the red blood cell: molecular biology competes with patch-clamp.* Front Mol Biosci, 2015. **2**: p. 46.
99. Gunn, R.B., et al., *Characteristics of chloride transport in human red blood cells.* J Gen Physiol, 1973. **61**(2): p. 185-206.

100. Balach, M.M., C.H. Casale, and A.N. Campetelli, *Erythrocyte plasma membrane potential: past and current methods for its measurement.* Biophys Rev, 2019. **11**(6): p. 995-1005.
101. Bae, C., F. Sachs, and P.A. Gottlieb, *The mechanosensitive ion channel Piezo1 is inhibited by the peptide GsMTx4.* Biochemistry, 2011. **50**(29): p. 6295-300.
102. Forstermann, U., et al., *Calmodulin-dependent endothelium-derived relaxing factor/nitric oxide synthase activity is present in the particulate and cytosolic fractions of bovine aortic endothelial cells.* Proc Natl Acad Sci U S A, 1991. **88**(5): p. 1788-92.
103. Fraser, K.H., et al., *A quantitative comparison of mechanical blood damage parameters in rotary ventricular assist devices: shear stress, exposure time and hemolysis index.* J Biomech Eng, 2012. **134**(8): p. 081002.
104. Kirklin, J.K., et al., *Eighth annual INTERMACS report: Special focus on framing the impact of adverse events.* J Heart Lung Transplant, 2017. **36**(10): p. 1080-1086.
105. Connes, P., et al., *The role of blood rheology in sickle cell disease.* Blood Rev, 2016. **30**(2): p. 111-8.
106. Joiner, C.H., *Gardos pathway to sickle cell therapies?* Blood, 2008. **111**(8): p. 3918-9.
107. Stocker, J.W., et al., *ICA-17043, a novel Gardos channel blocker, prevents sickled red blood cell dehydration in vitro and in vivo in SAD mice.* Blood, 2003. **101**(6): p. 2412-8.
108. Brugnara, C., et al., *Therapy with oral clotrimazole induces inhibition of the Gardos channel and reduction of erythrocyte dehydration in patients with sickle cell disease.* J Clin Invest, 1996. **97**(5): p. 1227-34.
109. Nguetse, C.N., et al., *A common polymorphism in the mechanosensitive ion channel PIEZO1 is associated with protection from severe malaria in humans.* Proc Natl Acad Sci U S A, 2020. **117**(16): p. 9074-9081.
110. Rooks, H., et al., *A gain of function variant in PIEZO1 (E756del) and sickle cell disease.* Haematologica, 2019. **104**(3): p. e91-e93.
111. Grau, M., et al., *High red blood cell nitric oxide synthase activation is not associated with improved vascular function and red blood cell deformability in sickle cell anaemia.* Br J Haematol, 2015. **168**(5): p. 728-36.
112. Belanger, A.M., et al., *Effects of nitric oxide and its congeners on sickle red blood cell deformability.* Transfusion, 2015. **55**(10): p. 2464-72.
113. Fermo, E., et al., *'Gardos Channelopathy': a variant of hereditary Stomatocytosis with complex molecular regulation.* Sci Rep, 2017. **7**(1): p. 1744.
114. Glogowska, E., et al., *Novel mechanisms of PIEZO1 dysfunction in hereditary xerocytosis.* Blood, 2017. **130**(16): p. 1845-1856.
115. Filatova, O.V., A.A. Sidorenko, and S.A. Agarkova, *[The Rheological Properties of Blood Depending on Age and Sex].* Fiziol Cheloveka, 2015. **41**(4): p. 110-8.
116. Baskurt, O.K., et al., *New guidelines for hemorheological laboratory techniques.* Clin Hemorheol Microcirc, 2009. **42**(2): p. 75-97.
117. Kuck, L., *Biochemical and physical responses of red blood cells with shear exposure*, in *School of Medical Science*. 2018, Griffith University.
118. Hardeman, M.R., P. Goedhart, and D. Breederveld, *Laser diffraction ellipsometry of erythrocytes under controlled shear stress using a rotational viscosimeter.* Clin Chim Acta, 1987. **165**(2-3): p. 227-34.
119. Bor-Kucukatay, M., et al., *Effects of nitric oxide on red blood cell deformability.* Am J Physiol Heart Circ Physiol, 2003. **284**(5): p. H1577-84.

120. Mozar, A., et al., *Red blood cell nitric oxide synthase modulates red blood cell deformability in sickle cell anemia.* Clin Hemorheol Microcirc, 2016. **64**(1): p. 47-53.
121. Fisslthaler, B., et al., *Phosphorylation and activation of the endothelial nitric oxide synthase by fluid shear stress.* Acta Physiol Scand, 2000. **168**(1): p. 81-8.
122. Suthipintawong, C., A.S. Leong, and S. Vinyuvat, *Immunostaining of cell preparations: a comparative evaluation of common fixatives and protocols.* Diagn Cytopathol, 1996. **15**(2): p. 167-74.
123. Dimmeler, S., et al., *Activation of nitric oxide synthase in endothelial cells by Akt-dependent phosphorylation.* Nature, 1999. **399**(6736): p. 601-5.
124. Masilamani, V., et al., *Cancer diagnosis by autofluorescence of blood components.* Journal of Luminescence, 2004. **109**(3-4): p. 143-154.
125. Bland, J.M. and D.G. Altman, *Statistical methods for assessing agreement between two methods of clinical measurement.* Lancet, 1986. **1**(8476): p. 307-10.
126. Zhu, R., et al., *Optical Tweezers in Studies of Red Blood Cells.* Cells, 2020. **9**(3).
127. Schmid-Schonbein, H., R. Wells, and J. Goldstone, *Influence of deformability of human red cells upon blood viscosity.* Circ Res, 1969. **25**(2): p. 131-43.
128. Lanotte, L., et al., *Red cells' dynamic morphologies govern blood shear thinning under microcirculatory flow conditions.* Proc Natl Acad Sci U S A, 2016. **113**(47): p. 13289-13294.
129. Rabai, M., et al., *Deformability analysis of sickle blood using ektacytometry.* Biorheology, 2014. **51**(2-3): p. 159-70.
130. McNamee, A.P., et al., *Acute Free-Iron Exposure Does Not Explain the Impaired Haemorheology Associated with Haemochromatosis.* PLoS One, 2016. **11**(1): p. e0146448.
131. Yagi, H., et al., *Impaired blood rheology is associated with endothelial dysfunction in patients with coronary risk factors.* Clin Hemorheol Microcirc, 2016. **62**(2): p. 139-50.
132. Turpin, C., et al., *Enhanced oxidative stress and damage in glycated erythrocytes.* PLoS One, 2020. **15**(7): p. e0235335.
133. Mohanty, J.G., E. Nagababu, and J.M. Rifkind, *Red blood cell oxidative stress impairs oxygen delivery and induces red blood cell aging.* Front Physiol, 2014. **5**: p. 84.
134. Balagopalakrishna, C., et al., *Production of superoxide from hemoglobin-bound oxygen under hypoxic conditions.* Biochemistry, 1996. **35**(20): p. 6393-8.
135. Kiefer, C.R. and L.M. Snyder, *Oxidation and erythrocyte senescence.* Curr Opin Hematol, 2000. **7**(2): p. 113-6.
136. Boas, F.E., L. Forman, and E. Beutler, *Phosphatidylserine exposure and red cell viability in red cell aging and in hemolytic anemia.* Proc Natl Acad Sci U S A, 1998. **95**(6): p. 3077-81.
137. Cloos, A.S., et al., *Interplay Between Plasma Membrane Lipid Alteration, Oxidative Stress and Calcium-Based Mechanism for Extracellular Vesicle Biogenesis From Erythrocytes During Blood Storage.* Front Physiol, 2020. **11**: p. 712.
138. Delaney, M., et al., *Transfusion reactions: prevention, diagnosis, and treatment.* Lancet, 2016. **388**(10061): p. 2825-2836.
139. Yoshida, T., M. Prudent, and A. D'Alessandro, *Red blood cell storage lesion: causes and potential clinical consequences.* Blood Transfus, 2019. **17**(1): p. 27-52.

140. Yurkovich, J.T., et al., *Quantitative time-course metabolomics in human red blood cells reveal the temperature dependence of human metabolic networks.* J Biol Chem, 2017. **292**(48): p. 19556-19564.
141. Heddle, N.M., et al., *Effect of Short-Term vs. Long-Term Blood Storage on Mortality after Transfusion.* N Engl J Med, 2016. **375**(20): p. 1937-1945.
142. Barshtein, G., et al., *Storage-induced damage to red blood cell mechanical properties can be only partially reversed by rejuvenation.* Transfus Med Hemother, 2014. **41**(3): p. 197-204.
143. Cluitmans, J.C., et al., *Red blood cell deformability during storage: towards functional proteomics and metabolomics in the Blood Bank.* Blood Transfus, 2012. **10 Suppl 2**: p. s12-8.
144. Li, Y., et al., *Blood banking-induced alteration of red blood cell oxygen release ability.* Blood Transfus, 2016. **14**(2): p. 238-44.
145. Hod, E.A., *Red blood cell transfusion-induced inflammation: myth or reality.* ISBT Sci Ser, 2015. **10**(Suppl 1): p. 188-191.
146. Bosman, G.J., *Survival of red blood cells after transfusion: processes and consequences.* Front Physiol, 2013. **4**: p. 376.
147. Luten, M., et al., *Survival of red blood cells after transfusion: a comparison between red cells concentrates of different storage periods.* Transfusion, 2008. **48**(7): p. 1478-85.
148. Simmonds, M.J. and H.J. Meiselman, *Prediction of the level and duration of shear stress exposure that induces subhemolytic damage to erythrocytes.* Biorheology, 2016. **53**(5-6): p. 237-249.
149. Horobin, J.T., S. Sabapathy, and M.J. Simmonds, *Repetitive Supra-Physiological Shear Stress Impairs Red Blood Cell Deformability and Induces Hemolysis.* Artif Organs, 2017. **41**(11): p. 1017-1025.
150. McNamee, A.P., et al., *Sublethal Supraphysiological Shear Stress Alters Erythrocyte Dynamics in Subsequent Low-Shear Flows.* Biophys J, 2020. **119**(11): p. 2179-2189.
151. McNamee, A.P., G.D. Tansley, and M.J. Simmonds, *Sublethal mechanical shear stress increases the elastic shear modulus of red blood cells but does not change capillary transit velocity.* Microcirculation, 2020. **27**(8): p. e12652.
152. Baskurt, O.K., A. Temiz, and H.J. Meiselman, *Effect of superoxide anions on red blood cell rheologic properties.* Free Radic Biol Med, 1998. **24**(1): p. 102-10.
153. Hebbel, R.P., A. Leung, and N. Mohandas, *Oxidation-induced changes in microrheologic properties of the red blood cell membrane.* Blood, 1990. **76**(5): p. 1015-20.
154. Abay, A., et al., *Glutaraldehyde - A Subtle Tool in the Investigation of Healthy and Pathologic Red Blood Cells.* Front Physiol, 2019. **10**: p. 514.
155. Simmonds, M.J., et al., *Red blood cell mechanical sensitivity improves in patients with sickle cell disease undergoing chronic transfusion after prolonged, subhemolytic shear exposure.* Transfusion, 2018. **58**(12): p. 2788-2796.
156. Hardeman, M.R., J.G. Dobbe, and C. Ince, *The Laser-assisted Optical Rotational Cell Analyzer (LORCA) as red blood cell aggregometer.* Clin Hemorheol Microcirc, 2001. **25**(1): p. 1-11.
157. Mc, G.J., A.R. Jones, and A.G. Steinberg, *The hematocrit of capillary blood.* N Engl J Med, 1955. **253**(8): p. 308-12.
158. Chien, S. and K. Jan, *Ultrastructural basis of the mechanism of rouleaux formation.* Microvasc Res, 1973. **5**(2): p. 155-66.

159. Schindelin, J., et al., *Fiji: an open-source platform for biological-image analysis.* Nat Methods, 2012. **9**(7): p. 676-82.
160. Baskurt, O.K., et al., *Parameterization of red blood cell elongation index--shear stress curves obtained by ektacytometry.* Scand J Clin Lab Invest, 2009. **69**(7): p. 777-88.
161. McNamee, A.P., et al., *Biphasic impairment of erythrocyte deformability in response to repeated, short duration exposures of supraphysiological, subhaemolytic shear stress.* Biorheology, 2016. **53**(3-4): p. 137-149.
162. Kuck, L., M. Grau, and M.J. Simmonds, *Recovery time course of erythrocyte deformability following exposure to shear is dependent upon conditioning shear stress.* Biorheology, 2018. **54**(5-6): p. 141-152.
163. Klein, H.G., D.R. Spahn, and J.L. Carson, *Red blood cell transfusion in clinical practice.* Lancet, 2007. **370**(9585): p. 415-26.
164. Chen, Z., et al., *Shear stress and blood trauma under constant and pulse-modulated speed CF-VAD operations: CFD analysis of the HVAD.* Med Biol Eng Comput, 2019. **57**(4): p. 807-818.
165. Kuhn, V., et al., *Red Blood Cell Function and Dysfunction: Redox Regulation, Nitric Oxide Metabolism, Anemia.* Antioxid Redox Signal, 2017. **26**(13): p. 718-742.
166. McNamee, A.P., et al., *Oxidative Stress Increases Erythrocyte Sensitivity to Shear-Mediated Damage.* Artif Organs, 2018. **42**(2): p. 184-192.
167. Baskurt, O.K., *In vivo correlates of altered blood rheology.* Biorheology, 2008. **45**(6): p. 629-38.
168. Chen, R.Y., et al., *Effects of dextran-induced hyperviscosity on regional blood flow and hemodynamics in dogs.* Am J Physiol, 1989. **256**(3 Pt 2): p. H898-905.
169. Chien, S., et al., *Blood viscosity: influence of erythrocyte deformation.* Science, 1967. **157**(3790): p. 827-9.
170. Lazari, D., et al., *The Relationship Between Aggregation and Deformability of Red Blood Cells in Health and Disease.* Front Physiol, 2020. **11**: p. 288.
171. Ju, M., et al., *Effect of deformability difference between two erythrocytes on their aggregation.* Phys Biol, 2013. **10**(3): p. 036001.
172. Avsievich, T., et al., *Mutual interaction of red blood cells assessed by optical tweezers and scanning electron microscopy imaging.* Opt Lett, 2018. **43**(16): p. 3921-3924.
173. Eylar, E.H., et al., *The contribution of sialic acid to the surface charge of the erythrocyte.* J Biol Chem, 1962. **237**: p. 1992-2000.
174. Jan, K.M. and S. Chien, *Role of surface electric charge in red blood cell interactions.* J Gen Physiol, 1973. **61**(5): p. 638-54.
175. Vassar, P.S., et al., *Physicochemical effects of aldehydes on the human erythrocyte.* J Cell Biol, 1972. **53**(3): p. 809-18.
176. Nishikimi, M., N. Appaji, and K. Yagi, *The occurrence of superoxide anion in the reaction of reduced phenazine methosulfate and molecular oxygen.* Biochem Biophys Res Commun, 1972. **46**(2): p. 849-54.
177. Carr, R. and G. Cockelet, *Rheology of suspensions of normal and hardened erythrocytes and their mixtures.* Journal of Rheology, 1981. **25**(67): p. 67-82.
178. Roback, J.D., *Perspectives on the impact of storage duration on blood quality and transfusion outcomes.* Vox Sang, 2016. **111**(4): p. 357-364.
179. Bacher, A., et al., *Pentoxifylline attenuates the increase in whole blood viscosity after transfusion.* Acta Anaesthesiol Scand, 2005. **49**(1): p. 41-6.

180. Zimmerman, R., et al., *Posttransfusion Increase of Hematocrit per se Does Not Improve Circulatory Oxygen Delivery due to Increased Blood Viscosity.* Anesth Analg, 2017. **124**(5): p. 1547-1554.
181. Mohandas, N. and P.G. Gallagher, *Red cell membrane: past, present, and future.* Blood, 2008. **112**(10): p. 3939-48.
182. Koutsiaris, A.G., S.V. Tachmitzi, and N. Batis, *Wall shear stress quantification in the human conjunctival pre-capillary arterioles in vivo.* Microvasc Res, 2013. **85**: p. 34-9.
183. Dodson, R.A., T.R. Hinds, and F.F. Vincenzi, *Effects of calcium and A23187 on deformability and volume of human red blood cells.* Blood Cells, 1987. **12**(3): p. 555-64.
184. Watanabe, H., et al., *Alterations of human erythrocyte membrane fluidity by oxygen-derived free radicals and calcium.* Free Radic Biol Med, 1990. **8**(6): p. 507-14.
185. Cueff, A., et al., *Effects of elevated intracellular calcium on the osmotic fragility of human red blood cells.* Cell Calcium, 2010. **47**(1): p. 29-36.
186. Kaestner, L., et al., *Calcium imaging of individual erythrocytes: problems and approaches.* Cell Calcium, 2006. **39**(1): p. 13-9.
187. Nunomura, W. and Y. Takakuwa, *Regulation of protein 4.1R interactions with membrane proteins by Ca2+ and calmodulin.* Front Biosci, 2006. **11**: p. 1522-39.
188. Simmonds, M.J., et al., *Erythrocyte deformability responses to intermittent and continuous subhemolytic shear stress.* Biorheology, 2014. **51**(2-3): p. 171-85.
189. Meram, E., et al., *Shear stress-induced improvement of red blood cell deformability.* Biorheology, 2013. **50**(3-4): p. 165-76.
190. Hardeman, M.R., et al., *Laser-Assisted Optical Rotational Cell Analyzer (Lorca) .1. A New Instrument for Measurement of Various Structural Hemorheological Parameters.* Clinical Hemorheology, 1994. **14**(4): p. 605-618.
191. Harboe, M., *A method for determination of hemoglobin in plasma by near-ultraviolet spectrophotometry.* Scand J Clin Lab Invest, 1959. **11**: p. 66-70.
192. Meiselman, H.J., E.A. Evans, and R.M. Hochmuth, *Membrane mechanical properties of ATP-depleted human erythrocytes.* Blood, 1978. **52**(3): p. 499-504.
193. Renoux, C., et al., *Impact of surface-area-to-volume ratio, internal viscosity and membrane viscoelasticity on red blood cell deformability measured in isotonic condition.* Sci Rep, 2019. **9**(1): p. 6771.
194. Leo, J.A., M.J. Simmonds, and S. Sabapathy, *Shear-thinning behaviour of blood in response to active hyperaemia: Implications for the assessment of arterial shear stress-mediated dilation.* Exp Physiol, 2019.
195. Lang, P.A., et al., *Role of Ca2+-activated K+ channels in human erythrocyte apoptosis.* Am J Physiol Cell Physiol, 2003. **285**(6): p. C1553-60.
196. Wesseling, M.C., et al., *Phosphatidylserine Exposure in Human Red Blood Cells Depending on Cell Age.* Cell Physiol Biochem, 2016. **38**(4): p. 1376-90.
197. Malek, A.M., S.L. Alper, and S. Izumo, *Hemodynamic shear stress and its role in atherosclerosis.* JAMA, 1999. **282**(21): p. 2035-42.
198. Horobin, J.T., et al., *Shear-stress mediated nitric oxide production within red blood cells: A dose-response.* Clin Hemorheol Microcirc, 2019. **71**(2): p. 203-214.
199. Lew, V.L. and R.M. Bookchin, *Volume, pH, and ion-content regulation in human red cells: analysis of transient behavior with an integrated model.* J Membr Biol, 1986. **92**(1): p. 57-74.
200. Larsen, F.L., et al., *Physiological shear stresses enhance the Ca2+ permeability of human erythrocytes.* Nature, 1981. **294**(5842): p. 667-8.

201. Johnson, R.M., *Membrane stress increases cation permeability in red cells.* Biophys J, 1994. **67**(5): p. 1876-81.
202. Paul, R., et al., *Shear stress related blood damage in laminar couette flow.* Artif Organs, 2003. **27**(6): p. 517-29.
203. Platt, O.S., *Exercise-induced hemolysis in sickle cell anemia: shear sensitivity and erythrocyte dehydration.* Blood, 1982. **59**(5): p. 1055-60.
204. Bosch, F.H., et al., *Determinants of red blood cell deformability in relation to cell age.* Eur J Haematol, 1994. **52**(1): p. 35-41.
205. Mohandas, N., et al., *Analysis of factors regulating erythrocyte deformability.* J Clin Invest, 1980. **66**(3): p. 563-73.
206. Linderkamp, O., E. Friederichs, and H.J. Meiselman, *Mechanical and geometrical properties of density-separated neonatal and adult erythrocytes.* Pediatr Res, 1993. **34**(5): p. 688-93.
207. Huisjes, R., et al., *Squeezing for Life - Properties of Red Blood Cell Deformability.* Front Physiol, 2018. **9**: p. 656.
208. Asaro, R.J. and P. Cabrales, *The RBC's road to ghost and removal: splenic clearance.* Blood Adv, 2021. **5**(21): p. 4422-4425.
209. Gottlieb, Y., et al., *Physiologically aged red blood cells undergo erythrophagocytosis in vivo but not in vitro.* Haematologica, 2012. **97**(7): p. 994-1002.
210. Ingber, D.E., *Cellular mechanotransduction: putting all the pieces together again.* FASEB J, 2006. **20**(7): p. 811-27.
211. Kuck, L., J.N. Peart, and M.J. Simmonds, *Piezo1 regulates shear-dependent nitric oxide production in human erythrocytes.* Am J Physiol Heart Circ Physiol, 2022.
212. van Wijk, R. and W.W. van Solinge, *The energy-less red blood cell is lost: erythrocyte enzyme abnormalities of glycolysis.* Blood, 2005. **106**(13): p. 4034-42.
213. Magnani, M., et al., *The age-dependent metabolic decline of the red blood cell.* Mech Ageing Dev, 1983. **22**(3-4): p. 295-308.
214. Bernstein, R.E., *Alterations in metabolic energetics and cation transport during aging of red cells.* J Clin Invest, 1959. **38**: p. 1572-86.
215. Kuck, L., J.N. Peart, and M.J. Simmonds, *Calcium dynamically alters erythrocyte mechanical response to shear.* Biochim Biophys Acta Mol Cell Res, 2020. **1867**(11): p. 118802.
216. Syeda, R., et al., *Chemical activation of the mechanotransduction channel Piezo1.* Elife, 2015. **4**.
217. Lutz, H.U., et al., *Density separation of human red blood cells on self forming Percoll gradients: correlation with cell age.* Biochim Biophys Acta, 1992. **1116**(1): p. 1-10.
218. Grau, M., et al., *Sub-Fractions of Red Blood Cells Respond Differently to Shear Exposure Following Superoxide Treatment.* Biology (Basel), 2021. **10**(1).
219. Frederiksen, H., *Dehydrated hereditary stomatocytosis: clinical perspectives.* J Blood Med, 2019. **10**: p. 183-191.
220. Waldvogel Abramowski, S., *Hemolysis: Mechanism and clinico-biological consequences.* Transfus Clin Biol, 2021. **28**(4): p. 364-366.
221. Thangaraju, K., et al., *Extracellular Vesicles from Red Blood Cells and Their Evolving Roles in Health, Coagulopathy and Therapy.* Int J Mol Sci, 2020. **22**(1).
222. Minetti, G., et al., *Red cell investigations: art and artefacts.* Blood Rev, 2013. **27**(2): p. 91-101.

223. Romero, P.J. and E.A. Romero, *Differences in Ca2+ pumping activity between sub-populations of human red cells.* Cell Calcium, 1997. **21**(5): p. 353-8.
224. Schatzmann, H.J., *ATP-dependent Ca++-extrusion from human red cells.* Experientia, 1966. **22**(6): p. 364-5.
225. Simmonds, M.J., J.A. Detterich, and P. Connes, *Nitric oxide, vasodilation and the red blood cell.* Biorheology, 2014. **51**(2-3): p. 121-34.
226. Horobin, J.T., et al., *Shear Stress and RBC-NOS Serine1177 Phosphorylation in Humans: A Dose Response.* Life (Basel), 2021. **11**(1).
227. Nagarajan, S., et al., *Mechanical perturbations trigger endothelial nitric oxide synthase activity in human red blood cells.* Sci Rep, 2016. **6**: p. 26935.
228. Nagaoka, T. and A. Yoshida, *Noninvasive evaluation of wall shear stress on retinal microcirculation in humans.* Invest Ophthalmol Vis Sci, 2006. **47**(3): p. 1113-9.
229. Gladwin, M.T. and D.B. Kim-Shapiro, *The functional nitrite reductase activity of the heme-globins.* Blood, 2008. **112**(7): p. 2636-47.
230. Jia, L., et al., *S-nitrosohaemoglobin: a dynamic activity of blood involved in vascular control.* Nature, 1996. **380**(6571): p. 221-6.
231. Cosby, K., et al., *Nitrite reduction to nitric oxide by deoxyhemoglobin vasodilates the human circulation.* Nat Med, 2003. **9**(12): p. 1498-505.
232. Lipton, A.J., et al., *S-nitrosothiols signal the ventilatory response to hypoxia.* Nature, 2001. **413**(6852): p. 171-4.
233. Herrera, M., N.J. Hong, and J.L. Garvin, *Aquaporin-1 transports NO across cell membranes.* Hypertension, 2006. **48**(1): p. 157-64.
234. Cinar, E., et al., *Piezo1 regulates mechanotransductive release of ATP from human RBCs.* Proc Natl Acad Sci U S A, 2015. **112**(38): p. 11783-8.
235. Wan, J., W.D. Ristenpart, and H.A. Stone, *Dynamics of shear-induced ATP release from red blood cells.* Proc Natl Acad Sci U S A, 2008. **105**(43): p. 16432-7.
236. Sprague, R.S., et al., *Participation of cAMP in a signal-transduction pathway relating erythrocyte deformation to ATP release.* Am J Physiol Cell Physiol, 2001. **281**(4): p. C1158-64.
237. Sridharan, M., et al., *Diamide decreases deformability of rabbit erythrocytes and attenuates low oxygen tension-induced ATP release.* Exp Biol Med (Maywood), 2010. **235**(9): p. 1142-8.
238. Racine, M.L. and F.A. Dinenno, *Reduced deformability contributes to impaired deoxygenation-induced ATP release from red blood cells of older adult humans.* J Physiol, 2019. **597**(17): p. 4503-4519.
239. Lipowsky, H.H. and B.W. Zweifach, *Methods for the simultaneous measurement of pressure differentials and flow in single unbranched vessels of the microcirculation for rheological studies.* Microvasc Res, 1977. **14**(3): p. 345-61.
240. Botello-Smith, W.M., et al., *A mechanism for the activation of the mechanosensitive Piezo1 channel by the small molecule Yoda1.* Nat Commun, 2019. **10**(1): p. 4503.
241. Li, J., et al., *Using diaminofluoresceins (DAFs) in nitric oxide research.* Nitric Oxide, 2021. **115**: p. 44-54.
242. Fischer, T.M., et al., *Selective alteration of erythrocyte deformabiliby by SH-reagents: evidence for an involvement of spectrin in membrane shear elasticity.* Biochim Biophys Acta, 1978. **510**(2): p. 270-82.

243. Becker, P.S., C.M. Cohen, and S.E. Lux, *The effect of mild diamide oxidation on the structure and function of human erythrocyte spectrin.* J Biol Chem, 1986. **261**(10): p. 4620-8.
244. Sinha, A., et al., *Single-cell evaluation of red blood cell bio-mechanical and nano-structural alterations upon chemically induced oxidative stress.* Sci Rep, 2015. **5**: p. 9768.
245. Sugisawa, E., et al., *RNA Sensing by Gut Piezo1 Is Essential for Systemic Serotonin Synthesis.* Cell, 2020. **182**(3): p. 609-624 e21.
246. Wang, L., et al., *Mechanical sensing protein PIEZO1 regulates bone homeostasis via osteoblast-osteoclast crosstalk.* Nat Commun, 2020. **11**(1): p. 282.
247. Mousavi, S.A.R., et al., *PIEZO ion channel is required for root mechanotransduction in Arabidopsis thaliana.* Proc Natl Acad Sci U S A, 2021. **118**(20).
248. Beech, D.J. and A.C. Kalli, *Force Sensing by Piezo Channels in Cardiovascular Health and Disease.* Arterioscler Thromb Vasc Biol, 2019. **39**(11): p. 2228-2239.
249. Zarychanski, R., et al., *Mutations in the mechanotransduction protein PIEZO1 are associated with hereditary xerocytosis.* Blood, 2012. **120**(9): p. 1908-15.
250. Zama, D., et al., *A novel PIEZO1 mutation in a patient with dehydrated hereditary stomatocytosis: a case report and a brief review of literature.* Ital J Pediatr, 2020. **46**(1): p. 102.
251. Lewis, A.H. and J. Grandl, *Inactivation Kinetics and Mechanical Gating of Piezo1 Ion Channels Depend on Subdomains within the Cap.* Cell Rep, 2020. **30**(3): p. 870-880 e2.
252. Saotome, K., et al., *Structure of the mechanically activated ion channel Piezo1.* Nature, 2018. **554**(7693): p. 481-486.
253. Zhao, Q., et al., *Structure and mechanogating mechanism of the Piezo1 channel.* Nature, 2018. **554**(7693): p. 487-492.
254. Zhao, Q., et al., *Ion Permeation and Mechanotransduction Mechanisms of Mechanosensitive Piezo Channels.* Neuron, 2016. **89**(6): p. 1248-1263.
255. Webb, A.J., et al., *Mechanisms underlying erythrocyte and endothelial nitrite reduction to nitric oxide in hypoxia: role for xanthine oxidoreductase and endothelial nitric oxide synthase.* Circ Res, 2008. **103**(9): p. 957-64.
256. Wang, S., et al., *Endothelial cation channel PIEZO1 controls blood pressure by mediating flow-induced ATP release.* J Clin Invest, 2016. **126**(12): p. 4527-4536.
257. Ranade, S.S., et al., *Piezo1, a mechanically activated ion channel, is required for vascular development in mice.* Proc Natl Acad Sci U S A, 2014. **111**(28): p. 10347-52.
258. Wood, K.C., et al., *Circulating blood endothelial nitric oxide synthase contributes to the regulation of systemic blood pressure and nitrite homeostasis.* Arterioscler Thromb Vasc Biol, 2013. **33**(8): p. 1861-71.
259. Jarrett, H.W. and J. Kyte, *Human erythrocyte calmodulin. Further chemical characterization and the site of its interaction with the membrane.* J Biol Chem, 1979. **254**(17): p. 8237-44.
260. Nicholson-Fish, J.C., M.A. Cousin, and K.J. Smillie, *Phosphatidylinositol 3-Kinase Couples Localised Calcium Influx to Activation of Akt in Central Nerve Terminals.* Neurochem Res, 2016. **41**(3): p. 534-43.
261. Kuchel, P.W. and D. Shishmarev, *Accelerating metabolism and transmembrane cation flux by distorting red blood cells.* Sci Adv, 2017. **3**(10): p. eaao1016.
262. Molina, E.J., et al., *The Society of Thoracic Surgeons Intermacs 2020 Annual Report.* Ann Thorac Surg, 2021. **111**(3): p. 778-792.

263. Couto, N., J. Wood, and J. Barber, *The role of glutathione reductase and related enzymes on cellular redox homoeostasis network.* Free Radic Biol Med, 2016. **95**: p. 27-42.
264. Beckman, J.S. and W.H. Koppenol, *Nitric oxide, superoxide, and peroxynitrite: the good, the bad, and ugly.* Am J Physiol, 1996. **271**(5 Pt 1): p. C1424-37.
265. Buerck, J.P., et al., *Production of erythrocyte microparticles in a sub-hemolytic environment.* J Artif Organs, 2021. **24**(2): p. 135-145.
266. O'Rear, E.A., et al., *Increased intracellular calcium and decreased deformability of erythrocytes from prosthetic heart valve patients.* Clinical Hemorheology and Microcirculation, 1984. **4**(5): p. 461-471.
267. Jeske, W.P., et al., *Blood cell microparticles as biomarkers of hemostatic abnormalities in patients with implanted cardiac assist devices.* Biomark Med, 2016. **10**(10): p. 1095-1104.
268. Rotordam, M.G., et al., *A novel gain-of-function mutation of Piezo1 is functionally affirmed in red blood cells by high-throughput patch clamp.* Haematologica, 2019. **104**(5): p. e179-e183.
269. Grootenboer, S., et al., *Pleiotropic syndrome of dehydrated hereditary stomatocytosis, pseudohyperkalemia, and perinatal edema maps to 16q23-q24.* Blood, 2000. **96**(7): p. 2599-605.
270. Fotiou, E., et al., *Novel mutations in PIEZO1 cause an autosomal recessive generalized lymphatic dysplasia with non-immune hydrops fetalis.* Nat Commun, 2015. **6**: p. 8085.
271. Andolfo, I., et al., *Novel Gardos channel mutations linked to dehydrated hereditary stomatocytosis (xerocytosis).* Am J Hematol, 2015. **90**(10): p. 921-6.
272. Ridone, P., M. Vassalli, and B. Martinac, *Piezo1 mechanosensitive channels: what are they and why are they important.* Biophys Rev, 2019. **11**(5): p. 795-805.
273. Cox, C.D., et al., *Removal of the mechanoprotective influence of the cytoskeleton reveals PIEZO1 is gated by bilayer tension.* Nat Commun, 2016. **7**: p. 10366.
274. Devika, N.T. and B.M. Jaffar Ali, *Analysing calcium dependent and independent regulation of eNOS in endothelium triggered by extracellular signalling events.* Mol Biosyst, 2013. **9**(11): p. 2653-64.
275. McCabe, T.J., et al., *Enhanced electron flux and reduced calmodulin dissociation may explain "calcium-independent" eNOS activation by phosphorylation.* J Biol Chem, 2000. **275**(9): p. 6123-8.
276. Helms, C. and D.B. Kim-Shapiro, *Hemoglobin-mediated nitric oxide signaling.* Free Radic Biol Med, 2013. **61**: p. 464-72.
277. Suriany, S., et al., *Individual red blood cell nitric oxide production in sickle cell anemia: Nitric oxide production is increased and sickle shaped cells have unique morphologic change compared to discoid cells.* Free Radic Biol Med, 2021. **171**: p. 143-155.